SYNTHESIS, CHARACTERIZATION AND STUDY OF ELECTRICAL AND MAGNETIC PROPERTIES OF FINE PARTICLE Mn-Zn FERRITES BY NITRILOTRIACETATE PRECURSOR METHOD

A THESIS
SUBMITTED TO

GOA UNIVERSITY

FOR THE DEGREE OF

DOCTOR OF PHILOSOPHY

IN

PHYSICS

By

SATISH H. P. KELUSKAR

DEPARTMENT OF PHYSICS
GOA UNIVERSITY
TALEIGAO PLATEAU
TALEIGAO- GOA 403206.
July 2006

To.....

My Father

STATEMENT

I hereby state that this thesis for the Ph.D. degree on "Synthesis, Characterization and study of Electrical and Magnetic properties of fine particle Mn-Zn ferrites by Nitrilotriacetate precursor method" is my original work and that it has not previously formed the basis for the award of any degree, diploma, associateship and fellowship or any other similar title to the best of my knowledge and information.

Satish H. P. Keluskar

(candidate)

CERTIFICATE

As required under the University ordinance, we certify that the thesis entitled "Synthesis, Characterization and study of Electrical and Magnetic properties of fine particle Mn-Zn ferrites by Nitrilotriacetate precursor method" submitted by Shri Satish H. P. Keluskar for the award of Doctor of Philosophy in Physics is a record of research done by the candidate during the period of study under our guidance and that it has not previously formed the basis for the award to the candidate of any degree, diploma, associateship, fellowship or other similar titles.

Date :

R.B.Tangsali
Research guide,
Department of Physics,
Goa University.

J.S.Budkuley
Research Co-guide,
Department of Chemistry
Goa University.

ACKNOWLEDGEMENTS

I express my sincere thanks to my guiding teacher, Dr. Rudraji B. Tangsali, for suggesting the topic, continuous guidance throughout the course of this research. and discussions from time to time.

I wish to express my deep sense of gratitude to Prof. Jayant .S. Budkuley, research Co- guide, Department of Chemistry for the guidance, especially during synthesis and characterization.

I also thank:

1. Head, Department of Physics, Goa University for extending necessary facilities,
2. Head, Department of Chemistry, Goa University for extending necessary research laboratory facilities,
3. Management, Principal and staff of P.E.S's. College of Arts & Science, Farmagudi, for their cooperation.
4. Dr. G. K. Naik, Reader, Department of Chemistry, S.P.C. college, Margao, for his help during the course of this study,

5. Dr. S.C.Watwe, Department of Physics, Gogte College of Arts Science & Commerce, Ratnagiri for permitting use of laboratory facilities to carry out some experiments.

I also thank Prof. Narsihaman, Prof. Paulose, Mr.V. Kulkarni, Ms. Shilpa Chalke, Mr Sanjay Prabhu, Mr. Manish Ghag from Tata Institute of Fundamental Research Mumbai and Prof. S. Sunder Manoharan, I.I.T. Kanpur, NT-MDT Lab, Nanonics Lab for permitting me to collect the instrumental data of samples.

I thank faculty and non-teaching members of Department of Physics and Department of Chemistry, Goa University for their continuous cooperation.

I am grateful to University Grants Commission for sanctioning me Teacher Fellowship under Faculty Improvement Programme for two years, without which this work would not be possible.

I thank my research colleages, Vishwajit, Preeti , Shetkar, Ratan, Ashish for making my work in the laboratories comfortable.

Thanks are also due to Mr. Amol Desai for computer facility and Mr. Jaiprakash Kamat, USIC, Goa University, for his technical help.

Lastly, my special thanks to my mother, wife for their constant encouragement as well as continuous moral support and son Harish who had forgone my time with him which should have been rightly for him.

CONTENTS

CHAPTER I

CHAPTER II

CHAPTER III

3. PREPARATION OF MATERIALS

CHAPTER IV

CHAPTER V

CHAPTER VI

6. MAGNETIC PROPERTIES

CHAPTER VII

7. ELECTRICAL PROPERTIES

CHAPTER VIII

8. CONCLUSIONS

LIST OF FIGURES

CHAPTER I

CHAPTER II

CHAPTER IV

LIST OF TABLES

CHAPTER I

CHAPTER III

CHAPTER IV

CHAPTER V

CHAPTER VI

CHAPTER I

INTRODUCTION

1.1 GENERAL INTRODUCTION

The phenomenon of magnetism and the behavior of magnetic materials are well known. The domain structure, magnetic interaction and the basic properties of these materials are of considerable importance in modern technology. Magnetic materials have gained importance due to variety of applications. They form essential components in the form of magnetic cores in audio-video equipment, high frequency transformers, memory units in computers, magnetic amplifiers, power inductors, broad band pulse transformers, electromagnetic interference (EMI) suppressors, asymmetric digital subscriber line (ADSL) and splitter application, mobile communication, microwave absorbers for special applications in defence etc.

The first naturally occurring magnetic material known to man having chemical formula Fe_3O_4 was lodestone or magnetite [1]. This material has been extensively studied by number of researchers. D.U.Bois made the saturation magnetization measurements of magnetite in 1890 [2]. The magnetic properties such as saturation magnetization and Curie temperature were studied by Pierre Weiss [3]. However Hilpert [4] was the one who suggested the basic formula for ferrites. The formula was MFe_2O_4 where M is a divalent metal ion. The performance of ferrites at high frequencies was studied by Snoek [5] by maintaining the accurate oxygen content and homogeneous product.

The structural studies on ferrites taken up by some researchers [6, 7] reported spinel structure for ferrites. Barth and Posnjak [8] discovered normal and inverted spinel structures of ferrites on the basis of X-ray analysis.

The fundamental theory of ferrimagnetism was introduced by Neel [9]. He introduced the concept of magnetic sub lattices, triangular or canted arrangements of these sub-lattices by applying molecular field theory to ferrites. Naturally occurring magnetite is a 'hard' ferrite, possesses weak magnetism, which is essentially permanent. Subsequently, man-made 'hard' ferrites with superior properties were developed but producing an analogous soft magnetic material in the laboratory proved elusive.

Magnetic materials are classified into different groups on the basis of their magnetic properties and temperature dependence of these properties viz: diamagnetic, paramagnetic, ferromagnetic, antiferromagnetic and ferrimagnetic. However the last three that is ferromagnetic, antiferromagnetic and ferrimagnetic are classified on the basis of ordered arrangement of spins over space lattice. Origin of magnetism is a well known fact; the same originates from the magnetic moment exhibited by rotational motion of charged particles. An electron of charge **e** revolving in an orbit with velocity **v**, making n revolutions per second, is equivalent to current loop and behaves like a magnetic shell or tiny magnetic dipole possessing a magnetic moment **p** given by the expression

$$p = nev \quad \text{----------} \quad 1.1.1$$

In case of electron revolving around the nucleus in an atom magnetization originates from the spin motion as well as its orbital motion.

Diamagnetic Materials

In diamagnetic materials, the orbital magnetic moment and the spin magnetic moment cancel each other. Hence there is no permanent dipole moment. When such a material is placed in a non- uniform magnetic field, the orbital speeds of the electrons undergoes a change due to which a moment is developed in the direction opposite to the applied field. An electron in a magnetic field, will precess around the field with a Larmor frequency

$$\nu = eB/2m \quad \text{----------} \quad 1.1.2$$

This precession is known as Larmors precession.

Since the magnetic moments induced by the applied magnetic field always oppose the applied field i.e. there is repulsion, the diamagnetic material has a negative susceptibility which is independent of temperature.

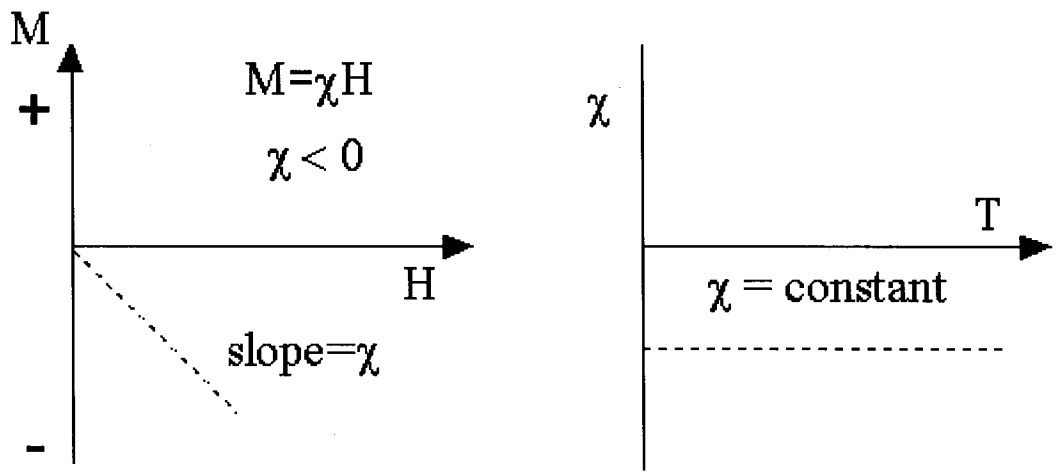

Diamagnetism

Paramagnetic Materials

The paramagnetic materials have incompletely filled outermost orbits and hence they have a permanent dipole moment. However due to thermal agitation, these moments are oriented in a random direction at room temperature. When placed in an external magnetic field, these dipoles experiences a torque and they tend to orient themselves in the direction of the applied field producing a net magnetization. Since the applied field has to overcome the thermal motion, the paramagnetic susceptibility decreases with increasing temperature. Langevin assumed that the randomization of the dipoles is due to thermal agitational energy and according to Weiss; there exist a molecular field which causes the dipoles to be parallel to the field. These substances have small positive susceptibility.

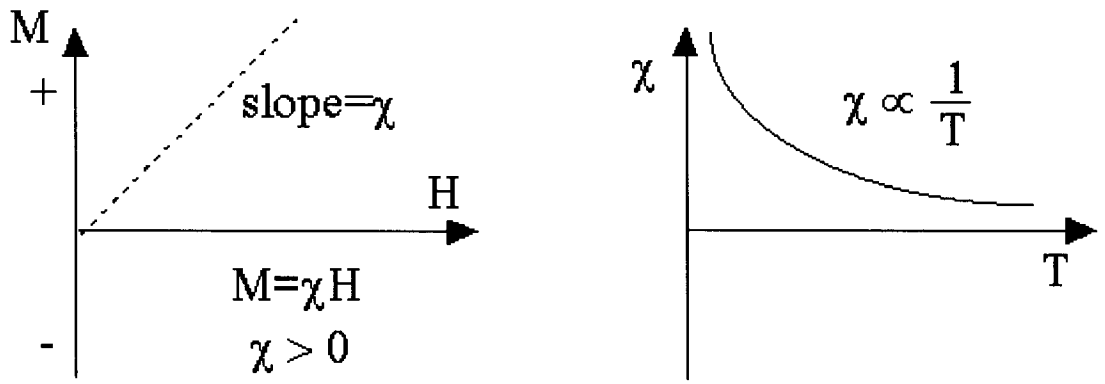

Paramagnetism

Ferromagnetic Materials

In these materials, the contribution of spin magnetic moment to the total magnetic moment is large. Neighboring atoms having magnetic moments

aligned in the same direction as illustrated in the (fig.1.1) form small regions called domains. This behavior is the result of strong exchange coupling between the atoms. This interaction arises due to coupling of spins on adjacent atoms. The exchange energy between the neighboring dipoles is positive, such that the lowest energy state is one in which all the dipoles are aligned with their magnetic moments parallel.

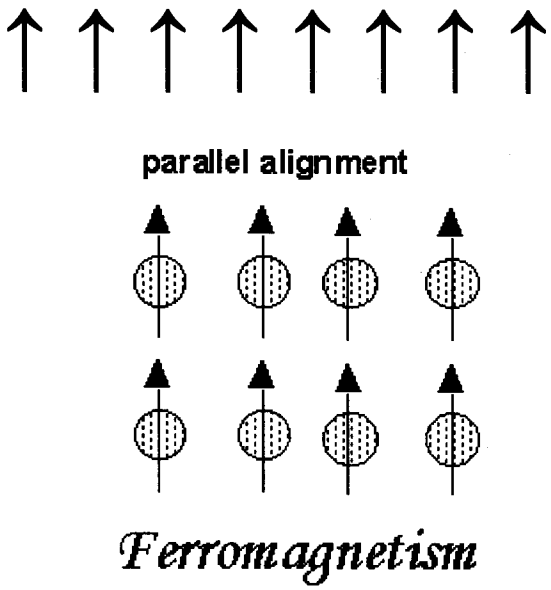

Fig.1.1

A ferromagnet has spontaneous magnetic moment even in zero applied field. The electron spins and magnetic moments are arranged in regular manner, which is supposed to occur, due to an field produced within the material that is proportional to magnetization of the sample.

Antiferromagnetic Materials

The material in which the atomic moments from two sub lattices are such that the moment on one equals in magnitude but aligned antiparallel to

that on the other. Thus the net magnetic moment is zero and the material is said to be antiferromagnetic (Fig1.2)

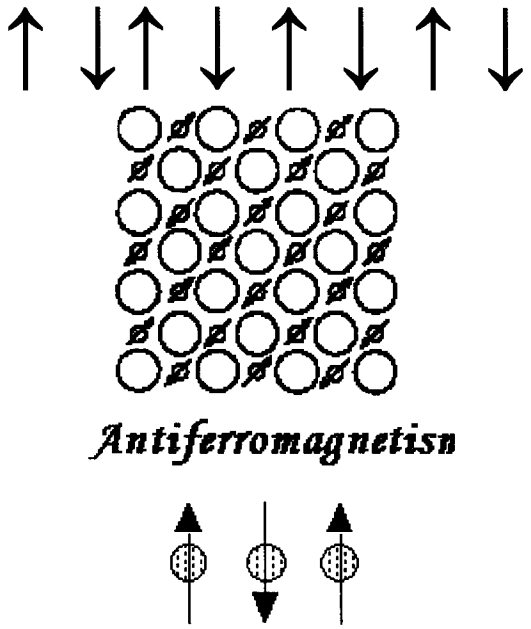

Fig.1.2

They do not produce any net magnetization at absolute zero temperature.

Ferrimagnetic Materials

Ferrimagnetism exists in those materials in which atomic moments are aligned antiparallel but magnetic moments are unequal as shown in (fig.1.3).

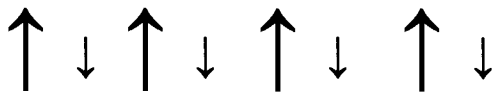

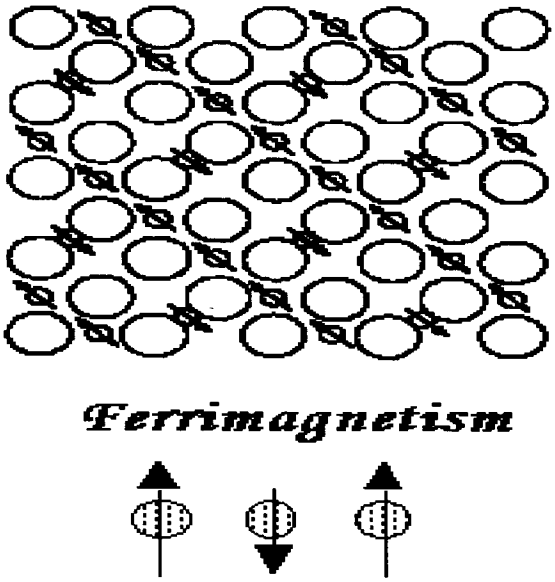

Fig.1.3

This is due to the fact that the opposing magnets have different moments or the number of atoms having one spin direction is different from that having opposite spin direction thus giving a magnetic moment.

Table 1.1: Materials classified by their magnetic properties

Class	**χ dependant on B**	**Dependant on temperature**	**Hysteresis**	**Example**
Diamagnetic	No	No	No	water
Paramagnetic	No	Yes	No	Aluminium
Ferromagnetic	Yes	Yes	Yes	Iron
Antiferromagnetic	Yes	Yes	Yes	Terbium
Ferrimagnetic	Yes	Yes	Yes	$MnZn(Fe_2O_4)_2$

Several magnetic oxides have been found to be magnetic; of these, ferrimagnetic oxides, popularly known as ferrites are of immense importance due to their special characteristics. Mixed metal oxides with iron oxides as their main components are known as mixed ferrites.

In 1952, C. L. Hogan from Bell Labs made the first non-reciprocal microwave devise at 9 GHz that was based on the Faraday rotation effect. Valuable research was carried out to improve the properties of the spinel ferrites by varying cation substitutions. These substitutions led to the modification of the magnetic properties and helped the production of magnetic devices for different frequency ranges, power requirements, and phase shift applications.

Ferrites crystallize in three different crystal types namely spinel, garnet and magnetoplumbite. The spinel and garnet have cubic structure while plumbite has hexagonal structure.

The general formula of simple spinel ferrites is $A^{II}\ Fe_2O_4$ where A^{II} is divalent metal ion.

The interesting and useful electrical and magnetic properties of spinel ferrites are governed by distribution of the ion and divalent metal ions among octahedral and tetrahedral sites of spinel lattice [10-14]. The tetrahedral and octahedral sites are conventionally called A and B sites respectively.

1.2 Scope and Organization of thesis

On going through the research articles in Proceedings of 8th international Conference on Ferrites (Kyoto Japan, 2000) one can realize the importance of Mn-Zn ferrite especially due to its fascinating properties. It finds wide applications in electronic industry. Ministry of Science and Technology and Department of Science and Technology, Government of India in its document **"Vision for R&D"** had given stress on innovative and new materials to promote research in frontier and emerging areas. The thrust areas included were high technology ceramics, smart sensors development of novel materials, advanced magnetic materials like Mn-Zn ferrite as the same formed the backbone of industrial growth. Mn-Zn ferrite is a soft magnetic material and enjoys a large spectrum of applications due to its high performance. Efforts are on to enhance the performance of this material in particular. The performance of this material is dependent on great number of factors. Some of the factors are the degree of Zn concentration in the sample, method of preparation, the grain size, sintering temperature, method and conditions at sintering etc. As per the available reports [15, 16] the most important parameter for high performance is small grain size. In Mn-Zn ferrite the grain boundaries exhibit different chemical and physical properties than the usual ferrite grains of other type. Ultra fine grain size materials have gained lot of attention and importance due to recent developments in the area of nanotechnology and development of newer methods for their synthesis as well as the fascinating properties exhibited by them. The present work is undertaken to explore a new synthetic route for preparation of high performance Mn-Zn ferrite of different compositions. Further, it is aimed at

studying the electrical and magnetic properties of the materials so obtained by using various known instrumental techniques

For this study the following work plan was executed

Step1: Synthesis of ultra fine particle $Mn_x Zn_{(1-x)}Fe_2O_4$ with

x= 0.3,0.35,0.4,0.45,0.5,0.55,0.6,0.65,0.7

Step2: Characterization of powder samples.

Step3: Grain size measurements of powder samples.

Step4: Study of Magnetic properties of powder samples.

Step5: Sintering of ultra fine grain size samples under different conditions for production of bulk material.

Step6: Study of Magnetic properties of sintered samples.

Step7: Study of Electrical properties of sintered samples.

Based on the above work plan, systematic experimental work and investigations were undertaken. The results of this study are presented in the thesis.

References

[1] M. R. Ananthraman, K. Seshan, D. K. Chakrabarty and H. V. Keer, Bull. Mater. Sci., 3(3) (1981) 275.

[2] H. E. Du Bois, Phil Mag., 29 (1890) 293.

[3] P. J. Weiss, J. Phys., 6(4) (1907) 66.

[4] S. Hilpert, Ber. Deut. Chem.Ges., 42 (1909) 2247.

[5] J. L. Snoek in ' New Development in Ferromagnetic Materials' Elsevier Press. Inc, New York. (1947).

[6] Y. Kato and T. Takei, J. Institute of Electrical Engineers, Japan, 53 (1953) 408.

[7] H. Forestier, Ann. Chemie Xe Series Tome, 9 (1928)353.

[8] T. F. Barth and E. Posnjac, Z. Krist, 82 (1952) 325.

[9] L. Neel, Ann. Phys., 3 (1948) 137.

[10] Jan Smit, Magnetic Properties of Materials, McGraw-Hill, New York , (1971), 20.

[11] J. Smit and H. P. J. Wijn, Ferrite, Philips Technical Library, Eindhoven, The Netherlands, (1959) 137.

[12] E.W. Gorter Philips, Res. Rept., 9 (1954) 302.

[13] A. Broese Van Groenev, P. F. Bongers and A. L. Stuyts, Materials Science and Engineering , 3 (1968-69) 317.

[14] E. J. W. Verwey, F. De Boer and J. H. Van Santen, J. Chem. Phys., 16 (1948) 1091.

[15] M. Drofenik, A. Znidarsic and I. Zajc J. Appl. Phys., 82 (1) (1997) 333-340.

[16] H. Inaba, T. Abe, Y. Kitano, J. Shimomura,

Solid State Chemistry, 121 (1996) 117-128.

CHAPTER II

LITERATURE SURVEY

2.1 THE IRON OXIDES

Iron oxide exists in a variety of chemical compositions and with varying magnetic properties. Materials of interest to magnetically guidable systems are iron oxides such as MFe_2O_4 (where M is divalent ion) because they display ferrimagnetism. As mentioned in previous chapter, ferrimagnetic iron oxides inherently display a lower magnetic response than ferromagnetic material such as the transition metals [1]. However, the iron oxides are also less sensitive to oxidation and therefore maintain stable magnetic responses. Ferrites are mixed metal oxides of magnetic nature in which iron is the main component.

In general, ferrites show four different types of crystal structures namely,

1] ferrospinel structure.

2] hexagonal structure.

3] garnet structure.

4] orthoferrite structure.

Ferrospinels

They have the general formula $MeFe_2O_4$, where Me is divalent metal ion or a mixture of ions having average valence of two. The unit cell is cubic. The oxygen ions forms a nearly close-packed face centered cubic structure and the metal ions are distributed over tetrahedral and octahedral holes.

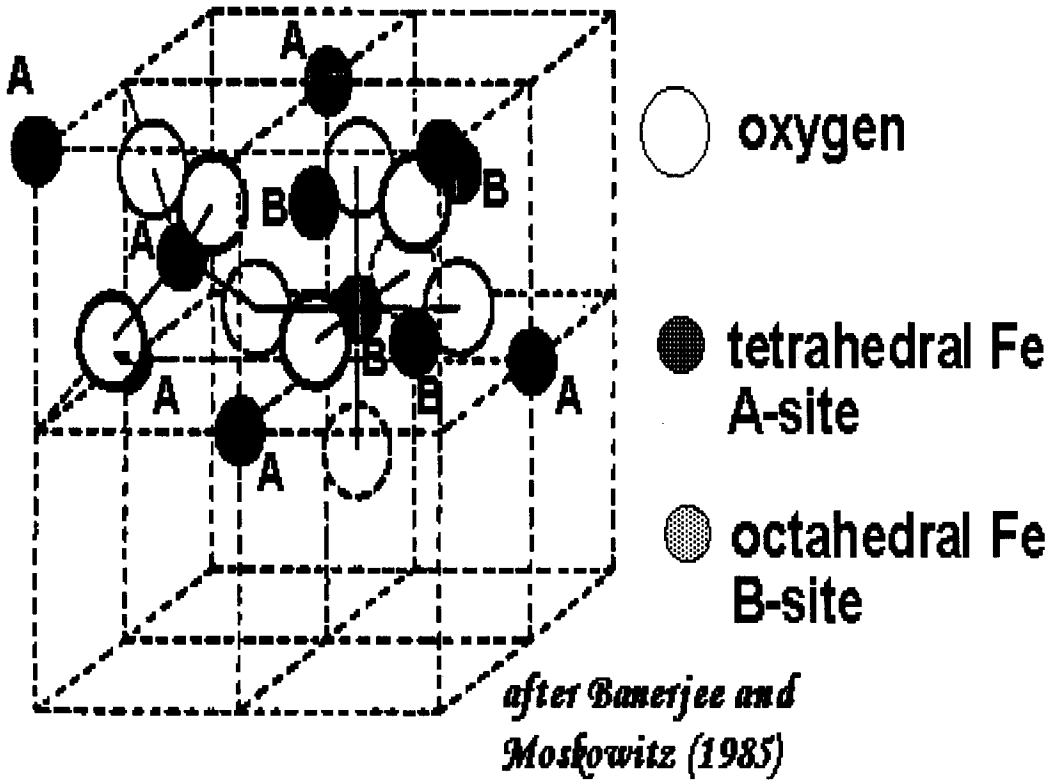

Hexagonal

They have the general formulae $MeFe_{12}O_{19}$ where Me is a divalent metal ion with large atomic radius. They crystallize in hexagonal structure e.x. Barium ferrite.

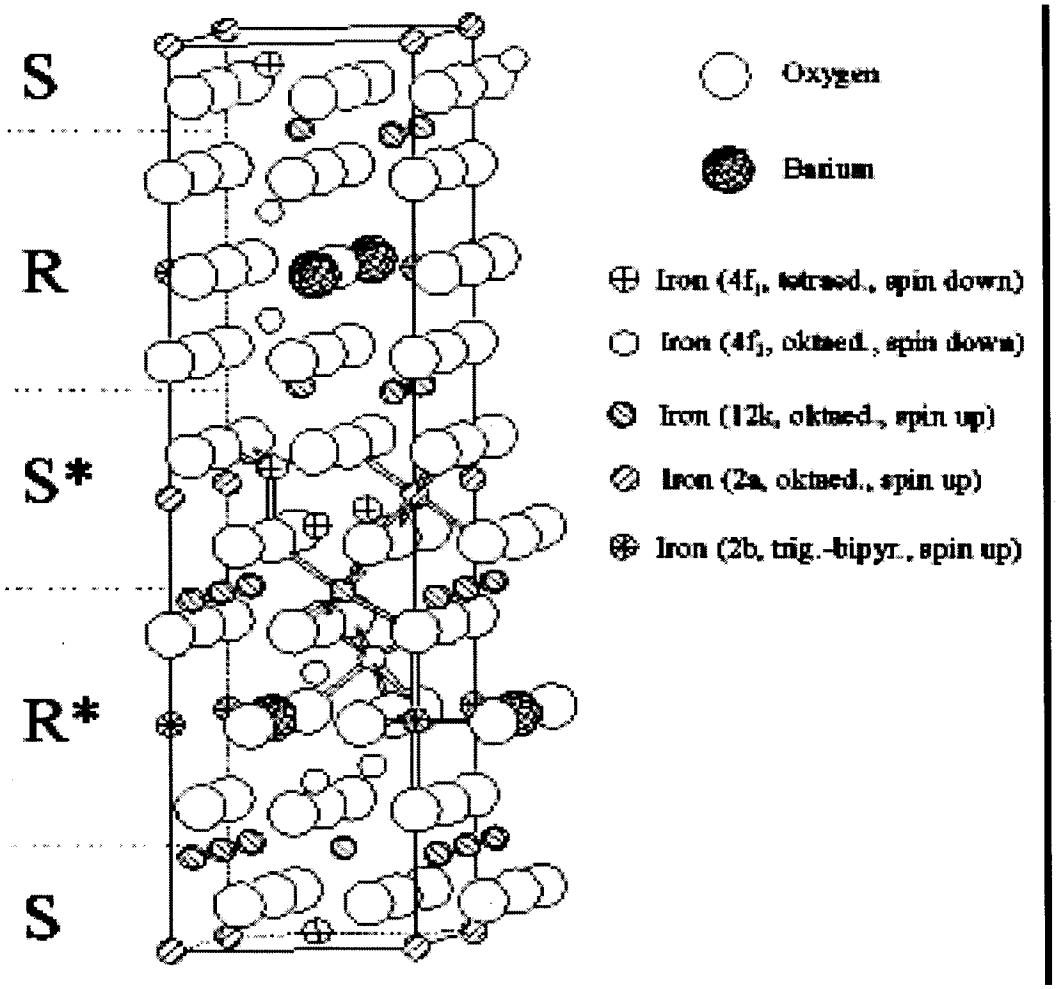

Garnet

They have the general formulae $Me_3Fe_5O_{12}$ where Me is a trivalent ion such as rare-earth. The unit cell is cubic and contains eight molecules of $Me_3Fe_5O_{12}$. Garnets are well known for their microwave applications.

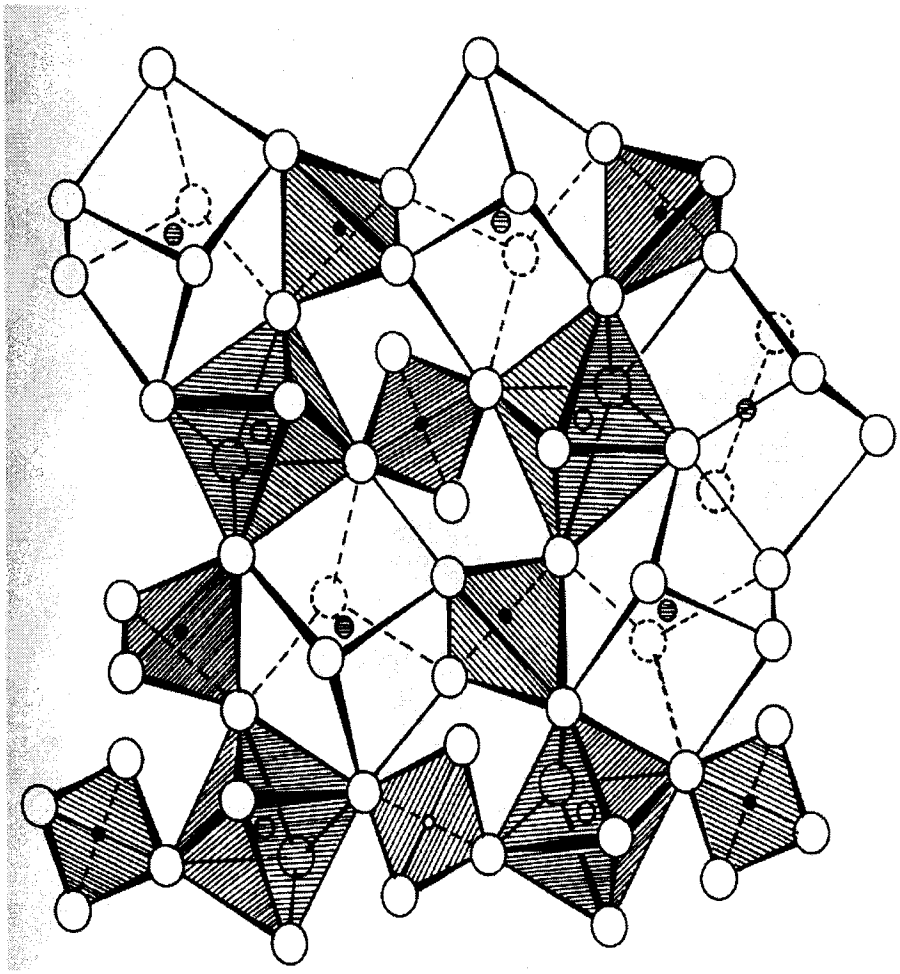

Orthoferrite

They have the general formulae $MeFeO_3$ where Me is a trivalent ion such as rare-earth. They crystallize in a distorted perovskite structure with a orthorhombic unit cell. They are used for bubble domains.

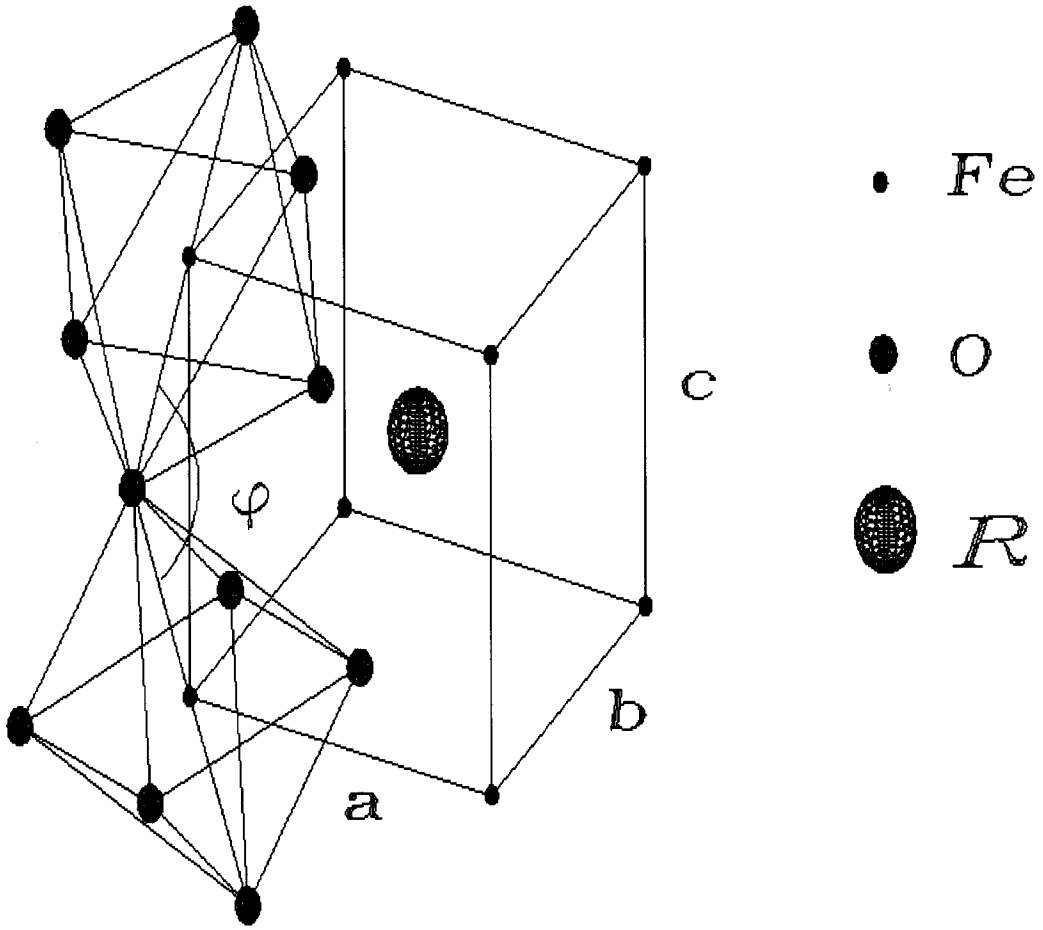

Ferrospinel structure group covers most of the technologically important oxide magnetic materials.

2.2 STRUCTURE OF SPINEL

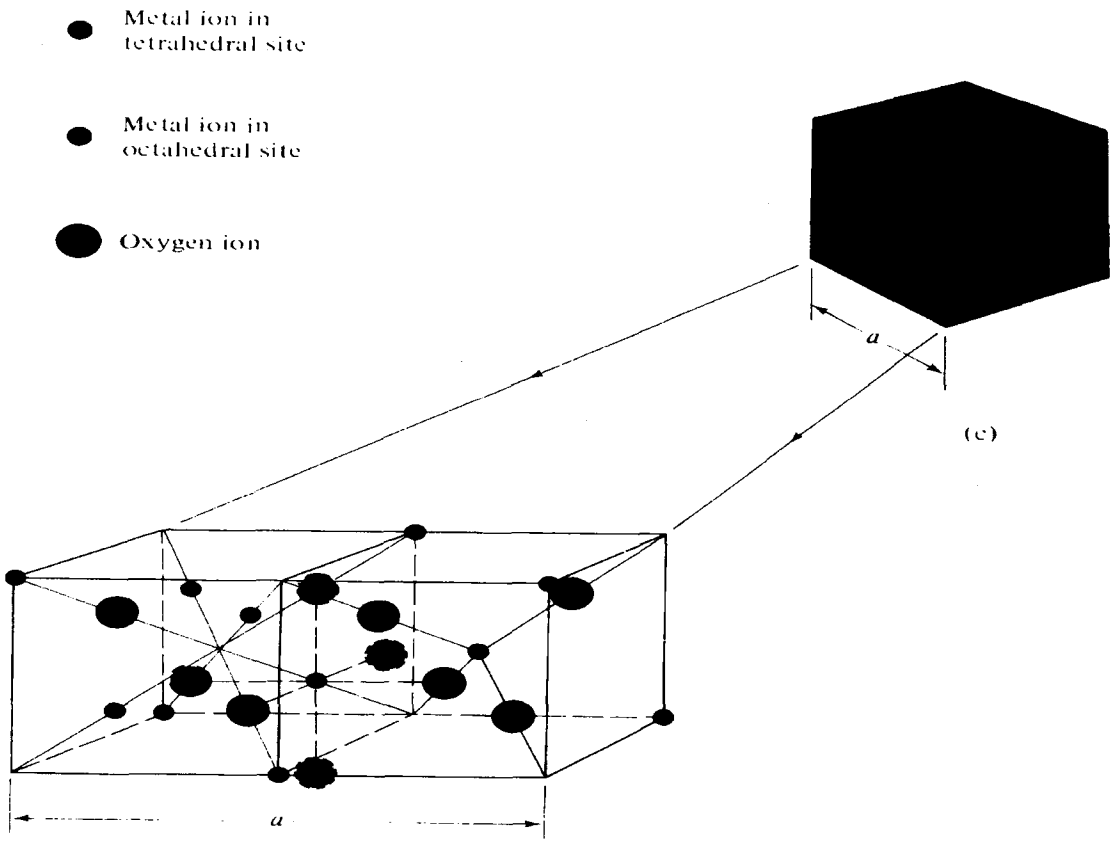

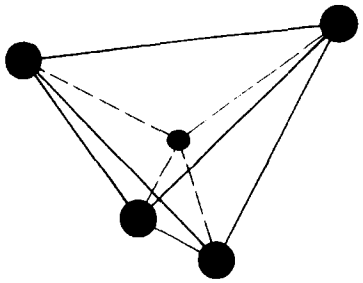

(a) Tetrahedral *A* site

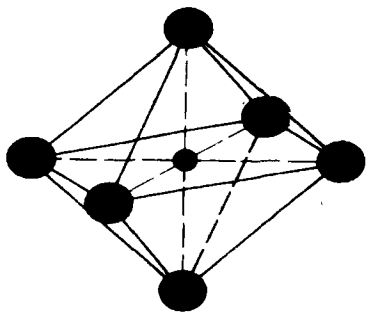

(b) Octahedral *B* site

In a unit cell eight tetrahedral and sixteen octahedral sites are occupied by metal ions designated as A and B sites. A site has tetrahedral symmetry and in a unit cell there are sixty four such vacancies, while B sites have octahedral symmetry and in a unit cell there are thirty two vacancies. Of these vacancies sixteen B sites and eight A sites are occupied by metal ions. The distribution of metal ions over two sites is governed by relative site preference, energies of cations present. This governs the intrinsic properties of ferrites.

Some divalent ions have very low octahedral preference. Therefore they enter A site of the lattice resulting in normal ferrites and some have preference for octahedral sites resulting in inverse ferrites. On the basis of cation distribution ferrites are classified into Normal ferrites, Inverse ferrites and Random or Mixed ferrites.

2.2.1 Normal Ferrites

In which all divalent metal ions occupy A sites and all the Fe^{3+} occupy B sites.

e.x. $Zn^{2+}[Fe_2^{3+}]O_4$

Zn^{2+} ions have a very low octahedral preference; therefore they enter the A-sites of the lattice, resulting in normal ferrites.

2.2.2 Inverse Ferrites

In which all divalent metal ions and half the Fe^{3+} ions occupy B sites while remaining Fe^{3+} occupy A sites.

e.x. $Fe^{3+}[Fe^{3+}Ni^{2+}]O_4$

2.2.3 Mixed Ferrites

In which all divalent metal ions and Fe^{3+} ions are uniformly distributed over the tetrahedral and octahedral sites.

Mn-Zn ferrite is a mixed spinel ferrite, which has general formulae

$A^{II}{}_x B^{II}{}_{1-x} Fe_2O_4$ where A=Mn; B=Zn

$Zn_{1-x} Fe^{3+}{}_{1-x} [Fe^{3+}{}_{1+x} Mn_x{}^{2+}] O_4$

Zn^{2+} ions occupy tetrahedral sites while Mn^{2+} ions occupy octahedral sites, whereas Fe^{3+}ions are distributed uniformly over octahedral and tetrahedral sites.

Interactions in ferrites between the ions in the two sites are A-A, A-B, and B-B type. Out of these only A-B interactions predominating, the spins of the ions, in ferrites will be oppositely magnetized sub lattices A and B with a resultant magnetic moment equal to the difference between those of Aand B ions [2].

In general the value of saturation magnetic moment for the B lattice (M_B) is greater than that of A lattice (M_A) so that the resultant saturation magnetization

$$Ms=M_B-M_A.$$

Magnetic characteristics of ferrites depend upon the concentration of magnetic and non-magnetic ions in mixed ferrites. In case of Mn-Zn ferrite, Zn^{+2} is non-magnetic ions and Mn^{+2} ion is magnetic weak ion. For small concentration of Zn^{+2} ions the saturation of mixed ferrite increases.

The behavior of the magnetization for a magnetic material can be explained on the basis of magnetic domains [3]. Ferrimagnetic grains can be (i) multidomain (MD) (ii) single domain (SD) and (iii) Super paramagnetic

(SP). In a crystallite there are regions called as domains where magnetic moments of all atoms are aligned in parallel. A large crystallite may consist of many domains resulting in multidomain state but for fine particles of few hundreds angstroms there can be only one domain in a crystallite, it is called SD state. The single domain particles at a particular temperature can have randomly oriented fluctuating domain moments; the state is termed as SP state. For multi domain grains magnetization is by displacement of the domain walls, hence coercivity is small but the magnetization of single domain results in large coercivity. In SP particles due to the thermal excitation coercively is less. Domain structure is a natural consequence of the various contributions to the energy namely (i) Exchange (ii) Anisotropy and (iii) Magnetostriction.

Nanomagnetic Mn-Zn Ferrite materials have gained a lot of importance due to the spectacular changes observed in the magnetic properties, electrical properties as well as its immense potential for wide ranging applications.

It is found that saturation magnetization, core loss, is fairly dependent on crystallite size. The most interesting characteristic is the behavior of mixed ferrites with different nonmagnetic ion concentration.

Zn^{+2} is non magnetic.

Mn^{+2} is magnetic ion.

For small concentration of Zn^{+2} ion, the saturation magnetization of mixed ferrites increases. This can be explained on the basis of Neel's theory of ferrimagnetism [4].

The saturation magnetization (Ms) in spinel ferrites is expressed as

$$Ms=|M_B-M_A|$$

The Zn^{+2} ions preferably occupy A sites and hence the value of M_A decreases therefore the value of M_S which is the difference between M_B which is unaffected by small amounts of Zn^{+2} substitution and M_A increases. This type of increase in saturation magnetization with small additions of nonmagnetic ions has been observed with substitution of non magnetic ions like Zn^{+2}.

Since the saturation magnetization is high, the permeability is high. The maximum permeability can also be obtained by bringing anisotropy const. K as close to zero as possible. This is achieved by bringing down the curie temperature by formation of solid solutions of Mn ferrite and Zn ferrite in appropriate ratio [4].

The performance of ferrites is greatly influenced by its synthesis techniques. It is well known that nano-particles have physical dimensions in the range of few nanometers to a few hundred nanometers.

Nanoparticles are unique as important changes occur in the electronic band structure. The size dependent properties of material are very interesting not only to fabricate technologically interesting devices but also to understand how starting from atoms, molecules ensemble or clusters evolve ending up into solid and how the structure bonding , electronic structure and other properties change during evolution. Magnetization in nano particles is considerably different from that of crystalline/ polycrystalline materials as they are characterized by a high value of surface to volume ratio with a large fraction of atoms residing at grains boundaries. Magnetic materials posses some type of anisotropy which affects their magnetic behavior.

In case of nano-structured materials the anisotropy, which are of significant importance, are magneto crystalline and shape anisotropy.

For high frequency applications it is essential to obtain fine-grained micro structure and low porosity materials [5]. All these properties depend on the preparative conditions so the processing has to be perfectly understood to have an optimum stoichiometry of ferrites which may otherwise change during cooling process.

The most common method of preparations of ferrites is the conventional ceramic method. In this case the resultant products are not necessarily stoichiometric and homogeneous on microscopic scale and do not always results in reproducible products. The non-stoichiometry is due to extensive grinding and high heating temperature involved in preparation process and also due to possibility of presence of un-reacted phases in the finished product. This also results in loss of fine particle size.

The wet chemical method of preparation overcomes the drawbacks of conventional ceramic methods. The stringent demands on the quality of high performance ferrites especially for applications requiring low loss at high frequencies have created the need for a more appropriate method for preparing compositionally and structurally perfect ferrites exhibiting low magnetic and electrical losses.

There are different wet chemical methods such as citrate precursor, sulphite hydrazinate, oxalate hydrazinate etc.

Precursor methods are simple, inexpensive, do not require elaborate experimental setup and is less time consuming. The ferrites prepared by this

method are found to exhibit better properties then those prepared by ceramic method [6].

In the present work Mn-Zn ferrites with different Zn concentration were prepared by nitrilotriacetate precursor method employing two different types of decomposition methods. This method is innovative, newly evolved and found to give good quality fine particles (nano size) ferrites [7]. The samples thus prepared were characterized by X-ray diffraction, infrared analysis and chemical analysis.

2.3 THEORETICAL UNDERSTANDING

Magnetic characteristics of ferrites depend upon the concentration of magnetic and non-magnetic ions in mixed ferrites [8].

The cation distribution in a spinel is based on the factors such as [i] electrostatic energy due to repulsion and attraction between the anions and cations [ii] anion polarization energy [iii] electronic configuration and crystal field stabilization energy [iv]ordering energy between different ions on the same sublattice resulting in gain of electrostatic energy and [v] magnetic ordering energy.

The site preference for individual cations is generally expressed in terms of particular site stabilization energy. In an ionic crystal, under the influence of the electrostatic field of the anions, the degeneracy of the d-electrons in the transition metal ions is lifted, resulting into crystal field splitting of the d- states and is associated with the stabilization energy, designated as crystal field stabilization energy (CFSE).

Maclure [9], Dunitz and Orgel [10] calculated theoretically the values of CFSE for various ions. These values explained the site preference by the cations in the spinel to a good approximation. Miller [11] extended CFSE calculations incorporating Madelung constant, as well as, short range energy terms such as, Coulomb and valence terms. Site preference energies have been calculated which can predict the ionic distribution in the spinels involving non transitional and transitional metal ions.

In case of Mn-Zn ferrites Zn^{2+} is the non-magnetic ion and Mn^{+2} is the magnetic ion. For small concentration of Zn^{2+} ion saturation magnetization of the mixed ferrites is found to increase. This phenomenon is explained on the basis of Neel's theory of ferrimagnetism. The saturation magnetization (Ms) in spinel ferrites can be expressed as

$$Ms=|M_B - M_A|$$

Zn^{2+} ions preferably occupy A sites and hence the value of M_A decreases. It is observed that saturation magnetization increases with small additions of non-magnetic ions. At higher concentration deviations occur due to weakening of A-B interaction and consequent stronger B-B interaction. But with the addition of non-magnetic ions the Curie temperature is decreased as the reduce value of M_A weakens A-B interaction.

Therefore the suitable variation of composition in the mixed ferrites brings about appreciable changes in magnetization and Curie temperature. The factors responsible for these changes are

(i) The magnitude of the sub-lattice magnetization at 0^oK

(ii) The ratio of magnitudes of exchanged interaction between sub-lattices. It is found that both M_A and M_B decrease with temperature. Hence the resultant Ms also decreases.

The dependence of M_A and M_B on temperatures is usually complex. This is because A site ions are situated in strong internal field provided by the B site ions find themselves in a weak field provided by A site ions. The change of temperature causes different changes in the individual magnetization.

The magnetization due to A lattice is not much affected by temperature and decreases slowly and rocks to zero sharply at a curie point where as B lattice magnetization falls steeply at a low temperature and approaches zero gradually. If a decrease in M_B with temperature is higher than that of M_A the resultant magnetization curve will pass through minimum. Such a magnetization curve is known as n type. When M_B is resistant towards increase of temperature, it will result into a curve with a maximum. Such a magnetization curve is known as p type.

The dependence of Magnetization on the direction of magnetization is known as magnetic anisotropy. The factors that contribute to magnetic anisotropy are energy of dipolar interaction and nature of magnetic ions. Energy of dipolar interaction between two magnetic dipoles and is dependent on the arrangement of magnetic spins in the lattice. The spin orbit interaction contributes to the anisotropy. The orbital angular momentum of the ions in the crystal lattice can differ appreciably from the value found when the ions are not incorporated in the crystal. Due to the crystal field the electronic states of the ions undergo as change.

Ions like Mn^{+2} have sevenfold degenerate 4f- state of the ground level as free ions and when they are in an octahedral crystal field , the ground state is a singlet and the orbital angular momentum of these ions is zero.

Some ions like Fe^{+2} in an octahedral crystal field possess a non-zero value for orbital angular momentum and hence interactions are possible between spin and angular momentum. As a result of these interactions spin aligns themselves in a direction perpendicular to the plane of the orbit, which is fixed with respect to crystal axis. Hence magnetization along one of the crystal axis is preferred. For cubic material the anisotropy energy can be expressed in terms of anisotropy constants K_1 and K_2, which are dependent on temperature, and material use. These constants determine the direction where E_A is minimum. Anisotropy contributes to magnetic susceptibility, permeability and hysteresis phenomenon. For most of ions like Mn^{2+} and Fe^{3+} have moderate value of anisotropy energy as the orbital moment is quenched and spin orbit interaction does not make any contribution to the anisotropy. An uniaxial anisotropy can be brought about by subjecting ferrites to an annealing treatment in a magnetic field. The magnitude of uniaxial anisotropy depends upon the duration of magnetic annealing and on the temperature at which it is carried out. The electrical conductivity of spinel ferrites is known to be low as compared to other magnetic materials. This factor is responsible for the wide use of ferrites at microwave frequencies. Spinel ferrites in general are semiconductors with their conductivity values varying between 10^{2} and $10^{-11} ohm^{-1} cm^{-1}$[12,13].

The conduction mechanism in ferrites is quite different from that in semiconductors [14]. In ferrites the temperature dependence of mobility

affects the conductivity and carrier concentration is almost unaffected by temperature variation. Electrical conductivity is given by

$$\rho = \rho_0 \exp [-E_0 / kT]$$

The charge carries in ferrites are localized at the magnetic atoms. In ferrites the cations are surrounded by closed pack oxygen anions and as a first approximation can well be treated as isolated from each other. This will be little direct overlap of the anion charge clouds or orbitals. The electron associated with particular ions will largely remain isolated and hence a localized electron model is more appropriate in case of ferrites rather than the collective electron (band) model. This accounts for basically insulating nature of this material. The factors that differentiate the electrical behaviour of ferrites from that of semiconductors led to hopping electron model [15, 16]. Many models have been suggested to account for electrical properties.

(i) Hopping model is based on the localized levels for electrons

(ii) Band Polaron model is based on electron transition between localized cells.

(iii) Small Polaron model has been introduced to explain electrical properties on the basis on thermally activated motion of electrons.

2.4 PROPERTIES OF FERRITES

The properties of ferrites are classified into two categories viz intrinsic and extrinsic.

Saturation magnetization, magnetostriction, anisotropy, permeability and Curie temperature are intrinsic properties whereas hysteresis, resistivity,

dielectric constant etc. are extrinsic properties. The extrinsic properties in general are structure sensitive properties.

2.4.1 Magnetic Properties

Magnetic properties are the most fundamental properties of any ferrite. The magnetic properties include saturation magnetization, retentivity, coercivity, permeability, susceptibility and Curie temperature.

2.4.1.1 Saturation Magnetization

The saturation magnetization is the maximum induced magnetic moment that can be obtained in a magnetic field (H_{sat}); beyond this field no further increase in magnetization occurs. Saturation magnetization is one of the intrinsic properties of ferrite and governed by the chemical composition, cation distribution and thermo-physical history. The normal spinels are paramagnetic at room temperature whereas the inverse spinels are magnetic at room temperature.

The Fe^{3+} ions on A-sites are coupled with their spins antiparallel to those of Fe^{3+} ions on B-sites. Therefore the net magnetic moment is only due to divalent M^{2+} metallic ions.

The saturation magnetization of Mn-Zn ferrite is known to depend on method of preparation and sintering temperature of the material.

2.4.1.2 Hysteresis

The lagging of magnetic induction to the magnetizing field is referred to as magnetic hysteresis. If an alternating magnetic field is applied to the material, its magnetization will trace out a loop called a hysteresis loop. The lack of retraceability of the magnetization curve is the property called hysteresis and it is related to the existence of magnetic domains in the material. Once the magnetic domains are reoriented, it takes some energy to turn them back again Hysteresis study of ferrites helps us to find out valuable information about retentivity, Coercivity, saturation magnetization, permeability etc. Ferrites with low coercive force are called 'soft ferrites' and with high coercive force are called called 'hard ferrites'.

2.4.1.3 Permeability

When a magnetic field is applied to a soft magnetic material, the resulting flux density is composed of that of free space plus the contribution of the allied domains.

$B= \mu_0 (H+J)$ or $B= \mu_0 (H+M)$ where $\mu_0 = 4\pi.x10^{-7}$ H/m, J is the magnetic polarization and M is the magnetization.

The initial permeability is measured in closed magnetic circuit (ring core) using very low field strength.

$$\mu_i = 1/\mu_0 \ (\Delta B/\Delta H)$$

Initial permeability is dependent on temperature and frequency.

2.4.1.4 A.C. Susceptibility

Magnetic susceptibility of a material is given by

$$\chi = M/H \text{ or } \chi = dM/dH$$

where M is the intensity of magnetization and H is the applied field. The incremental susceptibility in a.c. field can be expressed as

$$\chi_{inc} = M/H$$

The magnetization changes are reversible and the ratio M/H is defined as $\chi_{inc.}$ The domain state of spinel ferrite is studied by using ac susceptibility measurements.

AC susceptibility measurement explores the existence of multidomain (MD), single domain (SD) and super paramagnetic (SP) particles in the material. The variations of ac susceptibility with temperature have been reported by many workers [17, 18, 19]. These curves give the information about the Curie temperature and type of domain structure.

2.4.2 Electrical Properties

D.C. and A.C. electrical properties of spinel ferrites have gained a commercial importance. D.C. electrical property includes resistivity measurements and A.C. electrical property includes dielectric constant and loss measurements.

2.4.2.1 Resistivity

Spinel ferrites in general are semiconductors with their conductivity values varies between10^{2} to10^{-11} ohm $^{-1}$ cm^{-1}. The conductivity is due to the presence of Fe $^{2+}$ and Me $^{3+}$ ions. The presence of Fe $^{2+}$ results in n-type behavior and of Me $^{3+}$ in p-type behavior. The conductivity arises due to the mobility of the extra electron (from Fe $^{2+}$) or the positive hole (Me $^{3+}$) through the crystal lattice.

The resistivity of ferrites decreases with increase in temperature according to relation

$$\rho = \rho_0 \exp^{-\Delta E/RT}$$

Where E is the activation energy, K is the Boltzmann constant and T is the absolute temperature. The factors responsible for resistivity are the chemical inhomogeneity caused during preparation, the porosity, the grain size, sintering conditions etc.

2.4.2.2 Dielectric Behavior

The ac electrical properties of ferrites are of immense importance as the field of solid-state electronics continues to expand rapidly. Ferrites shows high dielectric constant and dispersion of dielectric constant in the frequency range from 50Hz to 1GHz. A dielectric material when subjected to an alternating electric field, the positive and negative charges within the material gets displaced with respect to on another and the system aquires an electric dipole moment. The dipole moment per unit volume is called polarization. The dielectric properties of ferrites are dependent upon several factors including the method of preparation, chemical composition, grain size and sintering

temperature. Koops gave a phenomenological theory of dispersion in the dielectric constant [20].

Nanoparticles are considered to have a size range from 1 to 100 nm. Particles within this size range usually have hybrid properties different from those of the bulk solid or the molecular/atomic species. The unique properties of nanoscale particles can be attributed to two basic phenomena. The first is that the number of atoms at the surface and/or interface in these materials is comparable to that of atoms located in the crystal lattice. Therefore the chemical and physical properties, which are normally determined by the structure of the bulk lattice, become increasingly dependent upon the atoms at the surface and interface. The high numbers of atoms on the surfaces of nanoparticles form a layer of "damaged" lattice with a higher energy state; therefore these particles are highly unstable and more reactive. The second phenomenon is the "quantum-size effect" or "quantum confinement effect." When particles approach the nanometer-size range, their electronic properties get significantly modified as a result of the absence of a few atoms in the lattice and the regional relaxation of the lattice structure [21].

The small size and rich surface/interface structure of magnetic nanomaterials can lead to properties quite different from those of the bulk. Studies on magnetic nanomaterials will not only provide information about the structure-property relations of magnetic nanomaterials but also help generating new ideas and technologies for the fabrication and application of these materials.

The emerging field of nanoscience and nanotechnology is leading to a disruptive technological revolution. Nanotechnology can be broadly defined as the ability to manipulate the structure of material at the nano length scale to produce engineered products with superior performance characteristics. By even the most conservative estimation, this field is expected to user in the new industrial age. Practically all sectors of the economy is expected to be profoundly influenced by nanotechnology in the very near future.

2.5 APPLICATIONS OF FERRITES

As nanomaterials possess unique, beneficial chemical, physical, and mechanical properties, they can be used for a wide variety of applications. Current research in this area of magnetic nanoparticles is being carried out by focusing on their applications were their unique properties will allow for significant advances in scientific technology. In the electronics field researchers are investigating the design of superstructures comprised of magnetic ordered arrays to enhance sensitivity in magnetic sensors [22].

Mn-Zn Ferrites with grain size in nanometer range posses interesting micro magnetic and electrical properties such as, magneto optic, magneto caloric effect, colossal and giant magnetic resistance etc. Their application in different devices like motors, transformers, sensors, inductors, insulators, and in ferrofluids [23] is on the rise. These materials are useful in a variety of applications in the electronic industry due to their high permeability, high saturation magnetization, high resistivity and low loss as these formed the key

impediments in downsizing of transformer cores deflection yokes, power inductors, antenna rods etc. in the world of miniaturization.

- Miniature drum for power inductors

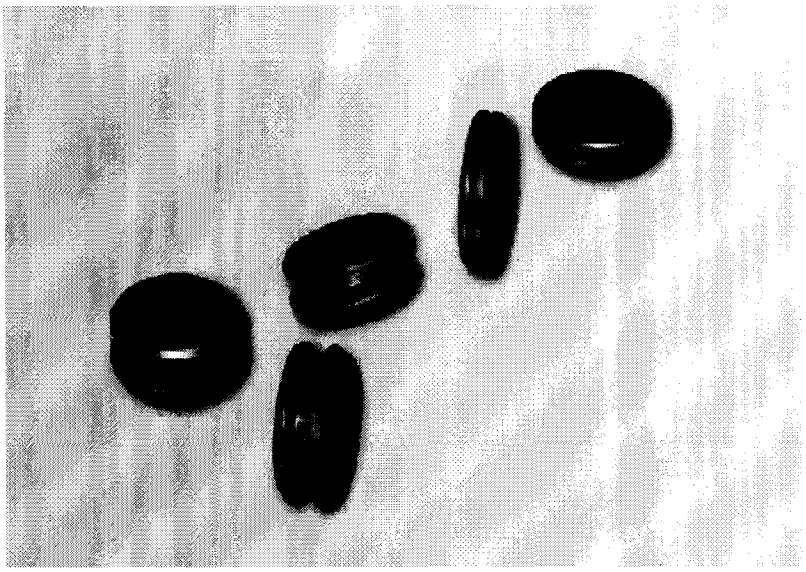

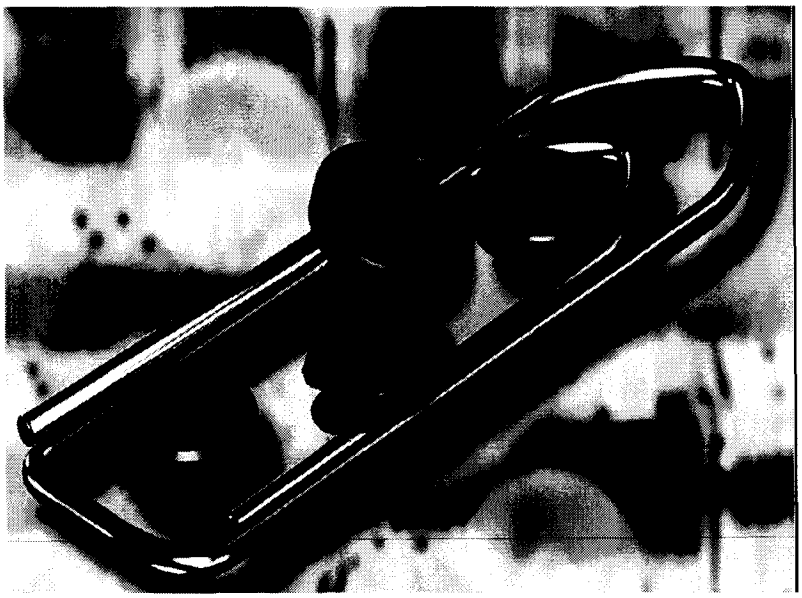

- Ferrite cores for quick charging systems

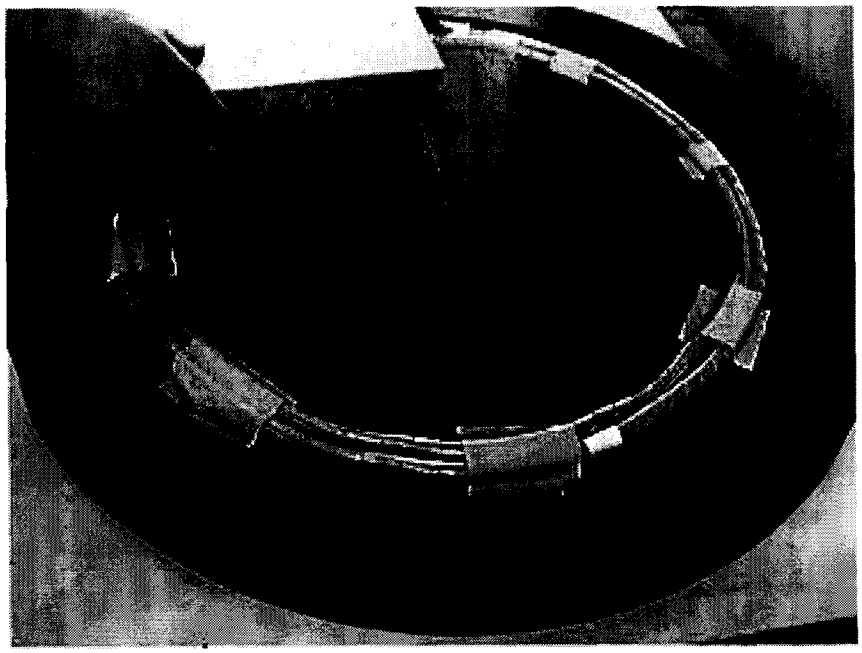

- Ferrites for power application

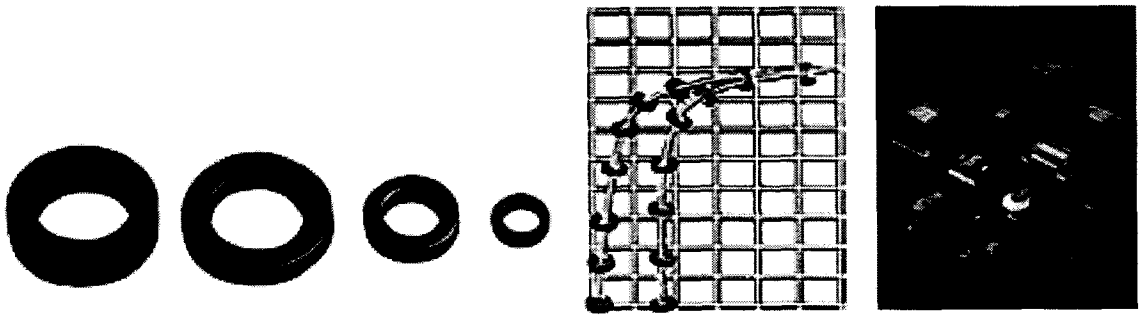

- Common mode chokes

Advantages of nanocrystalline material is compact size and covering a wide range of frequency, allowing operating temperatures up to 120°C. Applications are high power transformers for SMPS.

References

[1] R. M. Cornell, U. Schertmann, The Iron Oxides: Structure, Properties, Reactions, Occurrence and Uses, VCH Publishers, Weinheim, **1996**.

[2] E.W.Gorter, Philips Res. Rept. 9 (1954) 321.

[3] P.Weiss, Journal of Physics 6 (1907) 667.

[4] L. Neel, Ann. Phys. 3 (1948) 137.

[5] A.verma, T. C. Goel, R.G. Mendiratta, Material Science and technology 16 (2000) 712.

[6] K.C. Patil, S. Sudar Manoharan and D.Gajapathi, 'Handbook of Ceramics and Composites' (eds. Nicholas P.Cheremisinoff, Marcel Dekker, INC, New York) vol 1 p.469.

[7] A.A. Samokhvalov and A.G. Rustamov, Sov.Phys.Solid State, 7 (1965) 961.

[8] K. J. Standley, 'Oxide Magnetic Materials' (Oxford: Claredon Press, 1972).

[9] D. S. Maclure, J. Phys. Chem. Solids, 3 (1957) 311.

[10] J. D.Dunitz and L.E. Orgel, J. Phys. Chem. Solids, 3 (1957) 20.

[11] A. Miller, J. Appl. Phys. 30 (4) (1959) 245.

[12] J. Smit and H. P. J. Wijn, Ferrite, Philips Technical Library, Eindhoven, The Netherlands, (1959) 137.

[13] A. Broese van Groenev, P. F. Bongers and A. L. Stuyts, Materials Science and Engineering, 3 (1968-69) 317.

[14] L.R. Maxwell and S. J. Pickart, Phys. Rev. 96 (1954) 1501.

[15] E .J. W. Verwey, P.W. Haayman and F.C. Romeijin, J.Chem.Phys. 15 (1947) 181.

[16] A. A. Samokhvalov and A. G. Rustamov, Sov. Phys. Solid State, 6, (1964), 749.

[17] C. Radhakrishnamurthy, J. goel Soc.India 26 (9) (1985) 640.

[18] R.V. Upadhyay, G.J. Baldha and R.G. Kulkarni, Mater.Res.Bull. 21 (1986) 1015.

[19] G. J. Baldha and R.G. kulkarni, Solid Stat. Commun. 53 (1985) 11.

[20] C. G. Koops, Phys. rev., 83 (1951) 121.

[21] William R. Moser, Josef Find, Sean C. Emerson and Ivo M. Krausz Advances in Chemical Engineering Vol.27

[22] D. A. Thompson, J. S. Best, IBM Journal of Research and Development, 44 (2000) 311.

[23] P. K. Gallagher, E. M.Gyorgy, D.W. Johnson, W. David, M. Robbins and E. M.Vogel, J. Amer. Ceram. Soc. 66(7) (1983) C110.

Chapter III

PREPARATION OF MATERIALS

3.1 INTRODUCTION

Magnetism in nano particles is considerably different when compared to magnetism in bulk crystalline and polycrystalline materials since the nanoparticles are characterized by high value of surface to volume ratio with large fractions of atoms residing at grain boundaries. The properties of ferrites depend on the preparative conditions. The performance of ferrite material is greatly influenced by its history, especially with respect to its method of preparation. In general, research in solid state chemistry and physics of ferrites is focussed on the development of newer routes of synthesis, understanding the structures and studying their properties.

At present study in the field of nanoscience includes (a) nanoparticles, (b) nanocrystalline materials, and (c) nanodevices [1]. Here again, the most important aspect is still the development of new strategies for the synthesis of nanomaterials, particularly soft chemical routes.

Considerable chemical ingenuity is required in the synthesis of solid materials. Tailor-making materials of the desired structure and properties are one of the main goals of materials chemistry, but it is not always possible to do so by conventional methods. Rational approach to materials synthesis generally gives thermodynamically stable materials, but may miss new and novel metastable ones. This work is mainly involved in chemical approaches to the synthesis of oxides. Chemical methods of synthesis play a crucial role in designing and discovering new and novel materials and in providing less

cumbersome methods for preparing known materials. Chemical methods also enable the synthesis of metastable materials, which are otherwise difficult to prepare. In this chapter, the various methods of synthesizing oxide materials are briefly summarized with emphasis on soft-chemical routes.

3.2 PREPARATION OF MAGNETIC MATERIALS:

A variety of synthesis routes have been reported for the preparation of ferrites such as ceramic, hydrothermal [2,3], co-precipitation [4,5], solgel [6], precursor [7], vapour – phase, chimie- douce.

The new synthesis processes like plasma synthesis, reverse micelle synthesis, water–CTAB–hexanol microemulsions etc. have made possible preparation of nanostructured materials in a wide variety of compositions.

3.2.1 Ceramic Method

The ceramic method involves high temperature, which affects the fineness of the material thus produced [8]. The most common method of preparing inorganic solid materials is by the reaction of the component materials in the solid state at high temperatures [9]. In preparing oxides, one generally pelletizes the reacting materials and repeats the grinding, pelletizing and heating operations several times. Yet, the completion of the reaction or the phasic purity of the product is not assured. The ceramic method suffers from several disadvantages.

3.2.2 Hydrothermal

One of the techniques in synthesis of materials is hydrothermal oxidation. The method is based on the fact that many oxides are soluble in an alkali solution. The method has been most successfully applied to prepare ferrites. The advantage in the hydrothermal method is that it permits the

recrystallization of the powder and monitoring of grain size and shapes. However this method is time consuming.

3.2.3 Coprecipitation

In coprecipitation, the required metal cations taken as soluble salts (e.g. nitrates) are coprecipitated from a common medium, usually as hydroxides, car-bonates, oxalates or citrates. In actual practice, one takes oxides or carbonates of the relevant metals, digests them with an acid and then the precipitating reagent is added to the solution. The precipitate obtained after drying is heated to the required temperature in appropriate atmosphere to produce the final product. The decomposition temperatures of the precipitates are generally lower than the temperatures employed in the ceramic method.

Co-precipitation is a very simple method for the synthesis of powders. There are two co-precipitation routes possible for the preparation of Mn-Zn ferrites:

(i) The calcination route. The co-precipitation of hydroxides of Mn^{2+} , Zn^{2+} and Fe (usually Fe^{3+}) in the first stage is followed by calcination of the hydroxide precursors in the second stage:

$$\tfrac{1}{2}\, Mn^{2+} + \tfrac{1}{2}\, Zn^{2+} + 2Fe^{3+} + 8OH \rightarrow \tfrac{1}{2}\, Mn(OH)_2 + \tfrac{1}{2}\, Zn(OH)_2 + 2Fe(OH)_3$$

$$\xrightarrow{600\ ^{\circ}C} Mn_{0.5}\, Zn_{0.5}\, Fe_2O_4 + 4H_2O$$

(ii) The oxidation of Fe(II) hydroxide. The co-precipitation of hydroxides of Mn^{2+}, Zn^{2+} and Fe^{2+} in the first stage is followed by the oxidation of Fe(II) hydroxide in the second stage, which directly results (in situ) in the formation of the spinel ferrite according to Shikorr's reaction [10]

$$\tfrac{1}{2}\, Mn^{2+} + \tfrac{1}{2}\, Zn^{2+} + 2Fe^{2+} + 6OH^{-} + \tfrac{1}{2}\, O_2 \rightarrow Mn_{0.5}\, Zn_{0.5}\, Fe_2O_4 + 3H_2O.$$

One of the drawbacks of the co-precipitation method is the difficulty of controlling the particle size and morphology.

The problem of controlling the particle size and morphology during the synthesis is overcome by using a microemulsion method, which involves co-precipitation in water-in-oil microemulsions [11].

3.2.4 Sol-Gel

The Sol-gel method has provided a very important means of preparing inorganic oxides. It is a wet chemical method and a multistep process involving both chemical and physical processes such as hydrolysis, polymerization, drying and densification. In the sol-gel process, synthesis of inorganic oxides is achieved from inorganic or organometallic precursors. The important features of this method are better homogeneity compared to the traditional ceramic method, high purity, lower processing temperature, more uniform phase distribution in multicomponent systems, better size and morphological control, the possibility of preparing new crystalline and non crystalline materials.

3.2.5 Precursor

A precursor method involves preparation of an easily decomposible compound of metals and mixed metals, which yield the desired oxides on heating. One can obtain homogeneous, fine particle, high purity oxide materials from precursors. The preparation of ferrites from solutions of water soluble salts of the corresponding metals fall under wet chemical method category. These methods are reported to yield ferrite powders having

molecular level homogeneity, smaller grain size, low porosity and larger surface area [12].

In the last years, special focus has been placed on obtaining ferrite as a particulate environment through unconventional methods, especially chemical methods [13-15]. There are many methods that can be used to obtain the systems consisting of nano particles [16–21], but their application on a large scale is limited by their cost and the high purity of the starting material.

3.2.6 Vapour Phase

This is the method of chemical transport via the vapour phase. This method is used for the synthesis of new compounds, for the growth of single crystals or for the purification of a compound. In this method the gas phase is used as a transporting agent and has influence on reaction rates. Gases react much more quickly than solids because mobilities are increased. In addition, the gaseous phase is often important in normal solid state reactions under isothermal conditions, where mt may act as a rapid means of transporting matter from one grystal to another [22].

3.2.7 Chimie- Douce

The precursor method have the advantage that reaction takes place at much lower temperatures than when using normal solid state reaction procedures. Another use of precursor methods is in the wynthesis of new, metastable phases which cannot be prepared by other routes. Although these phases are thermodynamically metastable they are often kinetically stable to quite high temperatures. There is a close structural relationship between the precursor phase and final troduct. Often new phases therefore have unusual

structures and interesting properties. This method is termed as chimie-douce [22].

Crystallite sizes of the powder specimen can be obtained on calcinations at various temperatures. It is observed that size increases with calcination temperature. As the calcinations temperature affects the particle size, all parameters like Curie temperature, permeability, saturation magnetization dielectric properties, resistivity etc. are also affected the same. The ferrites have gained importance due to their microstructures. The magnetic properties of Mn-Zn ferrites depend on the microstructures. The microstructure of Mn-Zn ferrites is greatly influenced by sintering conditions as well, thus it is extremely important to control the same.

Chemical methods of synthesis play a crucial role in designing and discovering new and novel materials and in providing less cumbersome methods for preparing known materials. Chemical methods also enable the synthesis of metastable materials, which are otherwise difficult to prepare.

3.2.8 Plasma Synthesis

Plasma synthesis has shown to be a viable route to producing Mn-Zn ferrite nanoparticles [23]. The method uses metallic precursor's ball milled into fine powder using high energy ball mill and high energy rf induction thermal plasma system. The fine precursor powder is ejected through the plasma jet stream by Argon as carrier gas. Compressed air is also introduced in the reactor as an oxidizer [24-27]. This method of preparation is highly complex and involves complex systems.

3.2.9 Reverse Micelle Technique

Manganese–zinc ferrite nanoparticles can be synthesized using a reverse micelle technique [28, 29]. The basis for the technique is the use of a surfactant to stabilize varying aqueous droplet sizes in hydrocarbon medium. Metal salt precursors are contained in the aqueous portion and are transformed by a reactant from the hydrocarbon phase. Both the structure of the surfactant and the steric size are able to produce metals having a wide range of grain sizes. In this synthesis, two reverse micellar solutions are prepared, the first using the metal solution and the second one using ammonium hydroxide. Stock solutions of 0.5 M sodium dioctylsulfosuccinate (AOT) are prepared in 2,2,4-trimethylpentane ~isooctane!. It has been observed that precipitation of metals is influenced by pH and electrochemical potential of the solution; therefore, the initial ratio of metal precursors is modified to account for the reduction of metals in the precipitate and subsequently fired samples. In this method the micelle size can be controlled by the molar ratio of water to AOT, which is chosen to yield a fine particle size of in nm. The volume of aqueous solution and desired particle sizes are used to determine the amount of the precursor solution to be used. The ammonia solution is then added to the metal–salt solution under constant stirring. The reaction is allowed to proceed for about 2 hrs, until particle flocculation is induced by adding excess methanol. The particles are then collected using centrifugation and washed using methanol to remove excess surfactant, followed by a methanol: water solution to remove any additional unreacted ions. After final centrifugation, the material is dried overnight under a dynamic vacuum, and subsequently fired at 525 °C for 5 h under inert atmosphere to obtain the required product.

3.3 CTAB

Magnetic Mn-Zn ferrite nanoparticles with a narrow size distribution can be prepared in water–CTAB–hexanol microemulsions [30]. In this ferrite-nanoparticles are synthesized in the water pools of reverse micelles in a microemulsion system consisting of an aqueous phase, n-hexanol as the oil phase and n-hexadecyl trimethylammonium bromide (CTAB) as the surfactant. The synthesis of the magnetic ferrite occurrs in situ with the coprecipitation of hydroxides of Mn^{2+}, Zn^{2+} and Fe^{2+} ions in the first stage, followed by the oxidation of Fe(II) hydroxide in the second stage. The influence of the pH value after the precipitation of hydroxides on the nature of the product is determined.

The microemulsion containing an aqueous solution of the corresponding metal ions is mixed with a microemulsion containing an aqueous solution of precipitating agent. By varying the amount of the later microemulsion, different pH values between 4 and 13 can be set. The pH value needs to be approximately 8 and above to produce the spinel ferrite product after the oxidation of Fe (II) hydroxide; at lower pH values, FeOOH is obtained as the major product. Although the spinel product is obtained at room temperature, temperature has a large influence on the particle size [31].

It may be observed that many of the methods briefed above yield nanoparticle ferrites. These methods involve sophisticated instrumentation techniques, require expensive high purity starting materials, constant monitoring of temperature and other preparative condition, and are time consuming. Some of these methods use ball-milling. In the present work, an

alternate route for synthesis has been employed which uses low cost, moderate (AR) grade chemicals to yield high performance nanoparticle Mn-Zn ferrite.

3.4 SYNTHESIS OF $Mn_{(x)}Zn_{(1-x)}Fe_2O_4$ MIXED FERRITE IN PRESENT STUDY

Calculated amounts of manganese nitrate tetrahydrate and zinc nitrate hexahydrate were taken as per the various proportions of Mn^{+2} : Zn^{+2} ions mentioned in the Table 3(a & b) and dissolved in sufficient volume of distilled water to obtain solution mixture of two ions. Calculated amount of ferrous sulphate heptahydrate was taken such that the proportion of Fe^{+2} to Mn^{+2} and Zn^{+2} together was 2:1. This Fe^{+2} salt was dissolved in sufficient amount of distilled water and requisite volume of aqueous solution of barium nitrate was added to precipitate SO_4^{2-} (sulphate) as $BaSO_4$ (barium sulphate). Resultant mixture was filtered to remove insoluble $BaSO_4$ and washed with water to remove last traces of Fe^{2+} ions. Filtrate along with washings, which contained ferrous nitrate solution, was added to aqueous solution of manganese-zinc nitrate followed by appropriate amount of ligand solution.

This solution mixture was than processed to obtain the fine particle $Mn_{(x)}Zn_{(1-x)}Fe_2O_4$ ferrite material by two different techniques.

(a) The solution mixture was then heated slowly to dryness. The solid mass was then ignited to decompose to obtain the Mn-Zn mixed ferrite product.

(b) The solution mixture was heated slowly to dryness and was allowed to decompose by self ignition in a microwave oven to obtain Mn-Zn mixed ferrite product.

The samples obtained by these two techniques were used for characterization and study of physical, electrical and magnetic properties separately.

Table3(a):Amount of metal salts used in the synthesis of Mn-Zn mixed ferrites by thermal decomposition method .
Composition of $(Mn^{+2} + Zn^{+2}):Fe^{2+}$ is1: 2.

No.	Mn : Zn	Amount of $Mn(NO_3)_2 . 4H_2O$g (moles) Molecular Weight =250.94g	Amount of $Zn(NO_3)_2 .6H_2O$ g (moles) Molecular Weight =297.38g	Amount of $FeSO_4 7H_2O$ g (moles) Molecular Weight= 555.70g
1	0.30:0.70	7.5282 (0.03)	20.8166 (0.07)	111.14 (0.2)
2	0.35:0.65	8.7829 (0.035)	19.3297 (0.065)	111.14 (0.2)
3	0.40:0.60	50.0376 (0.040)	17.8428 (0.060)	111.14 (0.2)
4	0.45:0.55	11.2923 (0.045)	16.3559 (0.055)	111.14 (0.2)
5	0.50:0.50	12.5470 (0.050)	14.8690 (0.050)	111.14 (0.2)
6	0.55:0.45	53.8017 (0.055)	13.3821 (0.045)	111.14 (0.2)
7	0.60:0.40	15.0564 (0.060)	11.8952 (0.040)	111.14 (0.2)
8	0.65:0.35	16.3111 (0.065)	10.4083 (0.035)	111.14 (0.2)

Table3 (b): Amount of metal salts used in the synthesis of Mn-Zn mixed ferrites by microwave decomposition method .
Composition of $(Mn^{+2} + Zn^{+2}) : Fe^{2+}$ is 1: 2.

No.	Mn : Zn	Amount of $Mn(NO_3)_2 . 4H_2O$ g (moles) Molecular weight =250.94g	Amount of $Zn(NO_3)_2 . 6H_2O$ g (moles) Molecular Weight =297.38g	Amount of $FeSO_4 \cdot 7H_2O$ g (moles) Molecular Weight= 555.70g
1	0.40:0.60	10.0376 (0.040)	17.8428 (0.060)	111.14 (0.2)
2	0.50:0.50	12.5470 (0.050)	14.8690 (0.050)	111.14 (0.2)
3	0.60:0.40	15.0564 (0.060)	11.8952 (0.040)	111.14 (0.2)
4	0.63:0.37	15.80922 (0.063)	11.00306 (0.037)	111.14 (0.2)
5	0.65:0.35	16.3111 (0.065)	10.4083 (0.035)	111.14 (0.2)
6	0.67:0.33	16.81298 (0.067)	9.81354 (0.033)	111.14 (0.2)
7	0.70:0.30	17.5658 (0.070)	8.9214 (0.030)	111.14 (0.2)

References

[1] Suryanarayana C. and Koch C. C., Non-Equilibrium Processing of Materials, Pergamon Materials Series, (1999).

[2] Rozman M and Drofenik M , J. Am. Ceram. Soc. 78 (1995) 2449.

[3] Komarneni S, Fregeau E, Breval E and Roy R, J. Am.Ceram. Soc., 71 (1988) C26.

[4] Goldman A and Laing A M. , J. Phys. Coll. 4 (1977) C1 297.

[5] Robbins H, Ferrites ed H Watanabe, S Iida and M Sugimoto (Tokyo: Center for Academic Publications Japan), 1981.

[6] Seki M, Sato T and Usui S. , J. Appl. Phys. 63 (1988) 1424.

[7] Thakur A and Singh M, Ceram. Int. 29 (2003) 505.

[8] E.P.Wohlfarth, 'Ferromagnetic Materials' (North- Holland Publishing Co.) Vol.1 and 2, (1980).

[9] C.N.R. Rao and J. Gopalakrishnan, New Directions in Solid State Chemistry, Cambridge University Press, (1986).

[10] Schikorr G., Z. Allg. Chem., 212 (1938) 33.

[11] Pileni M. P., J. Phys. Chem. 97 (1993) 6961.

[12] K.C.Patil, S.Sudar Manoharan and D.Gajapath, 'Handbook of Ceramics and Composites' vol.1 (eds. Nicholas P.Cheremisinoff, Marcel Dekker, INC, New York) p.469.

[13] Fannin P. C., Charles S. W. and Dormann J. L., J. Magn. Magn. Mater. 201 (1999) 98

[14] Pannaparayil T., Komarneni S., Marande R. and Zadarko M., J. Appl. Phys. 67, 5509

355

[15] Yue Z., Zhou J., Li L., Zhang H. and Gui Z., J. Magn. Magn.Mater. 208 (2000) 55.

[16] Martinez B., Roig A., Molins E. and Monty C, J. Appl. Phys. 79 (1996) 2580.

[17] del Monte F., Morales M. P., Levy D, Fernandez A., Ocana M., Roig A., Molins E., O Grady K. and Cerna C. J. Langmuir 13 (1997) 3627.

[18] Cannas C., Gatteschi D., Musinu A., Piccalunga G. and Sangregorio C. J. Phys. Chem. B 102(1998) 7721.

[19] Jiang J. S., Gao L., Yang X. L.,Guo J. K. and Shen H. L. J. Mater. Sci. Lett., 18 (1999) 1781.

[20] Caizer C, Stefanescu M, Muntean C and Hrianca I 2000 3rd Int. Edition of Rom. Conf. on Advanced Materials (Bucharest, Romania, October r3–25) Contribution p 85

[21] Savii C., Popovici M., Enache M., Hrianca I., Zanfir A., Turicin R. and Caizer C. Int. Conf. on Chemical Sciences for Sustainable Development (Halkidiki, Greece, June 6–9) Contribution, (2000) 276.

[22] West, Anthony R., Solid State Chemistry and its applications, John Wiley & sons (1984)

[23] S. Son, R. Swaminathan, and M. E. McHenry Journal of applied physics 93 (10) (2003).

[24] Z. Tugut , PhD. Thesis CMU 2000.

[25] M. I. Boulos J. High Temp. Chem. Processes 1 (1992) 401.

[26] S. Son et al., J. Appl. Phys. 91 (10) (2002) 7589 .

[27] S.Yamamoto, N. Tanamachi, H. Kurisu, M. Matsuura and K. Ishida, 21 Aa I-6 digest 8th Int. Conf. on ferrites Kyoto Japan.

[28] P. Poddar, J. L. Wilson, H. Srikanth , S. A. Morrison and E. E. Carpenter, Nanotechnology (IOP publishing) 15 (2004) S570–S574

[29] S. A. Morrison , C. L. Cahill, E. E. Carpenter, S. Calvin, and V. G. Harris Journal of applied physics 93 (10) 2003 .

[30] D. Makovec, A. Kosak and M. Drofenik , Nanotechnology (IOP Publishing) 15 (2004) S160–S166.

[31] Kosak A., Makovec D. and Drofenik M. J. Metastab. Nanocryst. Mater. (2004).

Chapter IV

ANALYTICAL TECHNIQUE AND CHARACTERIZATION

4.1 INTRODUCTION

Characterization of materials forms an essential part of study in systematic development of materials and understanding their behavior. One of the principal objectives in the experimental study of bulk solids is the characterization of lattice structure and investigations of other physical properties. For a particular system, in material characterization, there are two classes of properties that need to be addressed. One is compositional (elemental) characterization and molecular or crystal structure of the material and second is the geometrical properties of the materials such as size, shape, polydispersity and surface characteristics of particulate matter. Among these, the compositional characteristics in general are independent of the microscopic form of the material while the geometric parameters are dependent on the microscopic form and are equally important in dictating the final properties of the product and its applications.

The challenges involved in material characterization are, to understand how specific instruments and analytical techniques can provide detail information about products formed. This information may be used to explain its behavior and develop materials with new improved properties to suit particular requirement.

This chapter deals with the different experimental techniques employed in the characterization of the final oxide products synthesized using nitrilotriacetate precursor method.

The techniques employed for the characterization of mixed spinel ferrite were

(i) Chemical analysis

(ii) Density measurement

(iii) Infra Red Spectroscopy (IR)

(iv) X-ray Diffraction Spectroscopy (XRD)

4. 2 CHEMICAL ANALYSIS

4.2.1 Characterization By Percentage Yield Method

One of the methods of ascertaining the formation of desired phase of oxide material is experimentally determining the percentage yield from the known amount of starting materials for the given composition.

4.2.2 Experimental

Experiments were carried out during initial stages of synthesis for all the samples as described earlier. Theoretically calculated percentage yields and experimentally determined percentage yields for the desired oxide material are given in Table.

4.2.3 Energy Dispersive X-Ray Analysis (EDAX)

Scanning Electron Microscopy (SEM) provides compositional information and elemental analysis through analyzing materials and physical properties of the sample. Along with the secondary electron emission that is used to form a morphological image of the surface in the SEM, a number of other signals are emitted as a result of the electron beam impinging on the surface. Each of these signals carries information about the sample that provides clues to its composition.

Two of the most commonly used signals for investigating composition are x-rays and backscattered electrons. X-ray signals commonly used to provide elemental analysis by the attachment of an Energy Dispersive Spectrometer to the SEM system. X-ray emission results from inelastic scattering between the beam electron and the electrons of the sample atoms. This interaction results in the ejection of an inner shell electron from the atom, acquired on this sample. As the electron beam of the SEM is scanned across the sample surface, it generates X-ray fluorescence from the atoms in its path. The energy of each X-ray photon is characteristic of the element, which produced it. The EDS microanalysis system collects the X-rays, sorts and plots them by energy, and automatically identifies and labels the elements responsible for the peaks in this energy distribution.

The EDS data are typically compared with either known or computer-generated standards to produce a full quantitative analysis showing the sample composition. Data output is either this element analysis, the original spectrum showing the number of X-rays collected at each energy, or maps of distributions of elements over areas of interest.

4.2.4 Experimental

EDS spectra along with the estimates of percentage content of Mn, Zn, Fe and O was obtained for the samples $Mn_{(x)} Zn_{(1-x)} Fe_2O_4$ where x=0.40/0.60/0.67 on Joel Model 840(SEM).

4.3 DENSITY MEASUREMENTS

The densities of powdered and sintered samples are measured by Pyknometric method. CCl_4 was used as a medium at room temperature. The density was calculated using expression,

$$\rho_{sample} = \frac{\text{weight of the sample}}{\text{(Weight of the liquid displaced)/ (Density of the liquid)}}$$

4.4 INFRA RED SPECTROSCOPY (IR)

Modern IR spectroscopy has become a versatile tool for both qualitative and quantitative analysis of molecular species. Infrared spectroscopy is a technique used to identify various functional groups in unknown substances through the identification of different covalent bonds that are present in the compound. By comparing the absorptions seen in an experimental spectrum to the literature of absorptions of various functional groups, one can determine a list of possible identities for the bonds present. One of the most important advantages of infrared spectroscopy over the other methods of structural analysis (X-ray analysis, electron spin resonance etc) is that it provides useful information about the structure of molecule quickly, without tiresome evaluation methods.

In this technique a chemical substance shows a marked selective absorption in the infra-red region. After absorption of IR radiations, the molecules of a chemical substance vibrate at many rates of vibration, giving rise to closed packed absorption bands, called an IR absorption spectrum which may extend over a wide wavelength range. Various bands will be present in IR spectrum corresponds to characteristic functional groups and bonds present in a chemical substance. Band intensities in IR spectrum may be expressed either as transmittance (T) or absorbance (A).

IR encompasses a spectral region from red end of visible spectrum ($12{,}500cm^{-1}$; 0.8mm) to the microwave ($10\ cm^{-1}$; 1000mm) in the electromagnetic spectrum and based upon application and instrumentation involved is conveniently divided into near-IR (12500 to 4000 cm^{-1}), mid- IR (4000 to 400 cm^{-1}) and far-IR (400 to $10cm^{-1}$). Mid-IR region is the most fundamental as it gives the important information about the vibrations of molecules, and hence about the structure of molecules.

When IR radiation is passed through sample, certain frequencies are absorbed by the molecule that corresponds to vibrational changes in the molecule. For this to occur there must be a mode of interaction between the incident radiation and the vibrational energy levels. This mode of interaction is an oscillating electric dipole induced by the vibration, which interacts with the oscillating electric field of the electromagnetic radiation. IR absorption occurs for each vibrational degree of freedom of the molecule provided that a change in the dipole moment of the molecule takes place during the vibration. For a large molecule with many vibrational degrees of freedom there may be many IR bands observed. Since each molecule has individual sets of energy levels,

the absorption spectrum is characteristic of the fundamental groups that are in the molecule [2,3].

For example A carbon-carbon triple bond (-C ≡ C-) absorbs in the region 2300-2000 cm^{-1}, where as a double bond (C = C) is weaker and absorbs at lower frequency, 1900-1500 cm^{-1}.

The frequencies of peak maximum depend on O-H bond strength. This provides information on, for instance the location of O-H group, whether it belongs to water molecule and whether hydrogen bonding is present or not. Peaks associated with vibrational modes of covalently bonded groups such as oxyanions usually occur at high frequency. At lower frequency in the far region lattice vibration give rise to absorption peaks. At temperatures above absolute zero, all the atoms in molecules are in continuous vibration with respect to each other. Each atom has three degrees of freedom, corresponding to motions along any of the three Cartesian coordinate axes (x, y, z). A polyatomic molecule of n atoms has $3n$ total degrees of freedom. However, 3 degrees of freedom are required to describe translation, the motion of the entire molecule through space. Additionally, 3 degrees of freedom correspond to rotation of the entire molecule. Therefore, the remaining $3n - 6$ degrees of freedom are true, fundamental vibrations for nonlinear molecules. Linear molecules possess $3n - 5$ fundamental vibrational modes because only 2 degrees of freedom are sufficient to describe rotation. Among the $3n - 6$ or $3n - 5$ fundamental vibrations (also known as normal modes of vibration), those that produce a net change in the dipole moment may result in an IR activity and those that give polarizability changes may give rise to Raman activity. Naturally, some vibrations can be both IR- and Raman-active. The total

number of observed absorption bands is generally different from the total number of fundamental vibrations. It is reduced because some modes are not IR active and a single frequency can cause more than one mode of motion to occur. Conversely, additional bands are generated by the appearance of overtones (integral multiples of the fundamental absorption frequencies), combinations of fundamental frequencies, differences of fundamental frequencies, coupling interactions of two fundamental absorption frequencies, and coupling interactions between fundamental vibrations and overtones or combination bands (Fermi resonance). The intensities of overtone, combination, and difference bands are less than those of the fundamental bands. The combination and blending of all the factors thus create a unique IR spectrum for each compound. The major types of molecular vibrations are stretching and bending. The absorption involves discrete, quantized energy levels. However, the individual vibrational motion is usually accompanied by other rotational motions. These combinations lead to the absorption bands, not the discrete lines, commonly observed in the mid IR region.

The transmittance spectra provide better contrast between intensities of strong and weak bands because transmittance ranges from 0 to 100% T whereas absorbance ranges from infinity to zero.

A typical spectrometer comprises of components like radiation source, optical path and monochromator, radiation detector and sample holder.
Fourier Transform Infra Red spectrometers (FTIR) are superior to the dispersive IR spectrometers.

The measurement of transmission, reflection or even emission spectra has become significantly faster and with higher sensitivity in FTIR.

4.4.1 Experimental

IR spectra for all the samples were recorded on Shimadzu FTIR 8900 spectrometer.

The solid sample was finely ground along with pure and dry KBr, in the ratio 1:10. Fine grinding is essential as the sample should be well and evenly mixed with KBr. The pellet is pressed in a special die that can be evacuated in order to avoid entrapped air, which causes cloudiness in the pellet. The mixture was pressed in a hydraulic press to form a transparent pellet. This pellet was then placed mounted on the sample holder, and placed in the sample chamber of the IR spectrometer. The absorption spectra for the sample was recorded in the wavelength range $250cm^{-1}$ to $4000cm^{-1}$ as usual. Similar measurements were carried out on all the samples prepared using thermal decomposition as well as microwave decomposition technique.

4.5 X-RAY DIFFRACTION SPECTROSCOPY

X-ray powder diffraction (XRD), is an instrumental technique that is used to identify materials. XRD provides the researcher with a fast and reliable tool for routine material identification. XRD in particular can be used for identifying fine-grained minerals and mixtures or intergrowths of minerals that may not lend themselves to analysis by other techniques. Crystal structure cannot be visualized by visible light of wavelength approximately $5000A^{o}$ as arrangement of atoms or placement of atoms in the material is too close for resolution. The interatomic spacing in crystal is of the order of 10^{-8} cm., therefore a wave with wavelength of similar order will give rise to diffraction

phenomena. Diffraction provides information about arrangement of atoms in the crystals.

For crystal diffraction, X-rays are more suitable as the energy of X-ray quanta is

$$E=hc/\lambda \quad \text{----------} \quad 4.5.1$$

Where λ is of order 10^{-8}cm.

When X-ray radiation passes through matter, the radiation interacts with the electrons in the atoms, resulting in scattering of the radiation. If the atoms are organized in planes (i.e. the matter is crystalline) and the distances between the atoms are of the same magnitude as the wavelength of the X-rays, constructive and destructive interference occur. This diffracted X-rays are emitted at characteristic angles based on the spacings between the atoms organized in crystal planes. Each atom can belong to many sets of crystal planes. Each set of planes has a specific interplanar distance and will give rise to a characteristic angle of diffracted X-rays. The relationship between wavelength, atomic spacing (d) and angle is given by Bragg Equation. If the illuminating wavelength is known and the angle can be measured then the interplanar distance can be calculated

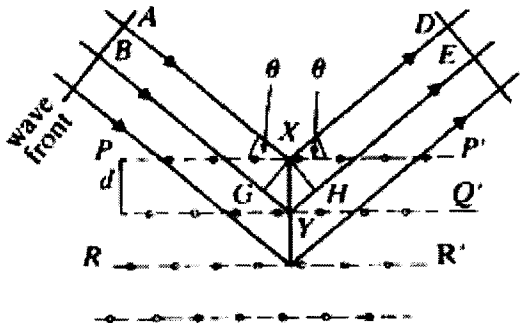

from the Bragg equation. A set of d-spaces obtained from a single compound will represent the set of planes that can be passed through the atoms and can be used for comparison with sets of d-spaces obtained from standard compounds. Diffraction of monochromatic X-rays by crystal takes place according to Bragg's law

$$2d\sin\theta = n\lambda \text{ ---------- } 4.5.2$$

λ=wavelength of X-rays

θ=Bragg angle

d=inter planar separations

n=order of diffraction

This condition helps in finding size, shape and orientation of crystallite unit cell. From Bragg's law it is seen that intensities are stronger only at certain values of θ for specific λ and d. This intensity depends on the atomic scattering factor of each atom and position of each atom in unit cell. The most widespread use of x-ray powder diffraction is for the identification of crystalline compounds by their diffraction pattern. One can determine crystallite size from analysis of peak broadening.

4.5.1 Line Broadening Analysis For Crystallite Dimension

As the particle size decreases the peaks get broadened due to incomplete destructive interference. The broadening caused by fine crystallites relate to size of the grains by Scherer formulae [1]

$$T=0.9\,\lambda/D_p\cos\theta \quad \text{----------} \quad 4.5.3$$

T = crystallite size, λ=wavelength, D_p = FWHM, θ=Bragg angle

The prime components of a powder diffractometer is the source of X-ray, usually called X-ray tube, the sample chamber, a goniometer for measuring angles, X-ray detector for measuring the intensity of diffracted X-ray beam. Besides there are several slits to reduce the divergence of the incident and diffracted beam and monochromator are also used.

4.5.2 Experimental

The X-ray diffraction patterns of the samples prepared by thermal decomposition were obtained on Microcomputer controlled Siemens D- 500 X-ray diffractometer using Cu Kα (λ=1.5406 AU). The X-ray diffraction patterns of the samples prepared by microwave-induced decomposition were obtained on X-pert PRO PANalytical Philips diffractometer .

4.6 RESULTS AND DISCUSSION

4.6.1 Chemical Analysis

4.6.1.1 Method of Determining % Yield

In a typical experiment, 0.7435g [0.0025 mole of Zn $(NO_3)_2 .6H_2O$] was dissolved in minimum quantity of distilled water. Similarly, 0.6274g (0.0025 mole) of Mn $(NO_3)_2 .4H_2O$ was dissolved in minimum quantity of water separately. These two solutions were mixed (water may added to the mixture to get clear solution).

In situ Fe $(NO_3)_2$ solution was prepared by slow addition of aqueous solution of barium nitrate [0.01mole i.e. 2.9734g of Ba $(NO_3)_2 2H_2O$] to aqueous solution of ferrous sulphate [0.01 mole i.e. 5.557g of $FeSo_4 7H_20$]. Resultant mixture was filtered to remove barium sulphate white precipitate. The precipitate on the filter paper was thoroughly washed and the filtrate, which contained ferrous nitrate, was collected and kept in stoppered airtight bottle.

Ferrous nitrate solution was added to the aqueous mixture of zinc nitrate and manganese nitrate. Appropriate amount of ligand solution was added to this mixture and then resultant solution was evaporated to dryness. Dry powder was decomposed in a previously weighed crucible by heating on bunsen burner, in order to know the weight of the residue left after decomposition.

Weights of the residues obtained after decomposition for known amount of starting materials, were thus experimentally found out to ascertain formation of mixed ferrites.

Theoretically calculated percentage yields and experimentally determined percentage yields for the desired oxide material are given in Table 4.6.1.1.

The values are in agreement within experimental errors suggesting the formation of Mn-Zn mixed ferrites as per the composition given in the Table.

Table 4.6.1.1: Theoretical and Experimental % yield of the oxide material after decomposition (a) thermal decomposition (b) microwave decomposition .

Sample	Experimental yield (g)	Theoretical yield (g)	% yield
$Mn_{0.3}Zn_{0.7}Fe_2O_4$	2.3564	2.3620	99.76
$Mn_{0.35}Zn_{0.65}Fe_2O_4$	2.3517	2.3557	99.83
$Mn_{0.4}Zn_{0.6}Fe_2O_4$	2.3611	2.3729	99.50
$Mn_{0.45}Zn_{0.55}Fe_2O_4$	2.3514	2.357	99.76
$Mn_{0.5}Zn_{0.5}Fe_2O_4$	2.3464	2.3553	99.62
$Mn_{0.55}Zn_{0.45}Fe_2O_4$	2.3579	2.3646	99.71
$Mn_{0.6}Zn_{0.4}Fe_2O_4$	2.3514	2.3622	99.54
$Mn_{0.65}Zn_{0.35}Fe_2O_4$	2.3586	2.3649	99.73
$Mn_{0.7}Zn_{0.3}Fe_2O_4$	2.3495	2.3638	99.39

(a)

Sample	Experimental yield (g)	Theoretical yield (g)	% yield
$Mn_{0.4}Zn_{0.6}Fe_2O_4$	22.5125	23.6874	95.04
$Mn_{0.5}Zn_{0.5}Fe_2O_4$	22.7462	23.5835	96.44
$Mn_{0.6}Zn_{0.4}Fe_2O_4$	22.8339	23.4796	97.25
$Mn_{0.63}Zn_{0.37}Fe_2O_4$	22.1175	23.4484	94.22
$Mn_{0.65}Zn_{0.35}Fe_2O_4$	22.5215	23.4276	96.13
$Mn_{0.67}Zn_{0.33}Fe_2O_4$	22.7514	23.4068	97.20
$Mn_{0.7}Zn_{0.3}Fe_2O_4$	21.9451	23.3757	93.88

(b)

4.6.1.2 EDS Data

Table 4.6.1.2(a): EDS results of Sample $Mn_{0.4}Zn_{0.6}Fe_2O_4$ prepared by thermal decomposition

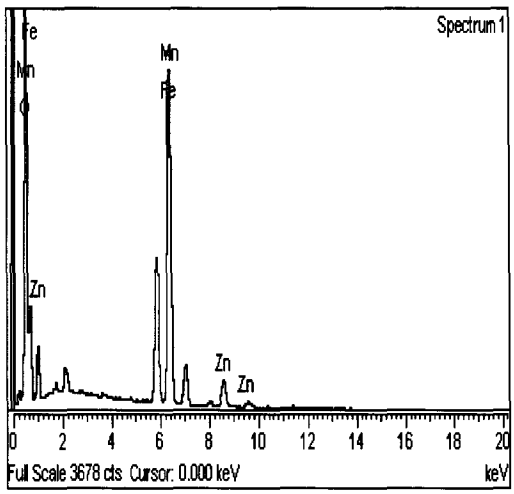

Element	Weight%	Atomic%
O K	28.56	58.94
Mn K	9.24	5.55
Fe K	47.47	28.06
Zn K	14.74	7.44
Totals	100.00	

Table 4.6.1.2(b) : EDS results of Sample $Mn_{0.60}Zn_{0.40}Fe_2O_4$

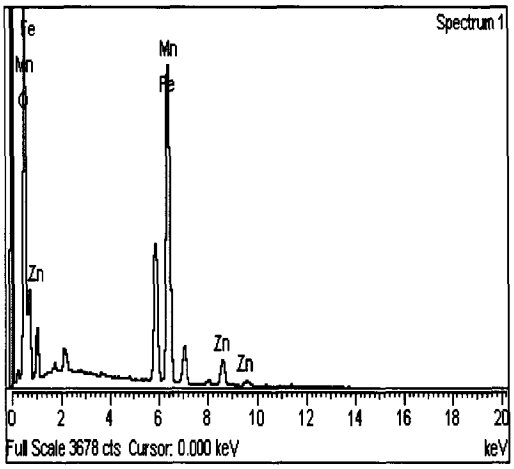

Element	Weight%	Atomic%
O K	26.23	55.87
Mn K	15.52	9.63
Fe K	46.43	28.34
Zn K	11.82	6.16
Totals	100.00	

Table 4.6.1.2(c): EDS results of Sample $Mn_{0.67}Zn_{0.33}Fe_2O_4$ prepared by microwave decomposition

Element	Weight%	Atomic%
O K	24.58	53.58
Mn K	18.55	11.78
Fe K	47.12	29.43
Zn K	9.75	5.20
Totals	100.00	

Estimated percentage contents of the elements Mn, Zn, Fe and O carried out with the help of EDS analysis of all the samples prepared by thermal decomposition and microwave induced decomposition (Table 4.6.1.2 a, b, c) are in good agreement with the theoretical estimated values thus confirming the preservation of stoichiometry [7].

4.6.2 Density Measurements

The density values for the powdered as well as sintered samples, calculated by pyknometric method.

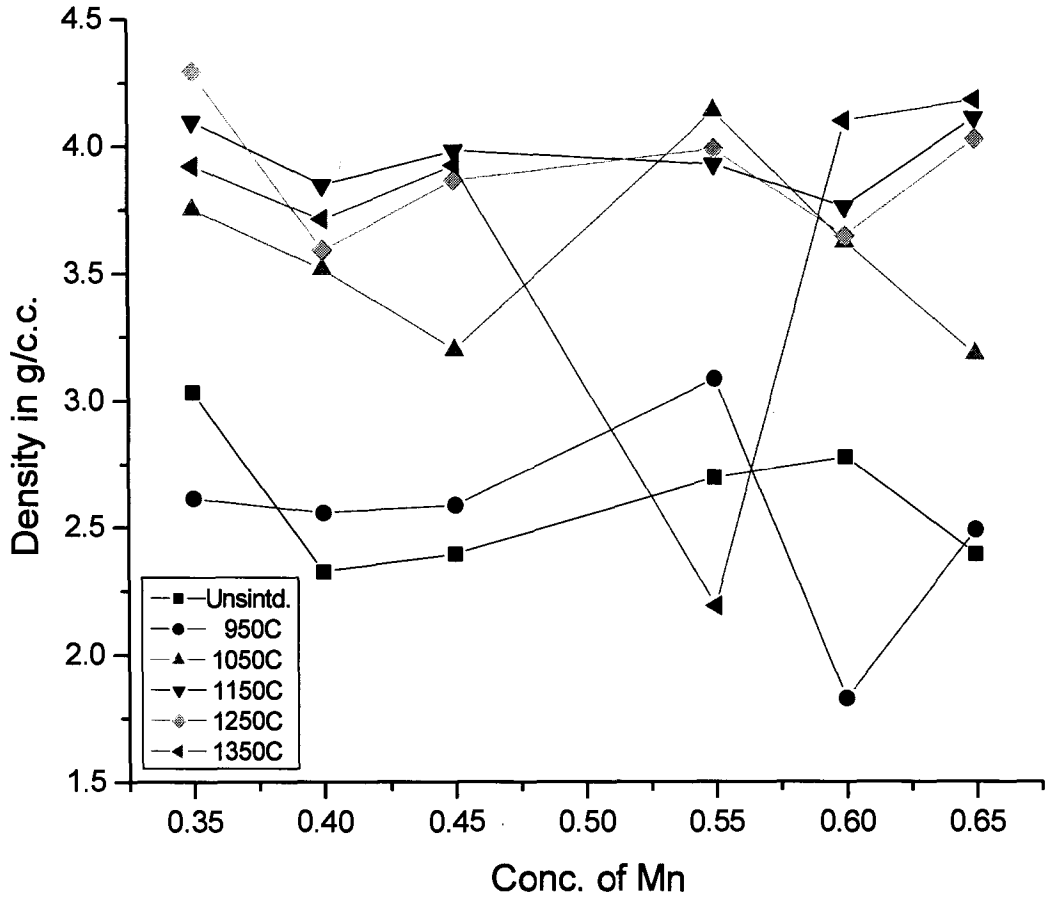

Fig.4.6.2 (a): Variation of density with conc. of Mn for various sintering temperatures prepared by thermal decomposition

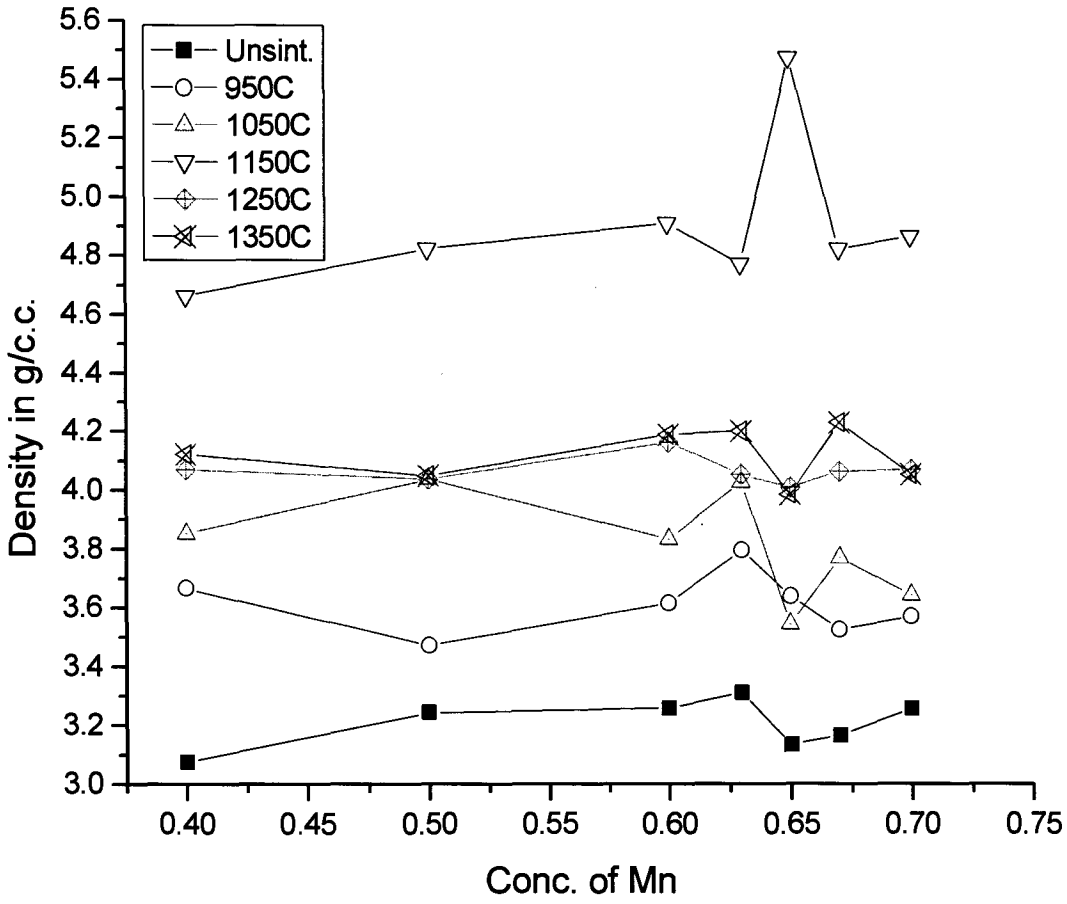

Fig.4.6.2(b): Variation of density with conc. of Mn for various Sintering temperatures prepared by microwave induced decomposition

The density values of the samples in general were found to show abrupt changes for samples sintered at 950°C 1050°C, 1150°C 1250°C and 1350°C. The density of sintered $Mn_x Zn_{(1-x)} Fe_2O_4$ ferrite material where x = 0.65, 0.6, 0.45 and 0.4 prepared by thermal decomposition (fig 4.6.2a) is found to be high when sintered at 1150°C and 1350°C whereas these values were low when these samples were sintered at 1050°C and 1250°C.The density for sample with x=0.55 was found to increase with sintering temperature whereas the same was observed to be lower for sample with x=0.35 sintered at 1350°C. Although density depends on the concentration of Mn in the sample the present unusual behavior observed in the density may be attributed to the existence of phase transitions, which occur during the crystal formation process while sintering. Density measurements shows increase in the densification rate with the increase in the sintering temperature. The density of the as prepared powdered samples (fig 4.6.2a) prepared using thermal decomposition technique was found to be in the range of 2.3273 g/c.c, to 3.0324 g/c.c. and for the samples prepared using microwave decomposition technique (fig4.6.2b) was in the range 3.075 g/c.c. to 3.2578 g/c.c. The density values for sintered samples prepared using thermal decomposition technique were found to be in the range of 1.8290 g/c.c. to 4.2953 g/c.c. whereas for samples prepared using microwave decomposition technique the same were found to be in the range of 3.1163 g/c.c. to 5.4721 g/c.c. the highest being 5.4721 g/c.c. for the sample $Mn_{0.65}Zn_{0.35}Fe_2O_4$ sintered at 1150°C which is higher than the reported values [8].

4.6.3 Infra Red Analysis

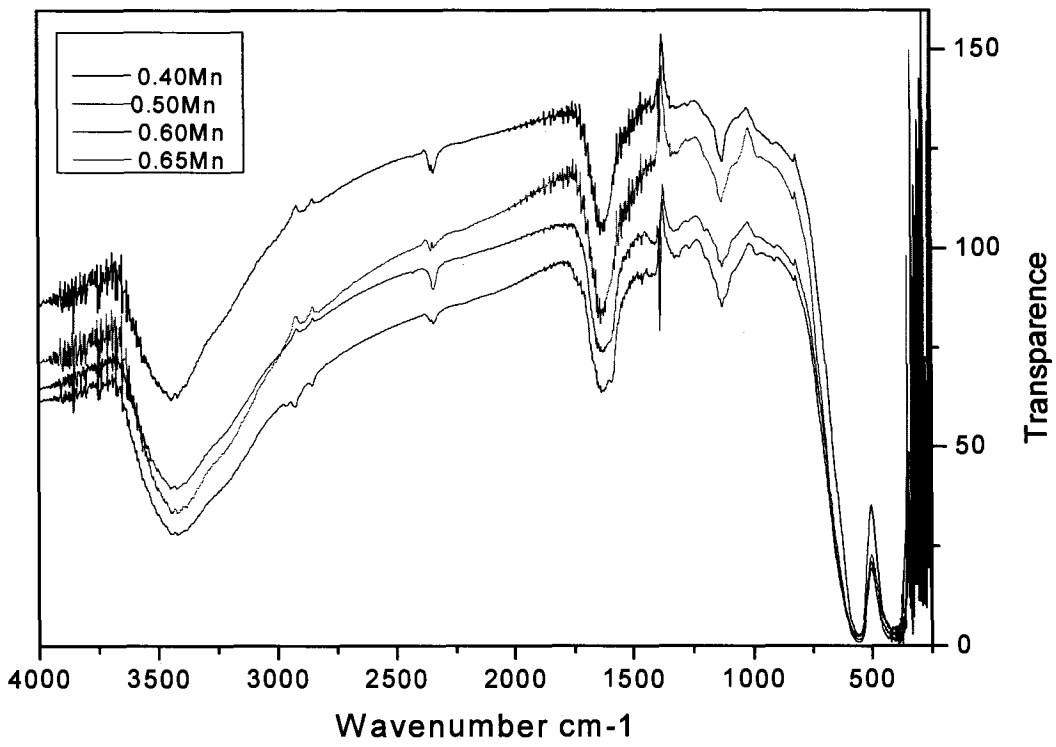

(a)

Fig. 4.6.3a : IR spectra of $Mn_{(x)} Zn_{(1-x)} Fe_2O_4$ ferrite where x=0.40/0.50/0.60/0.65 prepared by thermal decomposition

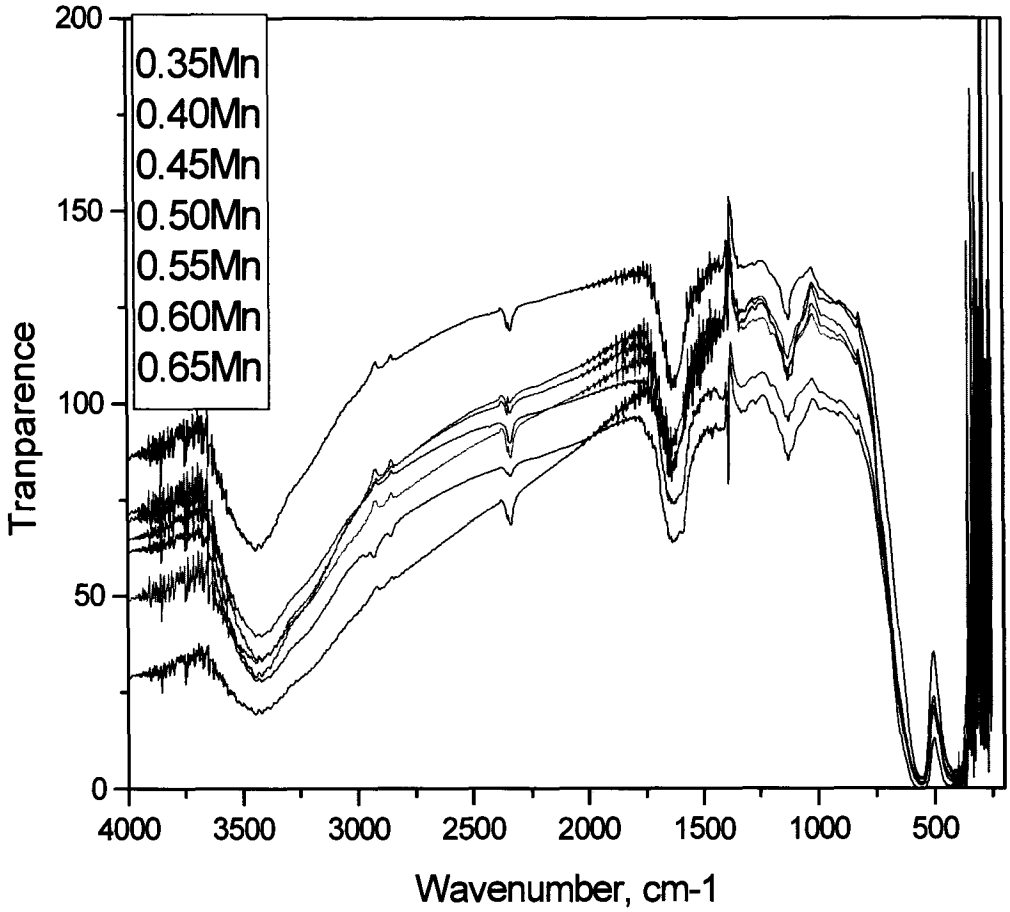

(b)

Fig. 4.6.3 b : IR spectra of $Mn_{(x)} Zn_{(1-x)} Fe_2O_4$ ferrite where x=0.40/0.50/0.60/0.63/0.65/0.67/0.70 prepared by microwave decomposition

IR absorption spectroscopy allows us to identify the spinel structure as well as a presence of certain types of chemical substances adsorbed on the surface of particles. IR spectra of dried samples were recorded in the waverange of 4000-250 cm^{-1}.

(1) Me_T O Me_O stretching vibration 600-550 cm^{-1}

(2) $Me_O \overset{\leftrightarrow}{—} O$ stretching vibration 450 -385 cm^{-1}

(3) $Me_T \overset{\leftrightarrow}{—} Me_O$ stretching vibration 350-330 cm^{-1}

Where O is oxygen, Me_O is metal in the octahedric site and Me_T -in the tetrahedric site. The metal-oxygen absorption bands (1) and (2) are pronounced for all spinel structures and essentially for ferrites. Usually the band (3) is less intense than bands (1) and (2), and sometimes found to merge with the band (2) resulting in a singlewide band at 420-330 cm^{-1}. In the IR absorption spectra recorded for the powdered samples, two broad bands (1) and (2) are observed in addition to a small narrow less intense third band in the range 350-330 cm^{-1} that has almost merged with band (2).

The metal oxygen absorption bands at 600-550 cm^{-1} and 450-385cm^{-1} are characteristically pronounced for all spinel structures and for ferrites in particular. The band 350-330 cm^{-1} is less intense and sometimes it merges with the band 450-385 cm^{-1} giving a single wide band at 420-330 cm^{-1}.

Fig 4.6.3(a & b) shows two broad bands at 600-550 cm^{-1} and 420-330 cm^{-1} for all the samples.

IR-spectra of samples very well matches with the reported one [5,6].

4.6.4 X-Ray Diffraction Analysis

In the present study X-ray diffraction is used to confirm the formation of spinel structure, to determine interplanar distances and the lattice constants. As the crystallites are randomly oriented, a reflection at the particular position is due to a set of atomic planes satisfying Bragg's condition.

Bragg's law is given as,

$$n\lambda = 2d_{hkl}\sin\theta \quad \text{----------} \qquad 4.6.4.1$$

Where d_{hkl} is the interplanar spacing of crystal planes of miller indices (hkl), θ is the glancing angle , λ is the wavelength of X-ray radiation and 'n' is the order of diffraction.

For a cubic lattice, the interplanar distance, d_{hkl} , lattice parameter 'a' and the miller indices(hkl) are related by relation,

$$d_{hkl} = \frac{a}{(h^2+k^2+l^2)^{1/2}} \qquad 4.6.4.2$$

Mn-Zn ferrite prepared by nitritriacetate method employing two different decomposition techniques was examined by powder X-ray diffraction analysis from 20 ° to 80 ° .

Formation of single-phase cubic spinel structure of $Mn_{(x)}Zn_{(1-x)}Fe_2O_4$ with x=0.35/0.40/0.45/0.55/0.60/0.65 was confirmed with the help of XRD patterns obtained for all the samples. Fig.4.6.4.1 (a) shows a typical XRD pattern for the sample $Mn_{0.50}Zn_{0.50}Fe_2O_4$ prepared by thermal decomposition and fig.4.6.4.1 (b) for the sample $Mn_{(x)}Zn_{(1-x)}Fe_2O_4$ with

x=0.40/0.5/0.6/0.63/0.65/0.67/0.70 prepared by microwave decomposition technique.. The XRD pattern clearly identifies a single phase of Mn-Zn ferrite. The patterns similar to the XRD patterns reported in the literature for Mn-Zn ferrite. The values of lattice constants *a* calculated from these were found to be in excellent agreement with reported values [4].

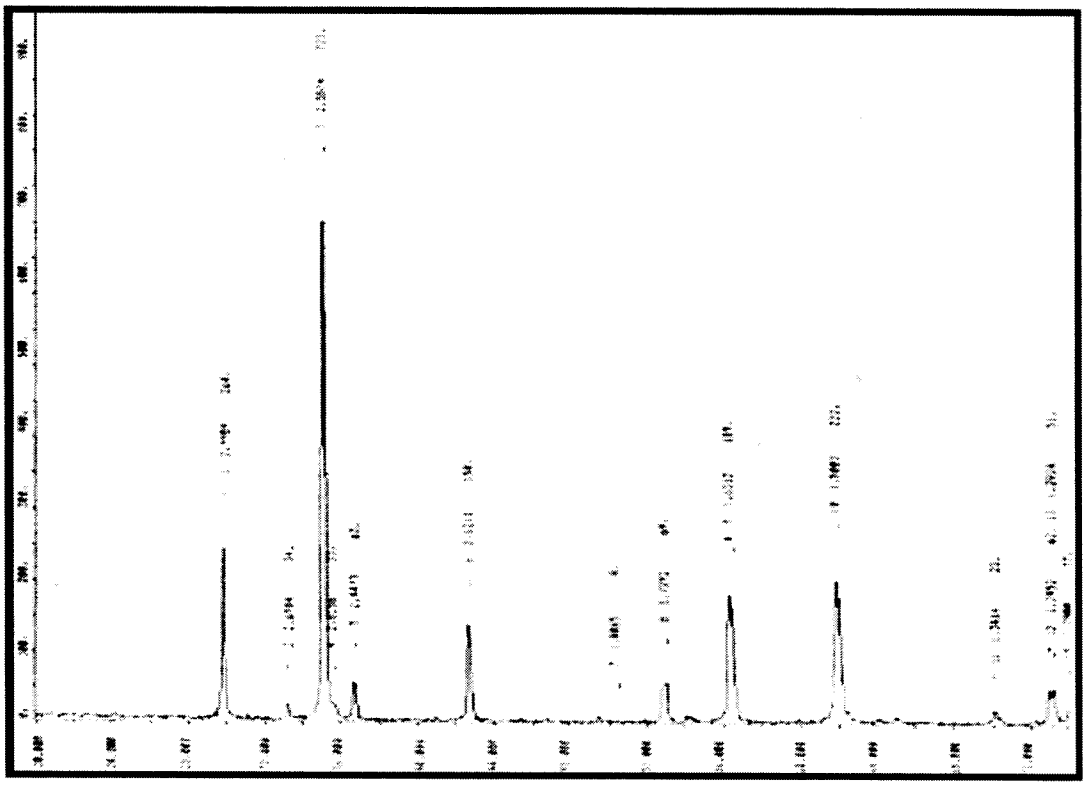

(a)

Fig.4.6.4.1: (a) Typical x-ray diffraction pattern obtained for $Mn_{(x)}Zn_{(1-x)}Fe_2O_4$ ferrite prepared by thermal decomposition

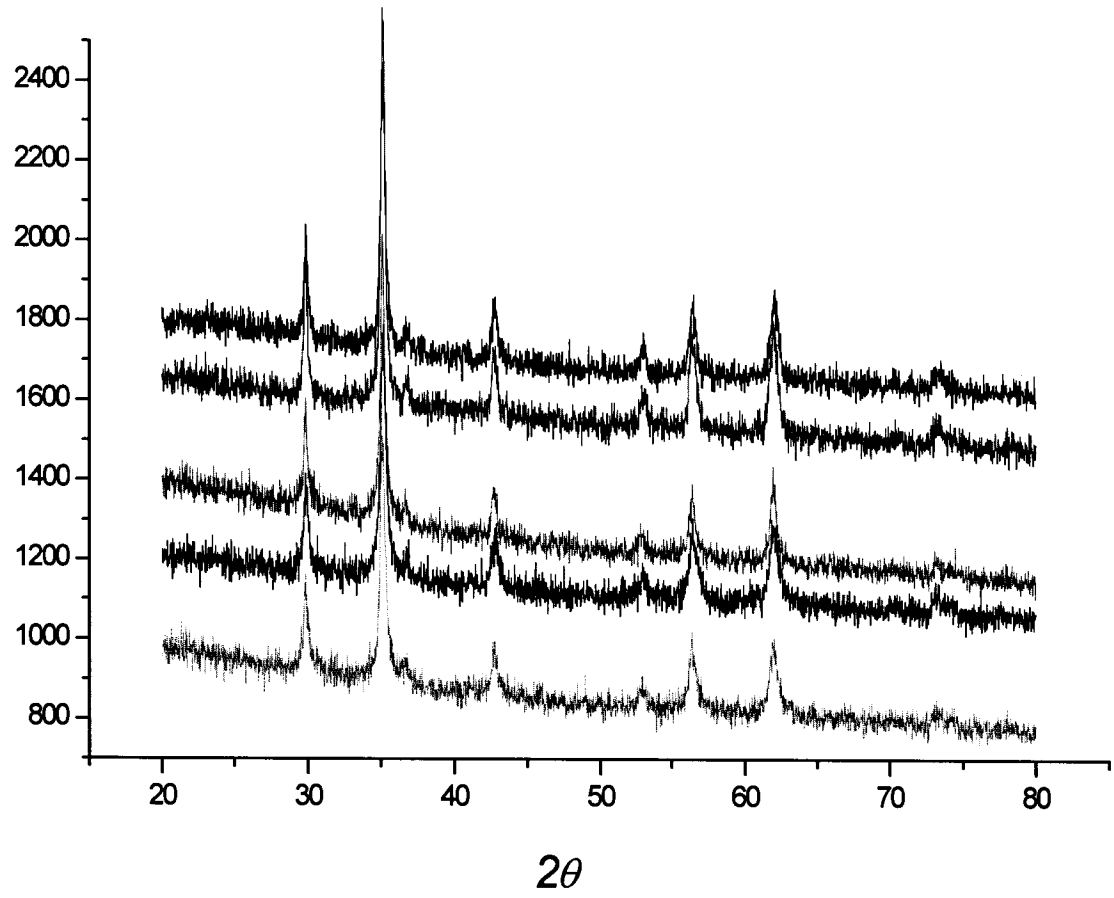

(b)

Fig.4.6.4.1(b): X-ray powder diffraction pattern for $Mn_{(x)}Zn_{(1-x)}Fe_2O_4$ ferrite prepared by microwave decomposition method.

Table 4.6.4.1: Structural parameters (lattice constant 'a') and particle size of Mn (x) Zn (1-x) Fe_2O_4 obtained from XRD pattern.

Sample	Experimental value for 'a' in AU	Average particle diameter D in nm.
$ZnFe_2O_4$	8.440	26.195
$Mn_{(0.3)}Zn_{(0.7)}Fe_{(2)}O_4$	8.455	7.20
$Mn_{(0.35)}Zn_{(0.65)}Fe_{(2)}O_4$	8.456	11.07
$Mn_{(0.4)}Zn_{(0.6)}Fe_{(2)}O_4$	8.457	21.461
$Mn_{(0.45)}Zn_{(0.55)}Fe_{(2)}O_4$	8.458	4.464
$Mn_{(0.5)}Zn_{(0.5)}Fe_{(2)}O_4$	8.459	18.543
$Mn_{(0.55)}Zn_{(0.45)}Fe_{(2)}O_4$	8.461	11.074
$Mn_{(0.6)}Zn_{(0.4)}Fe_{(2)}O_4$	8.463	25.278
$Mn_{(0.65)}Zn_{(0.35)}Fe_{(2)}O_4$	8.470	10.7274
$Mn_{(0.7)}Zn_{(0.3)}Fe_{(2)}O_4$	8.479	10.106
$MnFe_2O_4$	8.510	15.720

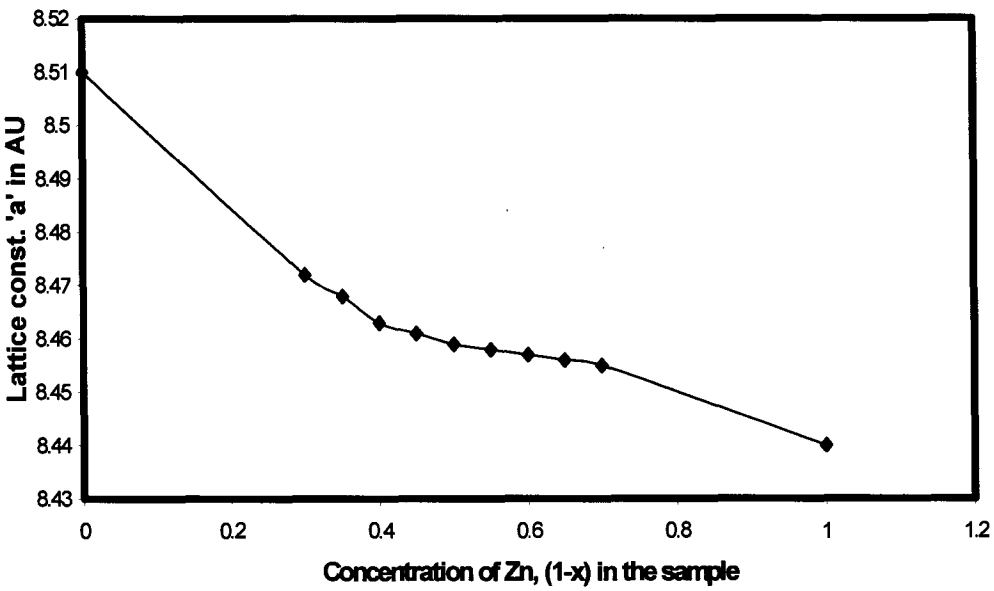

Fig.4.6.4.2: Variation of Lattice Constant with Conc. of Zn in Mn $_{(x)}$ Zn $_{(1-x)}$ Fe_2O_4

The values of lattice parameters show a smooth decrease in the lattice constant as the concentration (1-x) of zinc is increased. The lattice constant "a" for $Mn_{0.70}Zn_{0.30}Fe_2O_4$ (8.479Å) reduces smoothly to (8.455Å) for $Mn_{0.3}Zn_{0.7}Fe_2O_4$ as Zn-concentration is increased. This decrease could be easily explained on the basis of the ionic radii of Fe and Zn ions. Fe^{+3}-ions with radius (0.63Å), which are smaller, are replaced by Zn-ions with radius of (0.78Å) which are larger, as the concentration of Zn is increased in the sample[9].

References

[1] B. D. Cullity, Elements of X-ray Diffraction, 2nd edition, Addison Weseley (1978).

[2] R. W. Cahn, P . Haasen , E .J .Kramer, Material Science and Technology Vol.2A , VCH- Weinheim- Newyork.

[3] R. W. Cahn, P. Haasen, E. J. Kramer, Material Science and Technology Vol.2B, VCH- Weinheim- New York.

[4] Welch, R.G.; Neamtu, J.; Rogalski, M.S.; Palmer, S.B. Materials Letters 29, (1996) 199-203.

[5] J. LEMCOMTE, Enciclopedia of Physics, Springer Verlag, Berlin, 26, (1958) 244.

[6] V.C.FARMER, in "The Infrared Spectra of Minerals" ed. V.C.Farmer , Mineralogical Society, London , (1974) 18.

[7] S. Son, R. Swaminathan, and M. E. McHenry J. of Applied Physics 93(10) (2003).

[8] Andrej žnidaršič and Miha drofenik, Soft Magnetic Ferrite Materials, Mehko Magnetni Feritni Materiali.

[9] R.B. Tangsali, S.H. Keluskar, G.K.Naik, J.S.Budkuley , International J. of Nanoscience 3 (4 & 5) (2004) 1-9.

Chapter V

INSTRUMENTAL TECHNIQUES AND CHARACTERIZATION

5.1 INTRODUCTION

Particle characterization has become an indispensable tool in various fields of research and development, in the manufacture and quality control of many materials and products we use in high technology areas as well as in our everyday life. Microstructural analysis and estimation of particle size has become very important for all types of materials in recent times. Microstructural characterization broadly means ascertaining the morphology of phases, number of phases, structure of phases, identification of crystallographic defects and composition of the phases.

The characterization and manipulation of structures on the nanometer scale by itself, is an increasingly important area of research and development. Surface science has developed as a multidisciplinary field to study the physical and chemical properties of solid surfaces and interfaces. Many techniques have been developed involving particle scattering or emission to probe even the atomic, electronic and vibrational structure of surfaces.

In polycrystalline materials, the morphological parameters of the microstructure such as grain size, pore size and grain boundaries play a very important role in deciding the properties of the product.

The behavior of a particulate system and its physical parameters are highly dependent on its microscopic form. The specific surface area of a

particulate system is so large compared to the bulk material that it leads to many significant interfacial phenomena which consequently determines thermodynamic and kinetic stability of the system and final product performance.

Nanomaterials are single-phase or multiphase polycrystals with a typical crystal size of 1 to 100 nm in at least one dimension. Depending on the dimensions they can be classified into (a) nanoparticles, (b) layered or lamellar structures, (c) filamentary structures, and (d) bulk nanostructured materials [1]. The properties of nano-magnetic materials mainly depend on four features, namely (a) grain size and size distribution, (b) chemical composition, (c) presence of interfaces (grain boundaries, free surface), and (d) interactions between the constituent domains [2].

There are many technologies that have been developed and successfully employed for particle characterization. Among these, microscopy have always been indispensable tool due to the fact that it provide direct images of particles and information regarding size, shape and texture, which can be obtained in high resolution without any inherent assumptions or models.

The particle size estimates of as prepared samples were done using four different tools.

1. Particle size calculations through Scherrer formula.
2. Scanning Electron Microscope (SEM).
3. Transmission Electron Microscope (TEM).
4. Scanning Probe Microscope (SPM).

5.2 POWDER X-RAY DIFFRACTION

The powder X-ray diffraction is based on the principle of random orientation of the crystallites. There should be significant number of grains to assume random orientation. If particle size is larger, the statistics of the particles will be poor. However the very small particles deteriorate the peak shape due to particle size broadening. A proper optimization of these is essential for the proper X-ray diffractions.

Crystallite size can be calculated from analysis of peak broadening. As the particle size decreases the peaks get broadened due to incomplete destructive interference.

The broadening caused by fine crystallites relate to size of the grains by Scherrer formulae.

$$T=0.9\,\lambda/Dp\cos\theta$$

Where T = crystallite size, λ = wavelength, Dp = FWHM, θ = Bragg angle

5.3 SCANNING ELECTRON MICROSCOPE

The Scanning electron microscope (SEM) is the most widely used form of electron microscope in the field of materials sciences. SEM is an instrument, which is used to observe the morphology of a sample at higher magnification, higher resolution and depth of focus compared to an optical microscope. Herein, an accelerated beam of mono-energetic electrons is focused on to the surface of the sample and is scanned over it on a small area. Several signals are generated and appropriate ones are collected depending on the mode of its operation. The signal is amplified and made to form a

synchronous image on cathode ray tube, the contrast resulting from the morphological changes and variation of atomic number over the area probed.

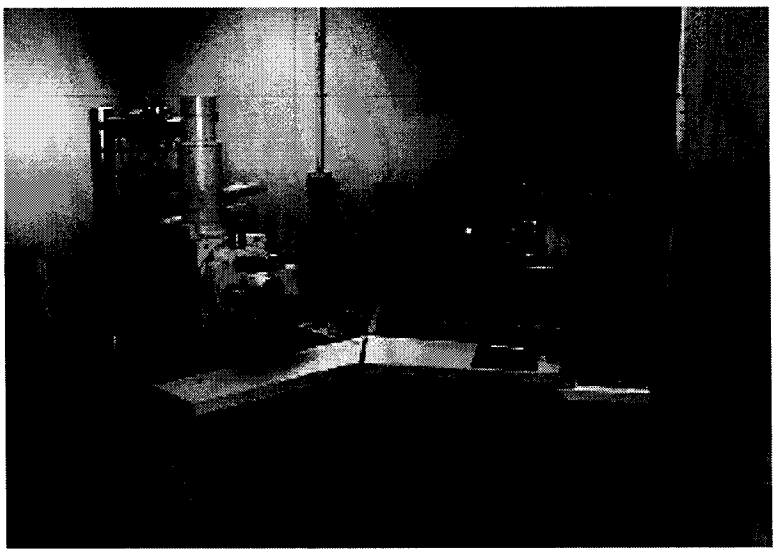

Fig.5.3(a) : JEOL Model 840(SEM)

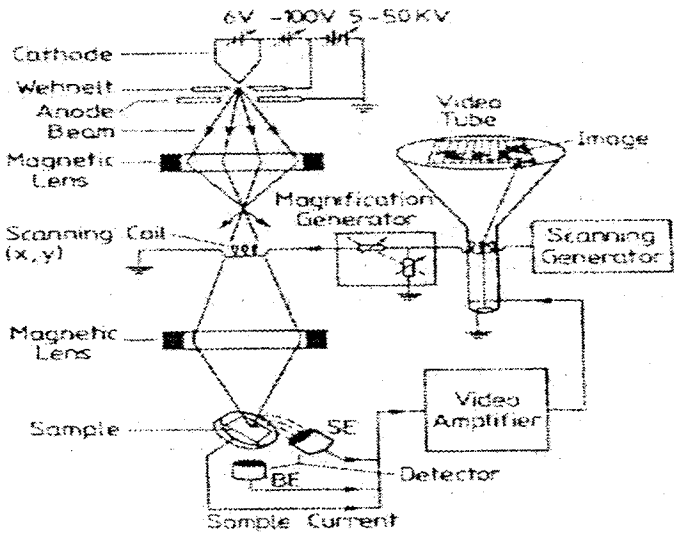

Fig.5.3 (b) : Line diagram of typical Scanning Electron Microscope

A camera is used to photograph the image or it may be digitized and processed on a computer. The characteristic X-rays emitted may be analysed for their energy and intensity energy absorption X-rays (EAX), the energy being the signature of the element emitting them and the intensity as to how much of it is present.

A well-focused mono-energetic (~25KeV) beam is incident on a solid surface giving various signals such as scattering electrons, secondary electrons, Auger electrons and X-rays. The SEM is therefore not restricted to imaging with radiations, which can be focused by lenses and can give many different views of the same specimen. Back-scattered electrons and secondary electrons are particularly pertinent for SEM applications, their intensity being dependent on the atomic number of the host atoms. Each may be collected, amplified and utilized to control the brightness of the spot on a cathode ray tube. To obtain signals from an area, the electron beam is scanned over the specimen surface by two pairs of electro-magnetic deflection coils and so is the C.R.T. beam in synchronization with this. The signals are transferred from point to point and signal map of the scanned area is displayed on a long persistent phosphor C.R.T. screen.

Changes in brightness represent changes of a particular property within the scanned area of the specimen. Some of these signals carry information about the sample which provide clues to its compositions. The performance of the SEM depends on a number of related factors; perhaps the most important is the output of the electron source.

5.4 TRANSMISSION ELECTRON MICROSCOPE

The Transmission Electron Microscope (TEM) has emerged as a powerful tool for probing the structure of metals and alloys. It can give morphological information of shape and size of particles in a microstructure. It can also reveal the nature of crystallographic defects. A detail study of both line defects and planar defects can be carried out in the TEM. Indirect structural information is obtained by making use of the various diffraction techniques available in the TEM. It is capable of yielding composition analysis at nanolevel. With its multifaced capabilities such as nano-beam diffraction and composition analysis and imaging abilities at angstrom level, it has emerged as an instrument for complete characterization of microstructure of materials. TEM's are available in several different forms, which are referred by different acronyms such as HRTEM (High resolution TEM), STEM (Scanning TEM) and AEM (Analytical TEM).

The basic TEM's comprise an electron gun, a vacuum system, electromagnetic lenses, high voltage generator, recording devices and the associated electronics. All TEM's need a source of electrons to illuminate the specimen. In order to get the best images, best diffraction effects and the chemical analysis capabilities, the best available electron source needs to be used. The resolution of the modern TEM is under 0.2 nm (point to point) even with a fair amount of specimen tilt. These microscopes are therefore capable of resolving the structure of different phases in most metals and alloys.

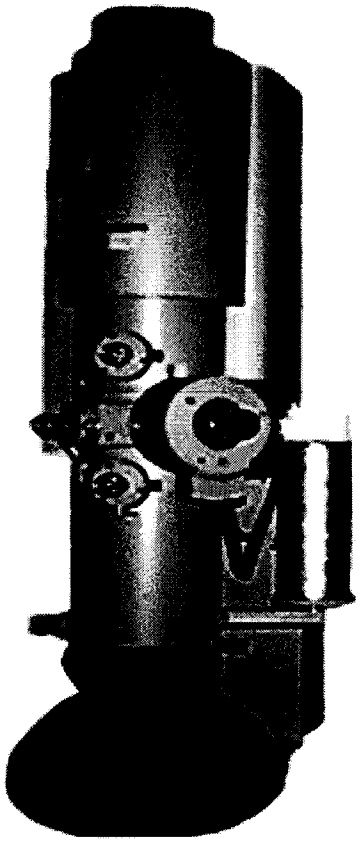

Fig.5.4(a): Philips model CM200 Transmission Electron Microscope

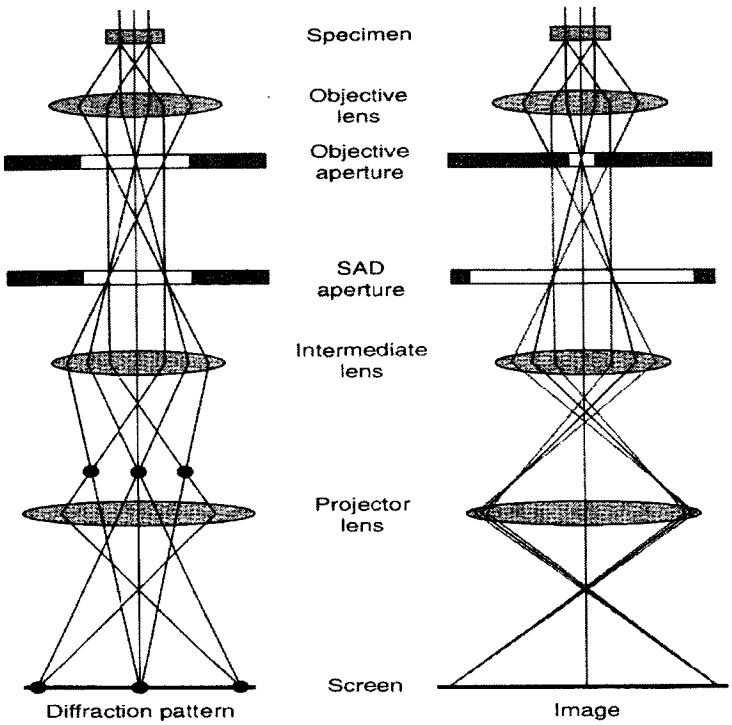

Fig.5.4(b) : Diffraction pattern and image of specimen obtained using TEM

Typically a modern day TEM has about five to six image forming lenses. The final image is projected on the screen. The diffraction pattern forms on the back focal plane of the objective lens and the first image forms on the back plane of the objective lens. If the image forming lenses following the objective lens are excited in such a way that these see the back focal plane of the objective lens as the object then what one sees on the screen is the diffraction pattern. However if the lenses are excited in such a way that these see the back image plane of the objective lens as an object then what we see on the screen is the image of specimen. Therefore in a modern TEM it is possible to switch from diffraction to imaging and vice-versa by changing the excitation of the lenses following the objective lens. TEM can be used to image the specimen by focusing the final image in the plane of the fluorescent screen or it can be used to image the diffraction pattern from the specimen.

Electron diffraction can be explained on the basis of concepts of Reciprocal lattice and Ewald sphere. When combined with the reciprocal lattice concept the Ewald sphere construction gives a very simple way of visualizing electron diffraction. Since the reciprocal of electron wavelength is much larger than the interplanar spacings in the reciprocal space, many reciprocal lattice points are simultaneously intersected by the Ewald sphere-giving rise to many diffracted rays even from a single crystal in case of electron diffraction. The diffraction patterns can be of various types i.e. selected area electron diffraction (SAED), Convergent beam electron diffraction (CBED), Reflective high-energy electron diffraction (RHEED), Low energy electron diffraction (LEED). Diffraction patterns forms the basis of all image formation in the TEM.

5.5 SCANNING PROBE MICROSCOPE

Scanning Probe Microscopes (SPMs) are a family of instruments used for studying properties of materials at localized regions at the surface from the atomic to micron level.

STM and AFM belong to the family of scanning probe microscopes. Scanning probe microscopes are rapidly gaining recognition as powerful tools for research, providing a wealth of information on the nature of solid surfaces, their topography, and their chemical and electronic structure. Among the most important impacts of SPM is in the area of nanotechnology – characterization and manipulation of structures on the nanometer scale. These instruments provide precise surface measurements using a tiny probe positioned in a very close proximity to the surface of the specimen under investigation. The instrument moves the probe across the surface in a controlled fashion, taking measurements at regular intervals. The sensitive probe of the instrument and its precise positional capability enable the SPM to make highly resolved spatial measurements of characteristics such as electron energy states, interatomic distances, magnetic field strengths and directions, thermal conductivity and many other properties.

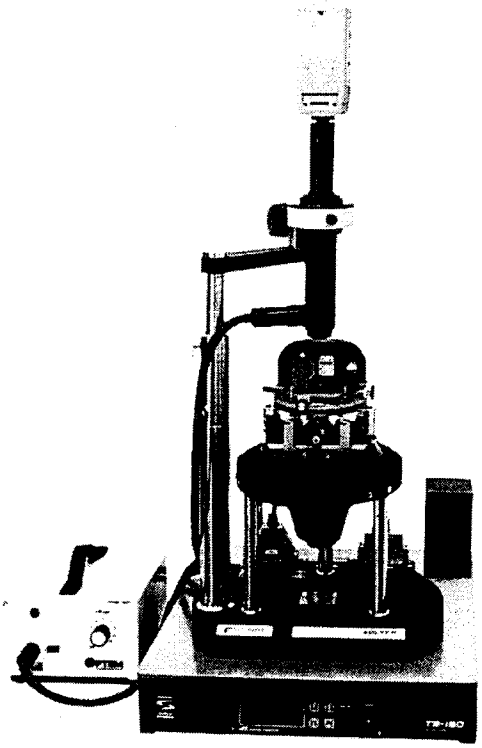

Fig.5.4(a): SOLVER PRO SPM.

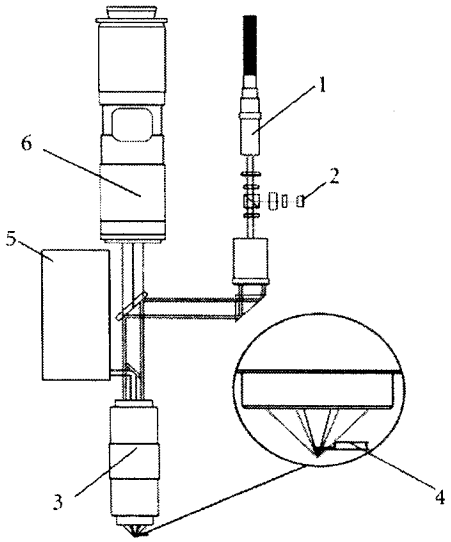

Scheme of the optical head

1 - fiber to the laser
2 - detector
3 - objective
4 - SPM probe
5 - registration system
6 - optical microscope

Fig.5.4 (b): Optical head of SPM

STM uses a sharpened, conducting tip with a bias voltage applied between the tip and the sample. When the tip is brought within about 10A° of the sample, electrons from the sample begin to "tunnel" trough the 10A° gap into the tip or vice versa, depending upon the sign of bias voltage. The resulting tunneling current varies with tip to sample spacing, and it is the signal used to create an STM image. STMs can image the surface of the sample with sub-angstorm precision vertically, and atomic resolution laterally. STMs can be used as surface analysis tools that probe the electronic properties of the sample surface with an atomic resolution.

The atomic force microscope (AFM) probes the surface of the sample with a sharp tip, a couple of microns long and often less than 100 A° in diameter. The tip is located at the free end of a cantilever that is 100 to 200 μm long. Forces between the tip and sample surface cause the cantilever to bend, or deflect. A detector measures the cantilever deflection as the tip is scanned over the sample, or the sample is scanned under the tip. The measured cantilever deflections allow a computer to generate a map of surface topography. AFMs can be used to study insulators and semiconductors as well as electrical conductors. Several forces contribute to the deflection of an AFM cantilever. The force most commonly associated with atomic force microscopy is an interatomic force called Van der Waals force. The Van der Waals force here depends upon the distance between the tip and the sample. There are two distance regimes labeled as contact regime and the non-contact regime. In the contact regime, the cantilever is held less than few angstroms from the sample surface, and the interatomic force between the cantilever and the sample is

repulsive. In the non-contact regime, the cantilever is held on the order of tens to hundreds of angstroms from the sample surface, and the interatomic force between the cantilever and the sample is attractive.

EXPERIMENTAL

Average grain size estimation of as prepared samples were done with the help of

(i) Scherrer Formula calculations using XRD peak broadening obtained on microcomputer controlled Siemens, Rigaku and X-pert PRO Analytical Philips Diffractometer.

(ii) Scanning electron micrographs of powdered samples obtained on JEOL Model 840(SEM), which also provided the surface morphology of the material under investigation.

(iii) Transmission electron micrographs are taken on Philips model CM200 Transmission electron Microscope with resolution 0-23nm having an electron beam of 200KeV.

(iv) Scanning probe micrographs are taken on NT-MDT SOLVER PRO SPM.

5.6 RESULTS AND DISCUSSION

(i) The particle size values obtained for samples $Mn_xZn_{1-x}Fe_2O_4$ using Scherrer formula are listed in table 5.6.1

Table 5.6.1: Particle size for (a) samples prepared by thermal decomposition
(b) samples prepared by microwave decomposition

Conc. of Mn X	Particle size in nm
0.30	7.20
0.35	11.07
0.40	21.46
0.45	4.46
0.50	18.54
0.55	11.07
0.60	25.27
0.65	10.72
0.70	10.10

(a)

Conc. of Mn X	Particle size in nm
0.40	46.38
0.50	38.62
0.60	23.18
0.63	32.04
0.65	41.67
0.67	32.05
0.70	29.75

(b)

Calculations indicate formation of ultra fine particle material with average grain size in the range of 5nm to 25nm for the samples prepared by thermal decomposition whereas for the samples decomposed using microwave technique it is in the range of 20nm to 50 nm. The particle size is found to depend on concentration of Mn in the sample.

(ii) The SEM micrographs of the samples and the particle size analysis made on the same can be seen in Fig.5.6.1 & 5.6.2 (a , b, c, d, e)

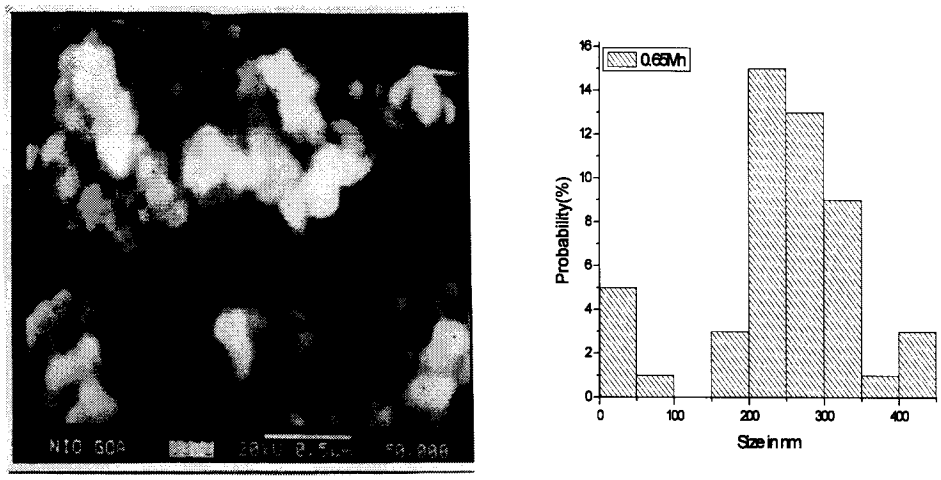

Fig 5.6.1: SEM micrograph and particle size hystogram of powdered sample $Mn_{0.65}Zn_{0.35}Fe_2O_{40}$ prepared by thermal decomposition method.

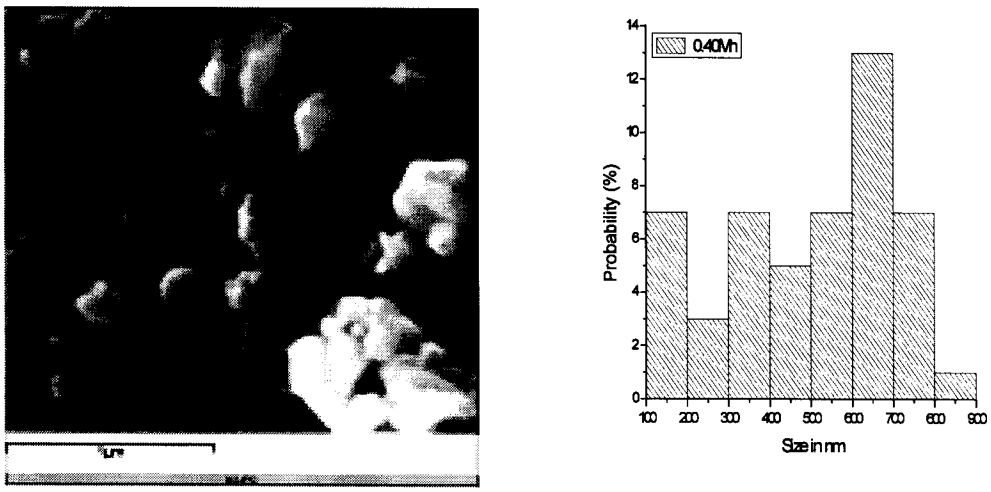

(a)

Fig 5.6.2.a: SEM micrograph and particle size hystogram of sample $Mn_{0.40}Zn_{0.60}Fe_2O_4$ after decomposing by microwave method

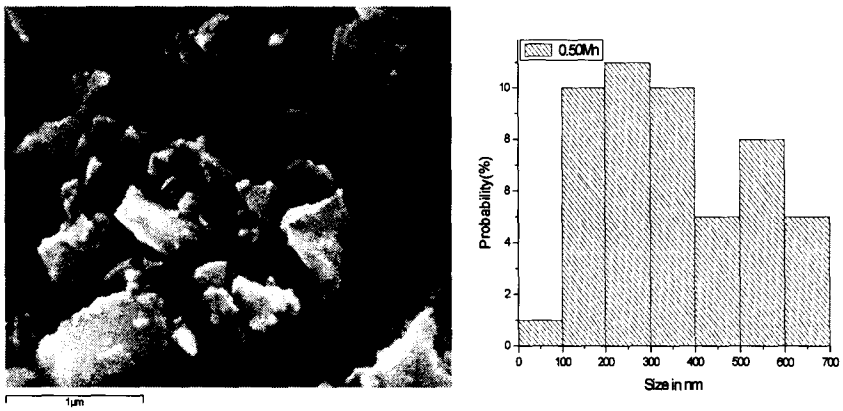

(b)

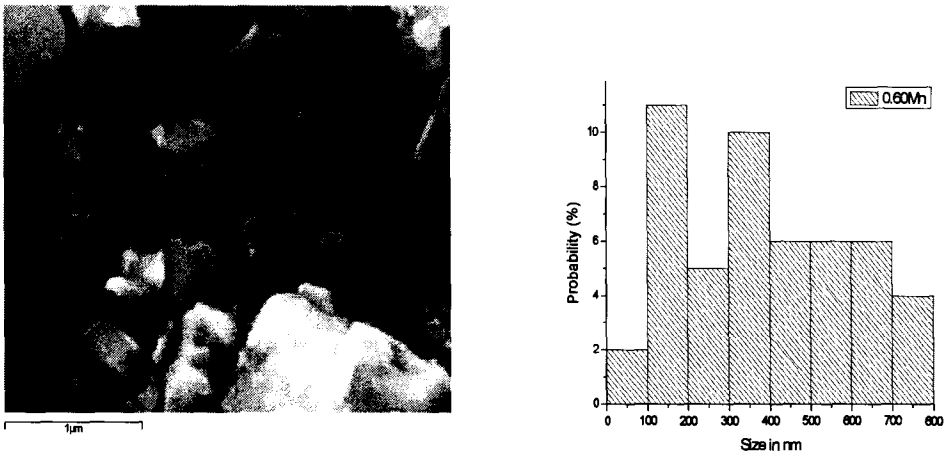

©

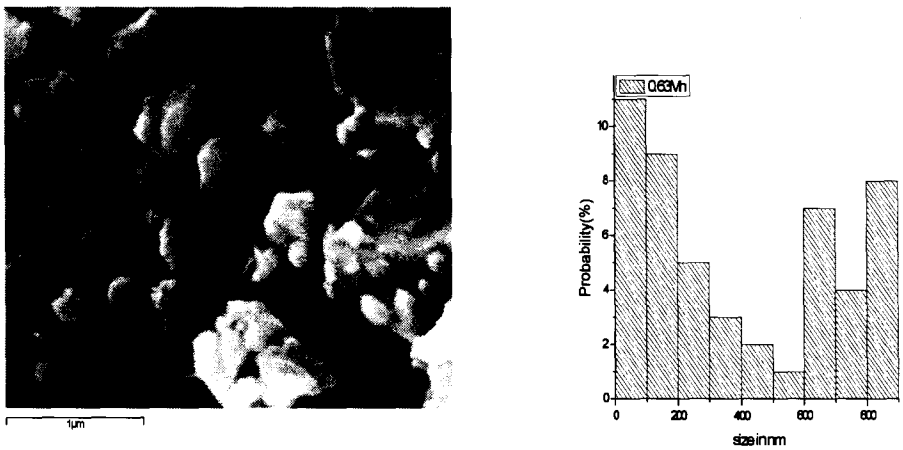

(d)

Fig 5.6.2: SEM micrograph and particle size hystogram of sample obtained after decomposing by microwave method (b) $Mn_{0.50}Zn_{0.50}Fe_2O_4$ (c) $Mn_{0.60}Zn_{0.40}Fe_2O_4$ (d) $Mn_{0.63}Zn_{0.37}Fe_2O_4$

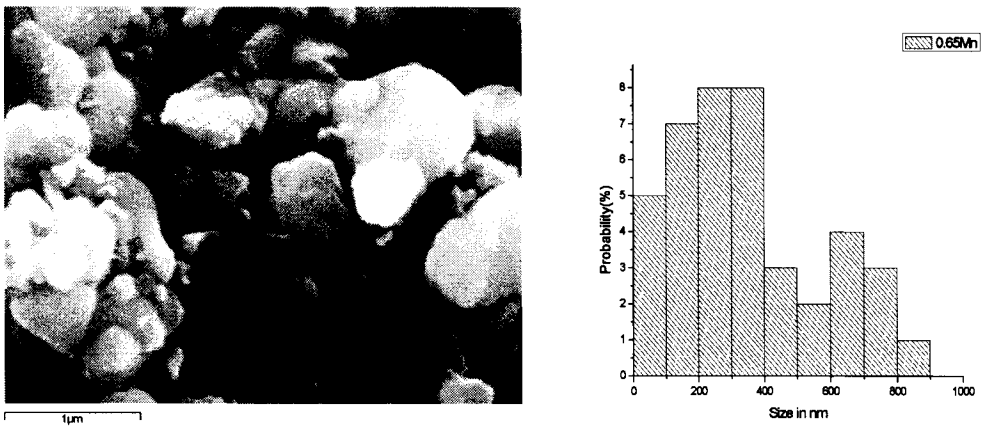

(e)

Fig 5.6.2.e: SEM micrograph and particle size hystogram of sample $Mn_{0.65}Zn_{0.35}Fe_2O_4$obtained after decomposing by microwave method

The size distribution has been determined from the histogram obtained by statistically measuring the size of around fifty individual particles size using SEM micrograph of powdered sample $Mn_{0.65}Zn_{0.35}Fe_2O_4$ prepared by thermal decomposition .It shows a variation of particle size in a range of 5nm to500nm.

The samples decomposed using microwave oven are found to be in the range of 5nm to 900nm. For the sample $Mn_xZn_{1-x}Fe_2O_4$ where x=0.60/0.63/0.65, particles size distribution is in the range of 100nm to 400nm where as for the samples x=0.4/0.5,it is in the range of 100nm to900nm.

(iii) The TEM micrographs of the samples and the particle size analysis made on the same can be seen in Fig.5.6.3 & 5.6.4

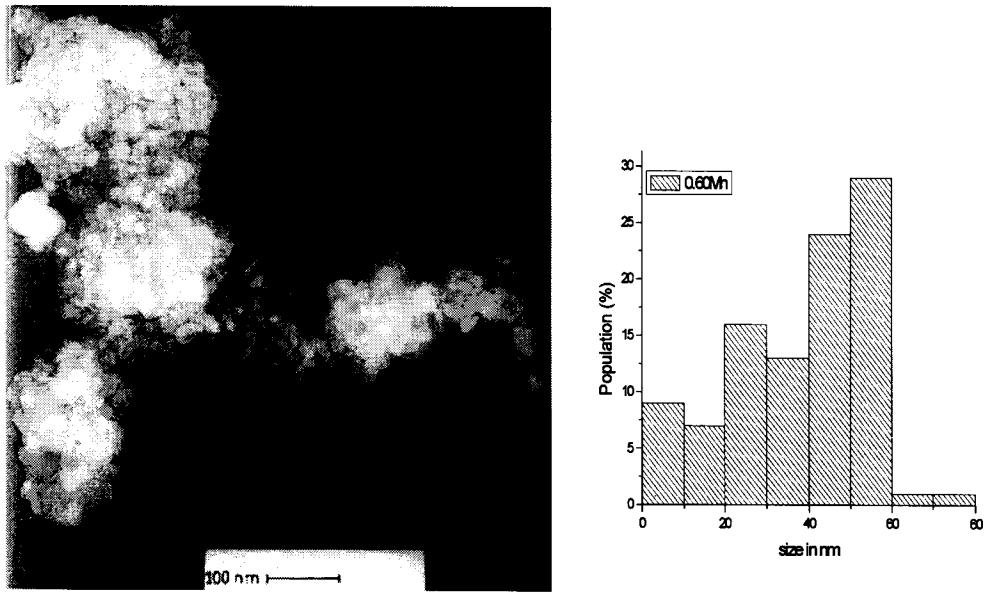

(a)

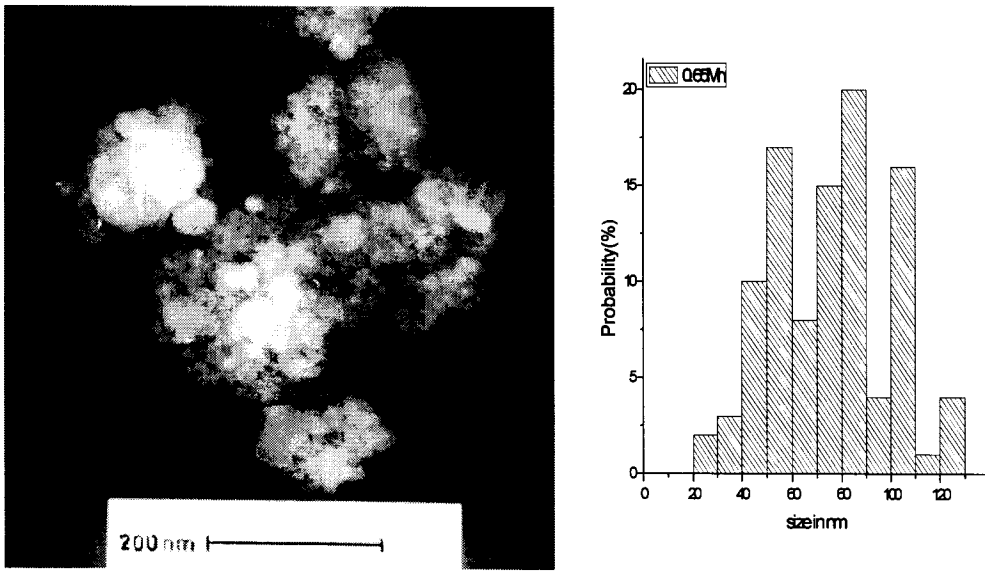

(b)

Fig.5.6.3 : TEM micrograph and particle size hystogram of sample obtained after decomposing by thermal method (a) $Mn_{0.60}Zn_{0.40}Fe_2O_4$ (b) $Mn_{0.65}Zn_{0.35}Fe_2O_4$

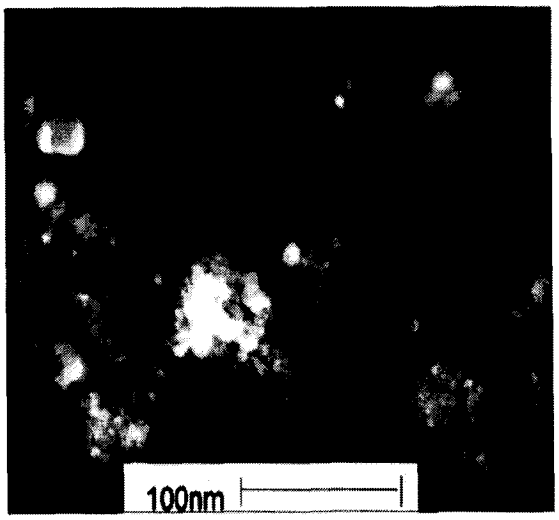

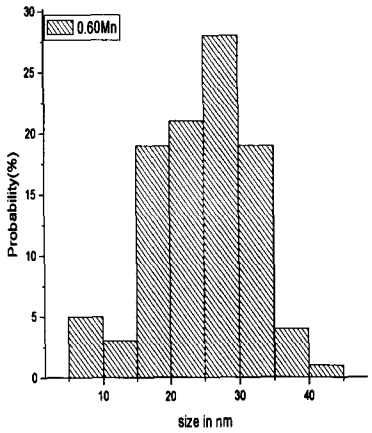

(a)

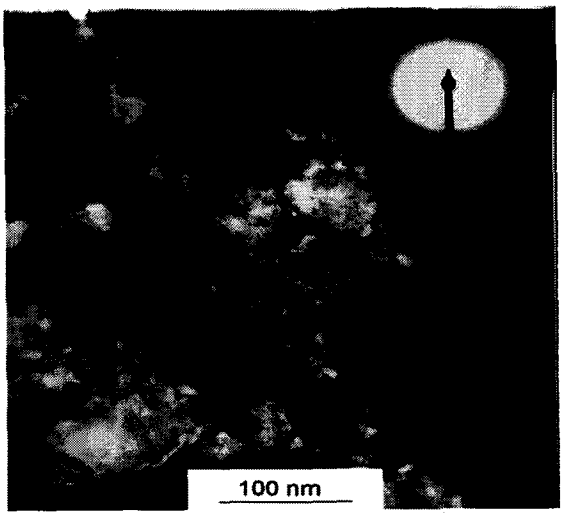

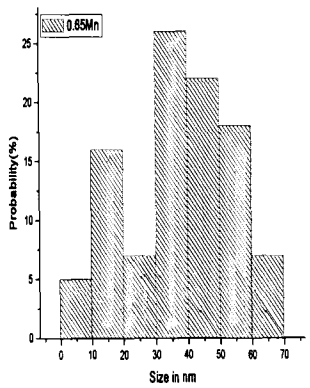

(b)

Fig.5.6.4 : TEM micrograph and particle size hystogram of sample obtained after decomposing by microwave method (a) $Mn_{0.60}Zn_{0.40}Fe_2O_4$ (b) $Mn_{0.65}Zn_{0.35}Fe_2O_4$

High resolution transmission electron microscopy (TEM) has been used to confirm the nanoparticle size and to determine the particle size distribution .the nanoparticles under TEM show a narrow size distribution. The size distribution has been determined from the histogram obtained by statistically measuring the size of around hundred individual particles. From the hystogram of sample $Mn_{0.60}Zn_{0.40}Fe_2O_4$ it is found that the maximum size distribution is in the range of 40nm to 60nm and for the sample $Mn_{0.65}Zn_{0.35}Fe_2O_4$ it is in the range of 50nm to 100nm. For the sample $Mn_{0.60}Zn_{0.40}Fe_2O_4$ prepared using microwave technique the maximum size distribution is in the range of 40nm to 60nm and for the sample $Mn_{0.65}Zn_{0.35}Fe_2O_4$ it is in the range of 50nm to 100nm. The high magnification TEM image shows clearly the lattice fringes of these nanoparticles (inset in Figure 5.6.4)

(iv) The SPM micrographs of the samples and the particle size analysis made on the same can be seen in Fig.5.6.5 & 5.6.6

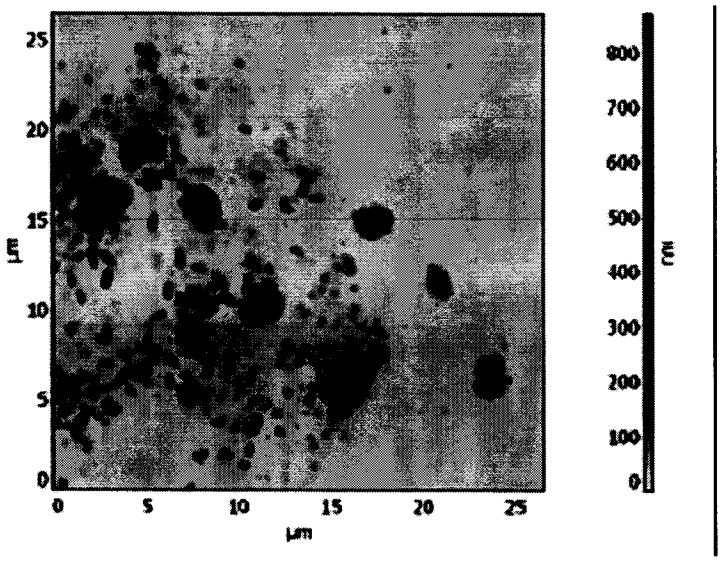

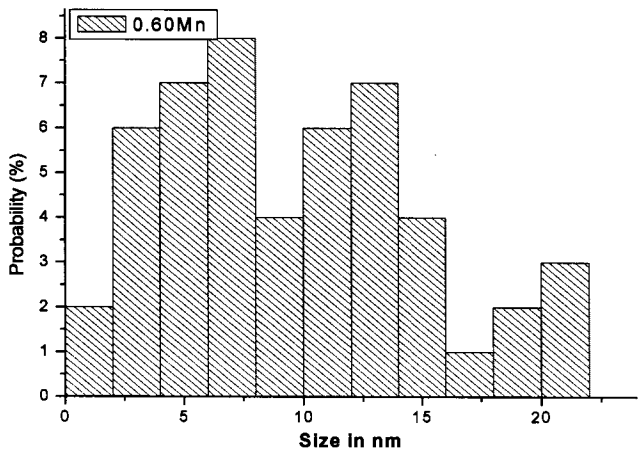

Fig.5.6.5 : SPM micrograph and particle size hystogram of sample $Mn_{0.60}Zn_{0.40}Fe_2O_4$obtained after decomposing by microwave method.

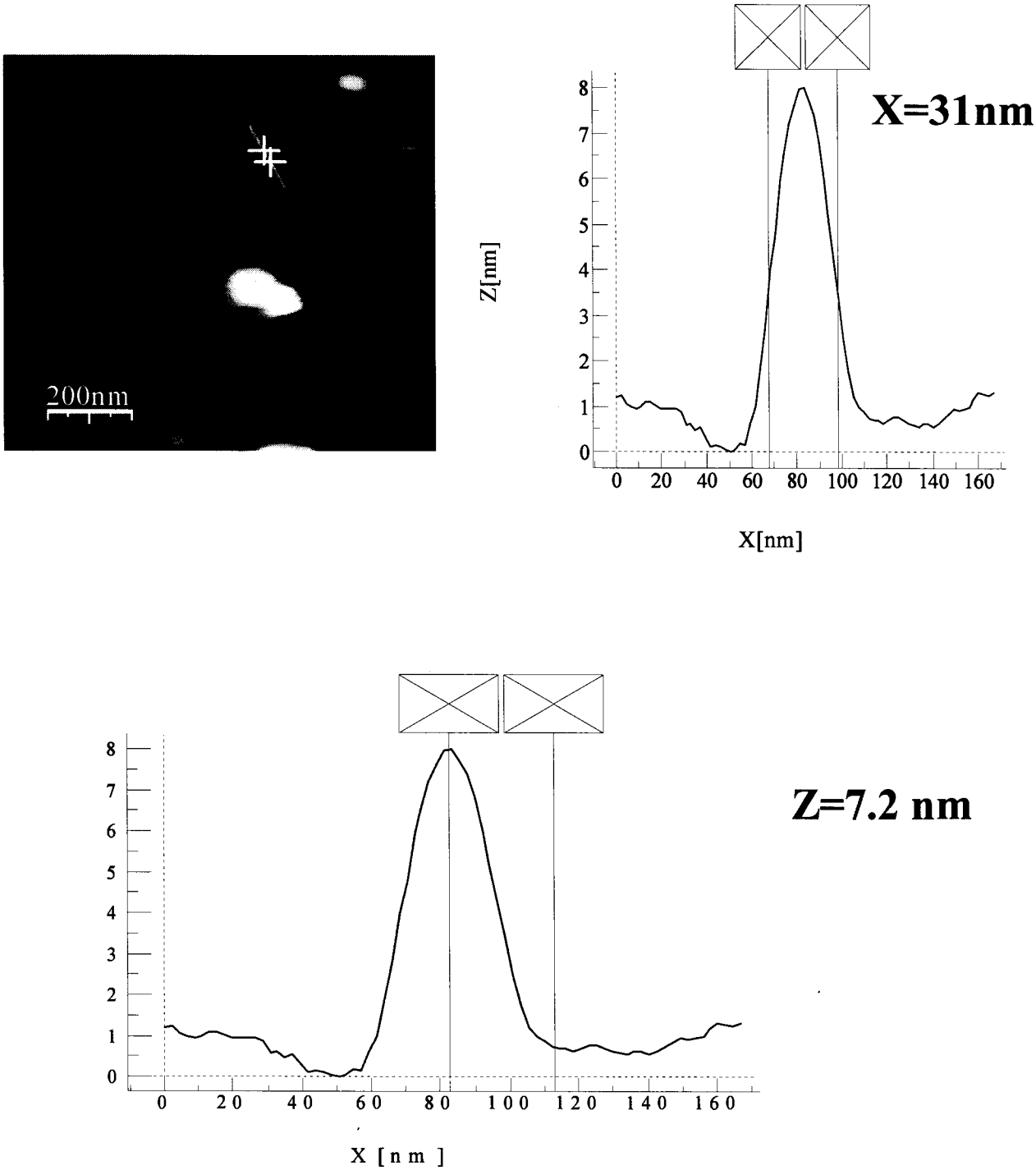

Fig.5.6.6: SPM micrograph and particle size hystogram of sample $Mn_{0.65}Zn_{0.35}Fe_2O_4$obtained after decomposing by microwave method.

The size distribution has been determined from the histogram obtained by statistically measuring the size of around fifty individual particles. From the hystogram of sample $Mn_{0.60}Zn_{0.40}Fe_2O_4$ it is found that the maximum size distribution is in the range of 5nm to 25nm. Scanning Probe Micrographs of sample $Mn_{0.65}Zn_{0.35}Fe_2O_4$ provided the information of particle size in two dimensions (Fig.5.6.6) shows the particle size below 10nm in one of the dimensions for one sample.

Particle size of as prepared sample seen from Scanning Electron Micrographs was found to be larger. However the average particle size of the same sample seen from Transmission Electron Micrograph is in excellent agreement with the particle size estimates made using Scherrer formulae. Particle size analysis carried out on SPM micrographs indicates formation of polycrystalline fine grain material.

Particle size of the as prepared sample seen from SEM micrographs is found to be larger and is not strictly consistent with the calculated values. This difference could be due to the type of probing technique, the energy difference of electron beams and the magnetic interaction between the sample and the scanning electron beam. The ultra fine sample particles were found to show high frequency oscillations when the electron beam in the scanning electron microscope while scanning the material.

References

[1] A. K. Dua, SEM & EDAX, Proceedings of National Workshop on Advanced Methods for Materials Characterization (NWMC – 2004).

[2] R. W. Cahn, P. Haasen, E. J. Kramer, Material Science and Technology Vol.2A ,VCH-Weinheim-Newyork.

[3] R. W. Cahn, P. Haasen, E. J. Kramer, Material Science and technology Vol.2B , VCH-Weinheim-Newyork.

[4] P.J. Goodhew and F. J. Humhreys, Taylor and Francis, Electron Microscopy and Analysis, London,(1988).

[5] D. B. Williams and C. B. Carter, Transmission Electron Microscopy, Plenum Press, Newyork, (1996).

[6] R. Pinto, Scanning Probe Microscopy, Proc. of National Workshop on Advanced Methods for Materials Characterization (NWMC – 2004).

[7] David Brandon and Wayne D. Kaplan, Microstructural Characterization of Materials, John Wiley & sons. New York, (2001).

Chapter VI

MAGNETIC PROPERTIES

6.1 INTRODUCTION

All materials display some magnetic response, however most effects are very small. Magnetism originates from the movement of electric charges. The electrons in an atom govern magnetic properties of matter in two different ways. The first is the electron acting as a spinning charged sphere, where the spin resembles the magnetic field of a tiny bar magnet. The spin is a quantum mechanical property and can be oriented in one of two directions, in the .up. (↑) direction or the .down. (↓) direction. The second is the effect of the electron circulating around the nucleus of the atom, which resembles a current loop [1]. The flow of charge in a circular current loop produces magnetic lines of force known as a dipole [2]. In a bar magnet the magnetic force lines flow around the dipole from north to south as depicted in Figure 6.1.

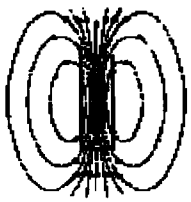

Figure 6.1 Magnetic field lines in a bar magnet

The magnetic moment of a material is the measure of the strength of the dipole. An electron in an atom has a magnetic moment due to its spin and orbital motion.

An orbiting electron's response to an applied magnetic field is governed by the spin configuration of the material. The orbital motions of electrons create atomic current loops, which generate the magnetic field. Therefore, all materials inherently possess magnetic fields generated by the orbital motions of their electrons.

6.2.1 Magnetization Terms

The quantities of magnetism are defined by fundamental concepts of magnetic dipoles consisting of equal and opposite moments. Free currents generate fields classified in terms of magnetic field strength or intensity (H) [3]. The magnetic induction (B) of a material is a function of H and the magnetization or polarization (M) (Equation 6.2.1.1).

$$B=H + 4\pi M \text{ ----------} \qquad (6.2.1.1)$$

The magnetization (M) can be understood as the density of net magnetic dipole moments (μ) in a material (Equation 6.2.1.2).

$$M = \mu \text{ total/ V----------} \qquad (6.2.1.2)$$

The 4π factor in Equation 6.2.1.1 originates from the unit field created by a unit polar on the surface of a sphere of 1 cm radius, which encloses the pole with a surface area of 4π cm2 [4, 5]. The magnetic susceptibility (κ) is a measure of the effectiveness of an applied magnetic field for inducing a magnetic dipole in the

material. Magnetic permeability (μ) is a ratio of the magnetic induction and magnetic field strength (Equation 6.2.1.3).

$$\kappa = \frac{M}{H} \qquad \mu = \frac{B}{H} \qquad \text{----------6.2.1.3}$$

If a material does not respond to an applied magnetic field the magnetic permeability is simply the magnetic permeability of space (μ_0), where

$\mu_0 = 4\pi \times 10^{-7}$ Tesla-m/A.

6.2.2 Magnetic Domains

The aligned spin arrangements in ferromagnetic, antiferromagnetic and ferromagnetic materials are subdivided into regions (domains) throughout the bulk material. Weiss proposed that the driving force for formation of magnetic domains is to minimize the field energy of a magnetized material. The balance of the energy necessary to form a domain wall and the energy conserved by the existence of domains defines the lower limit of a domain size and therefore domain formation is a finite process. The size of a domain is approximately 0.05 to 0.5 μm and is dependent on the intrinsic properties of each material [6]. The boundary between two neighboring domains is a domain wall, which consists of a rotation of the direction of the magnetic moment between discrete domains. Figure 6.2.2 Domain wall [7].

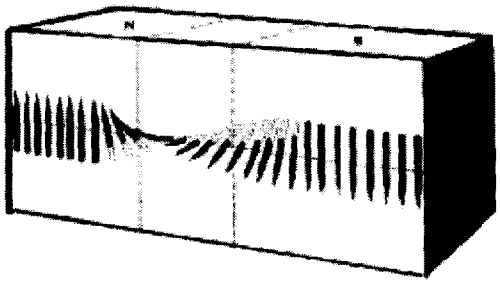

Figure 6.2.2 Domain wall

6.2.3 Hysteresis

In an unmagnetized ferromagnetic or ferrimagnetic material the collections of parallel spins in a domain are randomly oriented throughout the material and therefore collectively self-cancel resulting in a minimal to zero net magnetization. When placed in the presence of a sufficiently large external magnetic field, the spins in each domain rotate parallel to the direction of the applied magnetic field until all the dipoles are aligned. The plateau region of the magnetization curve is the saturation magnetization (Ms) (Figure 6.2.3). Ms is a measure of the magnetization (M) per gram basis and is given by

$$Ms = M/\rho \{emu/g\} \text{ ---------- } 6.2.3.1$$

where ρ is the density of the material (Equation 6.2.3.1). The smooth curve depicts the rotation of the vector moment in the domain wall as the magnetic field strength (H) is varied, actually occurs in very small jumps and is referred to as the Barkhausen effect [3].

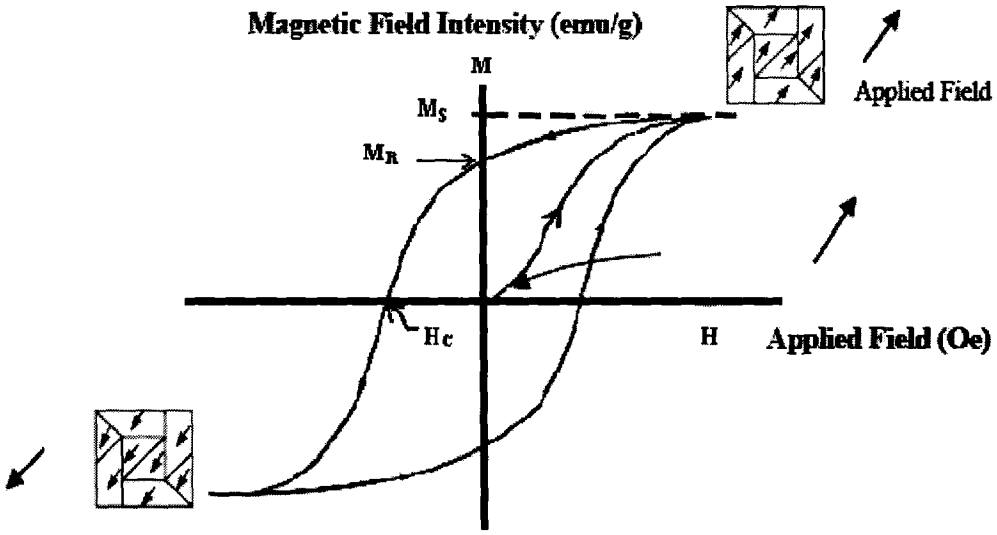

Figure 6.2.3 Magnetization (M) versus magnetic field strength (H) where Ms is the saturation magnetization (M_R) is the remanence magnetization, and Hc is the coercivity.

When the applied field is decreased magnetization decreases. In multi-domain bulk materials, demagnetization occurs primarily via spin rotation through the domain walls [2,7]. If the demagnetization curve, during the removal of the applied field, does not follow the initial magnetization curve, the material displays hysteresis, which is the lag observed in Figure 6.2.3.

Remanence magnetization (Mr) is the magnetization remaining at zero applied field (H = 0,). The magnetic field applied in the negative direction required to return the magnetization to zero is the coercive force (Hc) [8].

6.2.4 Magnetic Anisotropy

A magnetic material can be magnetized in any direction. The dependence of magnetization on the direction of magnetization is known as magnetic anisotropy.

The energy associated with the alignment of spins is described in its simplest form as a uniaxial system given by equation

$$E_a = K \sin^2\theta \quad \text{---------- 6.2.4.1}$$

where K is the magnetic anisotropy energy constant and θ is the angle between M_S and the easy axis. The easy axis of a crystalline specimen is the preferred direction of the total magnetization of the dipoles of a given material [3]. Magnetocrystalline anisotropy is derived from spin-orbit coupling, which is an intrinsic property dependent on the crystallographic orientation of the sample and is independent of particle shape [8]. The magnetic susceptibility is greatest when the saturation magnetization is induced along the easy axis of a material. Shape anisotropy is the effect of the induced magnetization on the physical shape of the specimen and is a significant factor for nonspherical materials [3].

6.2.5 Magnetic Properties of Small Particles Single Domain Particles

The width of a domain wall is a function of the magnetocrystalline anisotropy, the exchange energy and lattice spacing of the crystal structure. The domain wall is approximately a few hundred angstroms thick [9, 10]. As the particle size decreases, the number of magnetic domains per particle decreases

down to the limit where it is energetically unfavorable for a domain wall to exist [11, 12].

In 1930 Frenkel and Dorfman first formulated theories regarding the single domain nature of particles below a critical diameter in 1930 [13]. In this critical size range the nanoparticles are single domain materials. In the presence of an applied magnetic field, the spins orientation and subsequent magnetic saturation is achieved with lower field strengths than with the analogous bulk materials. The magnetic moment of each particle is ~105 times larger than for transition metal ions and saturation magnetization is reached at applied magnetic fields as low as 1 kOe [14]. When the field is decreased, demagnetization is dependent on coherent rotation of the spins, which results in large coercive forces. The large coercive force in single domain particles is due to magnetocrystalline and shape anisotropies for nonspherical particles. The coercive force is also dependent on particle size as shown in Figure 6.2.5.1

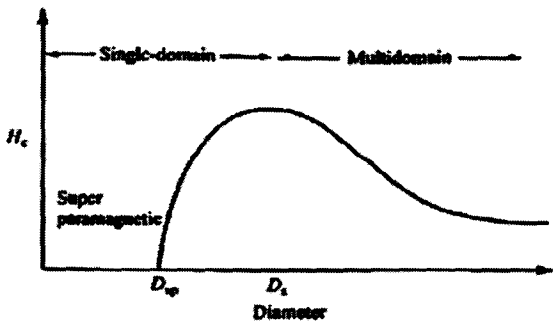

Figure 6.2.5.1 Coercivity as a function of particle sized (Dsp is the superparamagnetic size and Ds is the single domain particle size)

As particles the size of these single domain particles decreases, the coercive force decreases. Moreover, the shape anisotropy increases as the aspect

ratio of a particle increases. Therefore, elongated single-domain particles (Figure 6.2.5.1) can display large coercive forces [11,12].

Superparamagnetism

The magnetic anisotropy, which keeps a particle magnetized in specific direction, is generally proportional to the volume of a particle [15]. As the size of the particle decreases, the energy associated with the uniaxial anisotropy (K) decreases until thermal energy is sufficient to overcome any preferential orientation of the moment in the particle. A single domain particle that reaches magnetization equilibrium at experimental temperatures in short times relative to the measurement time is commonly referred to as superparamagnetic. (Figure 6.2.5.2) [11].

Figure 6.2.5.2: Domain structures observed in magnetic particles:
a) superparamagnetic b) single domain particle c) multi-domain particle

6.2.6 Magnetostriction

Magnetic materials experience changes in dimensions during magnetization .This phenomenon is related to the thermal anomalies shown by ferromagnetic substances around Curie point. For cubic materials, the changes in dimension are isotropic i.e. only volume changes, but for hexagonal ferrites the change of volume and shape is observed. These changes occur even when the

material is cubic but the magnetic order in non-cubic. This phenomenon is due to the dependence of exchange energy on inter-atomic spacing.

6.2.7 Low Field and Low Temperature Magnetization Measurements Using SQUID

Superconducting Quantum Interference Device (SQUID) is the most sensitive device for magnetic field detection. The device has been developed for traditional low temperature superconductors requiring cooling with liquid Helium to 4 Kelvin (-269 °C). This measurement device is capable of measuring magnetic fields in the order of femto tesla.

SQUID are the most sensitive detectors of magnetic flux. A SQUID is, in essence, a flux to voltage transducer providing an output voltage i.e. periodic in the applied flux with a period of one flux quantum, $\phi_o = h/2e$ .One is generally able to detect an output signal corresponding to flux change of much less than ϕ_o. SQUID is able to measure any physical quantity that can be converted to flux, ex. magnetic field, magnetic field gradient, current, voltage, displacement and magnetic susceptibility. SQUID combines two physical phenomenon, flux quantization and Josephson tunneling.

6.3 Initial Permeability

The origin of permeability of ferrites has been a subject of research for the last so many years. Basically two processes are responsible for permeability viz.

(i) rotations of domains

(ii) domain wall displacement

It is generally assumed that the initial permeability is caused by the reversible displacement of the domain walls, the contribution of rotation of spin inside each domain being negligibly small on account of relatively high crystal anisotropy. In polycrystalline ferrites, due to sintering, certain amount of pores are present. In such a structure, domain walls will extend from pore to pore so that they are not free to move. These pores have a considerable demagnetizing effect, which leads to rather intrinsic pattern of Weiss domains. Hence it is impossible to say in advance which kind of magnetization process will give the predominant contribution to the initial permeability.

For the reversible rotational process, Chikazumi [16] has given the permeability as

$$(\mu-1) = (\text{constant})\, Ms^2 \sin\theta / K1 \text{---------- } 6.3.1$$

where θ is the angle between Ms and μ, for reversible wall processes, permeability is ,

$$(\mu-1) = (\text{constant})\, Ms^2 S/\alpha \text{ ----------} 6.3.2$$

where S= wall surface area

α =Second order derivative of wall energy with respect to wall displacement.

At low frequency domain wall motion is a dominant mechanism. The second source of initial permeability viz. domain rotation is largely responsible for the high frequency permeability.

6.3.1 Models of Permeability

(i) Globus Model

Globus [17,18] has developed a model in which the initial permeability is mainly due to the reversible motion of domain walls under a very small magnetic field and contribution of the spin rotation is rather negligible. In this model the domain wall is pinned at the grain boundaries and they bulge under the application of magnetic field until the critical field is reached when the wall gets unpinned. In such a model

$$(\mu_i - 1) = 3\, Ms^2 D/16\gamma \text{ ---------- } 6.3.1.1$$

where Ms is saturation magnetization ,D is grain diameter and γ is domain wall energy per unit area as $\gamma \sim \sqrt{AK_1}$

$$\mu_i = Ms^2 D/|K_1| \text{ ----------} 6.3.1.2$$

Such a model can be extended to the case where the domain walls are pinned at intergranular pores i.e. span of domain wall.

Globus and co-workers [18, 19] realized that in polycrystalline ferrites the magnetization mechanism might be different due to granular structure of ferrites. They developed a model in which domain wall bulging of 180° instead of domain wall displacement is responsible for the initial permeability.

In another model they [20,21] used the existence of easy axis in each grain, the domain walls, under the influence of flux forces, tend to align themselves along the director circle as best as they can in order to minimize the demagnetizing field.

(iii) Non Magnetic Grain Boundary Model

The non-magnetic grain boundary model has been developed by Johnson[22]. This model can account for the entire grain size dependence of μ_i at low anisotropy as the Globus model cannot account for grain size dependence of permeability when intergranular domain walls are absent. This model describes the grain size dependence of rotational permeability in polycrystalline materials [23]. According to this model there is almost linear dependence of permeability on grain size for fine grained polycrystals where $D << \mu_i \delta$.

It is given by the relation

$$\mu_e = \mu_i D / (\mu_i \delta + D) \text{ ----------6.3.1.3}$$

where μ_e = effective permeability, μ_i = complex permeability ,

D= grain size, δ =grain boundary thickness

For larger grain size where $D >> \mu_i \delta$, the model predicts constant rotational permeability equivalent to that in single crystal of the same material i.e. $\mu_e \sim \mu_{is}$.

(iv) Two Pinning Model

In this model it is assumed that a component that varies with spatial co-ordinates along the grain boundary is responsible for permeability [24-27]. The microstress origin is due to disorientation of magnetic axis of the grains and their sources are located on the grain boundary. As a result of alternation of the region with best and worst coincidence on grain boundary, the magnetostrictional deformation creates the inhomogeneous stress along grain boundary. Thus domain wall is linked near grain boundary with the regions of increased anisotropy.

$$\Delta K = (| K| - | K_1|) \text{ ----------6.3.1.4}$$

6.3.2 Dependence of Initial Permeability

(i) Temperature Dependence

Temperature dependence of initial permeability is many times an important parameter in a magnetic component. From the graph of variation of initial permeability with temperature, the slope at a specific temperature can be expressed as a material parameter called the temperature factor which is defined as

$$Ti = \Delta T/ \Delta \mu_i^2 \text{ ----------6.3.2.1}$$

Where $\Delta \mu_i$ is the difference in permeability at temperatures T_1 and T_2 respectively and ΔT is the change in temperature.

The temperature factor can be used to predict the variation in magnetic properties of a magnetic component. A thermal hysteresis is observed when temperature is cycled from higher temperature above Tc to lower temperature.

This is explained by taking into account the domain wall pinning component between the intrinsic parameter Ms and K_1 around the transition point [28].

(ii) Microstructure Dependence

The initial permeability is dependent on grain size, density and porosity. Porosity causes hindrance to domain wall motion and it is very damaging to initial permeability [29]. Microstructure plays a very important role because of fine grains where there is reversal of magnetization by rotation since the domain walls are energetically favorable in fine grains. Also the coercive force increases with porosity because of internal demagnetizing field where the decrease in permeability is caused by same cause. The larger grain size causes reduction in initial permeability due to presence of voids that induce demagnetizing field and impede domain wall motion. thus the grain size is a very important parameter in the permeability. A duplex structure is undesirable because it lowers the permeability. It is often due to particle impurity, which produces rapid growth locally while other impeded areas are unaffected [13, 30].

(iii) Frequency Dependence

At low frequencies the domain wall motion is dominant mechanism and permeability is almost independent of frequency. The domain structure is responsible for high frequency permeability. At low frequencies, the applied field causes domain wall shift and this motion results in change in net magnetization. At high frequencies, the domain wall inertia precludes any appreciable wall motion but the mechanism can rotate within each domain. This mechanism is

same as ferromagnetic resonance. Smit and Wijn [31] have explained the extension of the loss over a relatively broad frequency region in terms of additional effects upon the resonance condition due to demagnetizing field in the domain structure.

6.4 A.C. Susceptibility

Curie temperature is one of the important parameters of any ferrite system. The ferrimagnetic materials show quite resemblance in their magnetic properties to those of ferromagnetic class. These materials show hysteresis and susceptibility below transformation temperature i.e. Curie temperature. It is intrinsic property of the spinel ferrites, which can be controlled by preparation conditions, sintering temperature and doping of additives [32]. The microstructure, porosity and grain size play dominant roles in deciding the a.c. susceptibility. A.C. Susceptibility studies explore the existence of multidomain (MD), single domain (SD) and super paramagnetic particles in the material. From the susceptibility curves, the Curie temperature and domain structure can be estimated.

The different magnetic properties of Mn-Zn ferrite samples prepared by both thermal decomposition technique and microwave decomposition technique viz Saturation magnetization, hysteresis loss, initial permeability, a.c. susceptibility, were studied.

6.5 EXPERIMENTAL TECHNIQUES

6.5.1 Saturation Magnetization and Hysteresis Loss

Sample preparation for measurement

Fine powders of samples $Mn_x Zn_{1-x} Fe_2 O_4$ obtained by both methods of decomposition were pressed into pellets of the size 10mm diameter and of thickness ranging between 2mm to 3mm under a pressure of 75KN applied for 3 minutes. Five sets of pellets were sintered in nitrogen atmosphere at temperatures, 950°C, 1050°C, 1150°C, 1250°C and 1350°C respectively for 3 hours separately in a programmable carbolite furnace by setting heating and cooling rate at 5 °C per minute.

The saturation magnetization and hysteresis loss measurements on the samples were carried out using a high field hysteresis loop tracer described by Likhite et al [33] and supplied by Arun electronics, Mumbai India. This instrument consists of three major parts, electromagnet, pick-up coil and balancing and integrating circuits.

The high field hysteresis loop tracer consists of an electromagnet working on 50Hz mains frequency. The alternating magnetic field of about 3600 Oersted is produced in an air gap of about 1 cm, in the instrument and a special balancing coil is used to measure the saturation magnetization of the sample in the air gap. Depending upon the magnetic induction in the specimen, pick-up coil produces a field proportional to the magnetic induction of the specimen. A supporting coil produces a signal which is equivalent to the strength of the magnetic field. When

the respective signals are supplied to the vertical and horizontal plates of an oscilloscope, it displays a hysteresis loop on the screen.

A digital AC voltmeter, which connected to the output, displayed the RMS value of the signal proportional to the saturation magnetization of the sample. The calibration of the instrument was carried out using pure nickel as a standard substance having magnetization of 53.34 emu/g.

Hysteresis loss was calculated by measuring the area of the loop.

Magnetic measurements were also carried out using vibrating sample magnetometer (VSM) OXFORD (Oxford Instruments) MagLabVSM and EV series VSM model EV-5 from ADE US. Retentivity and coercivity was also obtained from VSM data.

Temperature and low field dependence measurements MH at 35K upto 5 Tesla & MT at 100 Oe from 1.8K to 300K. were studied by Quantum Design MPMS-xl7 SQUID magnetometer. The Mn-Zn nanoparticles for temperature-dependent magnetization study was cooled from room temperature to 5K under zero magnetic field.

6.5.2 Initial Permeability

Sample preparation for measurement

The fine powders obtained by thermal decomposition were pressed into torroids of height ranging between 3mm. to 4mm. with inner and outer diameters of 1cm and 2cms respectively by application of 75kN pressure for 5mins. The torroids were sintered at 950°C /1050°C /1150°C /1250°C /1350°C in nitrogen atmosphere for 3hrs in a progressive manner. The heating and cooling rate was

fixed at 5°C /min during each sintering. Permeability measurements were carried out after each temperature sintering. A fresh new winding of 100 turns of super enameled doubly insulated copper wire of guage 33 was wound on each torroid after each temperature sintering to carry out initial permeability (μi) and loss factor measurements as a function of temperature and frequency.

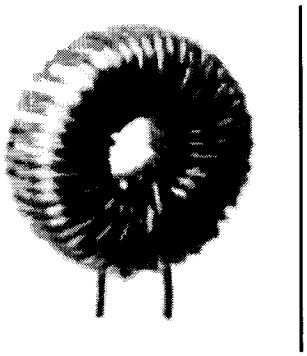

Inductance and loss factor values were recorded starting from room temperature to 500 °C with a frequency variation from 50Hz to1MHz using HP 4284A precision LCR meter.

The initial permeability (μi) was calculated from the formulae

$L=0.0046\mu i\ N^2\ h\ \ln (OD/ID)$

Where L is inductance in Henry, N is the number of turns of copper wire on torroid, h is height of the core in metres, OD is outer diameter of torroid in metres, and ID is the inner diameter of torroid in metres.

6.5.3 A.C. Susceptibility

A.C. Susceptibility measurements of the powdered as well as sintered samples were made using computerized Pulse field A.C. susceptibility apparatus described by Likhite et al [34].

The apparatus consists of Helmholtz coil, two pick-up coils, furnace, sample holder, a temperature measuring device, a control unit, data acquisition system, a power supply to run the furnace and a PC with related software to execute the run cycle. The Helmholtz coil is powered to produce pulsating magnetic field. To avoid over heating of coils, a glass jacket with water circulation was used. The furnace was inserted in glass jacket and was placed at the centre of the pick-up coil. The sample holder was made up of quartz tube fused at one end. The height of the sample holder was maintained at the centre of the coils. The sample of known weight was placed in the sample holder; The data, that is, magnetization (emu/gm) as a function of temperature collected by the data acquisition system is directly saved in a file on the PC which simultaneously shows the progress of the curve. The temperature of the furnace was maintained by a power supply and was measured by using platinum Rhodium thermocouple. The sample was gradually heated and the magnetic moments were recorded at various temperatures. The heating was continued till the magnetization (emu/gm) signal reduces to zero. This happens when curie temperature is achieved.

6.6 RESULTS AND DISCUSSION

6.6.1 Saturation Magnetization

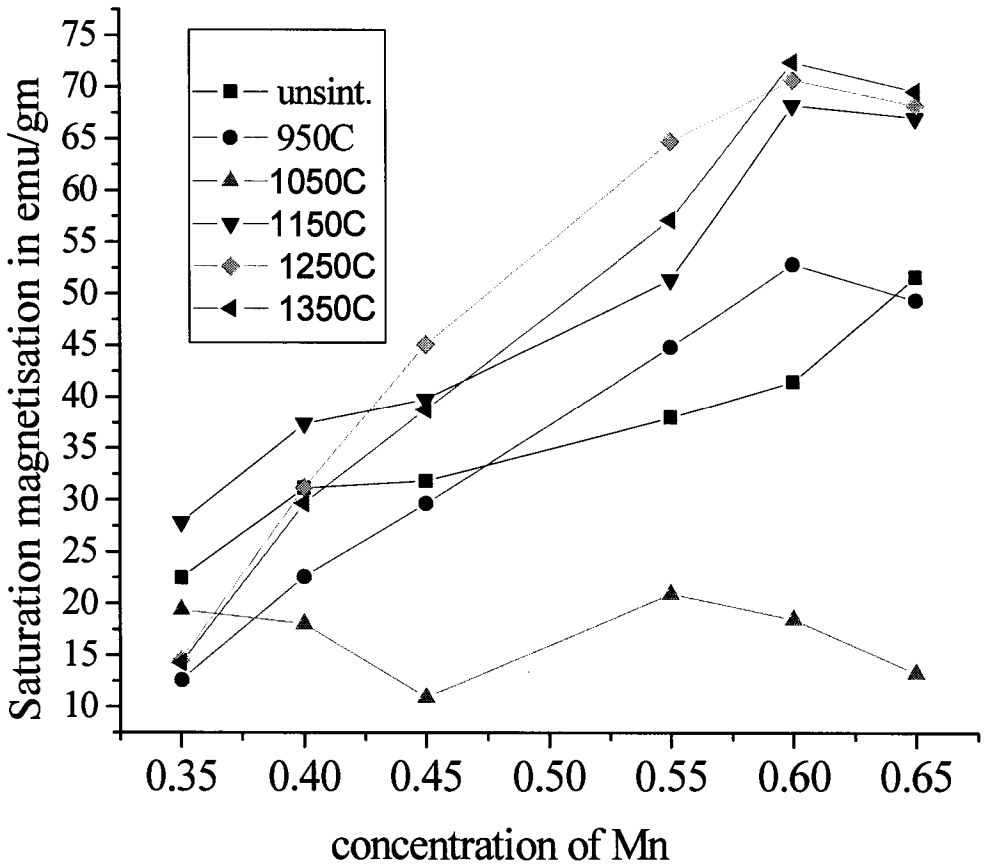

(a)

Fig. 6.6.1.1(a): Variation of Saturation magnetization with conc. of Mn for various sintering temperatures for the samples prepared by thermal decomposition

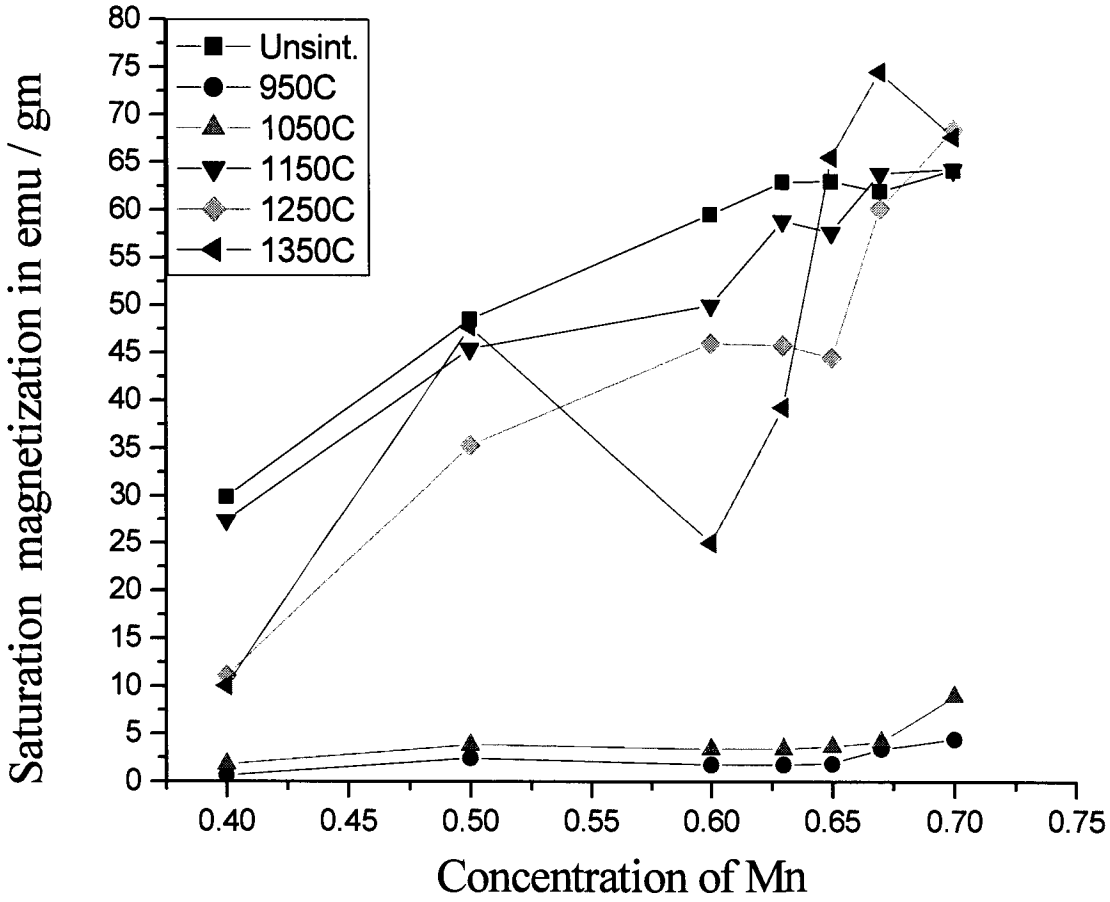

(b)

Fig. 6.6.1.1(b) :Variation of Saturation magnetization with conc. of Mn for various sintering temperatures for the samples prepared by microwave induced decomposition

The saturation magnetization for the samples prepared using thermal decomposition technique Fig 6.6.1.1(a) shows two peaks. A local maximum is found to appear for the sample $Mn_{0.4}Zn_{0.6}Fe_2O_4$ that becomes more prominent for sample sintered at 1150°C, the same is found to shift towards lower concentration $Mn_{0.35}Zn_{0.65}Fe_2O_4$ for sample sintered at 1050°C. The second maximum, which is more prominent, is seen to appear for $Mn_{0.60}Zn_{0.40}Fe_2O_4$ sintered at 950°C, 1150 °C,1250°Cand1350°C; this maximum is found to occur at a lower Mn concentration $Mn_{0.55}Zn_{0.45}Fe_2O_4$ for samples sintered at 1050°C with a dip for $Mn_{0.45}Zn_{0.55}Fe_2O_4$. The unsintered sample shows a maximum value of saturation magnetization, which is 51.63emu/gm for $Mn_{0.65}Zn_{0.35}Fe_2O_4$.

For the samples decomposed using microwave decomposition, the over all values of saturation magnetization for unsintered samples are found to be higher the highest being 63.03emu/g for the sample $Mn_{0.65}Zn_{0.35}Fe_2O_4$. The samples sintered at 950 °C are found to show a very unusual behavior almost all with exception of $Mn_{0.65}Zn_{0.35}Fe_2O_4$ and $Mn_{0.67}Zn_{0.33}Fe_2O_4$ are found to show a ferrimagnetic to paramagnetic phase transition. The ferrimagnetic behavior starts to re-appear in the set of samples sintered at 1050C with a peak appearing at $Mn_{0.63}Zn_{0.37}Fe_2O_4$. This peak is found to shift towards higher Mn concentration in the sample as can be seen in Fig 6.6.1.1(b). The unsintered sample and the sample sintered at 1250 °C and1350°C are found to show two prominent peaks for saturation magnetization. A high saturation magnetization of 74.54 emu/gm is observed for the sample $Mn_{0.67}Zn_{0.33}Fe_2O_4$ sintered at 1350 °C. This is higher as compared to the samples prepared by the thermal decomposition method [35].

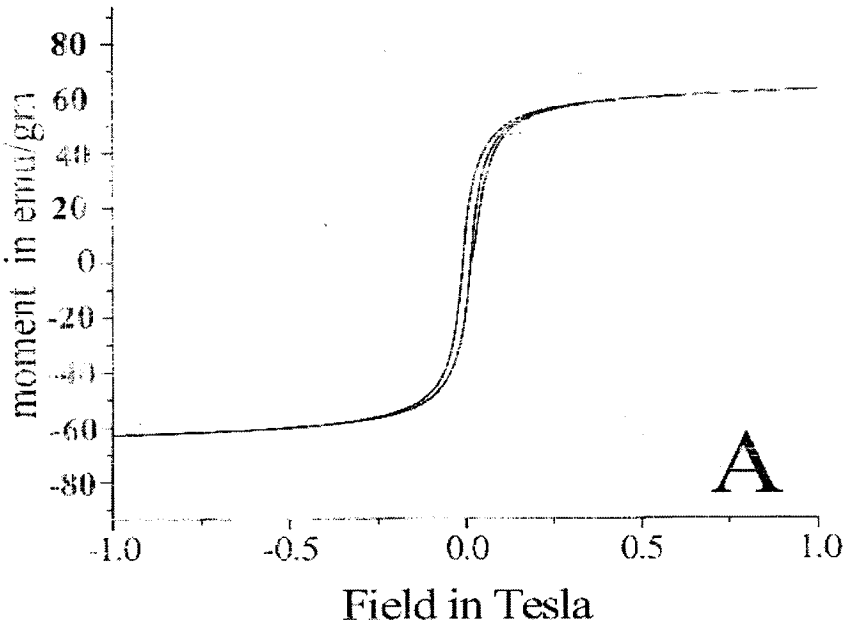

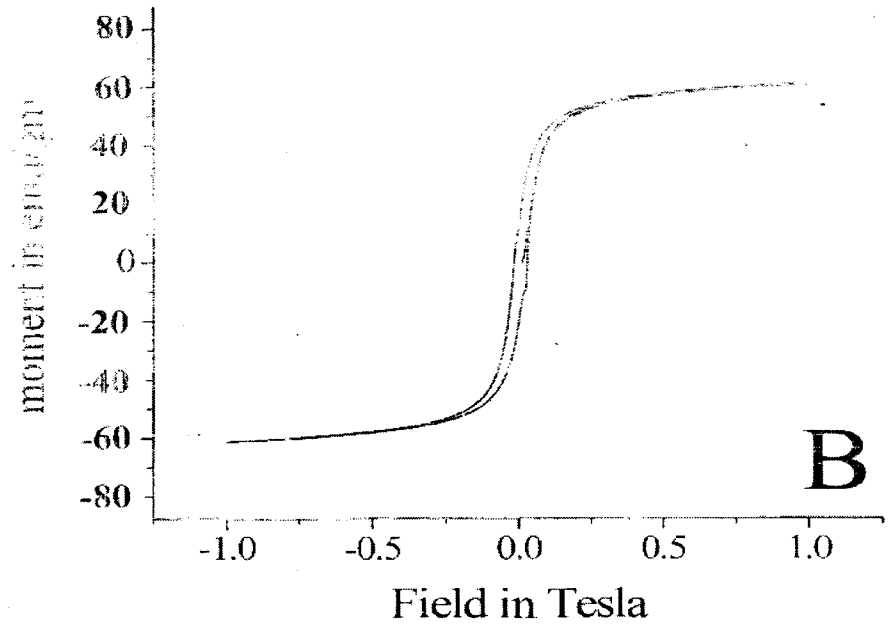

Fig 6.6.1.2.: Shows magnetic hysteresis curves obtained on VSM at room temperature for as prepared samples (A) $Mn_{0.65}Zn_{0.35}Fe_2O_4$ (B) $Mn_{0.67}Zn_{0.33}Fe_2O_4$.

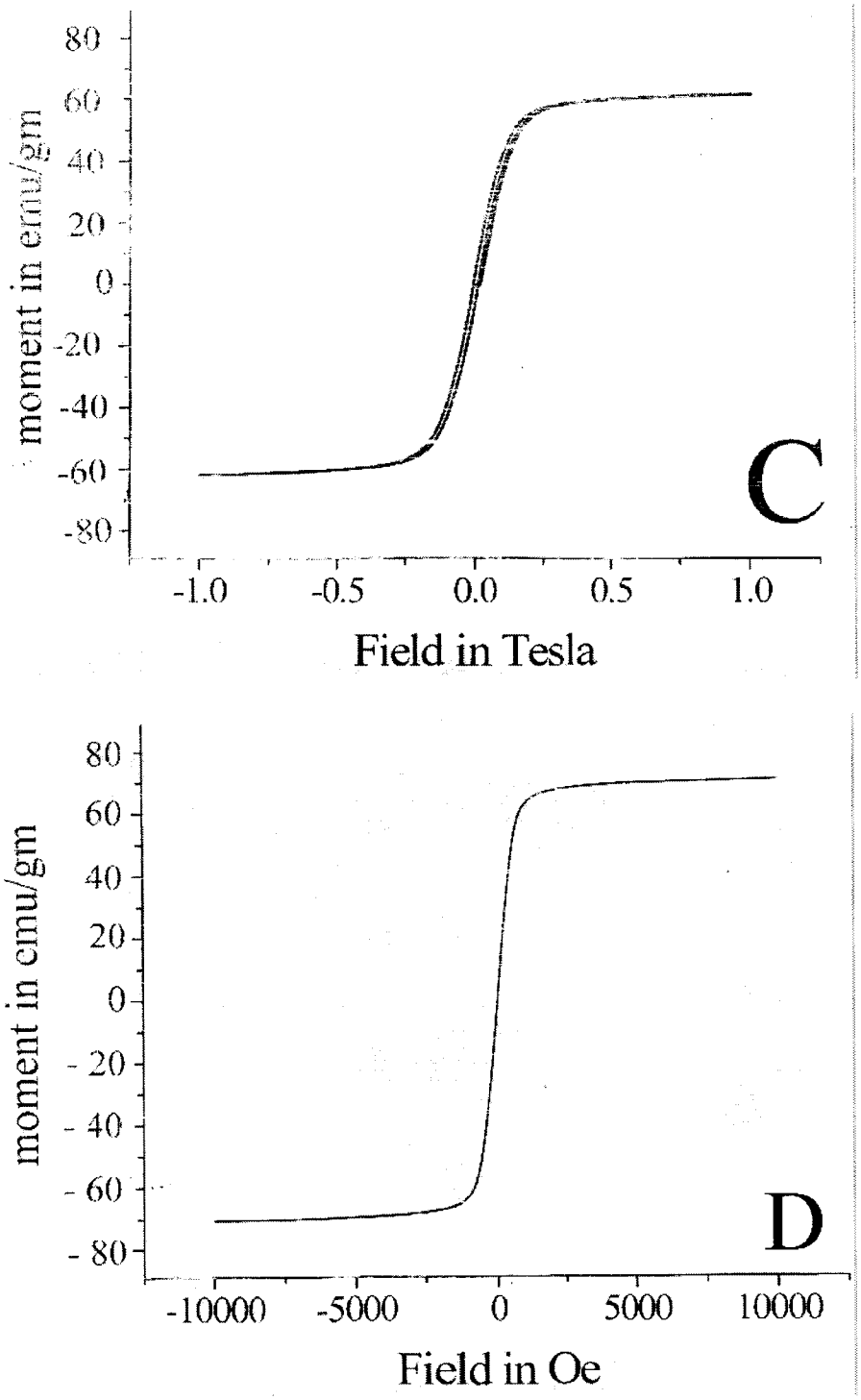

Fig 6.6.1.2.: Shows magnetic hysteresis curves obtained on VSM at room temperature for as prepared samples (C) $Mn_{0.65}Zn_{0.35}Fe_2O_4$ and (D) $Mn_{0.67}Zn_{0.33}Fe_2O_4$ sintered at 1350°C .

Table 6.6.1 Magnetic properties of $Mn_{0.65}Zn_{0.35}Fe_2O_4$ and $Mn_{0.67}Zn_{0.33}Fe_2O_4$ unsintered and sintered at 1350 °C.

Sample $Mn_xZn_{(1-x)}Fe_2O_4$	Sintering temperature °C	Retentivity **Mr** emu/gm	Saturation Magnetization **Ms** emu/gm	Squareness **Mr/Ms**	Coercivity **Hc** Oe
x=0.65	unsintered	30.74	63.20	0.65	86
x=0.67	unsintered	14.33	62.21	0.02	14.6
x=0.65	1350°C	5.3227	64.58	0.0956288	47.2
x=0.67	1350°C	0.1017	72.31	0.0015	1.06

A decrease in coercivity value ***Hc*** and squareness (***Mr /Ms***) is observed for sintered samples as well as for increasing *x* value. This decrease can be attributed to an increase in grain size and decrease in porosity of the sample.

The high values of retentivity ***Mr*** and the coercivity ***Hc*** for unsintered sample $Mn_{0.65}Zn_{0.35}Fe_2O_4$ tend to shows single domain (SD) behavior of the sample whereas the lower values of retentivity ***Mr*** and the coercivity ***Hc*** for unsintered sample $Mn_{0.67}Zn_{0.33}Fe_2O_4$ indicates multi domain (MD) behavior of the sample. MD samples contain more number of domain walls. The magnetization/demagnetization due to domain wall movement requires lower energy compared to that required for domain rotation [36]. Hence ***Mr*** and ***Hc*** values in MD samples are lower compared to SD samples. On sintering the samples the grain size increases and the material is expected to loose its SD behavior. This phenomenon can be seen in sample $Mn_{0.65}Zn_{0.35}Fe_2O_4$ which shows low values for ***Mr*** and ***Hc*** and a higher value for saturation magnetization *Ms* when the sample is sintered at 1350 °C.

When the sample $Mn_{0.67}Zn_{0.33}Fe_2O_4$ is sintered at 1350 °C it is found to show unusual behavior. The coercivity ***Hc*** drastically reduces to 1.06 Oe and the

squareness (***Mr /Ms***) reduces to 0.0015 which is extremely low. The saturation magnetization increases to 72.31 emu/gm with zero power loss.

Hysteresis Loss

The hysteresis losses as shown in (fig.6.6.1.3) are found to be quite low then reported [37,38] for unsintered as well as for sintered samples and are found to depend on concentration of Mn and sintering temperature.

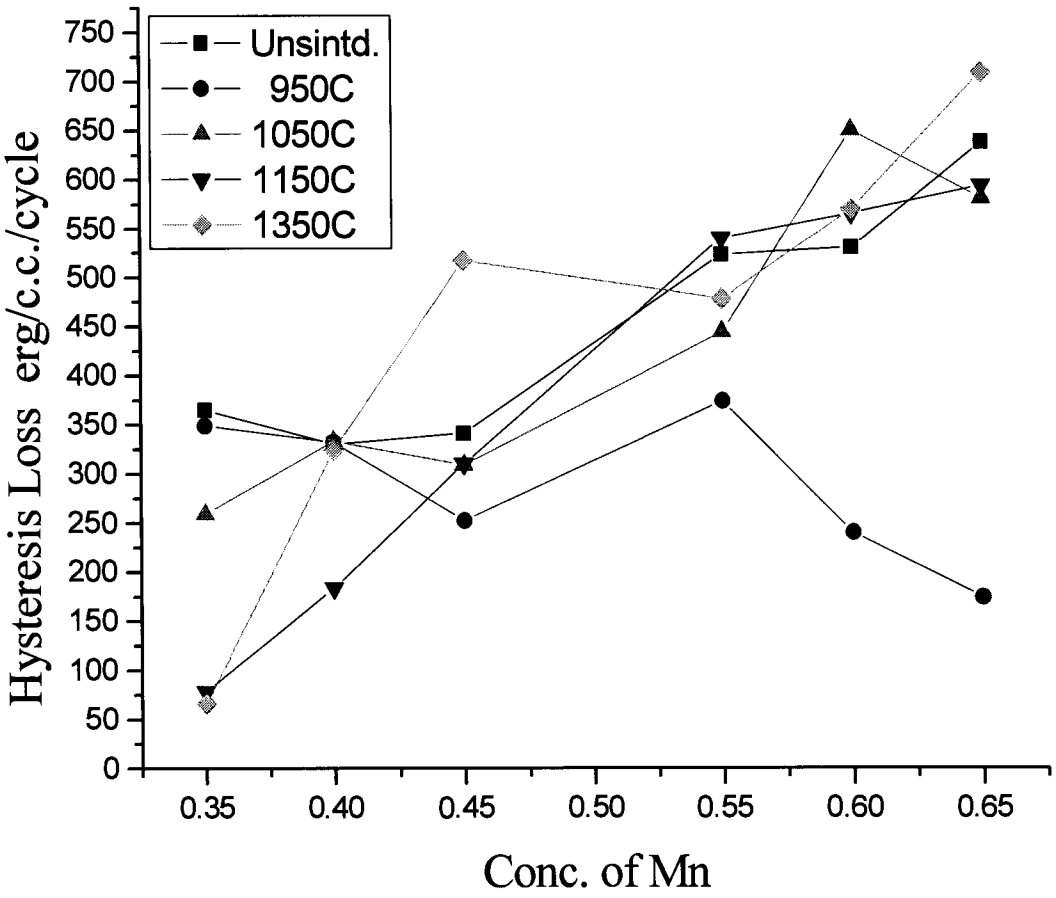

(a)

Fig. 6.6.1.3(a): Variation of Hysteresis loss with conc. of Mn for various sintering temperatures for the samples prepared by thermal decomposition.

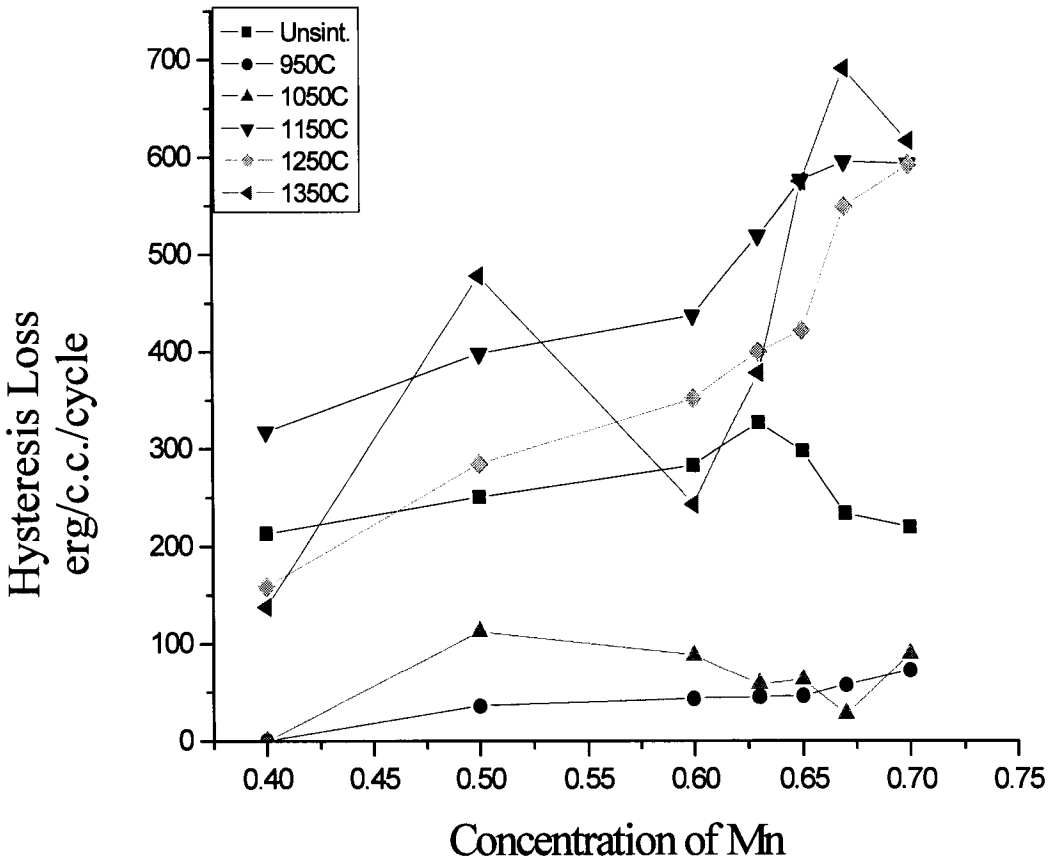

(b)

Fig. 6.6.1.3(b): Variation of Hysteresis loss with conc. of Mn for various sintering temperatures for the samples prepared by Microwave induced decomposition.

SQUID measurements

Field dependent data were taken by sweeping the field while holding the sample at fixed temperature, whereas the temperature dependence of the saturation magnetization was measured by applying field of 100Oe.

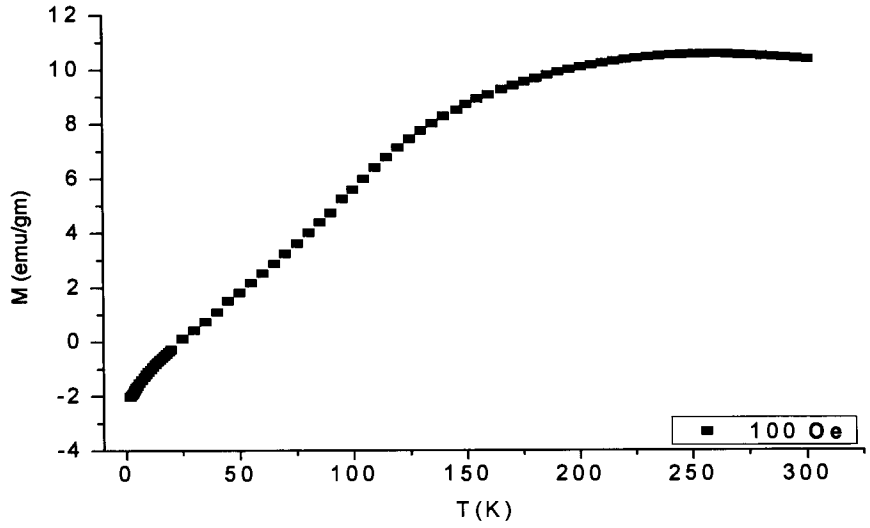

(a)

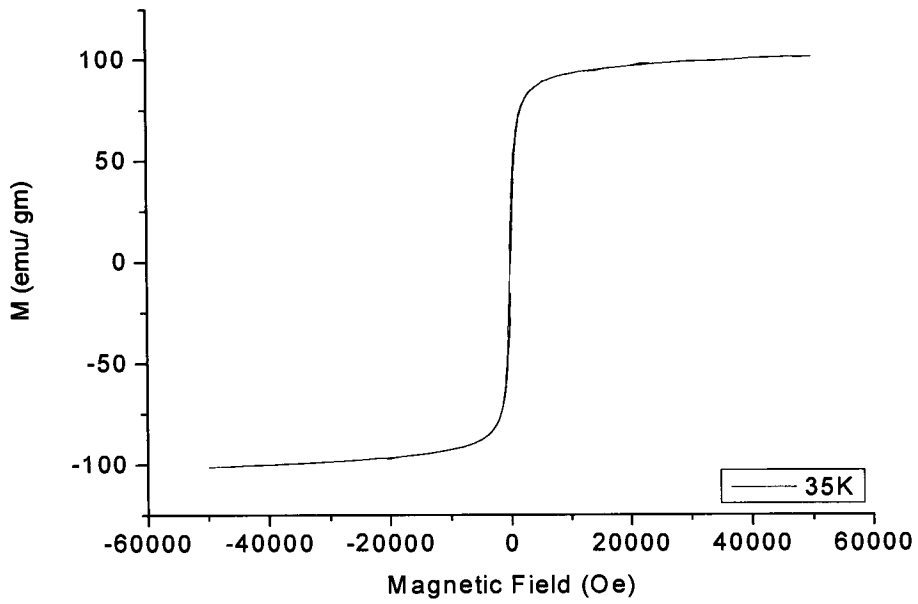

(b)

Fig.6.6.1.4: (a) Temperature dependence of magnetization (b) Field dependent magnetization for as prepared sample $Mn_{0.70}Zn_{0.30}Fe_2O_4$ prepared by Microwave decomposition.

SQUID measurements

Field dependent data were taken by sweeping the field while holding the sample at fixed temperature, whereas the temperature dependence of the saturation magnetization was measured by applying field of 100Oe.

The magnetization of the sample was measured with the increase in temperature when a field of 100Oe is applied (fig 6.6.1.4a). The total magnetization of the Mn-Zn nanoparticles is zero at 25K since the applied magnetic field is not strong enough to overcome the magnetic anisotropy alone. When the temperature rises, the magnetic anisotropy in some nanoparticles is overcome due to thermal activation and the magnetization directions of these nanoparticles align with the applied field, similar to a typical paramagnetic material. The magnetization increases with temperature and a maximum is reached at around 250K. This temperature is known as blocking temperature. Beyond this temperature the magnetization is found to decrease with increasing temperature. When the temperature reaches the blocking temperature, the magnetization directions of almost all of the nanoparticles point to the field directions and gives a high magnetization. As the temperature increases above the blocking temperature, the sample follows a typical paramagnetic behavior of decreasing magnetization [1,2].

The magnetic field dependence of magnetization of sample $Mn_{0.70}Zn_{0.30}Fe_2O_4$ is shown in fig 6.6.1.4b. The field dependent magnetization plot at 35K displays that the magnetization of the superparamagnetic nanoparticles changes direction in unison with the direction reversal of the

applied magnetic field. Therefore, the magnetization direction changes simultaneously with the reversal of the applied field at 35K [1,2]. A high magnetization of 101 emu /gm is obtained for the sample at 5T.

6.6.2 Permeability and Loss Factor

Initial permeability (μ_i) is an important magnetic parameter, which decides the suitability of a ferrite for particular application. It is technologically important extrinsic magnetic property, which is influenced by the microstructure, which in turn depends upon the method of preparation. The initial permeability is dependent on grain size, density and porosity of the material [39].

The Variation of permeability with the temperature for the samples prepared by thermal decomposition and sintered at 950°C, 1050°C, 1150°C, 1250°C and 1350°C is shown in Fig. 6.6.2.1(a, b, c, d & e) It is observed that initial permeability increases slowly, reaches peak value at a certain temperature and drops gradually to zero at Curie temperature. The maximum in initial permeability corresponds to the point of zero anisotropy field [40]. The increase in permeability with temperature is due to the fact that the anisotropy decreases faster with temperature than the saturation magnetization.

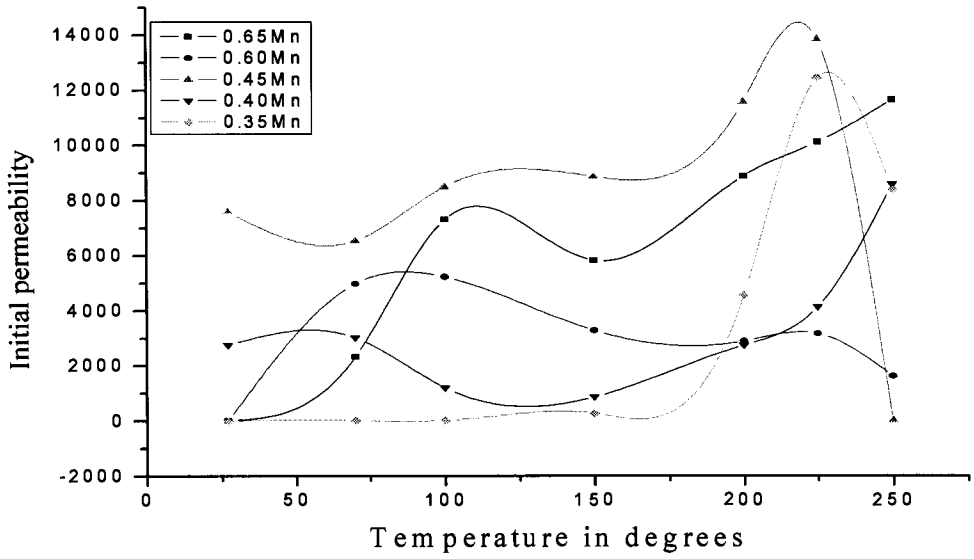

(a)

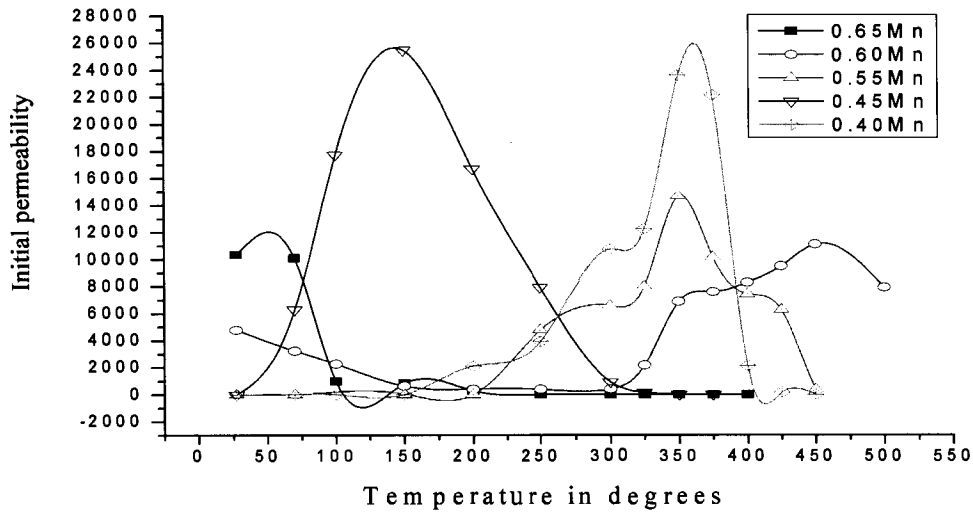

(b)

Fig.6.6.2.1: Variation of initial permeability with temperature for sample $Mn_xZn_{1-x}Fe_2O_4$ Sintered at (a) 950 °C (b) 1050 °C

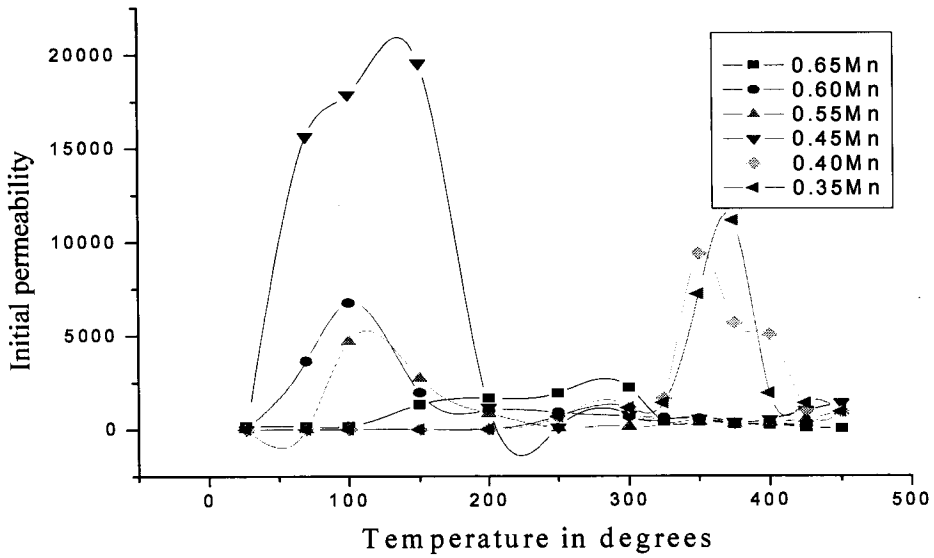

©

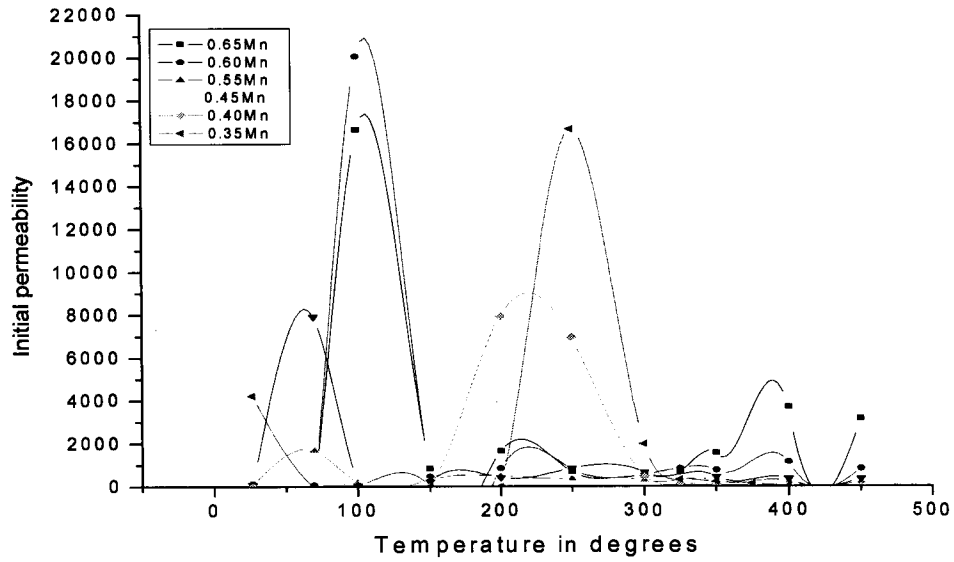

(d)

Fig.6.6.2.1: Variation of initial permeability with temperature for sample $Mn_xZn_{1-x}Fe_2O_4$ Sintered at (c) 1150 °C (d) 1250 °C

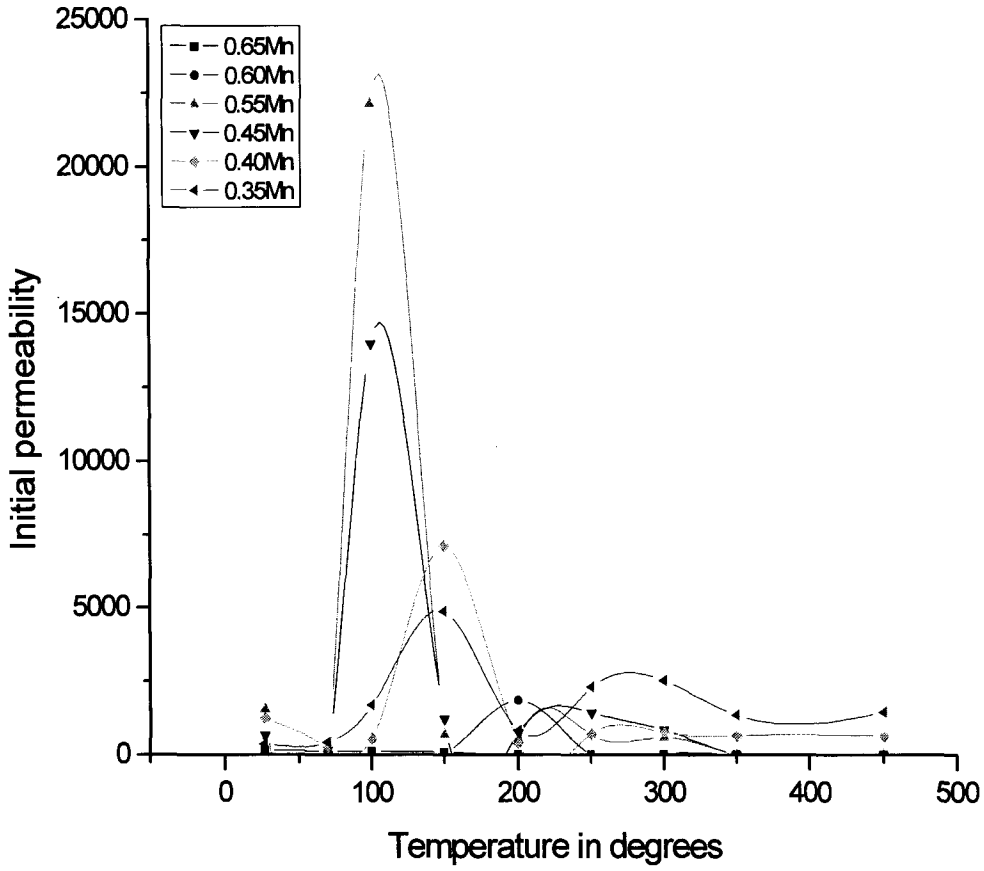

(e)

Fig.6.6.2.1e: Variation of initial permeability with temperature for sample $Mn_xZn_{1-x}Fe_2O_4$ Sintered at 1350 °C

The variation of initial permeability with temperature for the sample $Mn_{0.45}Zn_{0.55}Fe_2O_4$ sintered at 950 °C, 1050 °C, 1150 °C, 1250 °C and 1350 °C is as shown in Fig.6.6.2.1. The drops are observed near Curie temperature and a high value of initial permeability 25,472 at 150 °C for frequency 50Hz obtained for sample $Mn_{0.45}Zn_{0.55}Fe_2O_4$ sintered at 1050 °C is much higher than the reported values [41]. Samples $Mn_{0.35}Zn_{0.65}Fe_2O_4$, $Mn_{0.60}Zn_{0.40}Fe_2O_4$ and $Mn_{0.65}Zn_{0.35}Fe_2O_4$ when sintered at 950 °C shows very low room temperature permeabilities where as, sample $Mn_{0.40}Zn_{0.60}Fe_2O_4$ shows high value of 2,753 and the sample $Mn_{0.45}Zn_{0.55}Fe_2O_4$ shows a value of 13,831 for room temperature permeability. However, the overall permeabilities for this sample are found to increase as the temperature increases. Room temperature permeability values are drastically changed when the same samples are sintered at 1050 °C.

$Mn_{0.40}Zn_{0.60}Fe_2O_4$, $Mn_{0.45}Zn_{0.55}Fe_2O_4$ and $Mn_{0.55}Zn_{0.45}Fe_2O_4$ show very low values whereas $Mn_{0.60}Zn_{0.40}Fe_2O_4$ shows higher value of μ_i and the sample $Mn_{0.65}Zn_{0.35}Fe_2O_4$ shows highest room temperature value for μ_i which is higher than 10,000.

Sample $Mn_{0.45}Zn_{0.55}Fe_2O_4$ shows a high value of permeability i.e. 19,563 at 150°C when sintered at 1150 °C where as sample $Mn_{0.60}Zn_{0.40}Fe_2O_4$ shows a high value of permeability i.e. 20,042 at 100 °C when sintered at 1250 °C .Samples when sintered at 1350 °C, $Mn_{0.55}Zn_{0.45}Fe_2O_4$ showed a high value of initial permeability i.e.22,141 at 100 °C .All these samples show broad peaks followed by a gradual fall near Curie temperature as expected. For samples sintered at 950 °C the curie temperatures is beyond 250 °C where as for samples

sintered at 1050 °C the Curie temperature lies between 100 °C and 500 °C. Fig.6.6.2.2 (b)shows variation of maximum values of μ_i with Sintering temperature for sample $Mn_{0.45}Zn_{0.55}Fe_2O_4$. The variation of maximum value of the permeability for the sample is found to show a peak at 1050 °C and a fall followed by a rise at sintering temperature 1350 °C. Fig. 6.6.2.2 (a & b) can be related to the existence of different crystalline phases which the samples undergoes at different sintering temperatures [42] This is evident from the SEM photographs and TEM photograph depicted in Fig. 6.6.2.3 (a, b, c, d ,e & f)

The initial permeability of high permeability material depends to a large extent on mobility of the Bloch's domain walls. To obtain high permeability it is important to reduce the crystalline anisotropy and the magnetrostriction. Ferrites in particular are burdened with magnetic imperfections. Voids in bodies that are not completely densified, non-magnetic inclusions are the factors, which give, rise to internal magnetostatic energy. The stable domain configuration in a material is always such is to minimize this energy. The loss that occurs is proportional to imperfections of materials as well it's anisotropy, both crystalline and strain. High permeability may be expected in polycrystalline material that are homogeneous, dense and have composition that has very low value of anisotropy. Anisotropy is temperature dependent property. Effect of this depends on the composition. The anisotropy in Mn-Zn ferrite is highly dependent on the material composition. For some compositions of Mn-Zn anisotropy takes negative value at room temperature, increases monotonically with temperature to zero at Curie temperature whereas for certain combinations of Mn-Zn it takes a negative value

increases to zero, takes a positive value and decreases to attain a zero value at Curie temperature. This behavior is strongly reflected in the initial permeability of the material. The initial permeability rises to maximum at both zero anisotropy points with a saddle corresponding to the temperature at which anisotropy has a maximum positive value [42, 43]. Well-adjusted sintering conditions support the design of microstructure and resulting magnetic properties of the sample. SEM micrographs (Fig.6.6.2.3) show the morphology of sample $Mn_{0.45}Zn_{0.55}Fe_2O_4$ sintered at 950 °C, 1050 °C, 1150 °C, 1250 °C and 1350 °C respectively.

The sample sintered at 950 °C Fig. 6.6.2.3 (a) shows a more compact microstructure with well-developed grains, however the existence of non-magnetic voids is also large. The density of the sample is 2587Kg/m^3. The samples sintered at 1050 °C Fig. 6.6.2.3 (b) shows larger polycrystalline grains with less non-magnetic voids and a density of 3200Kg/m^3. The sample exhibits a high value of permeability. The samples sintered at 1150 °C fig. 6.6.2.3 (c) shows formation of well developed crystals and has a density of 3983Kg/m^3. The anisotropy for this sample is expected to be higher due to blocking of domain wall movement and the strain isotropy, which is a result of increase in lattice stress. The sample sintered at 1250 °C shown in fig. 6.6.2.3 (d) appears to be posses a very high value of anisotropy and magnetrostriction compared to other samples. This appears to be a stage with substantial magnetic imperfections and poor grain growth. The sample has a density of 3867 Kg/m^3. A different crystalline phase with fewer imperfections is obtained for sample sintered at 1350 °C (Fig. 6.6.2.3 e). The density of this sample is found to be 3925Kg/m^3.

The microstructures show different crystalline phases, which are responsible for variations in anisotropy and domain wall movement in the sample. Fig. 6.6.2.3 confirms the existence of polycrystalline phase in the sample sintered at 1050 °C, which is one of the factors for enhancing the permeability value of the sample.

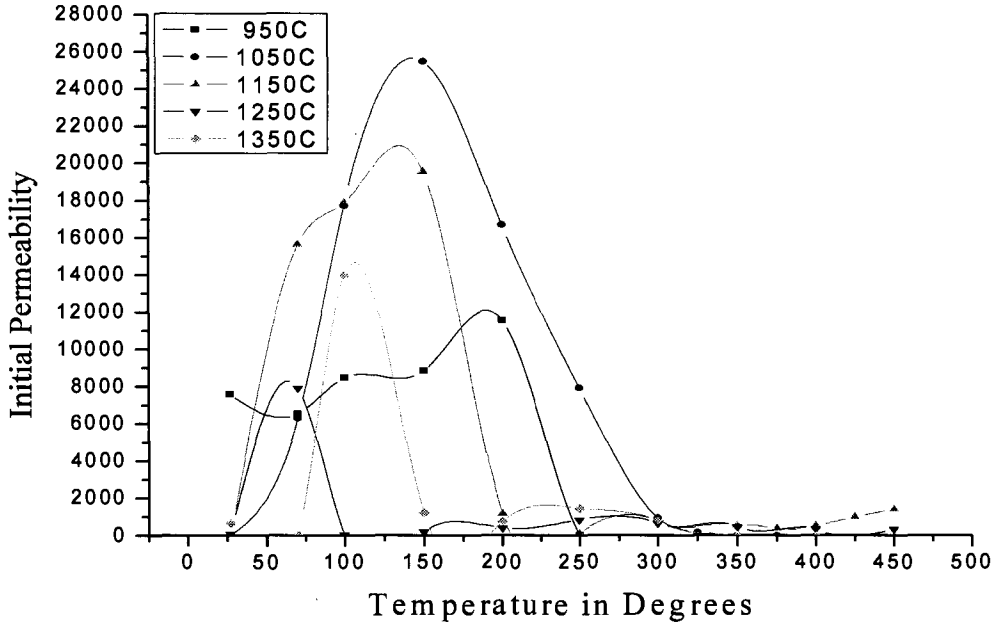

(a)

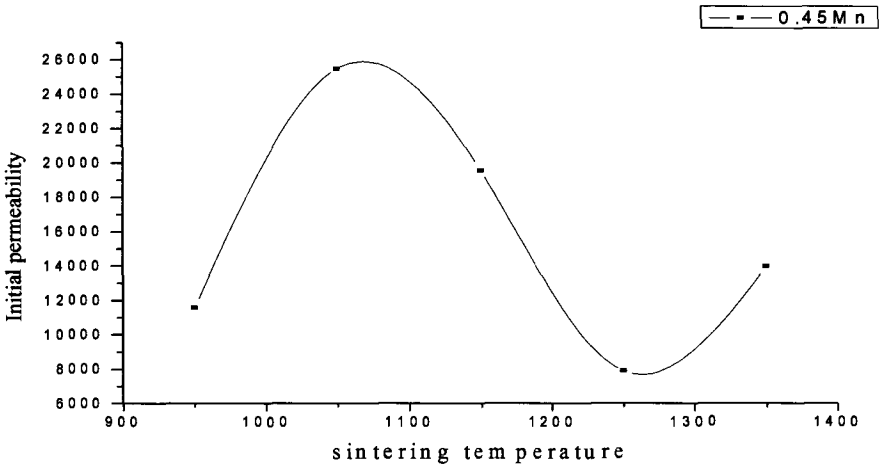

(b)

Fig.6.6.2.2: (a) The variation of Initial permeability with temperature for the sample $Mn_{0.45}Zn_{0.55}Fe_2O_4$ sintered at different temperatures.
(b) Variation of maximum value of initial permeability with sintering temperature for $Mn_{0.45}Zn_{0.55}Fe_2O_4$.

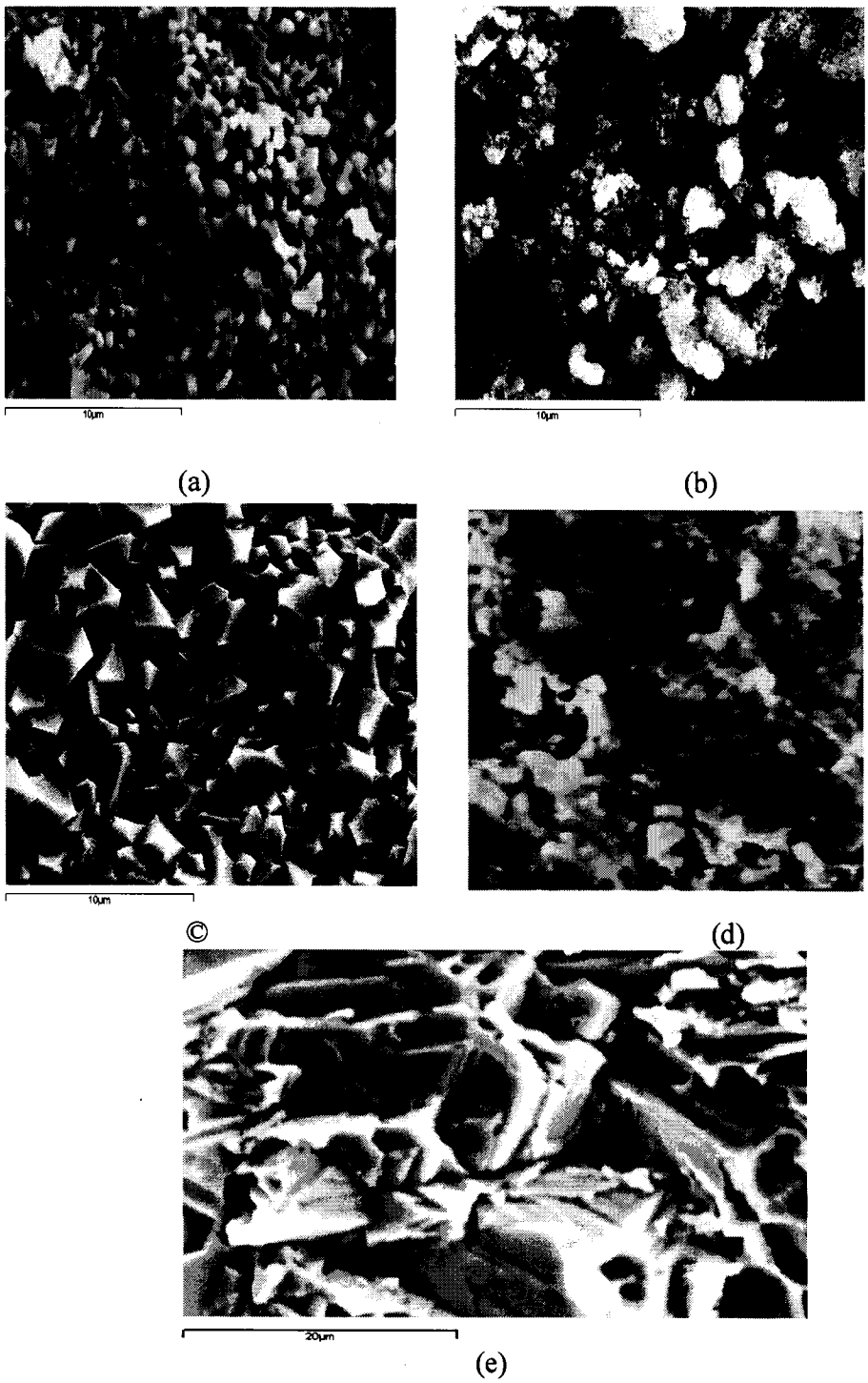

Fig.6.6.2.3: SEM Photographs of $Mn_{0.45}Zn_{0.55}Fe_2O_4$ sintered in nitrogen atmosphere for 3hours at, (a) 950C(b) 1050C, (c) 1150C, (d) 1250C (e) 1350C .

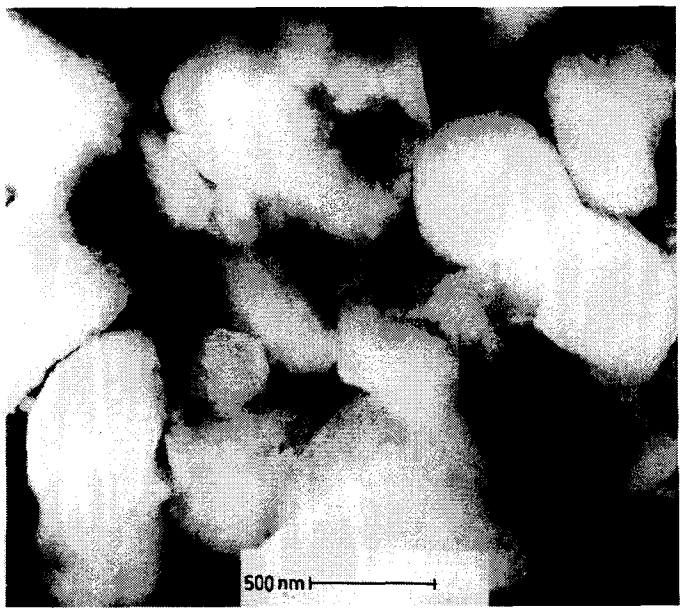

(f)

Fig.6.6.2.3: TEM Photograph of sample $Mn_{0.45}Zn_{0.55}Fe_2O_4$ sintered at 1050C.

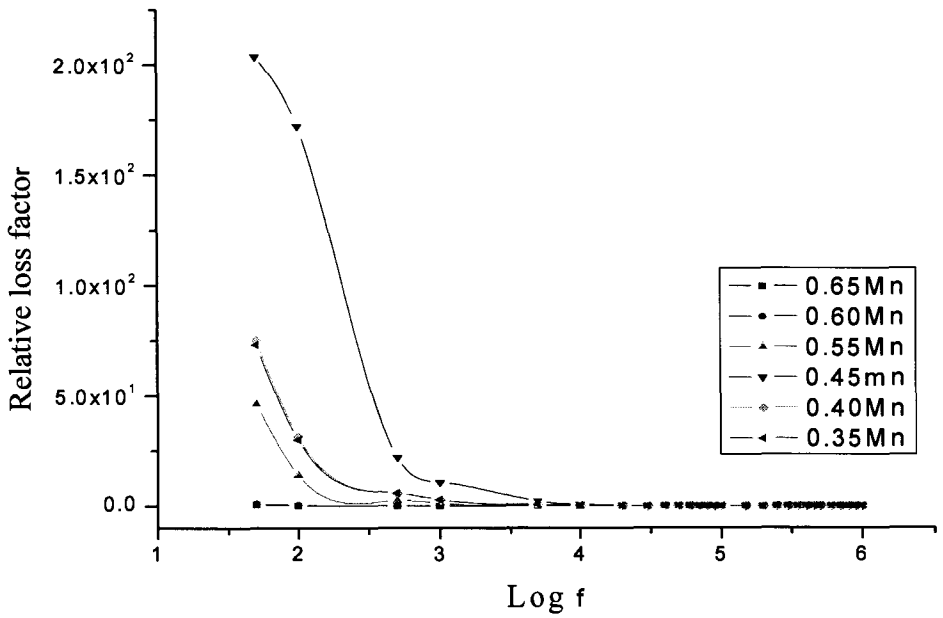

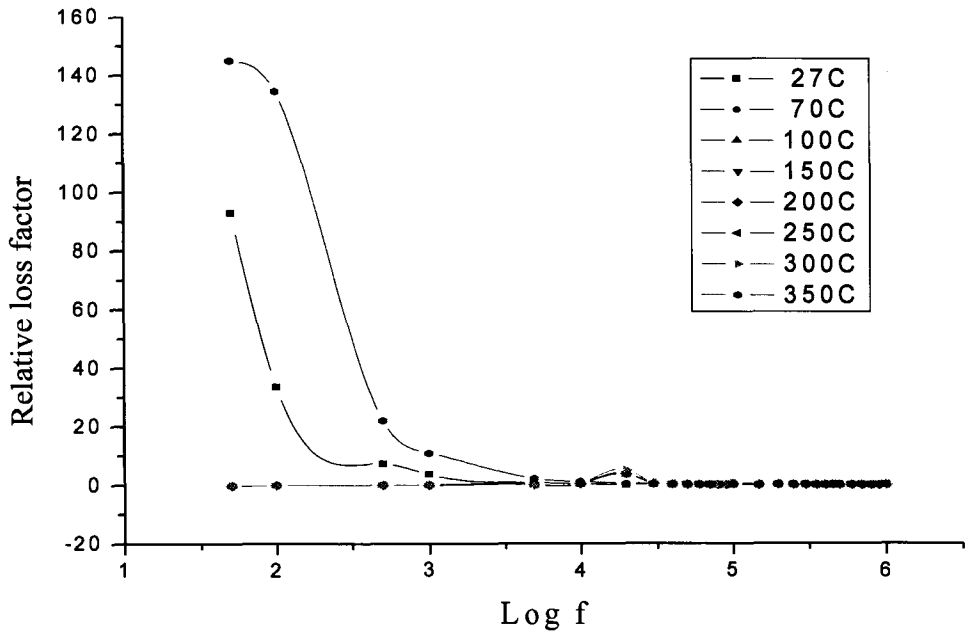

(b)

Fig.6.6.2.4 : Variation of relative loss factor with frequency (a) samples $Mn_xZn_{1-x}Fe_2O_4$ sintered at 1150 °C (b) Sample $Mn_{0.45}Zn_{0.55}Fe_2O_4$ sintered at 1050 °C at different temperatures.

The ratio tanδ to μ_i known as relative loss factor (rlf) is plotted against frequency as shown in fig.6.6.2.4. It is observed that for some samples the value of rlf rapidly decreases as the frequency is increased whereas it remains extremely low for most of the samples for all sintering temperatures. The rlf is found to depend on composition and microstructure of the sample, which is decided by sintering profiles of the sample. In the present work the rlf values obtained range from 10^2 to as low as 10^{-6}, in the frequency range 50Hz to1MHz

6.6.3 A.C. Susceptibility

For ferrimagnetic materials, the variation of a.c. susceptibility versus temperature has been reported by many workers [44-46]. From these curves the curie temperature and domain structure have been estimated. It has also been found that at curie temperature the curve drops almost to zero. Below curie temperature, ferrites exhibit ferrimagnetic nature. Above curie temperature, magnetic transition occurs from ferrimagnetic to paramagnetic.

In the present study, AC susceptibility measurements were carried out on low field a.c. susceptibility equipment as well as on pulse field a.c. susceptibility equipment.

The plots of the variation of normalized susceptibility (χ_T / χ_{RT}) with temperature (T) are shown in fig.6.6.3.1

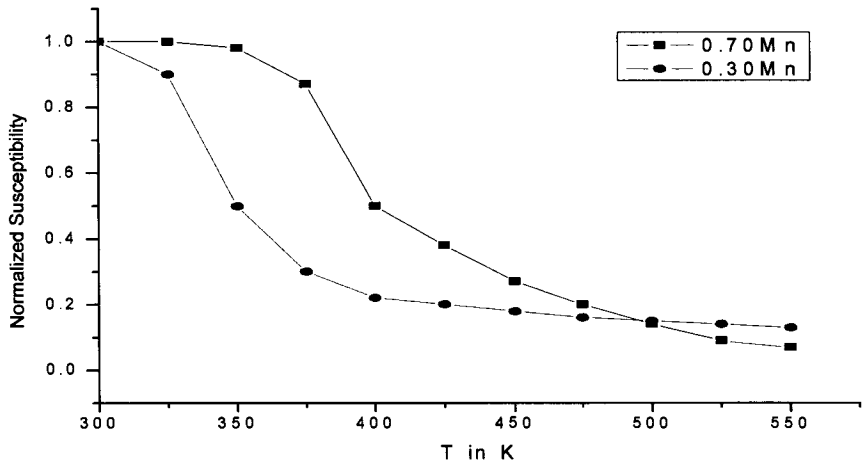

Fig. 6.6.3.1: Normalized susceptibility (ratio $\chi_T / \chi_{(300)}$) as a function of temperature for $Mn_x Zn_{1-x} Fe_2O_4$

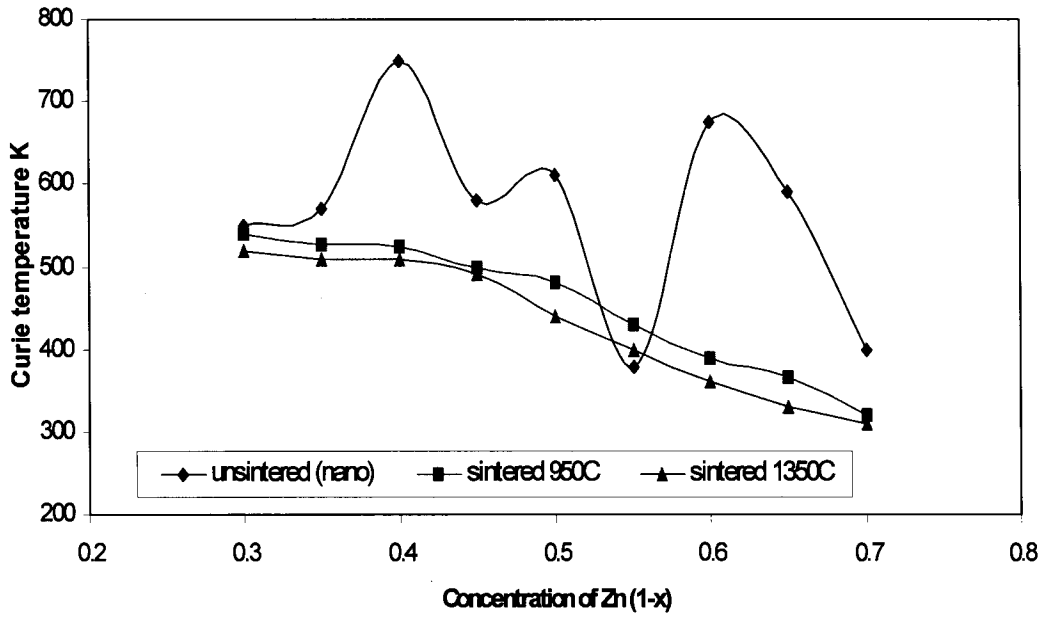

Fig 6.6.3.2: Variation of Curie temperature with concentration of Zn in $Mn_{(x)} Zn_{1-x} Fe_2O_4$

Table 6.6.3.1 : Experimentally determined curie temperatures for samples $Mn_x Zn_{1-x} Fe_2O_4$ prepared by thermal decomposition method

Zinc Conc.	Unsintered	Sintered 950C	Sintered 1350c
1-X	Tc	Tc	Tc
0.30	550	540	520
0.35	570	528	510
0.40	750	524	510
0.45	580	500	490
0.50	610	480	440
0.55	380	430	400
0.60	675	390	360
0.65	590	365	330
0.70	400	320	310

Curie temperature for samples in nano phase were found to be size dependent. A high Tc of 750K and a low Tc of 380K were observed for the samples. The A.C. susceptibility curves obtained on low field a.c. susceptibility equipment for unsintered and sintered samples prepared using thermal decomposition (fig.6.6.3.2) are typical to curves obtained for fine particle ferrite. The nature of the $\chi_{ac} - T$ plots for sample $Mn_{0.70} Zn_{0.30} Fe_2O_4$ exhibits SD behavior whereas sample $Mn_{0.30} Zn_{0.70} Fe_2O_4$ exhibits a mixture of SD and MD behavior with other samples with x= 0.65, 0.6,0.55,0.5,0.45,0.4,0.35 exhibiting near SD behavior [47]. It can therefore be concluded that, the normalized susceptibility versus temperature curves indicate ferrimagnetic behavior [48,49].

From these curves the curie temperatures of all the samples are determined. The lowest Tc of 310K and the highest Tc of 730K was obtained for $Mn_{0.30}Zn_{0.70}Fe_2O_4$ and $Mn_{0.70}Zn_{0.30}Fe_2O_4$ respectively. For sintered samples the curie temperature was found to decrease with increase in sintering temperature.

Fig 6.6 shows the susceptibility curves obtained on pulse field a.c. susceptibility equipment for the samples prepared by thermal decomposition.

A high Tc of 725K and a low Tc of 484K were observed for the samples $Mn_{0.45}Zn_{0.55}Fe_2O_4$ and $Mn_{0.55}Zn_{0.45}Fe_2O_4$ respectively.

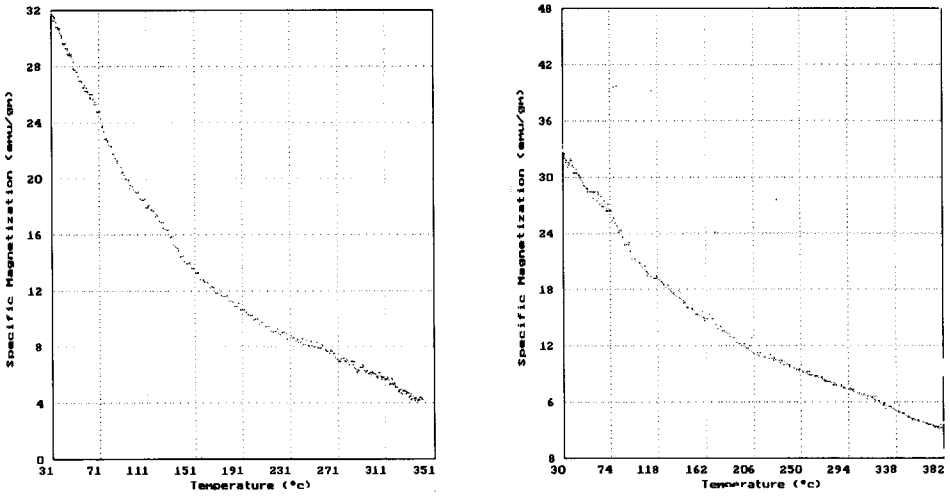

(a) (b)

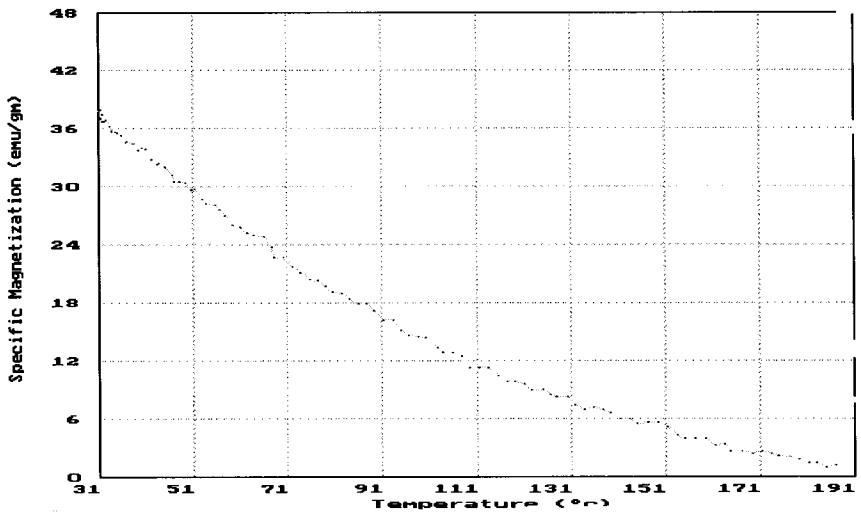

©

Fig 6.6.3.3: Variation of Specific magnetization with temperature for the samples (a) $Mn_{0.40}Zn_{0.60}Fe_2O_4$ (b) $Mn_{0.45}Zn_{0.55}Fe_2O_4$ and (c) $Mn_{0.55}Zn_{0.45}Fe_2O_4$

The pulse field A.C. susceptibility curves obtained for unsintered samples prepared using microwave decomposition are shown in (fig.6.6.1)

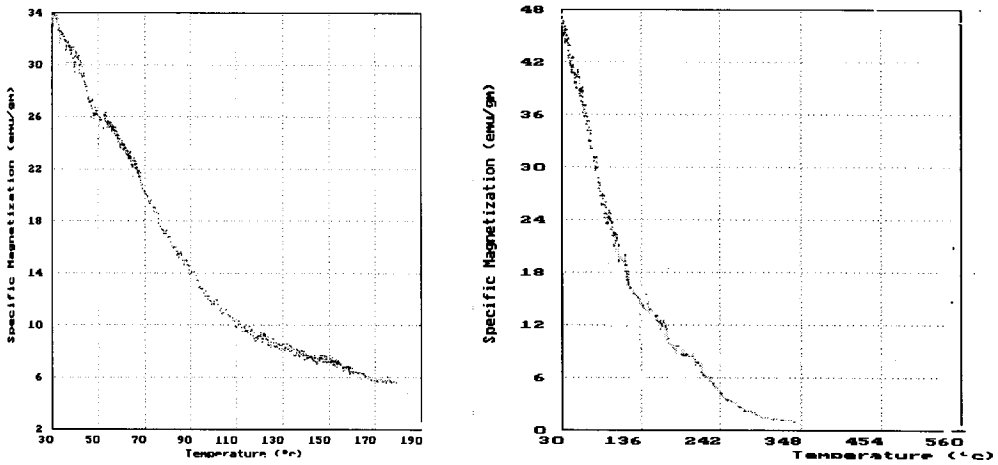

(a) (b)

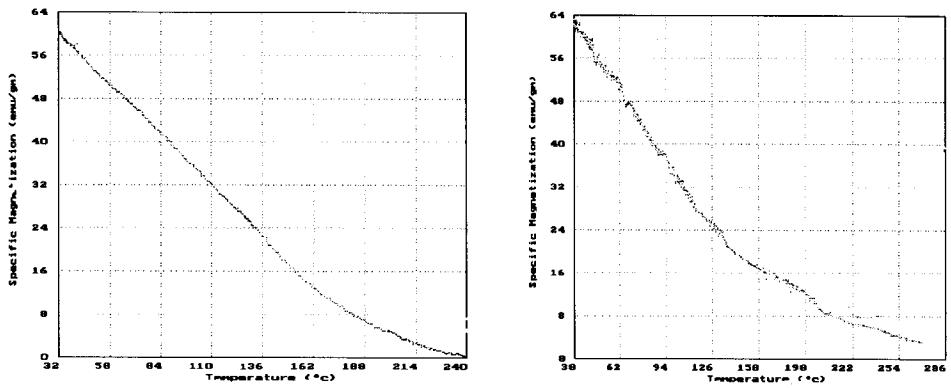

(c) (d)

Fig 6.6.3.4: Variation of Specific magnetization with temperature for the samples
(a) $Mn_{0.40}Zn_{0.60}Fe_2O_4$ (b) $Mn_{0.50}Zn_{0.50}Fe_2O_4$
(c) $Mn_{0.60}Zn_{0.40}Fe_2O_4$ (d) $Mn_{0.63}Zn_{0.37}Fe_2O_4$

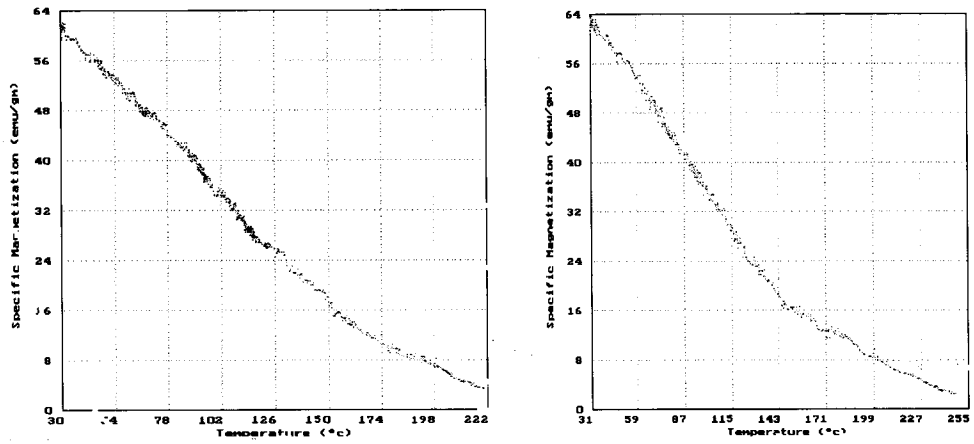

(e) (f)

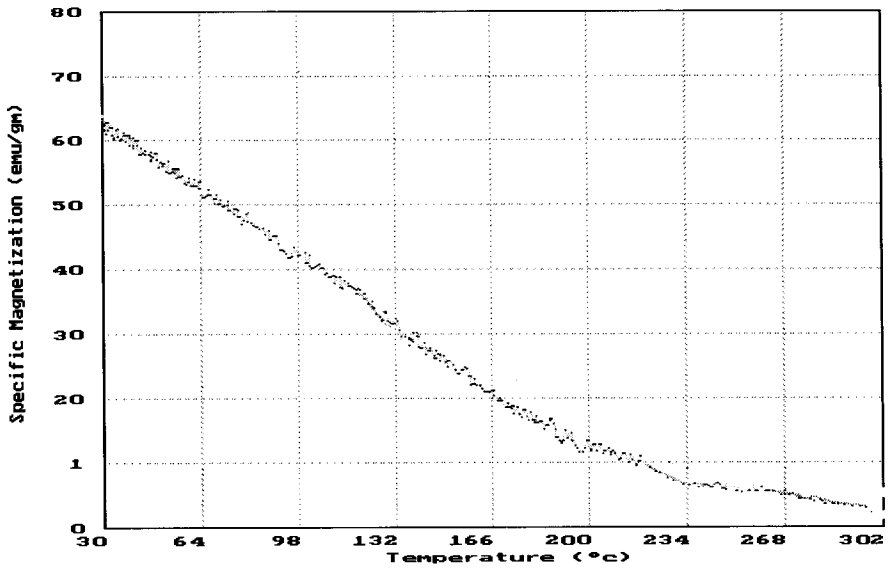

(g)

Fig 6.6.3.4: Variation of Specific magnetization with temperature for the samples
(e) $Mn_{0.65}Zn_{0.35}Fe_2O_4$ (f) $Mn_{0.67}Zn_{0.33}Fe_2O_4$ and
(g) $Mn_{0.70}Zn_{0.30}Fe_2O_4$

From these curves the curie temperatures of all the samples are determined.

Table 6.6.3.2 : Curie temperatures for samples $Mn_x Zn_{1-x} Fe_2O_4$ prepared by microwave decomposition method

Conc. of Mn	Unsintered
1-X	Tc in K
0.40	523
0.50	613
0.60	513
0.63	593
0.65	519
0.67	558
0.70	626

The lowest Tc of 519K and the highest Tc of 626K was obtained for $Mn_{0.60} Zn_{0.40} Fe_2O_4$ and $Mn_{0.70} Zn_{0.30} Fe_2O_4$ respectively. From the plots it appears that most of the samples prepared using microwave decomposition exhibits a mixed SD-MD behavior.

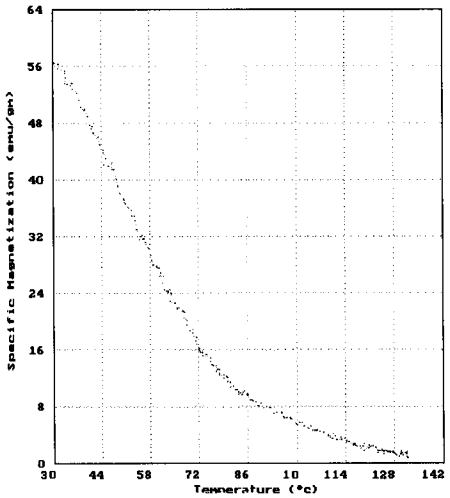

(a)

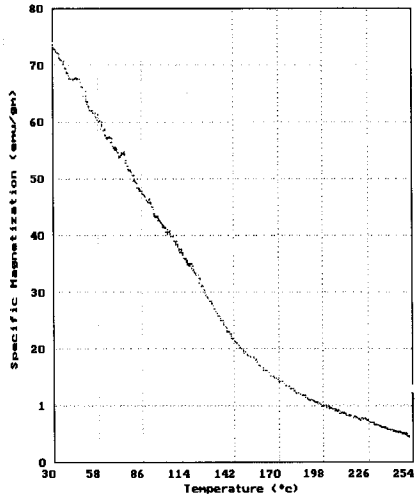

(b)

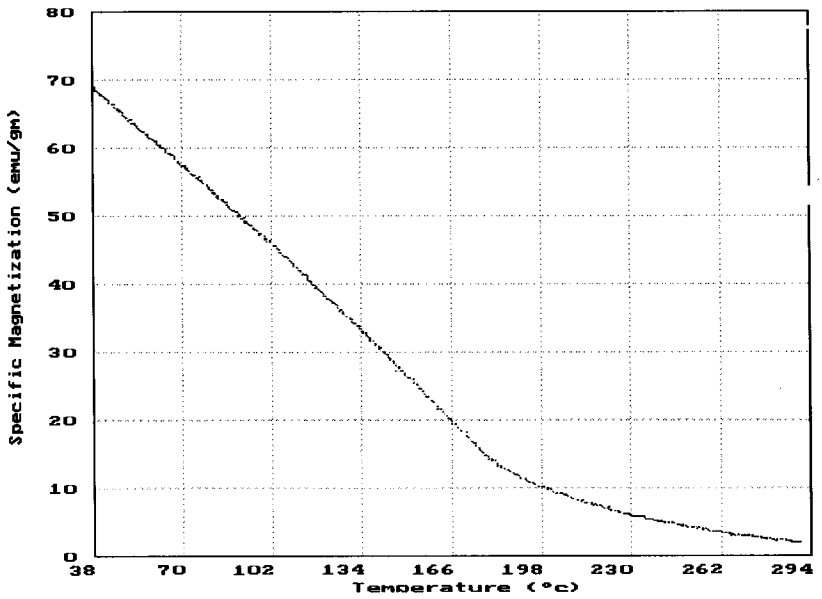

©

Fig 6.6.3.5: Variation of Specific magnetization with temperature for the samples sintered at 1350°C (a) $Mn_{0.55}Zn_{0.45}Fe_2O_4$ (b) $Mn_{0.60}Zn_{0.40}Fe_2O_4$ and (c) $Mn_{0.65}Zn_{0.35}Fe_2O_4$

For sintered samples the curie temperature was found to be in the range of 400K to 600K. It is observed that Curie temperature decreases with sintering temperature. Curie temperature was found to change with change in concentration of Zinc in the sample [50,51].

References

[1] A. Beiser, Modern Technical Physics, 2 ed., Cummings Publishing Company, Menlo Park, (1973).

[2] C. Kittel, Introduction to Solid State Physics, Wiley, New York, (1976).

[3] C. M. Sorensen, Nanoscale Materials in Chemistry , John Wiley and Sons, Inc., New York, (2001) 169.

[4] P. C. Scholten, J. of Magnetism and Magnetic Materials 57 (1995) 149.

[5] C. Chen, Magnetism and Metallurgy of Soft Magnetic Materials, Dover Publications,Inc., New York, (1986).

[6] D. J. Dunlop, Science 41,(1972) 176.

[7] S. R. Elliott, The Physics and Chemistry of Solids, John Wiley & Sons, New York, (1998).

[8] D. L. Leslie-Pelecky, R. D. Rieke, Chemistry of Materials 8 (1996) 1770.

[9] S. Wells, University of Wales (Wales), (1989).

[10] J. Smit, H. P. J. Wijn, Ferrites, John Wiley & Sons, New York, (1959).

[11] M. Ozaki, in Fine Particles: Synthesis, Characterization, and Mechanisms of Growth,Vol. 92 (Ed.: T. Sugimoto), Marcel Dekker, Inc., New York, 2000.

[12] E. P. Wohlfarth, J. of Magnetism and Magnetic Materials 39 (1983) 39.

[13] C. P. Bean, J. D. Livingston, J. of Applied Physics 30 (1959) 120.

[14] E. Blum, A. Cebers, M. M. Maiorov, Magnetic Fluids, Walter de Gruyter, Berlin, (1997).

[15] R. H. Kodama, A. E. Berkowitz, Physical Review B 59, (1999) 6321.

[16] S. Chikazumi "Physics of Magnetism" Wiely, New York (1996).

[17] A. Globus J.Physique Coll.,Cl (1963) C1.1-C1.15.

[18] A. Globus Cardiff Conf.USA, (1975).

[19] A. Globus and P. Duplex Phys.Stat Solidi , 31 (1968) 75.

[20] A. Globus and M. Gayut IEEE Transactions on magnetics, 6 (1970) 614.

[21] A. Globus, Thesis, Univ. of Paris, France (1963).

[22] M. T. Johnson and E.G.Vissar IEEE Trans. Magn. MAG-26 (1990) 1987.

[23] P. J. Vender Zaag, J.J.M.Ruigrok, A.Noordermeer,M.H.W.M.van Deiden, P.J.Por, Recveltk, D.M.Sonnet and J.N.Chapman. J.Appl.Phys,74 (6) (1993) 4085.

[24] H. Piscard and A.Globus , Phys. Rev. B 24 (1981) 6610.

[25] G. Rankis Bull. Latv. Acad.Sci., Phys Tech. Sci., N2 (1984) 27.

[26] A. Globus J.Phys. (France) 38 (1977) 1.

[27] J. Gieraltowski, "Interdependence between the grain size and the wall dimension in magnetically soft ferrites", Ferrites, Proc. International Conf., Japan (1980) 277.

[28] H.Rikukawa ,IEEE Trans. On Magn., 18 (1982) 1535.

[29] C.Guillaud Proc. IEEE, 704 (B) (1957) 165.

[30] C. Kittel, Physical Reviews, 70 (1946) 965.

[31] J. Smit and H.P.J.Wijn "Ferrites" John Wiley, New york, (1959).

[32] Sattar A A and El-Shokrofy K M J. Phys. IV France 7 Colloq (1997) , Cl-245.

[33] S.D.Likhite and C. Radhakrishnamurthy and P.W.Sahasrabudhe, Rev.Sci.Instr. 25, (1965), 302.

[34] S.D.Likhite and C.Radhakrishnamurthy,curr.sci. 35 (1966) 534.

[35] R.B. Tangsali, S.H. Keluskar, G.K.Naik, J.S.Budkuley , International J. of Nanoscience 3, (4 & 5) (2004) 1-9.

[36] A. Verma, T. C. Goel, R. G. Mendiratta, P. Kishan, J. Magn. Magn. Mater. 208 (2000) 13-19.

[37] S R Murthy, Bull. Mater. Sci., 26 (5) (2003) 499–503.

[38] M.Muroi, J.Amighian, R.Street and P.G.Mc Cormick, Digest of 8th int. Conf. Ferrites, Kyoto, Japan, 2000.

[39] Rondinone A. J., Samia A.C. S., Zhang Z. J. J. Phys. Chem. B, 103 (1999) 6876.

[40] Chao Liu, Bingsou Zou, Adam J. Rondinonen and Z. John Zhang J. of Phys. Chem. B, 104 (2000) 1141-1145.

[41] Goldman, »Modern Ferrite Technology«, Van Nostrand Reihold 1990, New York (1997) 286-287.

[42] K. J. Standley, 'Oxide Magnetic Materials' (oxford: claredon Press, 1972).

[43] S. H. Keluskar R.B. Tangsali , G.K.Naik, J.S.Budkuley, J. of Magnetism and magnetic Materials. (In Press)

[44]. J. Schnettler, »Physics of Electronic Ceramics, Part B«, Marcel Dekker, Inc, 1972 New York

[45] Verma, T. C. Goel, R.G. Mendiratta, P. Kishan, J. of Magnetism and Magnetic Materials 208 (2000) 13-19.

[46] C. Radhakrisnamurty, J.Geol. Soc.India, 26(9) (1985) 640.

[47] R.V. Upadhaya, G.J. Baldha and R.G. Kulkarni, Mater. Res. Bull. 21 (1986) 1015.

[48] G.J. Baldha and R.G. Kulkarni, Solid State Commun. 53 (1985)11.

[49] J. Hopkinson, Philos. Trans. R. Soc. (Lon.) 180 (1889) 443.

[50] C.Radhakrishnamurty, S.D. Likhite, E. R. Deutsch and G.S. Murthy, Phys. Earth and Planet. Inter., 130 (1982) 281.

[51] R.S.Chaughule, C.Radhakrinamurty, E.V.Sampathkumaran,S.K.Malik and R.Vijayraghavan, Mat Res. Bull. 18 (1983) 817.

[52] Radhakrishnamurthy C, Likhite S D and Sastry N P Philos.Mag. 23 (1971) 503.

[53] Radhakrishnamurthy C, Likhite S D and Sahasrabudhe P. W. Proc. Indian Acad. Sci. (Chem. Sci.) A87 (1978) 245.

Chapter VII

ELECTRICAL PROPERTIES

7.1 INTRODUCTION

Spinel ferrites score over the conventional magnetic materials in their application as their electrical conductivity is low when compared to those of other magnetic materials. In ferrites temperature dependence of mobility, affects the conductivity and the carrier concentration is almost unaffected by temperature variation.

In semiconductors the charge carriers occupy states in wide energy band, whereas the charge carriers in ferrites are localized at the magnetic atoms. The electrical properties of ferrites are affected by the distribution of cations in the sites, by non-magnetic and magnetic substitutions, by amount of Fe^{2+} present, sintering conditions, grain size and grain growth effects.

The ac electrical properties are of immense importance as the field of solid-state electronics continues to expand rapidly. The principle application of dielectric and the ac electrical properties is the capacitive element in electronic circuits and as electrical insulators, therefore the dielectric constant; dielectric loss factor and dielectric strength are the important parameters. Most of the high frequency applications related to electric properties are concerned with dielectrics. The advantages of ferrites, which are ceramic in nature, over the other available

dielectric materials are elastic properties, temperature performance and greater resistance to environmental changes particularly at higher temperature.

7.2 RESISTIVITY

Ferrites have very wide range of resistivities from 10^{-3} to 10^{11} Ohm.cm at room temperature [1]. This low and high resistivities of ferrites are mainly explained on the basis of actual location of cations in the spinel structure and hopping mechanism. Their high conductivity is due to simultaneous presence of ferrous and ferric ions in the crystallographically equivalent sites. The high resistivity in ferrites is associated with the occupation of B-sites by other divalent metal ions and trivalent iron ions. The spinel ferrites contain large number of oxygen ions and small number of metal ions in the interstial spaces. Both Fe^{2+} and Fe^{3+} ions are at B-site and conduction takes place when electrons move from $Fe^{2+}$to Fe^{3+} ions.

The conduction mechanism in ferrites is assumed to be related to d electrons and direct electron exchange between Fe^{2+} and M^{3+} ions is neglected due to small tunneling effect of d electrons.

The resistivity of ferrites is very sensitive to temperature. The diffusion of charge carriers from one state to other is possible only when their energy exceeds a certain minimum energy called activation energy. The thermal lattice vibrations consistently give rise to phonons and electrons hop between the pairs of states either by absorption or by emission of photons each time. In this way transport of charge carriers is achieved by hopping process through interaction with phonons.

On the basis of this the temperature dependence of resistivity of ferrites is given by the relation.

$$\rho = \rho_0 \exp(-\Delta E/kT) \quad \text{---------- 7.2.1}$$

where ρ_0 = Temperature dependent constant

ΔE = activation energy

K = Boltzmann constant

T = absolute temperature

In ferrites the cations are surrounded by close packed oxygen anions and as first approximation can well be treated as isolated from each other. There will be little direct overlap of the anion charge clouds or orbitals. Alternatively, the electrons associated with particular ion will largely remain isolated and hence a localized electron model is more appropriate in the case of ferrites rather than the collective electron (band) model.

These factors that differentiate the electrical behavior of ferrites from that of semiconductors, led to the different models such as hopping model of electrons, small polaron model and Phonon induced tunneling.

The mechanism of transport phenomenon in ferrites can be represented as [2] The two mechanism of conductivity can be represented as

$$Fe^{2+} + Fe^{3+} \longleftrightarrow Fe^{3+} + Fe^{2+} + \Delta E \quad \text{---------- 7.2.2}$$

$$M^{2+} + Fe^{3+} \longleftrightarrow M^{3+} + Fe^{2+} + \Delta E \quad \text{---------- 7.2.3}$$

Where ΔE is activation energy, the energy required for transfer of electron from M^{2+} to Fe^{3+} and vice versa. The valence states of two ions get interchanged.

Under the influence of an electric field these extra electrons can be regarded to constitute the current, by jumping or hopping process [3].

The free electron model cannot explain the electrical conductivity of ferrites because of the fact that the electrons in ferrites are not free and energy band model is not suitable to explain the electrical conductivity for the lack of Bloch type wave functions for electrons in ferrites. The conductivity of ferrites can be, however, explained in terms of electronic charge carriers, like electrons and holes, by the relation

$$\sigma = e[n_e\mu_e + n_h\mu_h] \text{---------- } 7.2.4$$

where n and μ are the concentration and mobility of electrons and holes respectively.

In ferrite lattice, the electrostatic interaction between electron and the neighbouring ions results into the polarization field called polaron. When such association is weak, it constitutes large polaron. Such polarons are found in ionic crystals.

When electron plus lattice deformation have a linear dimension smaller than lattice constant, they constitutes small polarons. Such polarons are found in covalent crystals.

The electrical resistivity, the change in activation energy at curie temperature and the relation of activation energies with composition can be explained and discussed in the light of the mechanism of hopping of polarons, which has been successfully employed to explain the electrical properties of

ferrites [4-5]. These polarons have low activation energy in magnetic region, while more activation energy in non-magnetic regions.

The electrostatic interaction between a conduction electron or hole and nearby ions may result in a displacement of the latter and hence in polarization of the surrounding region. So the carrier becomes situated at the centre of the polarization potential well. If this well is deep enough, a carrier may be trapped at a lattice site and its transition to a neighboring site may be determined by thermal activation. If this activation is sufficient, the conduction can take place by hopping of electrons, from one lattice to another.

In ferrites, having spinel structure, the B-B distances are smaller than A-A and A-B distances. Even then, the B-B distance is much larger than the sum of ionic radii of the cations involved, indicating a little or no overlap between d-d wave functions of ions on adjacent octahedral sites. This gives rise to a situation in which electrons are not free to move through the crystal but remain fixed on B-sites, necessitating a hopping process. However, in the ferrite samples, conductivity is decided mainly by the availability of a pair of cations [6] that facilitate hopping.

7.2.1 Hopping Model

Jonker [2] has observed in ferrites that the transport properties differ considerably from those of normal semiconductors, as the charge carriers are not free to move through the crystal lattice but jump from ion to ion. It is also observed that in this type of materials the possibility exists of changing the valency of a considerable fraction of metal ions and especially that of iron ions.

Assuming the number of electrons contributing to be equal to the number of Fe^{2+} ions and the number of electron holes to be equal to the number of Co^{3+} ions Jonker has calculated from resistivity data extremely low values of mobilities for electron and holes, and showed a fairly strong exponential dependence of resistivity on temperature. The temperature dependence of conductivity arises only due to mobility and not due to number of charge carriers in the sample.

7.2.2 Small Polaron Model

A small polaron is a defect created when an electron carrier becomes trapped at a given site as a consequence of the displacement of adjacent atoms or ions. The entire defect then migrates by an activated hopping mechanism. Small polaron formation can take place in materials whose conduction electrons belong to incomplete inner (d or f) shells, which due to small electron overlap; tend to form extremely narrow bands. The possibility for the occurrence of hopping conductivity in certain low mobility semiconductors, especially oxides, has been widely recognized for some time, and extensive theoretical literature has been developed which considers the small polaron model and its consequences [7-12].

The small polaron model also explains the low value of mobility, temperature independent, Seebeck coefficient and thermally activated hopping. In addition to these properties if the hopping electron becomes localized by virtue of its interaction within phonons, then a small polaron is formed and the electrical conduction is due to hopping motion of small polarons.

7.2.3 Phonon Induced Tunneling

Electrical properties of ferrites have been explained on the basis of tunneling of electrons amongst Fe^{2+} and Fe^{3+} atoms on B sites [13]. It has been assumed that the electrons, which participate in the $Fe^{2+} \rightarrow Fe^{3+} + e$ exchange process, are strongly coupled to the lattice and tunnel from one site to other due to a phonon-induced transfer mechanism.

7.3 EXPERIMENTAL TECHNIQUE

Fine powders of $Mn_x Zn_{1-x} Fe_2 O_4$ were pressed into pellets of the size 10mm diameter and of thickness ranging between 2mm to 3mm under a pressure of 75KN applied for 3minitues. Four sets of pellets were sintered in nitrogen atmosphere at temperatures, 1050°C, 1150°C, 1250°C and 1350°C respectively for 3 hours by setting heating and cooling rate at 5 degrees centigrade per minute. The pellets were silver pasted on either side for establishing good ohmic contacts with the electrodes. The dc resistivity measurements on these samples were then made using standard two-probe method.

7.4 DIELECTRIC CONSTANT

Ferrites act as dielectric materials in the low frequency regions. The dielectric constant of poly crystalline ferrites depends upon operating frequency. When alternating electric field is applied on the ferrite materials, there occurs dielectric displacement. They have abnormally high dielectric constant that shows the frequency dispersion. The dielectric constant of ferrites depends upon method of preparation [14], chemical composition and substitution [15], porosity and

grain size [16]. Krammer [17] has explained the relation between grain size and dielectric constant.

The dielectric dispersion can be explained on the basis of Koop's two layer model and Maxwell-Wagner polarization theory. To interpret the frequency response of dielectric constant in ferrite materials, Koops [18] suggested a theory in which relatively good conducting grains and insulating grain boundary layers of ferrite material can be understood as given by an inhomogeneous dielectric structure, as discussed by Maxwell [19] and Wagner [20]. Since an assembly of space requires finite time to line up their axes parallel to an alternating electric field, the dielectric constant naturally decreases, if the frequency of the field reversal increases.

The dielectric material reacts to an electric field differently from free space because it contains charge carriers that can be displaced. For an alternating field the time required for polarization shows phase retardation of the charging current instead of 90 ^{o} advanced .

It is advanced by some angle 90-δ where δ is the loss angle, which gives,

$$\text{Tan } \delta = K'' / K = \varepsilon'' / \varepsilon' \quad \text{---------- 7.4.1}$$

Where K's represent dielectric constant and ε's the permittivities. The loss factor Tan δ is the primary criterion for usefulness of dielectric as an insulating material.

The frequency dependence can be explained with the help of Maxwell–Wagner two-layer Model or the heterogeneous model of the polycrystalline structure of ferrites (Koops 1951). According to this theory two layers formed

dielectric structure. The first layer consists of ferrite grains of fairly well conducting (ferrous ions), which is separated by a thin layer of poorly conducting substances, which forms the grain boundary. These grain boundaries are more active at lower frequencies; hence the hopping frequency of electron between Fe^{3+} and Fe^{2+} ion is less at lower frequencies. As the frequency of the applied field increases, the conductive grains become more active by promoting the hopping of electron between Fe^{2+} and Fe^{3+} ions, thereby increasing the hopping frequency. Thus we observe a gradual increase in conductivity with frequency. But at higher frequencies the frequency of hopping between the ions could not follow the applied field frequency and it lags behind it. This causes a dip in conductivity at higher frequencies.

7.4.1 Experimental Technique

Pellets of the size 10mm diameter and of thickness ranging between 2mm to 3mm under a pressure of 75KN applied for 3minitues were made. Five sets of pellets were sintered in nitrogen atmosphere at temperatures 950°C, 1050°C, 1150°C, 1250°C and 1350°C respectively for 3 hours by setting heating and cooling rate at 5 degrees centigrade per minute. The pellets were silver pasted on either side for establishing good ohmic contacts with the electrodes. The dielectric measurements were carried out from room temperature to 500 °C with the variation of frequency 50Hz to 1MHz using HP 4284A precision LCR meter.

The capacitance C was measured and the dielectric constant, was calculated using the relation

$$\varepsilon' = ct/\varepsilon_o A \quad \text{---------- 7.4.2}$$

where t = Thickness of pallet

A = Area of cross section

ε_o = permittivity of free space.

7.5. RESULTS AND DISCUSSION

7.5.1 Resistivity

Fig.7.5.1.1 (a, b, c, d) shows plots of log ρ v/s 1000/ T (K) for $Mn_x Zn_{(1-x)} Fe_2O_4$ ferrite. A semiconductor like general behavior is seen for all the samples as the samples undergo a second order ferrimagnetic to paramagnetic phase transition. Although the trends depend on the concentration of Mn in the sample these are more strongly dependent on the sintering temperature of the sample. Resistivity values at 300K are seen to vary between 3.789×10^7 ohm-cm and 1.898×10^6 ohm-cm for samples sintered at 1050°C the highest and the lowest being observed for $Mn_{0.35}Zn_{0.65} Fe_2O_4$ and $Mn_{0.4}Zn_{0.6} Fe_2O_4$ respectively. A considerable variation in the resistivity is observed for samples sintered at 1150°C. The resistivity at 300K is found to vary between 7.5×10^8 ohm-cm and 2.832×10^6 ohm-cm with the highest for $Mn_{0.65}Zn_{0.35} Fe_2O_4$ sample. These values are found to be much lower for samples sintered at 1250°C and are found to range

between 2.285 $\times 10^6$ ohm-cm and 6.08 $\times 10^5$ ohm-cm. A large variation in the resistivity values is observed for samples sintered at 1350°C both at 300K and at higher temperatures with the highest being 1.624 $\times 10^9$ ohm-cm. for $Mn_{0.6}Zn_{0.4}Fe_2O_4$ at 300K. It may be seen that large variations in resistivity at 300K are observed for samples sintered at 1150°C and 1350°C. This may be due to formation of definite small grain shapes with high resistive boundaries in between any nearby neighbors and is evident from the SEM photographs (fig.7.5.1.3) [21]. In ferrites electron conduction mechanisms have been studied by many investigators [22]. Various models were proposed; however, the thermally activated hopping model is found to be more appropriate in explaining qualitatively the electrical behavior of Mn-Zn ferrites. In the hopping process the additional electron on a ferrous (Fe^{2+}) ion requires little energy to move to an adjacent (Fe^{3+}) on the equivalent lattice sites (B sites). In presence of the electric field, these extra electrons hopping between iron ions give rise to the electrical conduction. Therefore, any change in the (Fe^{2+}) ion content in the spinel ferrite lattice and/or the distance between them is crucial to the intrinsic resistivity of Mn-Zn ferrite grains, including the intrinsic grain boundaries. If the introduction of another cation into the lattice causes a change in the valency distribution on the B sites, then the number of electrons potentially available for transfer will be altered. On the other hand, the incorporation of foreign (addition of impurity) ions can change the distance between the B lattice sites, which is crucial for the conduction mechanism. Thus, the formation of an intrinsic grain boundary in doped samples by the segregation of aliovalent ions must increase the resistivity.

This gives rise to polycrystalline Mn-Zn ferrite with nonferrimagnetic grain boundary, ferrimagnetic outer grain region and ferrimagnetic conductive core. Thus the contribution to the bulk resistivity may be considered as resistivity contribution coming from three different regions. To establish a relation between the Power loss due to eddy currents and the average grain diameter a hypothetical brick wall model is applied. As per the model each layer can be represented by a resistance – capacitance (R-C) lumped circuit of high Ohmic layers. When the resistivity of the bulk is much lower than the grain boundary layers, the equivalent circuit of the ferrite can be represented by a series of lumped R-C circuits of the grain boundary layers [23].

As the samples under investigation are sintered from nanoparticle Mn-Zn ferrite in a reducing atmosphere with no additives there is no possibility of formation of high resistivity ferrimagnetic outer grain boundary. Thus the total contribution should come only from the non-ferrimagnetic grain boundaries and ferrimagnetic conductive core. It is evident from Fig.7.5.1.2 that due to phase transitions samples sintered at 1150°C and 1350°C show small grain sizes with large nonferrimagnetic grain boundaries more over the total surface area of the sample also increases due to formation of fine crystals which results in high resistivity for the samples [24]. The samples sintered at 1050°C and 1250°C do not show formation of perfect crystals or small grain shapes which results in low surface area and less high resistivity nonferrimagnetic grain boundaries which accounts for low value of resistivity at 300K for this samples as compared to

samples sintered at 1150°C and 1350°C. The resistivity values obtained are much higher as compared to the reported resistivity values of 10^5 ohm-cm [25,26].

The unusual behavior observed in the resistivity trends of the samples may be attributed to the existence of phase transitions, which occur during the crystal formation process while sintering [24].

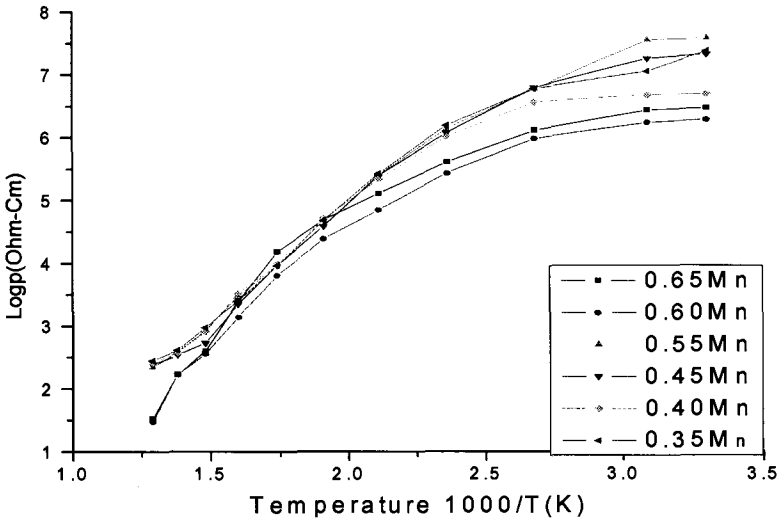

(a)

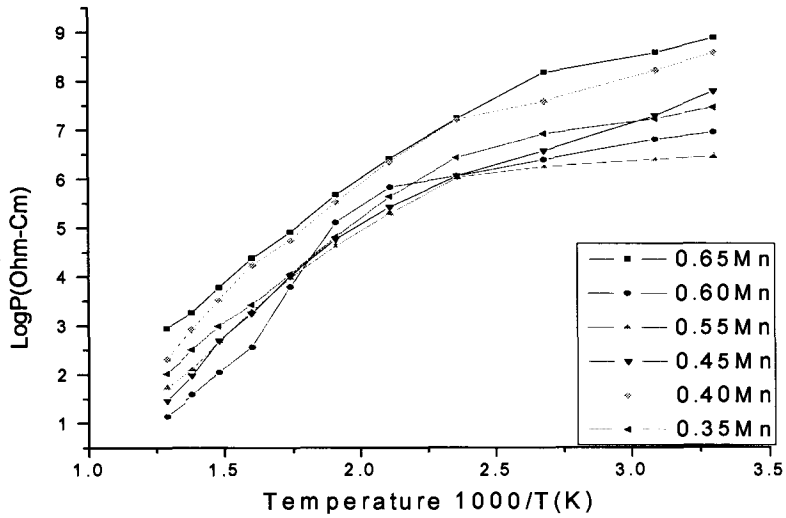

(b)

Fig.7.5.1.1: Variation of resistivity for the samples of different compositions, sintered at (a) 1050°C (b) 1150°C

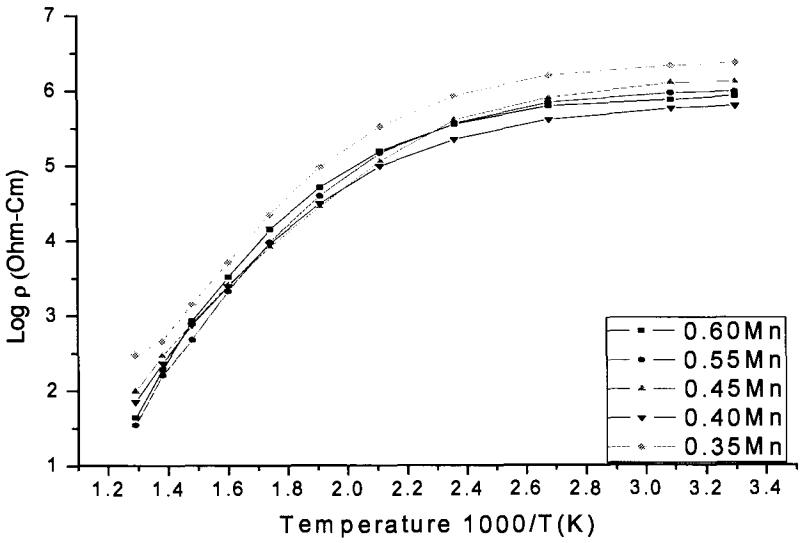

©

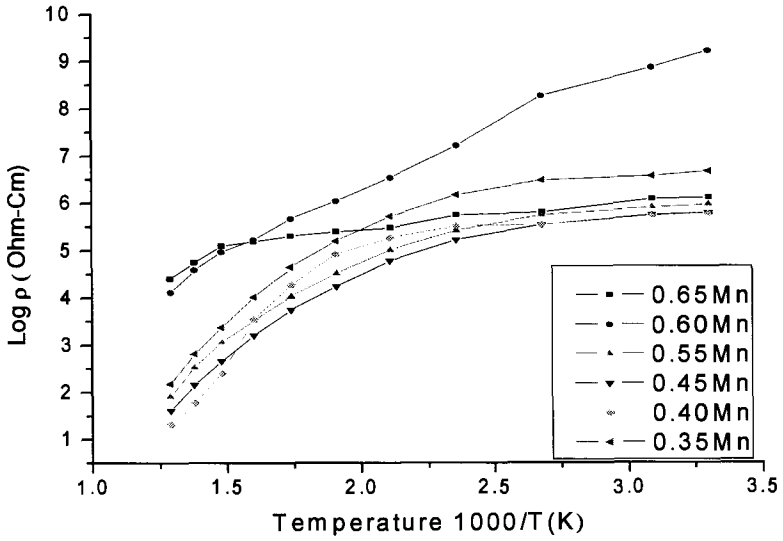

(d)

Fig.7.5.1.1: Variation of resistivity for the samples of different compositions, sintered at (c) 1250°C & (d) 1350°C

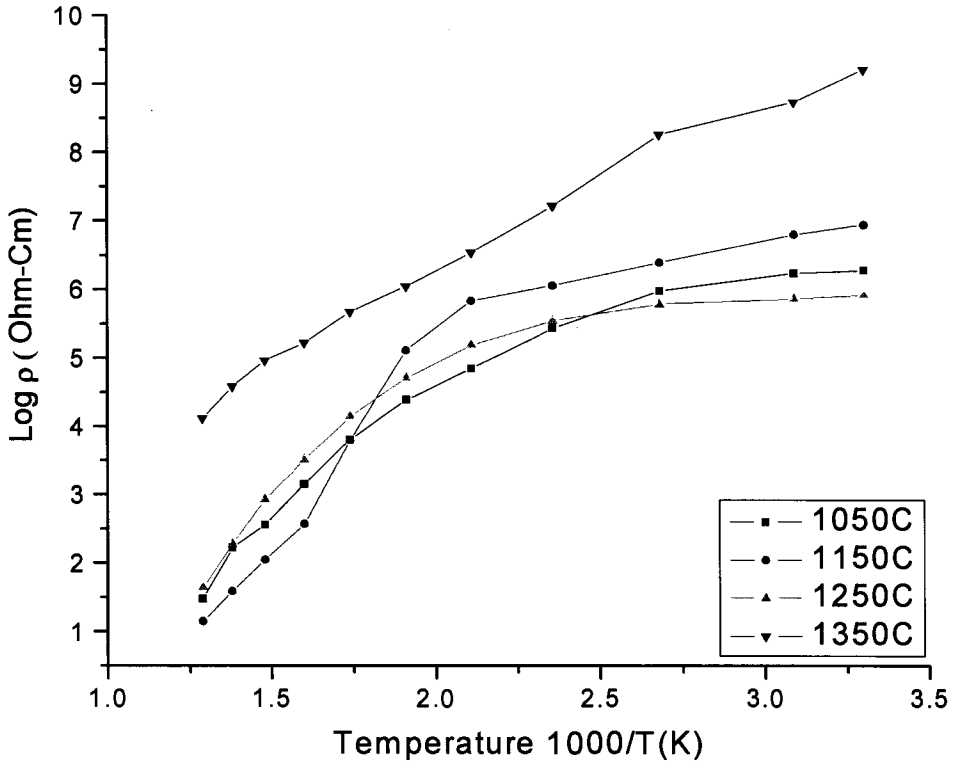

Fig.7.5.1.2: Variation of resistivity for the sample $Mn_{0.6}Zn_{0.4}Fe_2O_4$ sintered at various temperatures

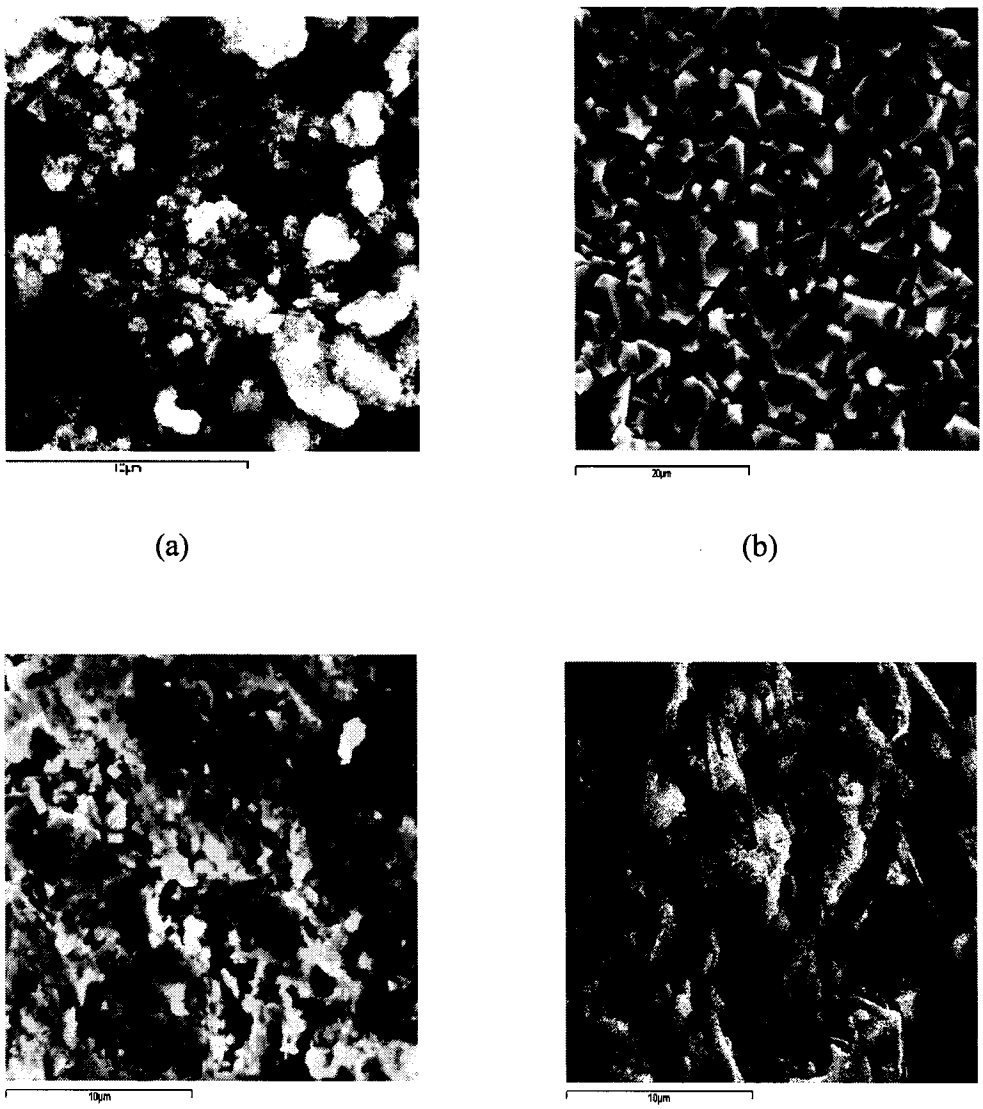

(a) (b)

© (d)

Fig.7.5.1.3: SEM Photographs of $Mn_{0.60}Zn_{0.40}Fe_2O_4$ sintered in nitrogen atmosphere for 3 hours at (a) 1050°C (b) 1150°C (c) 1250°C & (d) 1350°C

7.5.2 Dielectric Constant

7.5.2.1 Frequency Dependence of Dielectric Constant

Fig.(a, b, c, d & e) show the variation of dielectric constant (ε^{1}) with frequency for the $Mn_{(x)}Zn_{(1-x)}Fe_2O_4$ samples sintered at 950 °C, 1050 °C, 1150 °C, 1250 °C and 1350 °C.

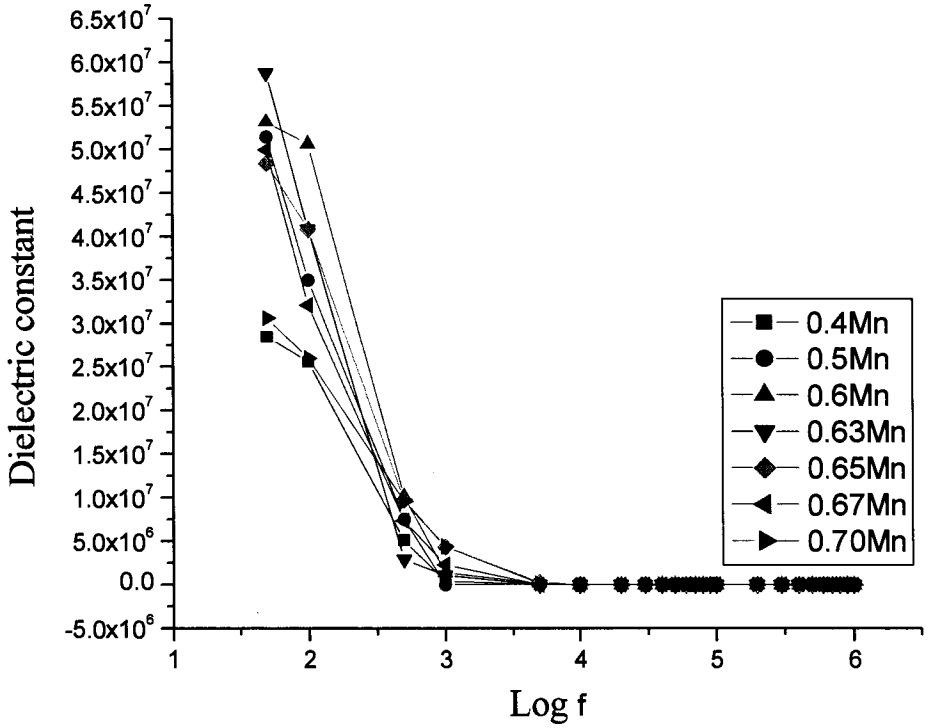

(a)

Fig.7.5.2.1(a): Variation of dielectric constant for the samples of different compositions, sintered at 950°C

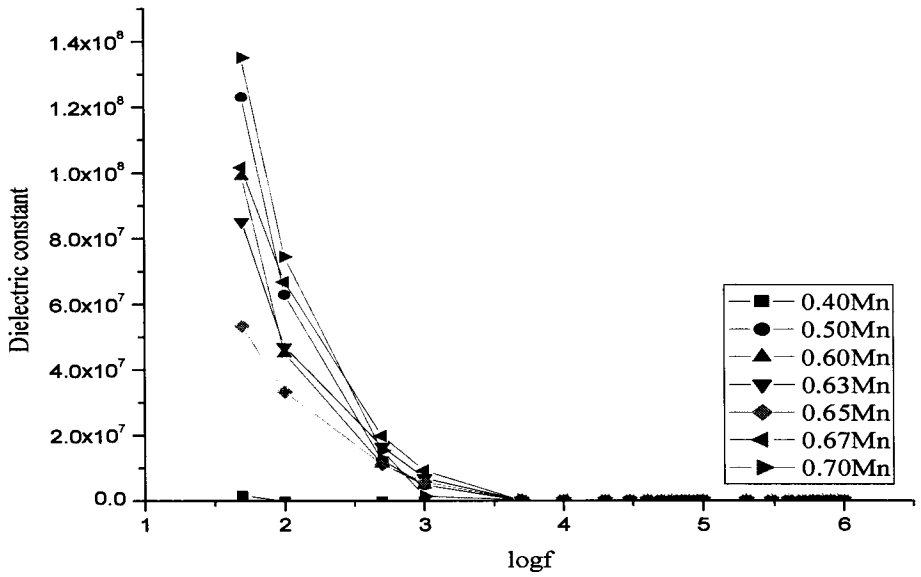

(b)

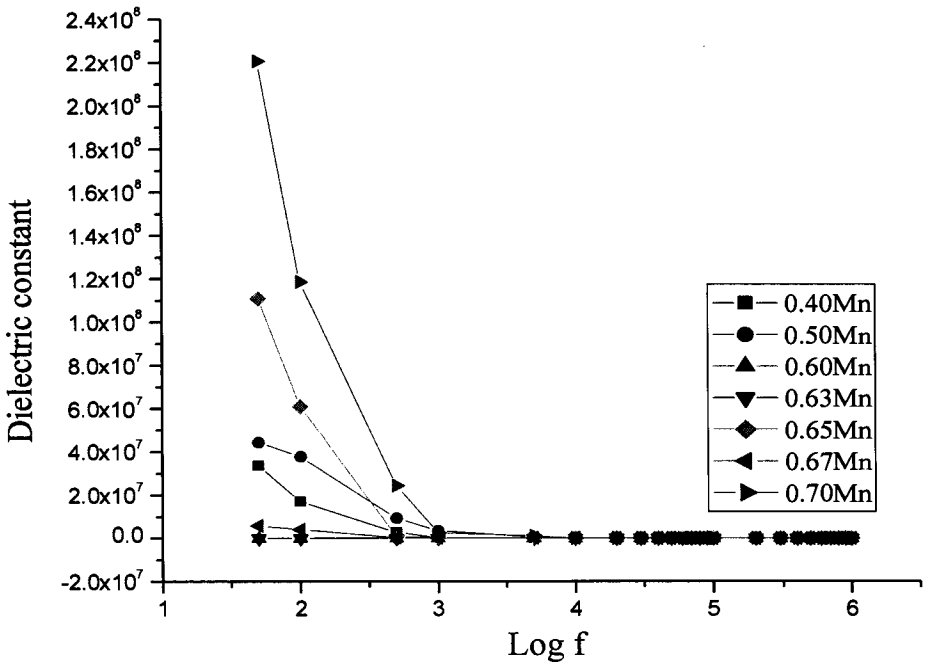

©

Fig.7.5.2.1: Variation of dielectric constant for the samples of different compositions, sintered at (b) 1050°C (c) 1150°C

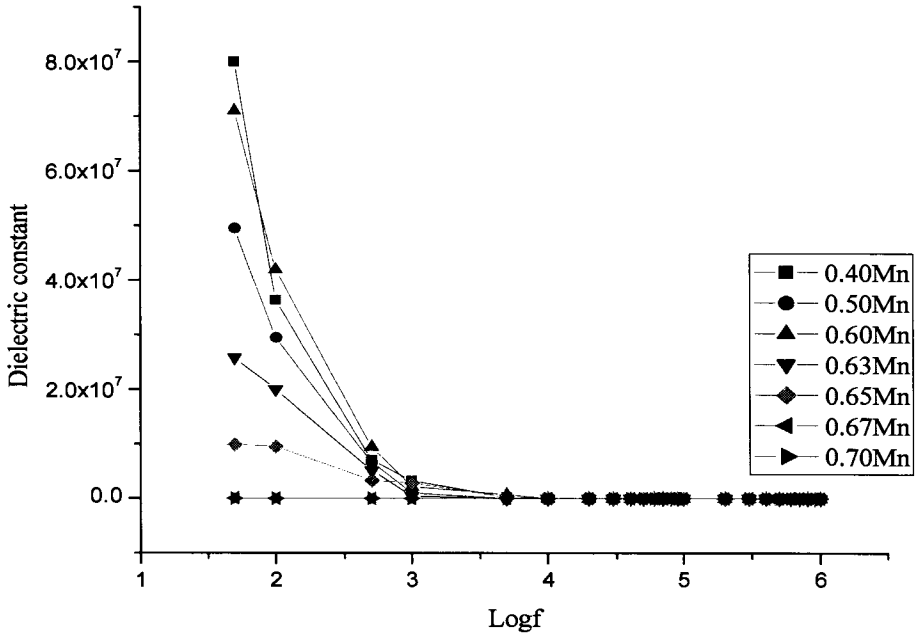

(d)

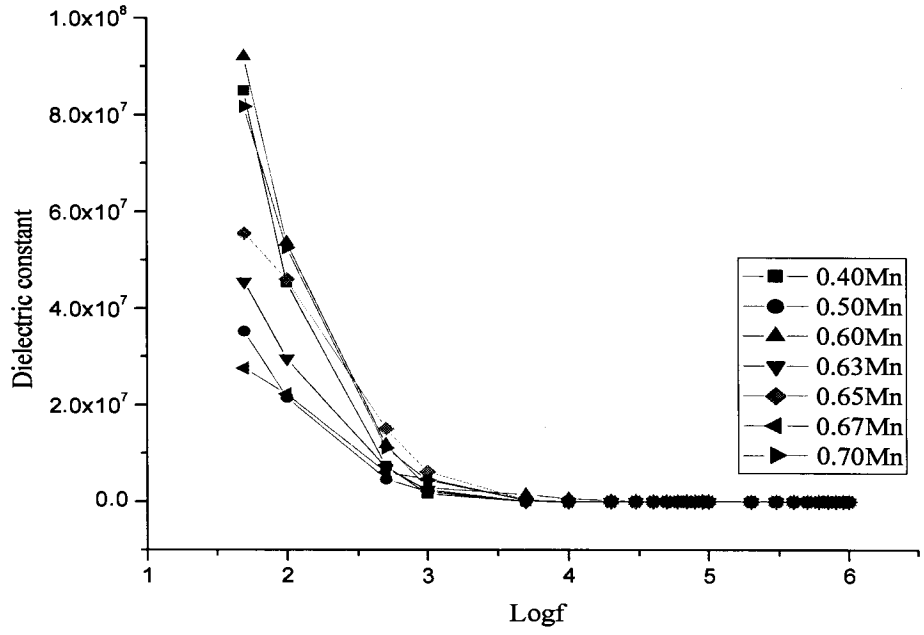

(e)

Fig.7.5.2.1: Variation of dielectric constant for the samples of different compositions, sintered at (d) 1250°C & (e) 1350°C

It can be seen from the figures that the dielectric constant is found to decrease with increase in frequency reaching a very low value at higher frequencies for all the samples sintered at various temperatures. The polarization decreases with increase in frequency and the changes are very negligible beyond a certain frequency limit. The variation of dielectric constant with frequency reveals the dispersion due to Maxwell-Wagner [27,28] type interfacial polarization in agreement with Koops phenomenological theory [29]. The decrease of dielectric constant with increase of frequency as observed in the case of mixed ferrites is a normal dielectric behavior. This normal dielectric behavior was also observed by several other investigators [30-32]. Reddy et.al. have studied the variation of dielectric constant with frequency for ferrites [33]. They have explained the behavior qualitatively as due to the fact that the electron exchange between Fe^{3+} and Fe^{2+} ions cannot follow the frequency of the externally applied alternating field beyond a certain limit. The large decrease in dielectric constant validates the two-layer model assumption [34]. The large values of dielectric constant at lower frequencies have been attributed to the predominance of the species like Fe^{2+} ions, interfacial dislocation pile ups, oxygen vacancies, grain boundary defects etc [27,28].

Appreciable changes in the values of dielectric constant is observed at room temperature for the same frequency as the samples are sintered at different temperature.

The values of dielectric constant at 300K and 50Hz frequency are seen to vary between 5.877×10^7 and 2.845×10^7 for samples sintered at 950°C the highest

and the lowest being observed for $Mn_{0.63}Zn_{0.37}Fe_2O_4$ and $Mn_{0.40}Zn_{0.60}Fe_2O_4$ respectively. For the samples sintered at 1050°C the values vary between 1.35×10^8 and 1.638×10^6, the highest and the lowest being observed for $Mn_{0.70}Zn_{0.30}Fe_2O_4$ and $Mn_{0.40}Zn_{0.60}Fe_2O_4$ respectively.

It can be seen that sample $Mn_{0.70}Zn_{0.30}Fe_2O_4$ sintered at 1150 °C exhibits the highest value of dielectric constant $2.21X\ 10^8$ at room temperature at 50Hz frequency which is comparable to reported values. The lowest value of dielectric constant $2.510X10^3$ is observed for the sample $Mn_{0.60}Zn_{0.40}Fe_2O_4$ sintered at same temperature. These values are found to be lower for samples sintered at 1250°C and are between 8×10^7 and 2.29×10^3 for the samples $Mn_{0.40}Zn_{0.60}Fe_2O_4$ and $Mn_{0.70}Zn_{0.30}Fe_2O_4$ respectively. The samples sintered at 1350 °C, dielectric constant ranges between 9.20×10^7 and 2.759×10^7 for $Mn_{0.60}Zn_{0.40}Fe_2O_4$ and $Mn_{0.67}Zn_{0.33}Fe_2O_4$ respectively.

The values of dielectric constant for all other samples sintered at different temperatures lie between $2.21X\ 10^8$ and $2.510X10^3$.

It has been reported that there is strong correlation between the conduction mechanism and the dielectric behavior of the ferrites starting with the conjecture that the mechanism of the polarization process in ferrites is similar to that of the conduction process [35,36]. They observed that the electronic exchange between $Fe^{2+} \Leftrightarrow Fe^{3+}$ results in local displacements that determine the polarization behavior of the ferrites. The dependence of the dispersion of dielectric constant on composition can be explained on the basis of the available ferrous ions on octahedral sites [37]. As the frequency of the externally applied electric field

increases gradually, and though the same number of ferrous ions are present in the ferrite material, the dielectric constant decreases. This reduction occurs because, beyond a certain value of frequency of the externally applied field, the electronic exchange between ferrous and ferric ions cannot follow the alternating field that is the field changes are too fast. The variation of dispersion with composition can also be explained on same basis.

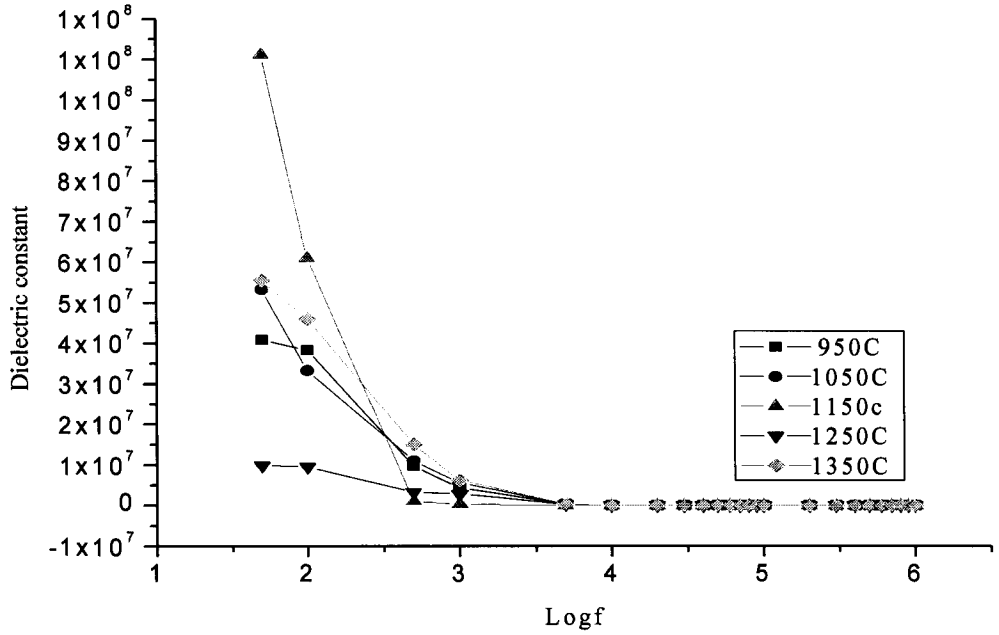

(a)

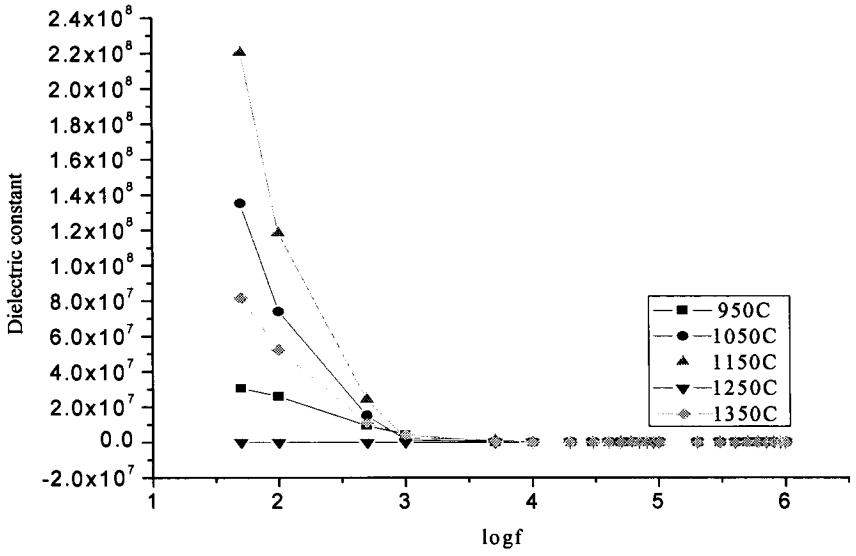

(b)

Fig.7.5.2.2: Variation of dielectric constant for the samples sintered at different temperatures (a) $Mn_{0.65}Zn_{0.35}Fe_2O_4$ and (b)$Mn_{0.70}Zn_{0.30}Fe_2O_4$

Fig7.5.2.2 shows variation of dielectric constant for samples $Mn_{0.65}Zn_{0.35}Fe_2O_4$ and $Mn_{0.70}Zn_{0.30}Fe_2O_4$. It can be seen that the dielectric constant values for the sample at 300K initially increases with the sintering temperature exhibiting a maximum value at 1150 °C. These values are found to be much lower for samples sintered at 1250°C. The dielectric constant values again found to be high for samples sintered at 1350°C both at 300K. It may be seen that large variations in dielectric constant at 300K are observed for samples sintered at 1150°C and 1350°C. This may be due to formation of definite small grain shapes. The present unusual behavior observed in the dielectric constant may be attributed to the existence of phase transitions which occur during the crystal formation process while sintering [24].

7.5.2.2 Temperature dependence of dielectric constant

Fig7.5.2.2 shows variation of dielectric constant for samples $Mn_{0.65}Zn_{0.35}Fe_2O_4$ and $Mn_{0.70}Zn_{0.30}Fe_2O_4$. It can be seen that the dielectric constant values for the sample at 300K initially increases with the sintering temperature exhibiting a maximum value at 1150 °C. These values are found to be much lower for samples sintered at 1250°C. The dielectric constant values again found to be high for samples sintered at 1350°C both at 300K. It may be seen that large variations in dielectric constant at 300K are observed for samples sintered at 1150°C and 1350°C. This may be due to formation of definite small grain shapes. The present unusual behavior observed in the dielectric constant may be attributed to the existence of phase transitions which occur during the crystal formation process while sintering [24].

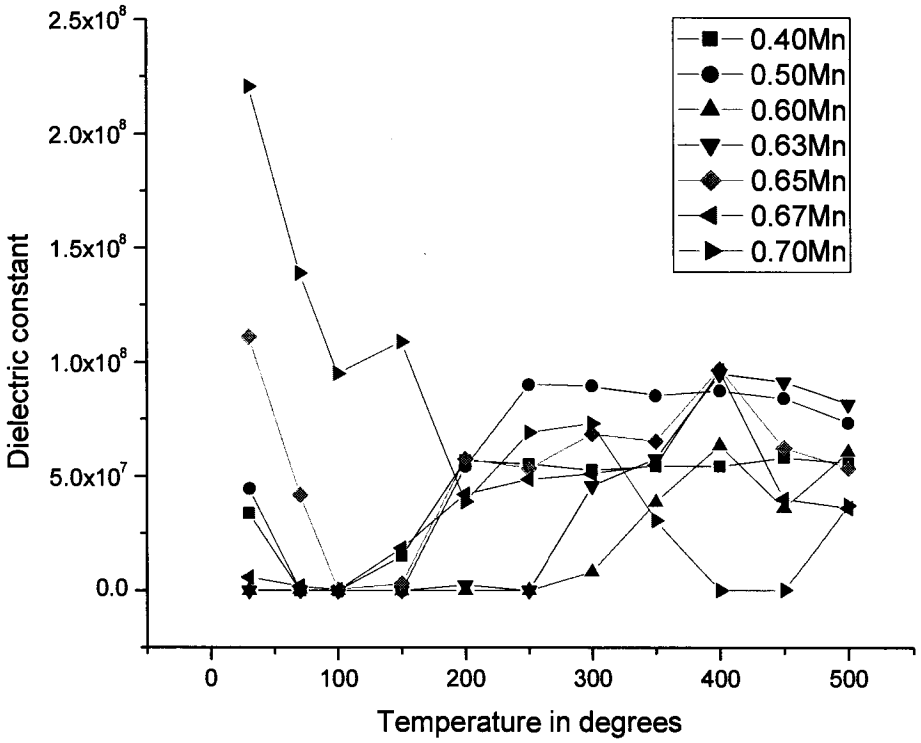
2.5x10^8
2.0x10^8
1.5x10^8
1.0x10^8
5.0x10^7
0.0
Dielectric constant
0
100
200
300
400
500
Temperature in degrees
0.40Mn
0.50Mn
0.60Mn
0.63Mn
0.65Mn
0.67Mn
0.70Mn

(a)

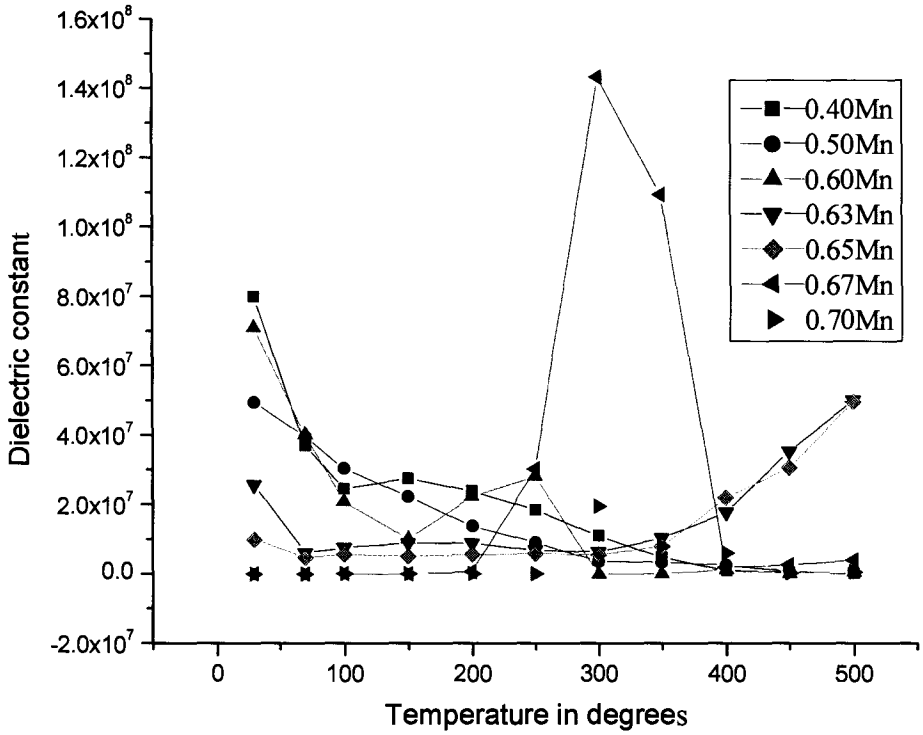

(b)

Fig.7.5.2.3: Variation of dielectric constant with temperature for the samples of different compositions, sintered at
(a) 1150°C (b) 1250°C

The temperature dependence of dielectric constant at selected frequencies for the different samples are as shown in fig. 7.5.2.3. It is observed that almost for all compositions the dielectric constant initially decreases as the temperature increases followed by a peak at certain temperature. In some samples a prominent peak is observed. The observed peaks may be attributed to two competitive effects, the first of which is the increase of the mobility of charge carriers with increasing temperature leading to an sudden increase in dielectric constant, as the conductivity and polarization is of the same origin, and the second opposing

effect is the hindrance of the charge carriers movements due to thermal agitation[38]. Also those peaks are attributed to the presence of two types of charge carriers as reported by Rezlescu [37].

7.5.2.3 Dielectric loss factor

The dielectric loss factor (tanδ) is plotted against frequency as shown in Fig. 7.5.2.4 (a & b). It is observed that for some of the samples the value of tanδ rapidly decreases as the frequency is increased whereas it remains extremely low for most of the samples for all sintering temperatures.

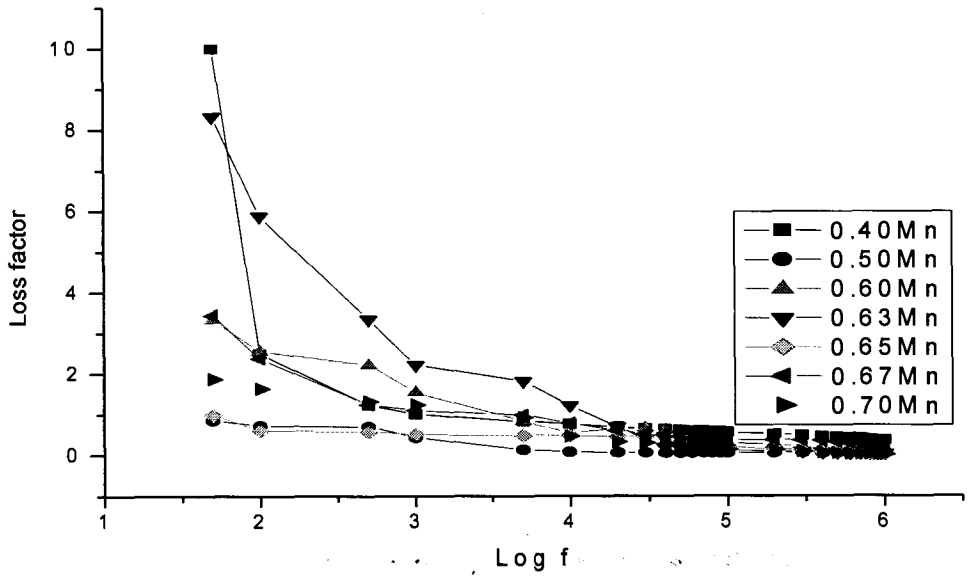

(a)

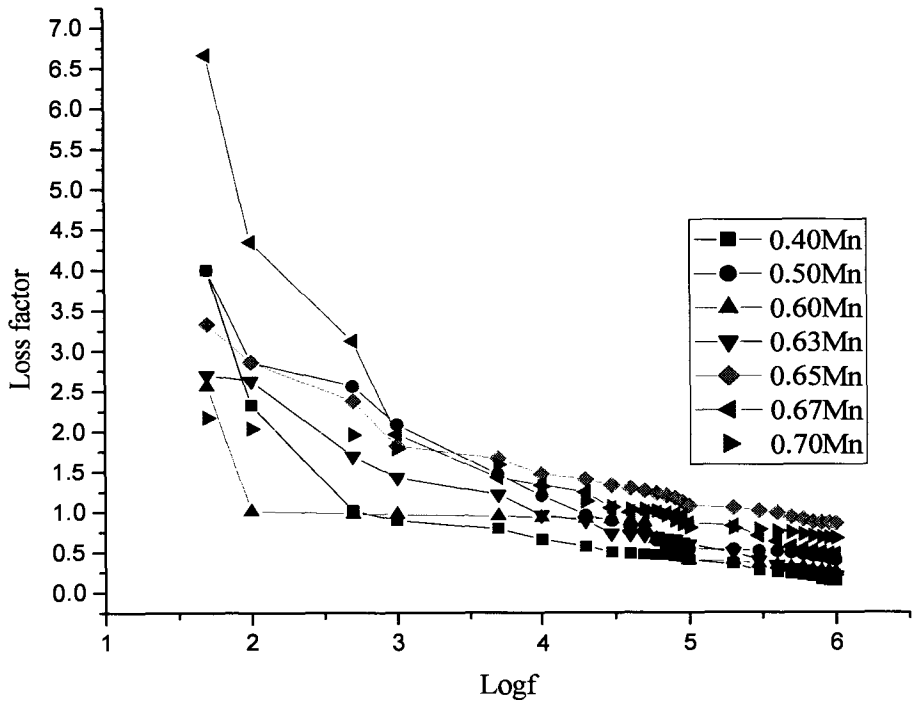

(b)

Fig.7.5.2.4: Variation of loss factor for the samples
(a) $Mn_{0.65}Zn_{0.35}Fe_2O_4$ and (b)$Mn_{0.70}Zn_{0.30}Fe_2O_4$

References

[1] L.G.Van Uitert, Proc.I.R.E. 44 (1956) 1294.

[2] G.H.Jonker, J.Phys. Chem. Solids, 9, (1959), 165.

[3] E.J.W. Verwey and J.H.de Boer, Reauil Ches Travaux chimques des Phys. Bas(Czeckh), 55(1936) 531.

[4] N. Rezlescu and E. Rezlescu, Solid State commun. 14 (1974) 69.

[5] Z. Sisma, J.Simsova and V.A.M.Borabers, in Proc. 11^{th} Int. Conf. on progr. Of semiconductors (Warsaw, Poland) 2 (1972) 1294.

[6] E.J.W.Verwey, P.W.Haayman, F.C.Romeijn and G.W.Van Oosterhout, Philips Res. Rep. 5 (1950) 173.

[7] J. Yamashita and T. Kurosawa, J.Phys. Chem. Solids, 5,34 (1958).

[8] T.Holstein, Ann.Phys., (N.Y.) 8, (1959), 343.

[9] J.Appel, Solid state Phys., 18, (1969), 41.

[10] I.G.Austin and N.F.Mott, Adv.Phys., 18 (1969).

[11] H.L.Tuller and A.S.Nowick; J.Phys. Chem. Solids, 38 (1977) 859.

[12] B.Gillot, Mat.Res.Bull, 11 (1976) 848

[13] G.Srinivasan and C.M.Srivastava, Phys. Stat.Solidi,108, (1981) 665.

[14] K.Iwauchi, Jpn, J.Appl. Phys. 10(1971) 1520.

[15] C.Prakash and J.S.Baijal, J.Less common Met. 107 (1985) 169.

[16] V.P. Miroshkin, Y.I.Panovaand, V.V.Passynrov, Phys. Stat. Sol.(a) 66 (1981) 779.

[17] G.P.Kramer, J. Ya Ponava and V.V.passynkov, Phys. Stat. Sol.(a) 86 (1993) 95.

[18] C.G.Koops, Phys. Rev.83 (1951) 121.

[19] J. C. Maxwell, A Treatise on Electricity and Magnetism, Clarendon Press, Oxford p.(1982) 328.

[20] K. W. Wagner, Ann. Physik 40, (1913) 817.

[21] S.H.Keluskar, R.B.Tangsali, G.K.Naik, J.S.Budkuley, J.Mag.& Mag. Mater. (in press)

[22] M. I. Klinger and A. A. Samokhvalov, Phys. Status Solidi B 79 (1977) 9.

[23] M. Drofenik, A. Znidarsic, I. Zajc, J. Appl. Phys. 82 (1) (1997) 333-340.

[24] R.B. Tangsali, S.H. Keluskar, G.K.Naik and J.S.Budkuley, Journal of Material science (in press).

[25] T. Nakamura Y. Okano, J. Appl. Phys. 79, (1996) 7129.

[26] E. Otsuki, S. Yamada, T. Oysuka, K. Shoji, and T. Sato, J. Appl. Phys. 69 (1996) 5942.

[27] J.C. Maxwell "Electricity and Magnetism" Oxford University press, N.Y.I (1950).

[28] K. W. Wagner, Ann. Physik, 40 (1913) 817.

[29] C. G. koops, Phycs., Rev., 83(1951) 121.

[30] Chandra Prakash and Bajal J. S. J. Less Common metals 51 (1985) 107.

[31] Ravinder D. Phys. Status Solidi (a) 139 K 69.

[32] Ramana Reddy, A.V.Ranga Mohan G., Ravinder D. and Boyanov B.S. J.Mater. Sci.34, (1999), 3169.

[33] M.B.Reddy and P.V.reddy Appl.Phys.(UK) 24, (1991), 975.

[34] R.Raman, V.R.K.murthy, B.Vishvanathan J. Appl. Phys.69(7) (1991) 4053.

[35] Rabinkin L.I. and Novikova Z.I. Ferrites Minsk (1960) 146.

[36] Iwauchi K Jap.J.Appl.Phys. 10 (1971) 1520.

[37] Rezlescu N. and Rezlescu E. Phys. Status Solidi A23 (1974) 575.

[38] M. M. El kestawy, Thesis Ph. D. Department of Physics,

Faculty of science, Tanta university (2003).

CHAPTER VIII

CONCLUSIONS

8.1 SUMMARY

This study is undertaken to examine nitrilotriacetate precursor method for synthesis of high performance fine particle **Mn - Zn** ferrite material having general formula $\mathbf{Mn_{(x)}\,Zn_{(1-x)}\,Fe_2O_4}$. This method was employed to synthesize these materials by varying concentration of Zn in the sample where

x = 0.30, 0.35, 0.40, 0.45, 0.50, 0.55, 0.60 and 0.65. Two different modes of decomposition of the precursor complex was used.

Samples obtained by combustion of precursor were found to yield expected ferrite materials, so confirmed by well known methods of characterization such as

i) Chemical analysis (percentage yield, EDAX)

ii) FTIR Spectra analysis

iii) X-ray diffraction analysis

The relevant data has been presented in chapter IV. Further Scanning Electron Micrographs taken on these samples show formation of fine particle samples, however the particles were found to agglomerate on large scale due to their fine nature. The average crystallite size calculated using Scherrer formula was in the range of 4.464 nm to 25.276 nm whereas the crystallite size as observed from the SEM micrographs are found to be slightly larger than expected. Saturation magnetization ($\mathbf{M_s}$) measurements made on the powdered samples show very high values for $\mathbf{M_s}$ compared to the reported values for nanoparticle sample. The

highest value was obtained for sample with x=0.55. The Curie temperature values (750K-380K) for the samples are found to be higher then the reported values (500K –300K). The hysteresis losses for the samples are found to be lower and the densities of the samples are found to be on the higher side. Dependence of lattice constant "a", particle size, saturation magnetization, Curie temperature, hysteresis loss and the density on Zn concentration are strongly noticed in this work. Similar measurements are also carried out on the bulk sample obtained by sintering of the nanoparticle samples. These measurements not only confirmed conclusions drawn from the results obtained on the nanoparticle sample but provide more information on the behavior of the bulk samples. In addition to the Zn concentration, the properties of the sample are found to depend on the microstructure of the sample. The microstructure of the sintered samples are different for different sintering temperature. Scanning electron micrographs of the samples sintered at 950°C, 1050°C, 1150°C, 1250°C and 1350°C showed development of different crystalline phases of the samples. The magnetic and the electrical property studies carried out on this samples indicate that control of Zn concentration in the sample is not the only factor that affected these properties but the same are strongly dependent on microstructure of the sample which in turn depended on the sintering conditions. The samples exhibited high values for saturation magnetization, low loss, high values for magnetic permeability, high values for resistivity, and high values for dielectric constant. The high value of saturation magnetization, high value of permeability (25,472), low relative loss factor (10^{2} to 10^{-6}), high value of room temperature resistivity (10^{9} ohm-cm),

high value of dielectric constant (10^8) and extremely low loss are essential parameters for high performance Mn-Zn ferrite.

Although the work carried out provide a better route for synthesis of high performance nano material, the quest for improved performance and to pinpoint the critical value of Zn concentration for optimization of the magnetic properties, are achieved with samples obtained by decomposing precursor using microwave decomposition technique.

$\mathbf{Mn_{(x)}Zn_{(1-x)}Fe_2O_4}$ ferrite samples with x= 0.40,0.50,0.60,0.63,0.65,0.67 and 0.70 were prepared and characterized. The newly prepared powdered samples show less tendency towards agglomeration. Particle size data was collected by employing four different techniques, and presented in Chapter V, which provide a strong evidence of synthesis of high quality nanoparticle Mn-Zn ferrite. The results obtained by Scherrer formula, Transmission Electron Microscopy and Scanning Probe Microscopy are found to show formation of nanoparticle sample with crystallite size in the range of 10nm to 80nm. The Scanning Electron Micrograph showed large size crystals, this is probably due to low energy electron beam and strong magnetic moment of the sample, suggesting that for strongly magnetic samples, SEM is not a suitable technique for crystallite size measurements. The magnetic properties in particular the saturation magnetization, retentivity, hysteresis loss, AC susceptibility, Curie temperature measurements and SQUID measurements made for these samples provide testimony to the

performance of these samples. The samples show high saturation magnetization at room temperature, the highest value of 63.03 emu /gm is obtained for $Mn_{(0.65)}Zn_{(0.35)}Fe_2O_4$. The hysteresis loss is extremely low and most of the samples exhibits a mixed SD-MD behavior except a few in particular $Mn_{(0.70)}Zn_{(0.30)}Fe_2O_4$ which shows SD behavior. The SQUID measurements carried out on this sample show a high of 101emu/gm for saturation magnetization at 35K. Low temperature hysteresis show superparamagnetic behavior with zero hysteresis loss for the sample there by confirming single domain behavior. The magnetic properties of the samples sintered at 950°C, 1050°C, 1150°C, 1250°C and 1350°C to obtain bulk Mn-Zn ferrite are studied employing hysteresis loop tracer, pulse field AC susceptibility equipment and vibrating sample magnetometer. The saturation magnetization measurements made on the samples show high values for saturation magnetization. A room temperature high of 74.54emu/gm is observedfor sample $Mn_{(0.67)}Zn_{(0.33)}Fe_2O_4$. The hysteresis loss is found to be extremely low and zero in some cases. The Mr/Ms ratio for the samples was found to be very low the lowest being 0.0015, which is less than the value set for superparamagnetic materials. This sample was found to exhibit superparamagnetic like behavior which is a rare phenomena in bulk materials. Other measurements like AC susceptibility on the sample suggested a mixed SD-MD behavior for the sample. The Curie temperatures obtained for the samples are found to be quite high than the reported values.

Thus, the detail analysis of the results of this investigation of samples obtained by two different decomposition techniques suggests that high performance nanoparticle Mn-Zn ferrite can be synthesized using nitrilotriacetate precursor method. Materials with enhanced properties can be synthesized by same method by decomposing the precursor employing microwave technique. The bulk samples produced by sintering of this nanoparticle Mn-Zn ferrite also exhibit enhanced, unique and very unusual behavior.

8.2 SCOPE FOR FUTURE WORK

Research, development and growth go hand in hand as the later two are dependent on the first. Since there is always a room for improvement and widening the areas of application, good amount of work can be taken up on these materials.

1. An in depth study to understand the structural properties of the sintered samples in particular can be taken up. This is to ascertain if there is occurrence of structural phase transition in the sintered materials sintered at 950°C, and 1050°C in particular.
2. Small Angle X-ray Scattering (SAXS) study to investigate the density fluctuations in the sample on a distance scale can be taken up.
3. Investigations by using Small Angle Neutron Scattering (SANS) for studying the variation of density, magnetization and concentration on a nanometer length scale could be interesting.

4. Study of magnetite properties at low temperature and low field employing VSM and SQUID to know about the softness of material or the behavior of superparamagnetism in nanosample as well as bulk samples could be interesting..

5. Study of resistivity and permeability of nanoparticles and sintered samples prepared by microwave-induced combustion can also be taken up.

6. Microwave absorption studies for application as good insulating magnetic oxide material could be interesting.

7. Study of phase transitions in sintered samples prepared by microwave induced combustion needs to be taken up.

8. Thermoelectric power studies which leads to its applications in sensor devices can be studied.

Thus a host of new studies can be taken up on these materials as the same are advanced materials and find applications in high technology areas.

International Journal of
NANOSCIENCE
www.worldscinet.com/ijn.html

Volume 3 • Numbers 4 & 5 • August & October 2004

Special Issue on
ICMAT 2003, Symposium N1: Surface and Nanoscale Science
Edited by H. C. Kang & W. S. Chin
(National University of Singapore, Singapore)

Effect of Sintering Conditions on Magnetic Properties of Nanoparticle Mn–Zn Ferrite Synthesized with Nitrilotriacetate Precursor Method

R. B. Tangsali, S. H. Keluskar, G. K. Naik and J. S. Budkuley

World Scientific
NEW JERSEY • LONDON • SINGAPORE • BEIJING • SHANGHAI • HONG KONG • TAIPEI • CHENNAI

International Journal of Nanoscience
Vol. 3, Nos. 4 & 5 (2004) 589–597

World Scientific
www.worldscientific.com

EFFECT OF SINTERING CONDITIONS ON MAGNETIC PROPERTIES OF NANOPARTICLE Mn–Zn FERRITE SYNTHESIZED WITH NITRILOTRIACETATE PRECURSOR METHOD

R. B. TANGSALI
Department of Physics, Goa University
Taleigao Plateau, Goa, India 403206

S. H. KELUSKAR
Department of Physics, P.E.S. College of Arts and Science
Ponda, Goa, India 403401

G. K. NAIK and J. S. BUDKULEY
Department of Chemistry, Goa University
Taleigao Plateau, Goa, India 403206

Nitrilotriacetate precursors have been used for synthesis of oxide materials. High permeability Mn–Zn ferrite with general formula $Mn_xZn_{1-x}Fe_2O_4$ where $x = 0.3/0.35/0.4/0.45/0.5/0.55/0.6/0.65/0.7$ were prepared using this novel method. Formation of cubic spinel structure was confirmed by XRD, which also provided information on formation of fine particle material. The magnetic properties of these materials were investigated after sintering the same at 950°C, 1150°C, 1250°C and 1350°C in nitrogen atmosphere and at 1050°C in air and were found to be interesting.

Keywords: Nitrilotriacetate; hydrezinium; nanoparticle; sintering; hysteresis; domain.

1. Introduction

Research in nanomaterials is growing at a dramatic pace since reduced dimensions in the nanometer range alter the properties of the materials. This has opened up enormous possibilities to meet the challenges in different fields like electronics, optoelectronics, medicine, biotechnology, engineering, defense, information technology, etc. Production of efficient devices with new technology can save tremendous amounts of energy, decrease their size and increase efficiency.

Ferrofluids is a relatively new class of magnetic materials, consisting of magnetic nanoparticles colloidally dispersed in a carrier liquid, exhibit both fluid and magnetic properties.[1] This gives rise to the numerous unusual fundamental phenomena as well as to interesting applications. One of their promising applications is as liquid heat carriers in different heat-exchange devices as well as in devices for

magnetocaloric energy conversion. Such systems may require ferrofluids with high thermomagnetic coefficients. However, the most widely used ferrofluids with the magnetite nanoparticles do not satisfy these requirements. Therefore the development and synthesis of special temperature-sensitive magnetic nanoparticles for ferrofluids is of great interest. Among the different temperature-sensitive magnetic materials, Zn containing spinel type ferrites $Me_xZn_{1-x}Fe_2O_4$ are important substances in which variation of content of initial components (Zn substitution degree $1-x$) allows to change their magnetic parameters[2,3] in a wide range of values. This helps to obtain materials exhibiting different thermomagnetic coefficients. Moreover, Zn containing ferrites can be obtained in the form of ultra fine particles by using different chemical methods[4] such as coprecipitation method, different precursor methods, sol–gel method, hydrothermal synthesis,[5] mechanochemical processing, etc.[6,7] Among different Zn substituted ferrites Mn–Zn ferrites are preferred due to their lower Curie temperatures and high magnetization, which lead to rather high thermomagnetic coefficients. Crystalline and magnetic properties of bulk Mn–Zn ferrites are well-known. However, properties of ferrite nanoparticles significantly differ from those of a bulk material. Therefore a detailed study of conditions of synthesis and their influence on properties of Mn–Zn ferrite nanoparticles is necessary. Magnetization measurements of these nanoparticles under different conditions may shed some light on the regularities of behavior of their magnetic parameters.

In the present work for synthesis, precursor method which yields ferrites at low temperature with good homogeneity is employed. The samples were characterized using standard techniques. Half-level width of the maximum peak was substituted in Scherrer's formula to obtain the average size of particles. Samples sintered at different temperatures and environment were then studied for their magnetic properties. The result of this study is quite fascinating.

2. Sample Preparation

The samples were prepared by mixing aqueous solution of metal salts in stoichiometric quantities and aqueous solution of dihydrazinium nitrilotriacetate. Nitrilotriacetate hydrazinate precursor of mixed metal ions, so formed in solution, was obtained in dry form and ignited. Autocombustion of dry product results in formation of mixed oxides. As the mixed oxides are produced at low temperature, the particle size obtained is small. The mixed oxide samples in powder form were subjected to chemical analysis, XRD, IR spectroscopy and SEM. The percentage yield, X-ray diffraction pattern, IR pattern, and the lattice constant confirm the formation of mixed ferrites. The broadening of XRD peaks indicates formation of fine particle material. The fine powdered samples were then pressed into pellets of dimension 1 cm diameter and thickness, ranging between 2 mm and 3 mm for further investigations.

3. X-Ray Powder Diffraction

X-ray powder diffraction allows identification of crystalline structure of the samples. X-ray powder diffraction patterns were obtained on the automated Rigaku and Siemens diffractometer, Cu-Kα radiation source with the wavelength $\lambda = 1.54183$ Å was used for the purpose.

A typical X-ray powder diffraction pattern obtained for Mn–Zn ferrite fine particle powder ($Mn_{0.5}Zn_{0.5}Fe_2O_4$) is shown in Fig. 1. Widening of peaks is related to the size of crystallites. The mean diameter of particles was determined from the measurements of the widening at half height using Scherrer's formula. The mean diameter of the particles calculated was found to vary from 4.46 nm to 25.276 nm.

From the experimental values of θ, "a" the lattice constant was calculated using standard method. The values obtained are in good agreement with the reported values. The decrease in the lattice constant with increase in Zn concentration $(1-x)$ may be attributed to the replacement of small size Fe^{+3} ions by large size Zn^{+2} ions in the tetrahedral site. Fe^{+3} has an ionic radius of 0.63 Å whereas Zn^{+2} has an ionic radius of 0.78 Å.

4. Scanning Electron Microscopy (SEM)

Pictures of samples taken on Scanning Electron Microscope, Fig. 2, shows surface morphology of unsintered $Mn_{0.6}Zn_{0.4}Fe_2O_4$ sample and when pellets of the same sample are sintered in nitrogen atmosphere.

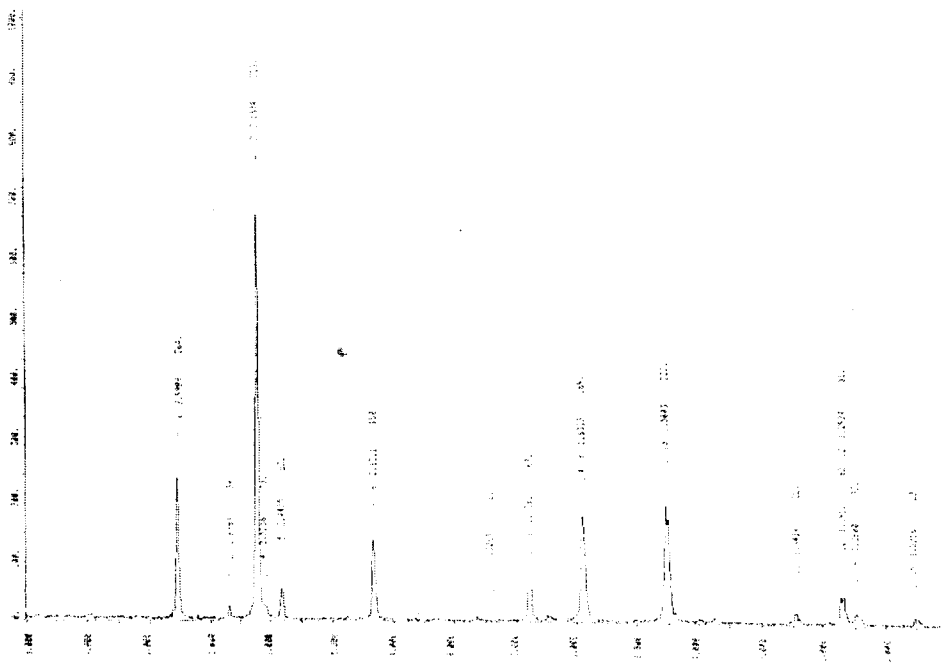

Fig. 1. Typical X-ray powder diffraction pattern obtained for $Mn_xZn_{1-x}Fe_2O_4$ fine particles.

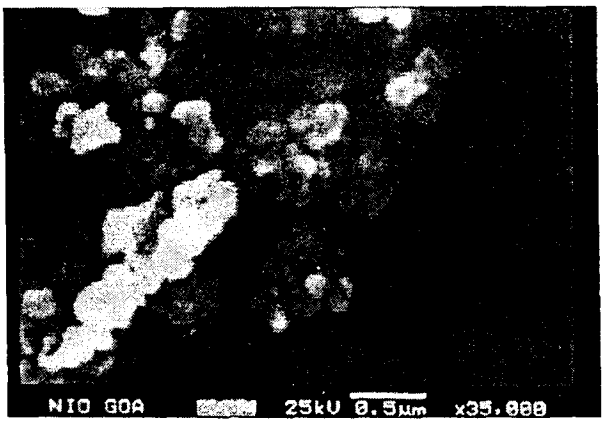

(a)

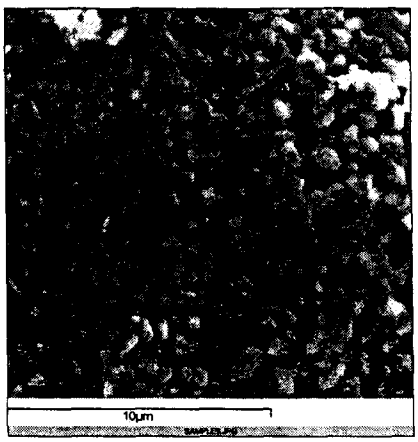

(b)

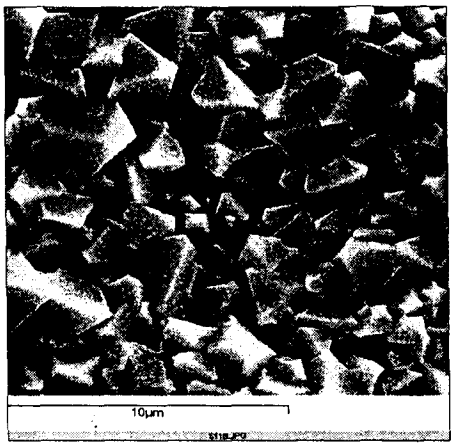

(c)

Fig. 2. (a) Unsintered sample; (b) sintered at 950°C in N_2; and (c) sintered at 1150°C in N_2.

5. Infra-Red (IR) Absorption Spectroscopy

IR absorption spectroscopy allows us to identify the spinel structure as well as a presence of certain types of chemical substances adsorbed on the surface of particles. IR spectra of dried samples were recorded in the waverange of 4000–200 cm^{-1}.

(1) Me_T — $\overset{\leftrightarrow}{O}$ — Me_O stretching vibration 600–550 cm^{-1},

(2) Me_O $\underset{\longrightarrow}{\leftrightarrow}$ O stretching vibration 450–385 cm^{-1},

(3) Me_T $\leftrightarrow$ Me_O stretching vibration 350–330 cm^{-1},

where O is oxygen, Me_O is metal in the octahedral site and Me_T — in the tetrahedral site. The metal–oxygen absorption bands (1) and (2) are characteristically

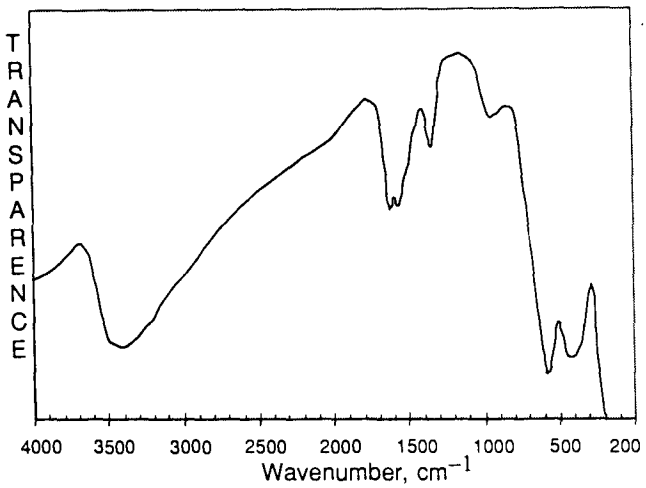

Fig. 3. Typical IR spectra obtained for $Mn_xZn_{1-x}Fe_2O_4$.

pronounced for all spinel structures and for ferrites in particular. The band (3) is less intensive than bands (1) and (2). Sometimes it merges with the band (2) and gives one wide band at 420–330 cm^{-1} as seen in the absorption spectra, Fig. 3.

Comparison of the IR-spectra of samples taken for different values of "x" as well as comparison of the same with Mn–Zn ferrite treated at high temperature allows understanding of the product structure transformations. The chemical compositions were confirmed by chemical analysis, EDS studies were carried out on Joel Model 840 (SEM) to confirm the composition and to determine percentage content of Mn, Zn, Fe and O.

6. Magnetic Properties

Sample preparation for measurements:

(i) The fine powders were pressed into pellets of the size 10 mm in diameter and thickness ranging between 2 mm and 3 mm were used for measurements. Saturation magnetization, AC susceptibility measurements, and Curie temperature measurements were made for the powdered sample.

(ii) Five sets of pellets were then sintered in the furnace at 950°C, 1050°C, 1150°C, 1250°C and 1350°C in nitrogen atmosphere for 3 h and were allowed to cool at a natural cooling rate. The pellets were then used for making similar measurements as in (i).

(iii) Another set of pellets were sintered at 1050°C for 24 h in air. There was no control over heating rate as well as cooling rate of the sample. Measurements on these samples were then made as in (i).

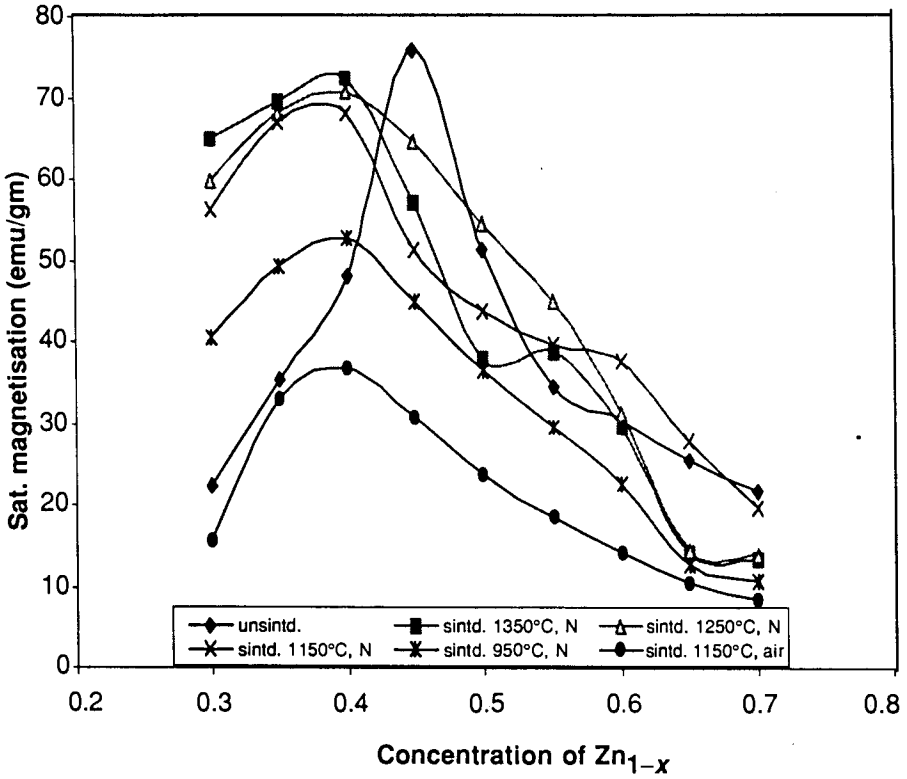

Fig. 4. Saturation magnetization with concentration of Zn_{1-x} in $Mn_xZn_{1-x}Fe_2O_4$.

Saturation magnetization curves, Fig. 4, show a high value for M_s equal to 75.9 emu/g for unsintered $Mn_{0.55}Zn_{0.45}Fe_2O_4$ sample whereas profiles of all sintered samples show maxima for $Mn_{0.6}Zn_{0.4}Fe_2O_4$ sample. The maximum saturation magnetization values for sintered samples are lower, as compared to the fine particle unsintered sample. The highest being 72.44 emu/g observed for sample sintered at 1350°C. Samples sintered in air at 1050°C show very low values for saturation magnetization.

Curie temperature for samples in nano phase were found to be size dependent. A high T_c of 750 K and a low T_c of 380 K were observed for samples with particle size varying between 25.276 nm and 4.464 nm. For samples sintered in N_2 atmosphere, the Curie temperature was found to decrease with increase in sintering temperature. In both cases Curie temperature was found to change with change in concentration of Zinc in the sample, Fig. 5.

The AC susceptibility curves obtained for unsintered samples in Fig. 6 are typical to curves obtained for fine particle ferrite. The density of the samples in Fig. 7 was found to depend on concentration of Zinc in the sample, the sintering temperature and at large on the grain size of the sample. The highest density was

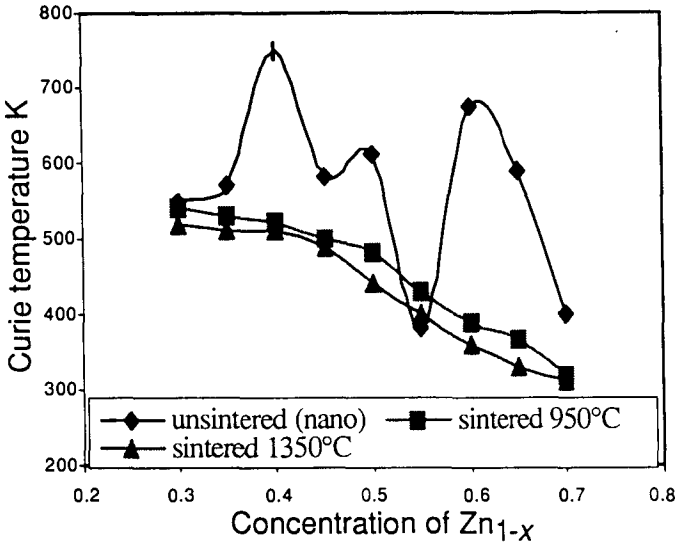

Fig. 5. Curie temperature with concentration of Zn_{1-x} in $Mn_xZn_{1-x}Fe_2O_4$.

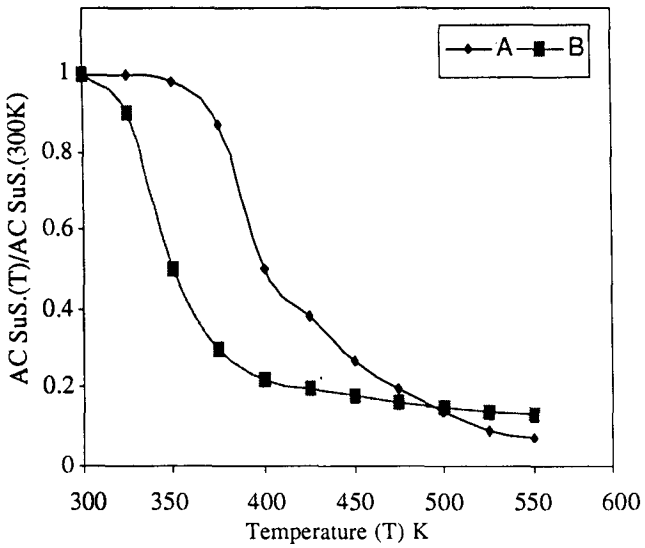

Fig. 6. Ratio X_T/X_{300} as a function of temperature for $Mn_{0.7}Zn_{0.3}Fe_2O_4$ and $Mn_{0.7}Zn_{0.7}Fe_2O_4$.

obtained for samples sintered at 1350°C in N_2 atmosphere. The hysteresis losses indicated in Fig. 8 are quite low and are found to depend on concentration of Zinc. There was only a marginal increase in the hysteresis loss for samples sintered in N_2 atmosphere.

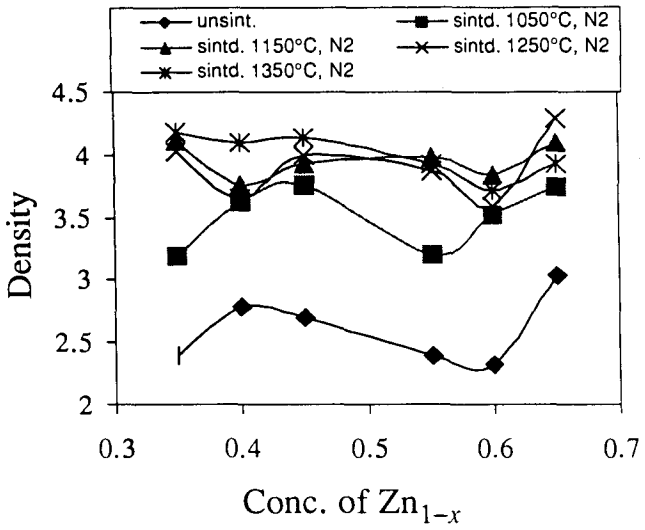

Fig. 7. Variation of density with Conc. of Zn_{1-x}.

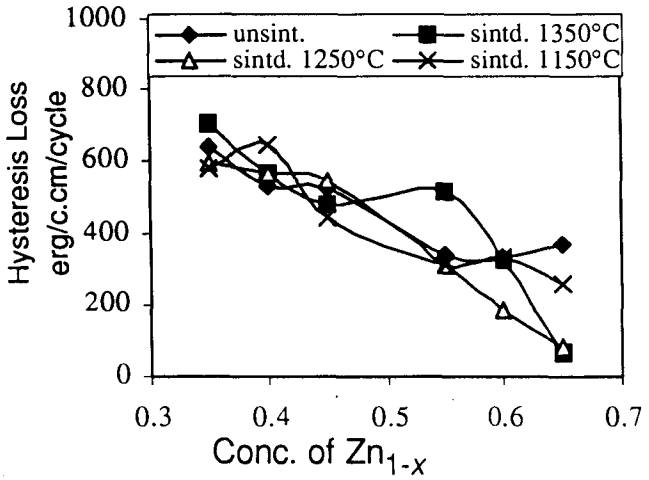

Fig. 8. Hysteresis loss versus Conc. of Zn_{1-x}.

7. Results and Conclusion

- The precursor method employed yields nanoparticle ferrites.
- The nanomaterial produced by this method shows high values of saturation magnetization[6] both in nano phase as well as in the bulk mode when sintered at 1350°C without addition of any additives.
- Mn–Zn Ferrite being a soft ferrite, the Curie temperature ranges from 500 K to 300 K for materials which are prepared by conventional ceramic method. The

samples prepared by the present method gives a higher Curie temperature which ranges between 750 K to 380 K for materials in the nano phase and are found to depend on particle size. The same varies from 520 K to 320 K in bulk mode when the samples are sintered at 1350°C in N_2 atmosphere. Sintering of sample changes the microstructure[5] which increases grain size there by reducing total surface area of the sample. Curie temperatures for samples sintered at 950°C are higher than those obtained for samples sintered at 1350°C. This indicates strong dependence of Curie temperature on particle size.[8,9]

- It has been reported that the values of saturation magnetization decreases with decrease in particle size.[6,10] However, such a variation was not observed for the samples prepared using nitrilotriacetate precursor method.
- The preparative conditions could be monitored more carefully for tailor-made particle size and clustering of particles could be overcome by providing more energy to the particles after decomposition.

References

1. A. Grants, A. Irbitis, G. Kronkalns and M. Maiorov, *J.M.M.M.* **85**, 129 (1990).
2. J. Smith and H. P. J. Wijn, *Ferrites* (John Wiley and Sons, New York, 1959).
3. B. Viswanathan and V. R. K. Murthy (eds.), *Ferrite Materials Science and Technology* (Narosa Publishing House, 1990).
4. T. Pannaparayil, R. Marande and S. Komarneni, *J. Appl. Phys.* **64**, 5641 (1988).
5. D. Makovee, M. Drofenik and A. Znidarsic, *Digest of 8th Int. Conf. Ferrites*, Kyoto, Japan, 2000.
6. M. Muroi, J. Amighian, R. Street and P. G. McCormick, *Digest of 8th Int. Conf. Ferrites*, Kyoto, Japan, 2000.
7. P. D. Popa, E. Rezlescu and N. Rezlescu, *Digest of 8th Int. Conf. Ferrites*, Kyoto, Japan, 2000.
8. T. Kuroda, H. Saita, N. Sato and T. Nomura, *Digest of 8th Int. Conf. Ferrites*, Kyoto, Japan, 2000.
9. Z. X. Tang, C. M. Sorensen and K. J. Klabunde, *Phys. Rev. Lett.* **67**, 3602 (1991).
10. Y. Matsuo, T. Mochizuki, M. Ishikura and I. Sakaki, *J. Mag. Soc. Jpn.* **20**, 429 (1996).

Available online at www.sciencedirect.com
ScienceDirect
Journal of Magnetism and Magnetic Materials 305 (2006) 296–303
Journal of magnetism and magnetic materials
www.elsevier.com/locate/jmmm

High permeability of low loss Mn–Zn ferrite obtained by sintering nanoparticle Mn–Zn ferrite

S.H. Keluskar[a,*], R.B. Tangsali[a], G.K. Naik[b], J.S. Budkuley[c]

[a]*Department of Physics, Goa University, Taleigao Plateau, Goa 403206, INDIA*
[b]*S.P.C. College of Arts and Science Margao Goa, INDIA*
[c]*Department of Chemistry, Goa University, Taleigao Plateau, Goa 403206, INDIA*

Received 11 November 2005; received in revised form 1 December 2005
Available online 6 February 2006

Abstract

Nanoparticle ferrite having general formulae $Mn_xZn_{1-x}Fe_2O_4$ with $x = 0.35/0.40/0.45/0.55/0.60/0.65$ were prepared using nitrilotriacetate precursor method. Production of fine grain size material at low temperature is the unique feature of this method. Bulk $Mn_xZn_{1-x}Fe_2O_4$ ferrite material produced by sintering nanoparticles 950/1050/1150/1250/1350 °C progressively in nitrogen atmosphere showed high values for initial permeability. Scanning electron microscopy and transmission electron microscopy were especially employed in order to elucidate the microstructure and understand the dependence of permeability and relative loss factor on the material grain size.

Keywords: Magnetic materials; Sintering; Magnetic properties; Electrical properties

1. Introduction

A tremendous surge in research on nanomaterials and bulk materials produced from nano-sized grains has been observed in the last few years since these materials are to shape the future advanced technology. The demand for high performance and miniaturization of electronic devices is on rise. This exclusively needs soft magnetic materials as its basic component. Soft ferrite material is extensively used in inductors, transformers, antenna rods, loading coils, deflection yokes, choke coils, recording heads, magnetic amplifiers, electromagnetic interference (EMI), power transformer and splitter applications, which forms a basic requirement in high technology areas. Mn–Zn ferrite material adequately suits these demands. Nano sized Mn–Zn grains are also found to be of great use in medical applications. For high performance the permeability and resistivity of this materials needs to be increased. An important parameter for high performance is small grain size Drofenik et al. [1], Inaba et al. [2]. Power ferrites should have low power loss characteristics under driving conditions. Low power loss Mn–Zn ferrites demands uniformly sized grains of high-fired density. Currently electronic modules are becoming smaller and lighter, the power supplies must likewise be reduced. The core loss, consisting of hysteresis loss, eddy current loss and residual loss, vary considerably with operating frequency and magnetic flux density. These losses can be reduced by production of material with uniform microstructure. This type of material facilitates better domain wall movements, as they are free from lattice defects, pores and impurities. Along with this low mechanical stress, low magneto crystalline anisotropy and low magnetostriction are also essential.

The factors responsible for controlling the grain size of the material are the method of preparation and conditions at preparation. Ferrite materials prepared using precursor method which is a solution technique produces material with improved microstructure Verma et al. [3]. In the present work a novel nitrilotriacetate precursor method is used for preparing compositionally and structurally perfect fine particle Mn–Zn ferrite. This method results in the samples exhibiting low magnetic and electrical losses as

*Corresponding author. Tel.: +91 832 2451345; fax: +91 832 2451184.
E-mail address: shpk@rediffmail.com (S.H. Keluskar).

0304-8853/$ - see front matter © 2006 Elsevier B.V. All rights reserved.
doi:10.1016/j.jmmm.2006.01.018

compared to those prepared by the conventional ceramic and other wet chemical methods. Fine particle Mn–Zn ferrite material synthesized using precursor method has a unique advantage of producing the material at very low processing temperature. These nanoparticles, when sintered in nitrogen atmosphere, using suitable sintering profile, show high values for permeability and low relative loss. Occurrence of phase transitions while sintering is also observed for these materials.

2. Experimental

Mn–Zn ferrite samples in form of ultra fine powders having general formula $Mn_xZn_{1-x}Fe_2O_4$ with $x = 0.35/0.4/0.45/0.5/0.55/0.6/0.65$ were synthesized using nitrilotriacetate precursor method as in Tangsali et al. [4]. XRD patterns for the samples were obtained on microcomputer controlled Siemens D-500 X-ray diffractometer and X-pert PRO PANalytical Philips diffractometer using CuKα ($\lambda = 1.5406$ Å). FTIR absorption spectra for all the samples were recorded on Shimadzu FTIR 8900 spectrometer. Estimation of metal ions was carried out by titrimetry. Estimation of Mn, Zn, Fe and O by EDAX was carried out using JEOL Model 840(SEM). Average grain size estimation was done with the help of Scherrer Formula. SEM photographs of prepared samples were obtained on JEOL Model 840(SEM), which provided the surface morphology of the material under investigation. TEM photographs were taken on Philips model CM200 with resolution 0–23 nm with an electron beam of 200 KeV Transmission electron Microscope to confirm formation of ultra fine particle size of the samples and to know grain size of unsintered and sintered samples. The fine powders were pressed into torroids of height ranging between 3–4 mm with inner and outer diameters of 1 and 2 cms, respectively by application of 75 kN pressure for 5 min. The torroids were sintered at 950/1050/1150/1250/1350 °C in nitrogen atmosphere for 3 h in a progressive manner. The heating and cooling rate was fixed at 5 °C/min during each sintering. Permeability measurements were carried out after each temperature sintering. A winding of 100 turns of super enameled doubly insulated copper wire of guage 33 was done on each torroid to carry out initial permeability (μ_i) and loss factor measurements as a function of temperature and frequency. Inductance values were recorded starting from room temperature to 500 °C with a frequency variation from 50 Hz to1 MHz using HP 4284A precision LCR meter.

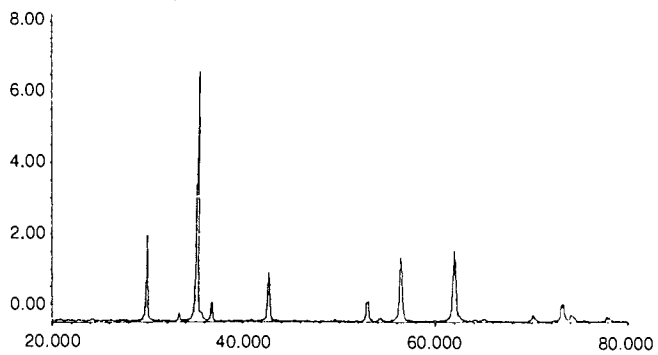

Fig. 1. XRD pattern for the sample of $Mn_{0.65}Zn_{0.35}Fe_2O_4$.

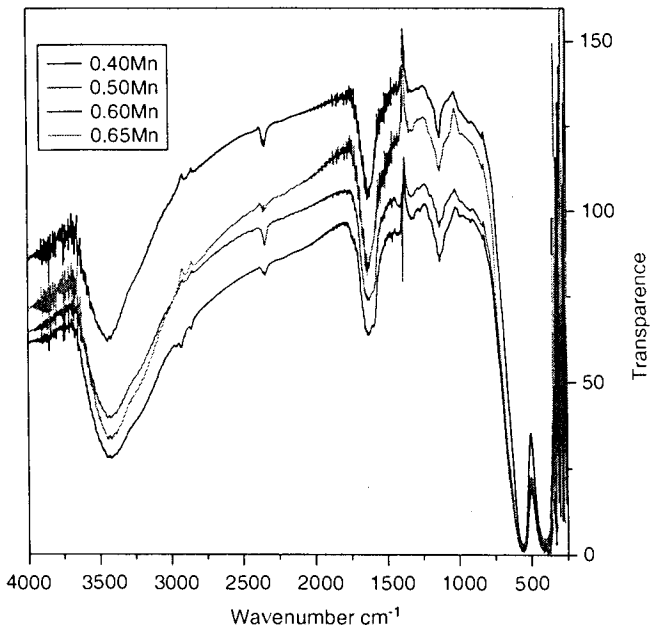

Fig. 2. FTIR spectra obtained for $Mn_xZn_{1-x}Fe_2O_4$ with $x = 0.40/0.50/0.60/0.65$.

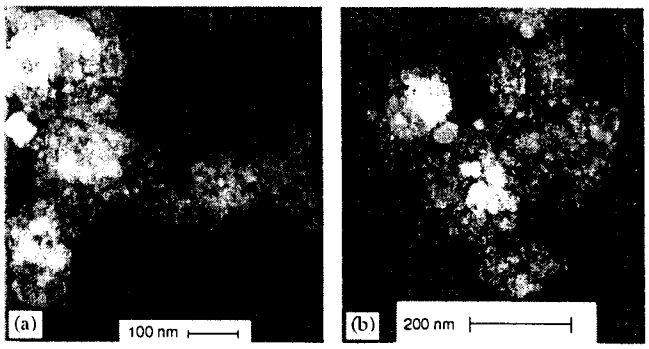

Fig. 3. TEM photographs of as prepared samples: (a) $Mn_{0.60}Zn_{0.40}Fe_2O_4$; (b) $Mn_{0.65}Zn_{0.35}Fe_2O_4$.

Table 1
EDS results obtained on sample of $Mn_{0.6}Zn_{0.4}Fe_2O_4$

Element	App (Conc.)	Intensity (Corrn.)	Weight%	Weight% (Sigma)	Atomic%
OK	104.10	1.6400	26.23	0.21	55.87
MnK	35.07	0.9334	15.52	0.15	9.63
FeK	107.50	0.9566	46.43	0.22	28.34
ZnK	24.75	0.8651	11.82	0.21	6.16
Totals			100.00		

SEM and TEM photographs of the sintered samples were recorded to obtain the information on grain size development of the sintered samples.

3. Results and discussion

3.1. X-ray analysis

Formation of single-phase cubic spinel structure of $Mn_xZn_{1-x}Fe_2O_4$ with $x = 0.35/0.40/0.45/0.55/0.60/0.65$ was confirmed with the help of XRD patterns obtained for all the samples under investigation. Fig. 1 shows a typical XRD pattern obtained on Siemens X-ray diffractometer using CuKα ($\lambda = 1.5406$ Å) radiation for the sample $Mn_{0.65}Zn_{0.35}Fe_2O_4$. The values of lattice parameters determined using Bragg's law shows a smooth decrease in the lattice constant as the concentration $(1 - x)$ of zinc is increased. The lattice constant "a" for $Mn_{0.7}Zn_{0.3}Fe_2O_4$ (8.479 Å) reduces smoothly to (8.455 Å) for $Mn_{0.3}Zn_{0.7}Fe_2O_4$ as Zn-concentration is increased. This decrease could be easily explained on the basis of the ionic radii of Fe and Zn ions. Fe^{+3}-ions with radius (0.63 Å), which are smaller, are replaced by Zn-ions with radius of (0.78 Å) which are larger, as the concentration of Zn is increased in the sample.

3.2. IR analysis

Analysis of IR spectra gives the information about product structure transformation as well as a presence of certain types of chemical substances adsorbed on the surface of particles. The metal oxygen absorption bands at 600–550 and 450–385 cm^{-1} are characteristically pronounced for all spinel structures and for ferrites in particular. The band 350–330 cm^{-1} is less intense and sometimes it merges with the band 450–385 cm^{-1} giving a single wide band at 420–330 cm^{-1}. Fig. 2 shows two broad bands at 600–550 cm^{-1} and 420–330 cm^{-1} for all the samples.

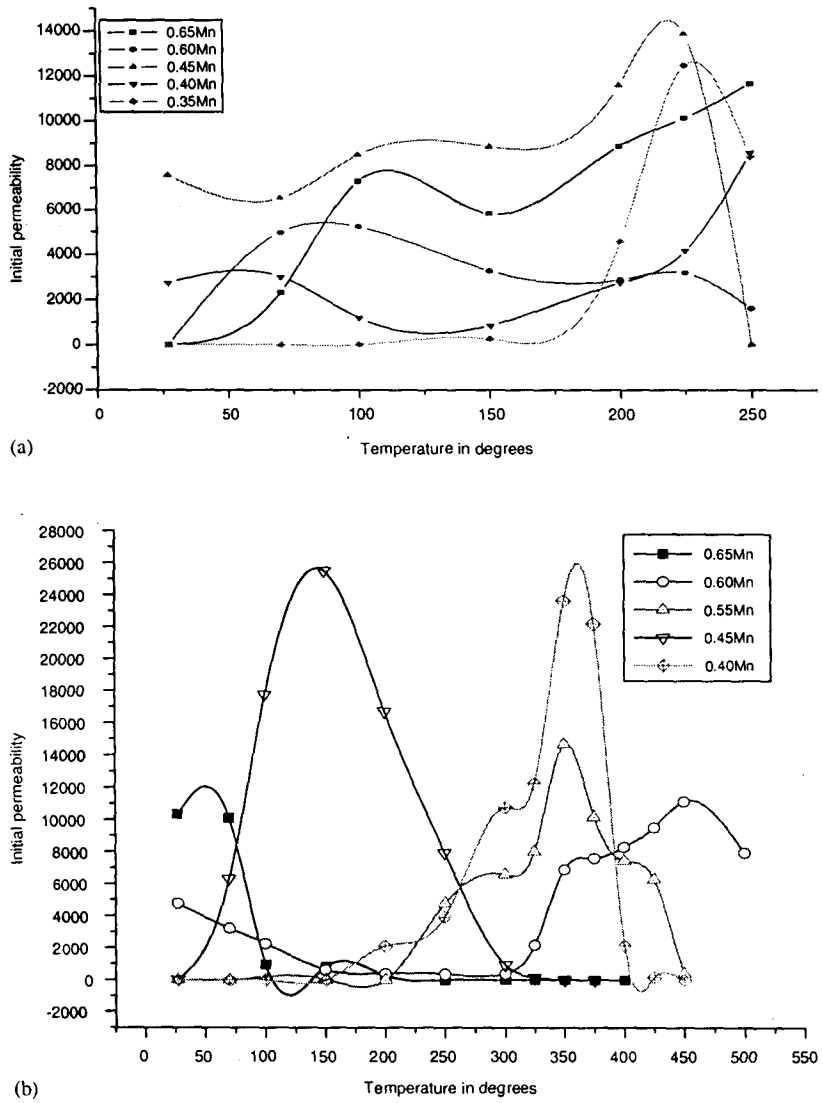

Fig. 4. Variation of initial permeability with temperature for samples $Mn_xZn_{1-x}Fe_2O_4$ sintered at: (a) 950 °C; (b) 1050 °C.

3.3. Particle size determination

The particle size estimates of as prepared samples were done using three different tools. Particle size calculations through Scherrer formulae based on XRD peak widening showed formation of ultra fine particle material with average grain size in the range of 10–80 nm and are found to depend on Zn concentration in the sample. The average particle size of the samples as seen from TEM photographs Fig. 3(a) and (b) are in excellent agreement with the particle size estimates made using Scherrer Formula. The average particle size of the as prepared samples seen from TEM photographs is about 10 nm.

3.4. Chemical analysis

Estimated percentage contents of the elements Mn, Zn, Fe and O carried out with the help of EDS analysis of all the samples (Table 1 for $Mn_{0.6}Zn_{0.4}Fe_2O_4$) are in good agreement with the theoretical estimated values thus confirming the preservation of stoichiometry [5].

3.5. Permeability and loss factor

Initial permeability (μ_i) is an important magnetic parameter, which decides the suitability of a ferrite for particular application. It is technologically important extrinsic magnetic property, which is influenced by the microstructure, which in turn depends upon the method of preparation. The initial permeability is dependent on grain size, density and porosity of the material (Goldman [6]). Temperature dependence of initial permeability is a very important factor to be considered in designing any magnetic component.

The initial permeability (μ_i) was calculated from the formulae

$$L = 0.0046\mu_i N^2 h \ln(OD/ID)$$

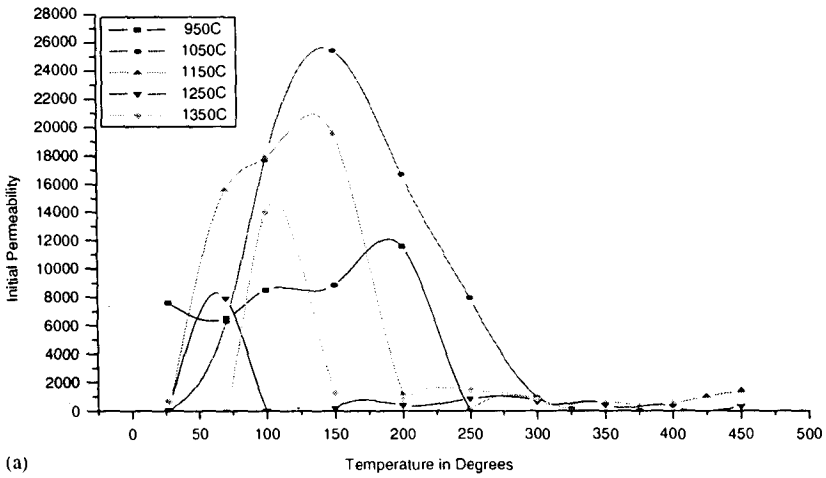

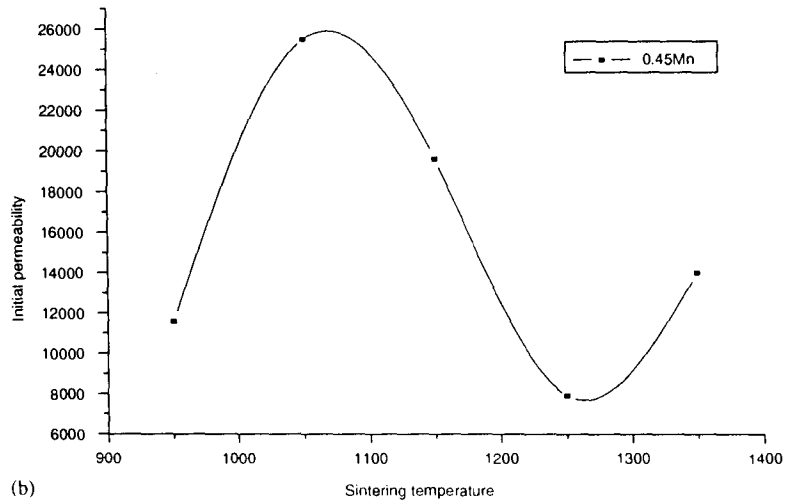

Fig. 5. (a) The variation of initial permeability with temperature for the sample $Mn_{0.45}Zn_{0.55}Fe_2O_4$ sintered at different temperatures; (b) Variation o maximum value of initial permeability with sintering temperature for $Mn_{0.45}Zn_{0.55}Fe_2O_4$.

where L is inductance in Henry, N is the number of turns of copper wire on torroid, h is height of the core in metres, OD is outer diameter of torroid in metres, and ID is the inner diameter of torroid in metres.

The variation of permeability with the temperature for the samples sintered at 950 and 1050 °C is shown in Fig. 4 (a and b). It is observed that initial permeability increases slowly, reaches peak value at a certain temperature and drops gradually to zero at Curie temperature. The maximum in initial permeability corresponds to the point of zero anisotropy field (Standley [7]). The increase in permeability with temperature is due to the fact that the anisotropy decreases faster with temperature than the saturation magnetization.

The variation of initial permeability with temperature for the sample $Mn_{0.45}Zn_{0.55}Fe_2O_4$ sintered at 950, 1050, 1150, 1250 and 1350 °C is as shown in Fig. 5(a). The drops are observed near Curie temperature and a high value of initial permeability 25,472 at 150 °C for frequency 50 Hz obtained for sample $Mn_{0.45}Zn_{0.55}Fe_2O_4$ sintered at 1050 °C is much higher than the reported values. Samples $Mn_{0.35}Zn_{0.65}Fe_2O_4$, $Mn_{0.60}Zn_{0.40}Fe_2O_4$ and $Mn_{0.65}Zn_{0.35}Fe_2O_4$ when sintered at 950 °C shows very low room temperature permeabilities (Fig. 4(a)) where as sample $Mn_{0.40}Zn_{0.60}Fe_2O_4$ shows high value of 2753 and the sample $Mn_{0.45}Zn_{0.55}Fe_2O_4$ shows a value of 13,831 for room temperature permeability. However, the overall permeabilities for this sample are found to increase as the

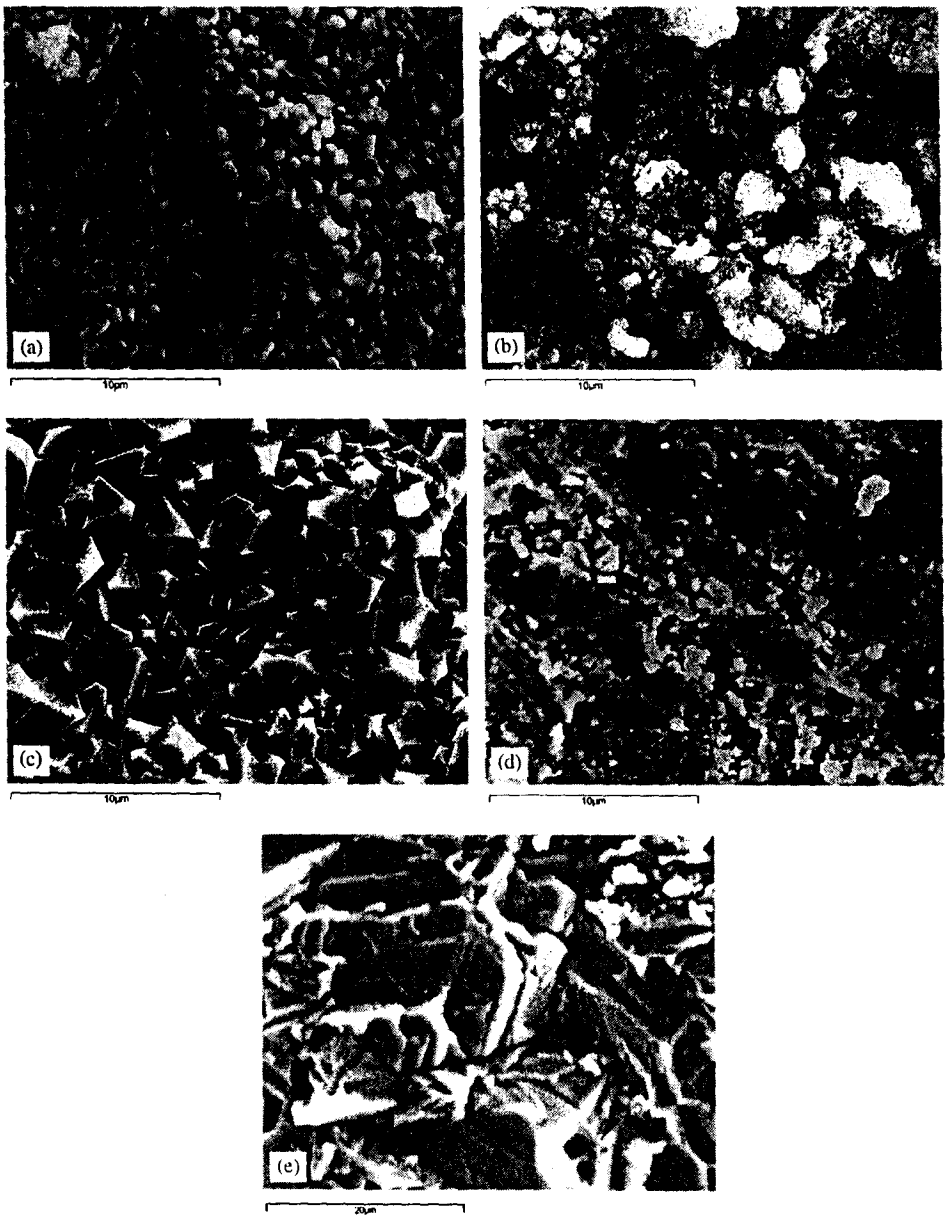

Fig. 6. SEM photographs of $Mn_{0.45}Zn_{0.55}Fe_2O_4$ sintered in nitrogen atmosphere for 3 h at: (a) 950 °C; (b) 1050 °C; (c) 1150 °C; (d) 1250 °C and (e) 1350 °C.

temperature increases. Room temperature permeability values (Fig. 4(b)) are drastically changed when the same samples are sintered at 1050 °C. $Mn_{0.40}Zn_{0.60}Fe_2O_4$, $Mn_{0.45}Zn_{0.55}Fe_2O_4$ and $Mn_{0.55}Zn_{0.45}Fe_2O_4$ show very low values whereas $Mn_{0.60}Zn_{0.40}Fe_2O_4$ shows higher value of μ_i and the sample $Mn_{0.65}Zn_{0.35}Fe_2O_4$ shows highest room temperature value for μ_i which is higher than 10,000.

All these samples show broad peaks followed by a gradual fall near Curie temperature as usual. For samples sintered at 950 °C the curie temperatures is beyond 250 °C where as for samples sintered at 1050 °C the Curie temperature lies between 100 and 500 °C. Fig. 5(b) shows variation of maximum values of μ_i with sintering temperature for sample $Mn_{0.45}Zn_{0.55}Fe_2O_4$. The variation of maximum value of the permeability for the sample is found to show a peak at 1050 °C and a fall followed by a rise at sintering temperature 1350 °C. This behavior and the initial permeability trends observed in Fig. 4(a) and (b) and Fig. 5(a) and (b) can be related to the existence of different crystalline phases which the samples undergoes at different sintering temperatures. This is evident from the SEM and TEM photographs depicted in Figs. 6 (a–e) and 7.

The initial permeability of high permeability material depends to a large extent on mobility of the Bloch's domain walls. To obtain high permeability it is important to reduce the crystalline anisotropy and the magnetrostriction. Ferrites in particular are burdened with magnetic imperfections. Voids in bodies that are not completely densified, non-magnetic inclusions are the factors, which give, rise to internal magnetiostatic energy. The stable domain configuration in a material is always such is to minimize this energy. The loss that occurs is proportional to imperfections of materials as well it's anisotropy, both crystalline and strain. High permeability may be expected in polycrystalline material that are homogeneous, dense and have composition that has very low value of anisotropy. Anisotropy is temperature dependent property. Effect of this depends on the composition. The anisotropy in Mn–Zn ferrite is highly dependent on the material composition. For some compositions of Mn–Zn anisotropy takes negative value at room temperature, increases monotonically with temperature to zero at Curie temperature whereas for certain combinations of Mn–Zn it takes a negative value increases to zero, takes a positive value and decreases to attain a zero value at Curie temperature. This behavior is strongly reflected in the initial permeability of the material. The initial permeability rises to maximum at both zero anisotropy points with a saddle corresponding to the temperature at which anisotropy has a maximum positive value [9], Verma et al. [8]. Well-adjusted sintering conditions support the design of microstructure and resulting magnetic properties of the sample. SEM micrographs Fig. 6(a–e) shows the morphology of sample $Mn_{0.45}Zn_{0.55}Fe_2O_4$ sintered at 950, 1050, 1150, 1250 and 1350 °C, respectively.

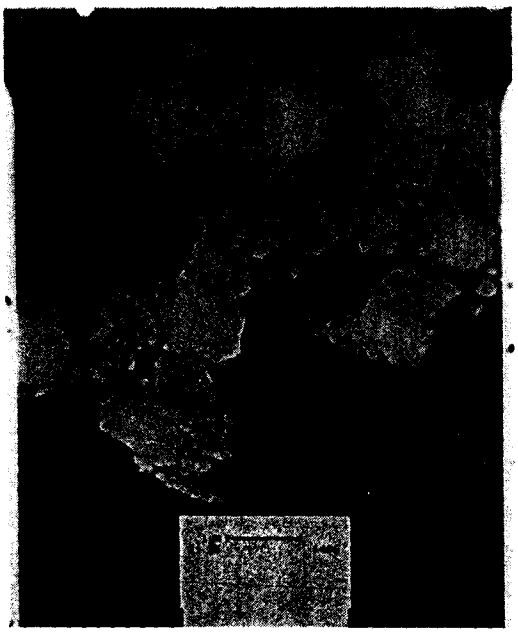

Fig. 7. TEM photograph of sample $Mn_{0.45}Zn_{0.55}Fe_2O_4$ sintered at 1050 °C.

The sample sintered at 950 °C Fig. 6(a) shows a more compact microstructure with well-developed grains, however the existence of non-magnetic voids is also large. The density of the sample is 2587 Kg/m^3. The samples sintered at 1050 °C (Fig. 6(b)) shows larger polycrystalline grains with less non-magnetic voids and a density of 3200 Kg/m^3. The sample exhibits a high value of permeability. The samples sintered at 1150 °C (Fig. 6(c)) shows formation of well developed crystals and has a density of 3983 Kg/m^3. The anisotropy for this sample is expected to be higher due to blocking of domain wall movement and the strain isotropy, which is a result of increase in lattice stress. The sample sintered at 1250 °C shown in Fig. 6(d) appears to possess a very high value of anisotropy and magnetrostriction compared to other samples. This appears to be a stage with substantial magnetic imperfections and poor grain growth. The sample has a density of 3867 Kg/m^3. A different crystalline phase with fewer imperfections is obtained for sample sintered at 1350 °C (Fig. 6(e)). The density of this sample is found to be 3925 Kg/m^3.

The microstructures show different crystalline phases which are responsible for variations in anisotropy and domain wall movement in the sample. Fig. 7 confirms the existence of polycrystalline phase in the sample sintered a 1050 °C, which is one of the factors for enhancing th permeability value of the sample.

The ratio $\tan\delta$ to μ_i known as relative loss factor (rlf) plotted against frequency as shown in Fig. 8(a) and (b). It observed that for some samples the value of rlf rapid decreases as the frequency is increased whereas it remai extremely low for most of the samples for all sinteri temperatures. The rlf is found to depend on compositi and microstructure of the sample, which is decided

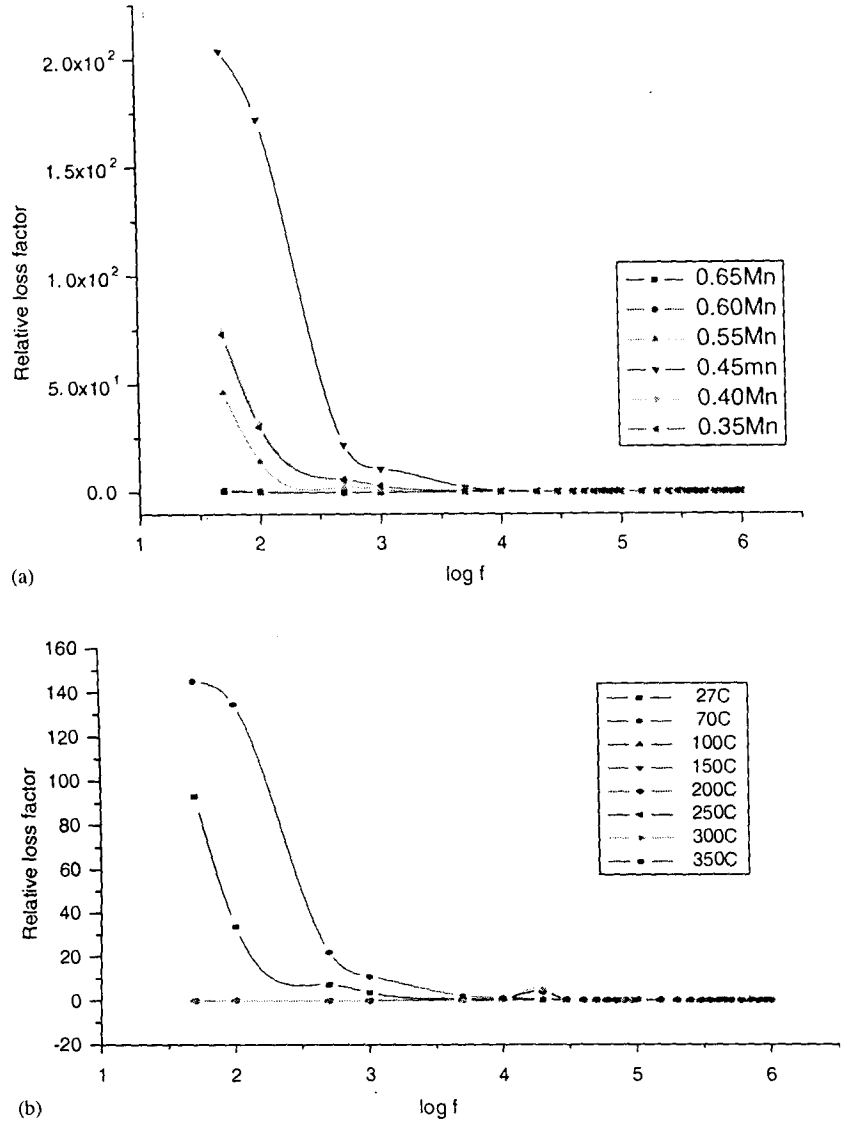

Fig. 8. Variation of relative loss factor with frequency: (a) Samples $Mn_xZn_{1-x}Fe_2O_4$ sintered at 1150 °C (b) Sample $Mn_{0.45}Zn_{0.55}Fe_2O_4$ sintered at 1050 °C at different temperatures.

sintering profiles of the sample. In the present work the rlf values obtained range from 10^2 to as low as 10^{-6}, in the frequency range of 50 Hz–1 MHz.

4. Conclusions

The materials prepared by sintering nanomaterial Mn–Zn ferrite prepared using nitrilotriacetate precursor method yield high performance materials. The samples are found to show high permeability and low loss, which are essential parameters for any present-day electronic and electromagnetic applications. The permeability and loss depends on the various factors such as stoichiometry, density and grain size. For electromagnetic application of ferrites it is necessary that the rlf values should be as low as possible over a large frequency range. The rlf values of the samples under investigation are found to be much lower.

Acknowledgements

The authors are thankful to Prof. K.L. Narciman, TATA Institute of Fundamental Research Mumbai, India, for providing XRD and imaging facilities and to Dr. S.C. Watve, Department of Physics, G.J. College, Ratnagri, Maharashtra, India, for permeability measurement facilities.

References

[1] M. Drofenik, A. Znidarsic, I. Zajc, J. Appl. Phys. 82 (1997) 333.
[2] H. Inaba, T. Abe, Y. Kitano, J. Shimomura, J. Solid State Chem. 121 (1996) 117.
[3] A. Verma, T.C. Goel, R.G. Mendiratta, Mater. Sci. Technol. 16 (2000) 712.
[4] R.B. Tangsali, S.H. Keluskar, G.K. Naik, J.S. Budkuley, Int. J. Nanosci. 3 (2004) 1.

[5] S. Son, R. Swaminathan, M.E. McHenry, J. Appl. Phys. 93 (2003) 7495.
[6] Goldman, Modern Ferrite Technology, Van Nostrand Reihold, New York, 1990.
[7] K.J. Standley, Oxide Magnetic Materials, Clarendon Press, Oxford, 1972.
[8] F.J. Schnettler, Physics of Electronic Ceramics, Part B, Marcel Dekker, New York, 1972.
[9] A. Verma, T.C. Goel, R.G. Mendiratta, P. Kishan, J. Magn. Magn. Mater. 208 (2000) 13.

Journal of Materials Science
Full Set - Includes 'Journal of Materials Science Letters'

10.1007/s10853-006-0017-8

Effect of sintering conditions on resistivity of nanoparticle Mn–Zn ferrite prepared by nitrilotriacetate precursor method

Rudraji B. Tangsali[1] ✉, **Satish H. Keluskar**[2], **Ganpat K. Naik**[3] and **J. S. Budkuley**[3]

(1) Department of Physics, Goa University, Taleigao Plateau, Panjim, Goa, 403206, India
(2) Department of Physics, P. E. S. College of Arts and Science, Ponda, Goa, India
(3) Department of Chemistry, Goa University, Taleigao Plateau, Panjim, Goa, 403206, India

✉ **Rudraji B. Tangsali**
Email: rbtangsali@unigoa.ac.in

Received: 20 October 2005 **Accepted:** 16 March 2006 **Published online:** 18 January 2007

Abstract Mn–Zn spinel ferrites are most important class of magnetic materials owing to their high saturation magnetization, high permeability, low loss and interesting applications in various fields. The magnetic as well as electrical properties of these ferrites depend on relative distribution of cations at different sites, grain size, sintering conditions as well as preparative conditions. Nanoparticle Mn–Zn ferrite material having general formula $Mn_x Zn_{1-x} Fe_2O_4$ with $x = 0.35/0.4/0.45/0.5/0.55/0.6/0.65$ were synthesized using nitrilotriacetate precursor method and characterized using standard techniques. The resistivity measurements of all these samples were carried out after sintering the same in nitrogen atmosphere at 1,050 °C/1,150 °C/1,250 °C/1,350 °C, respectively. High resistivity values obtained for the system of materials would provide a low eddy current loss material for wide ranging applications in electronics and telecommunications. Semiconductor like behavior of the material with resistivity variation over large range of temperature is ideal characteristic essential for materials in sensor applications.

Introduction

Research in nanomaterials is on growth as the reduced grain dimensions drastically alter the properties of materials. Nano sized magnetic oxides are becoming important materials due to their unique micro magnetic properties such as superparamagnetism, magneto optic, magneto caloric effect, colossal and giant magnetic resistance etc. These materials are useful in a variety of applications in the electronic industry due to their high permeability, high saturation magnetization, high resistivity and low loss as these formed the key impediments in downsizing of transformer cores deflection yokes, antenna rods in the world of miniaturization. The most important parameter for high performance is small grain size. Resistivity of bulk Mn–Zn Ferrite obtained by sintering ultra fine particle Mn–Zn ferrite

material is different from the one obtained by sintering material prepared by conventional methods like ceramic method and other wet chemical methods which yields large particle size. The performance of these materials is greatly influenced not only by its composition but also by the method of preparation and conditions at preparations. These factors are responsible for controlling the grain size of the material. The power loss per unit volume P_V for a Mn–Zn ferrite material can be divided into the hysteresis loss P_H, the eddy current loss P_E, and the residual loss P_R. The eddy current loss is dependent on the resistivity of the sample. The eddy current loss is given by $P_E = cL^2 B_m^2 f^2/\rho$; f is frequency, L^2 is equal to the A dimension of the circuit, B_m is the maximum flux density, ρ is the electrical resistivity of the bulk, and c is a coefficient related to the dimension of the circuit of the eddy current. Eddy currents in the core are related to material microstructure as the parameter L^2 may be replaced by D^2 the average diameter of the individual grains [1, 2].

Fine particle Mn–Zn ferrites were synthesized using nitrilotriacetate precursor method. Samples were characterized using standard techniques. The resisitivity of the bulk material obtained on sintering the nanoparticles at different temperatures was found to be very high which can account for sizable reduction in eddy current losses.

Experimental

Mn–Zn ferrites samples in form of ultra fine powders having general formula $Mn_xZn_{1-x}Fe_2O_4$ with x = 0.35/0.4/0.45/0.5/0.55/0.6/0.65 were synthesized using nitrilotriacetate precursor method [3]. The advantage of this method is that it produces nanoparticle Mn–Zn Ferrite material at much lower temperature. The decomposition of the complex precursor takes place at around 250 °C, which proceeds via auto-combustion method. XRD pattern for the samples were obtained on microcomputer controlled Siemens Diffractometer using Cu Kα (λ = 1.54183 AU). FTIR absorption spectra were recorded Shimadzu FTIR 8900 Spectrometer. Estimation of metal ions was carried out by titrimetry. Analysis for estimation of Mn, Zn, Fe and O by EDAX was also carried out by using Joel Model 840(SEM). Average grain size estimation was done using Scherrer Formula. TEM photographs were taken on Philips model CM200 Transmission electron Microscope with resolution 0–23 nm to confirm formation of ultra fine particle size of the samples. SEM photographs of sintered samples were obtained on Joel Model 840(SEM), which gave information on the microstructure of the materials under investigation. Fine powders of $Mn_xZn_{1-x}Fe_2O_4$ were pressed into pellets of the size 10 mm diameter and of thickness ranging between 2 and 3 mm under a pressure of 75 KN applied for 3 min. Four sets of pellets were sintered in nitrogen atmosphere at temperatures, 1,050, 1,150, 1,250 and 1,350 °C, respectively, for 3 h by setting heating and cooling rate at 5 °C per minute. The pellets were silver painted on either side for establishing good Ohmic contacts with the electrodes. Resistivity measurements on these samples were then made using standard two-probe method.

Results and discussion

A typical XRD pattern obtained for the sample is shown in Fig. 1. Similar patterns were recorded for all the samples. The *d* values, 2θ values and the values of lattice constants *a* calculated from these was verified and is found to be in excellent agreement with reported values. Formation of cubic spinel structure was thus confirmed by XRD data analysis. The particle size of these fine powders, as calculated from Scherrer formula using XRD data, was found to range between 10 and 80 nm.

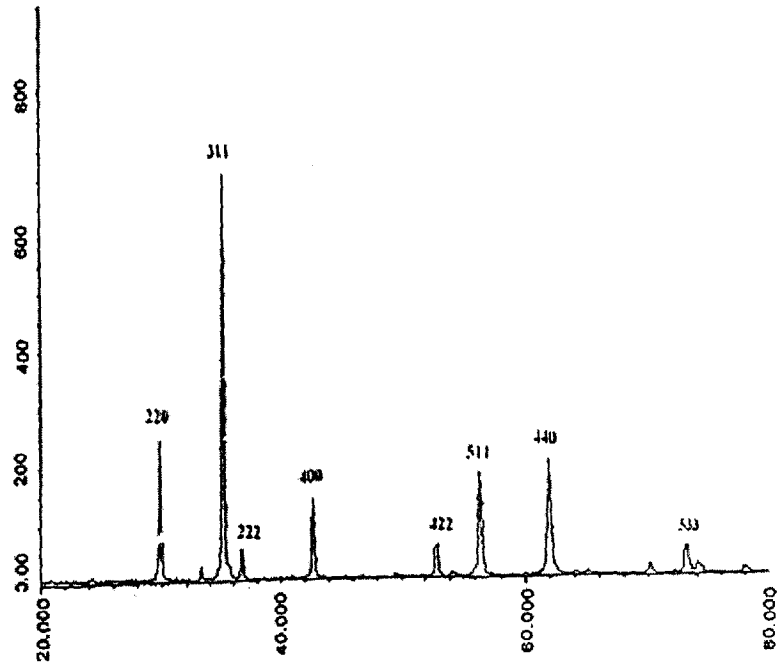

Fig. 1 XRD pattern obtained for as prepared powdered sample $Mn_{0.6}Zn_{0.4}Fe_2O_4$

Analysis of IR spectra gave the information about product structure transformation. The study of far-infrared spectrum is an important tool to get information about the positions of the ions in the crystal through the crystal's vibrational modes [4]. It also helps in identifying the spinel structure as well as a presence of certain types of chemical substances adsorbed on the surface of particles. In the IR spectra of the mixed oxides the following vibrations, with a corresponding wavenumber are possible.

$$Me_T - \overline{O} - Me_O \text{ stretching vibration } 600 - 550\,cm^{-1} \quad (1)$$

$$Me_O - \overline{O} \text{ stretching vibration } 450 - 385\,cm^{-1} \quad (2)$$

$$Me_T - \overline{Me_O} \text{ stretching vibration } 350 - 330\,cm^{-1}, \quad (3)$$

where O is oxygen, Me_O is metal in the octahedric site and Me_T in the tetrahedric site. The metal–oxygen absorption bands (1) and (2) are pronounced for all spinel structures and essentially for ferrites. Usually the band (3) is less intense than bands (1) and (2), and sometimes found to merge with the band (2) resulting in a singlewide band at 420–330 cm^{-1}. In the IR absorption spectra recorded for the powdered samples (Fig. 2), two broad bands (1) and (2) are observed in addition to a small narrow less intense third band in the range 350–330 cm^{-1} that has almost merged with band (2).

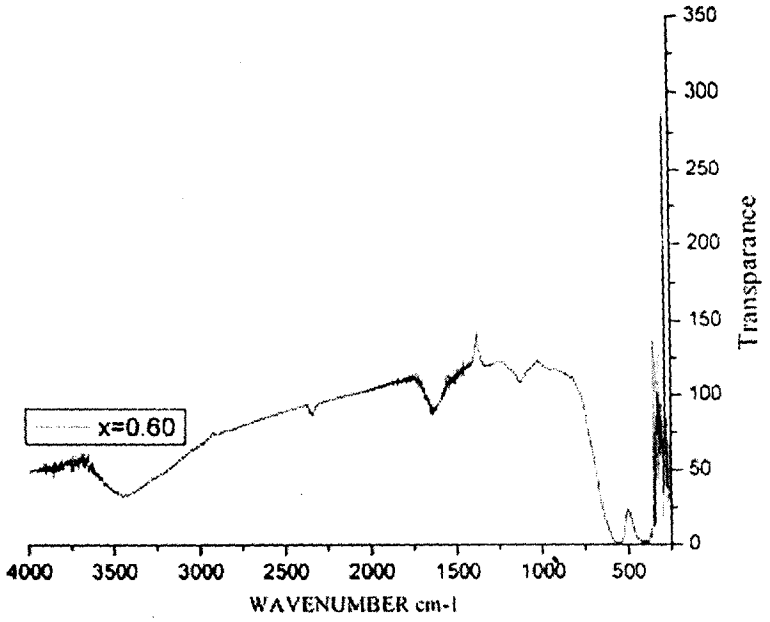

Fig. 2 IR spectra obtained for as prepared powdered sample $Mn_{0.6}Zn_{0.4}Fe_2O_4$

The grain size of the sample as seen from TEM photograph of Fig. 3 is in excellent agreement with values obtained for particle size using Scherer formula. . Preservation of stoichiometry was confirmed on analyzing the EDS results.

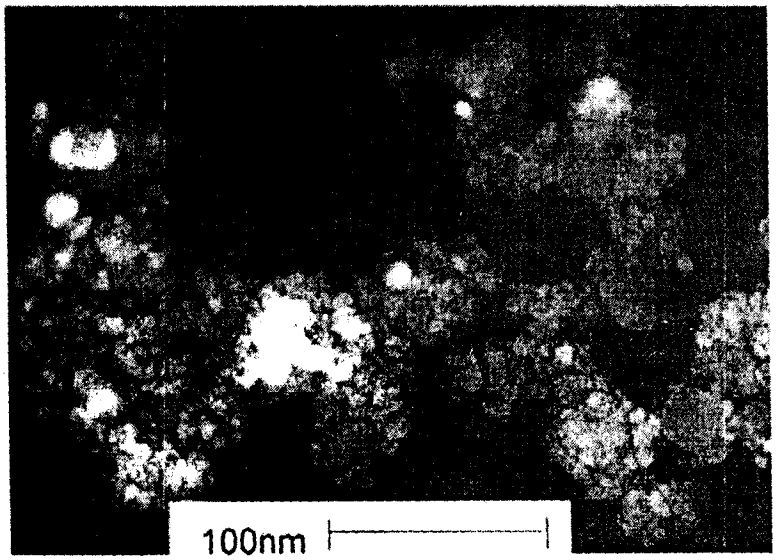

Fig. 3 TEM photograph of as prepared powdered sample $Mn_{0.6}Zn_{0.4}Fe_2O_4$

The density values of the samples (Table 1) are found to show abrupt changes on changing sintering temperature from 1,050 to 1,350 °C. The density of sintered $Mn_xZn_{(1-x)}Fe_2O_4$ ferrite material where $x = 0.65$, 0.6, 0.45 and 0.4 is found to be high when sintered at 1,150 and 1,350 °C whereas these values are low when these samples are sintered at 1,050 and 1,250 °C. The density for sample with $x = 0.55$ is found to increase with sintering temperature whereas the same is observed to be lower for sample with $x = 0.35$ sintered at 1,350 °C. Although density depends on the concentration of Mn in the sample the present unusual behavior observed in the density may be attributed to the existence of phase transitions which occur during the crystal formation process while sintering, as evident from SEM photographs depicted in Fig. 4. The investigation on fine structure of $Mn_xZn_{(1-x)}Fe_2O_4$ ferrite clearly indicates the influence of sintering conditions on the grain growth [5], density of the sample and crystalline phase of the sample [6]. The unusual trend in the density values is also observed in the resistivity trends of the samples. Figure 5a–d shows plots of log ρ v/s 1,000/T (K) for $Mn_xZn_{(1-x)}Fe_2O_4$ ferrite. A semiconductor like general behavior is seen for all the samples as the samples undergo a second order ferrimagnetic to paramagnetic phase transition. Although the trends depend on the concentration of Mn in the sample these are more strongly dependent on the sintering temperature of the sample. Resistivity values at 300 K are seen to vary between 3.789×10^7 ohm-cm and 1.898×10^6 ohm-cm for samples sintered at 1,050 °C the highest and the lowest being observed for $Mn_{0.35}Zn_{0.65}Fe_2O_4$ and $Mn_{0.4}Zn_{0.6}Fe_2O_4$, respectively. A considerable variation in the resistivity is observed for samples sintered at 1,150 °C. The resistivity at 300 K is found to vary between 7.5×10^8 ohm-cm and 2.832×10^6 ohm-cm with the highest for $Mn_{0.65}Zn_{0.35}Fe_2O_4$ sample. These values are found to be much lower for samples sintered at 1,250 °C and are found to range between 2.285×10^6 ohm-cm and 6.08×10^5 ohm-cm. A large variation in the resistivity values is observed for samples sintered at 1,350 °C both at 300 K and at higher temperatures with the highest being 1.624×10^9 ohm-cm for $Mn_{0.6}Zn_{0.4}Fe_2O_4$ at 300 K. It may be seen that large variations in resistivity at 300 K are observed for samples sintered at 1,150 and 1,350 °C. This may be due to formation of definite small grain shapes with high resistive boundaries in between any nearby neighbors and is evident from the SEM photographs (b) and (d) of Fig. 4.

Table 1 Table showing density of unsintered samples and density of samples sintered at 1,050, 1,150, 1,250 and 1,350 °C

Mn Conc. (x)	Unsintd. density (g/cc)	Sintd. 1,050 °C density (g/cc)	Sintd. 1,150 °C density (g/cc)	Sintd. 1,250 °C density (g/cc)	Sintd. 1,350 °C density (g/cc)
0.65	2.3941	3.1825	4.1127	4.0287	4.1824
0.6	2.7779	3.6226	3.7624	3.6477	4.0999
0.55	2.696	3.7536	3.9285	3.9909	4.1401
0.45	2.396	3.2007	3.9833	3.8674	3.9251
0.4	2.3273	3.5169	3.8471	3.5923	3.7124

0.35	3.0324	3.7512	4.0987	4.2953	3.9222

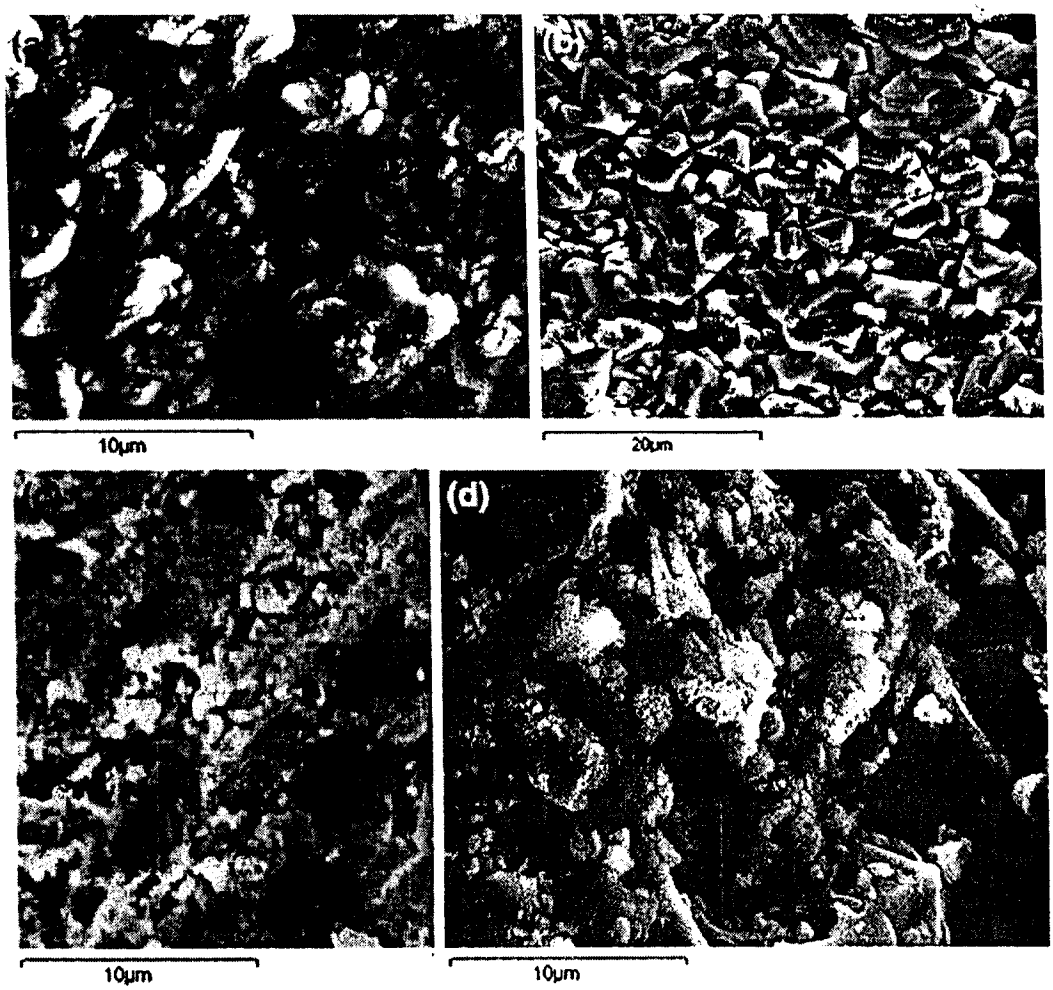

Fig. 4 SEM photographs of $Mn_{0.45}Zn_{0.55}Fe_2O_4$ sintered in nitrogen atmosphere for 3 h at (**a**) 1,050 °C, (**b**) 1,150 °C, (**c**) 1,250 °C and (**d**) 1,350 °C

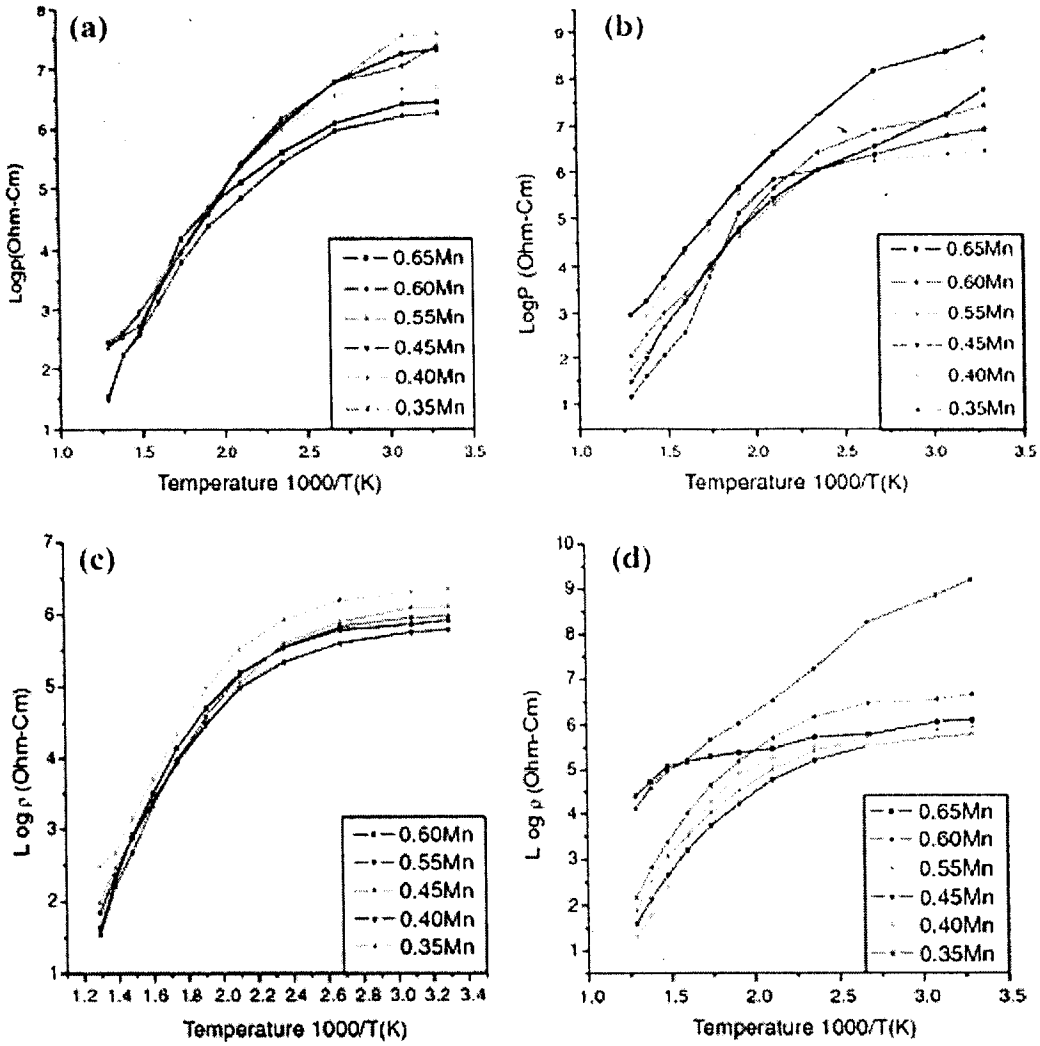

Fig. 5 Resistivity variation for the samples of different compositions, sintered at (**a**) 1,050 °C, (b) 1,150 °C, (**c**) 1,250 °C and (**d**) 1,350 °C

In ferrites electron conduction mechanisms have been studied by many investigators and reviewed by Klinger et al. [7]. Various models were proposed; however, the thermally activated hopping model is found to be more appropriate in explaining qualitatively the electrical behavior of Mn–Zn ferrites. In the hopping process the additional electron on a ferrous (Fe^{2+}) ion requires little energy to move to an adjacent (Fe^{3+}) on the equivalent lattice sites (B sites). In presence of the electric field, these extra electrons hopping between iron ions give rise to the electrical conduction. Therefore, any change in the (Fe^{2+}) ion content in the spinel ferrite lattice and/or the distance between them is crucial to the intrinsic resistivity of Mn–Zn ferrite grains, including the intrinsic grain boundaries. If the introduction of another cation into the lattice causes a change in the valency distribution on the B sites, then the number of electrons potentially available for transfer will be altered. On the other hand, the incorporation of foreign (addition of impurity) ions can change the distance between the B lattice sites, which is crucial for the conduction mechanism. Thus, the formation of an intrinsic grain boundary in doped samples by the segregation of aliovalent ions must increase the resistivity. This gives rise to polycrystalline Mn–Zn ferrite with non-ferrimagnetic grain boundary, ferrimagnetic outer grain region and ferrimagnetic conductive

core. Thus the contribution to the bulk resistivity may be considered as resistivity contribution coming from three different regions. To establish a relation between the Power loss due to eddy currents and the average grain diameter a hypothetical brick wall model is applied. As per the model each layer can be represented by a resistance–capacitance (R–C) lumped circuit of high Ohmic layers. When the resistivity of the bulk is much lower than the grain boundary layers, the equivalent circuit of the ferrite can be represented by a series of lumped R–C circuits of the grain boundary layers [2].

As the samples under investigation are sintered from Nanoparticle Mn–Zn ferrite in a reducing atmosphere with no additives there is no possibility of formation of high resistivity ferrimagnetic outer grain boundary. Thus the total contribution should come only from the non-ferrimagnetic grain boundaries and ferrimagnetic conductive core. It is evident from Fig. 4 that due to phase transitions samples sintered at 1,150 and 1,350 °C show small grain sizes with large non-ferrimagnetic grain boundaries more over the total surface area of the sample also increases due to formation of fine crystals which results in high resistivity for the samples. The samples sintered at 1,050 and 1,250 °C do not show formation of perfect crystals or small grain shapes which results in low surface area and less high resistivity non-ferrimagnetic grain boundaries which accounts for low value of resistivity at 300 K for this samples as compared to samples sintered at 1,150 and 1,350 °C. The resistivity values obtained are much higher as compared to the reported resistivity values of 10^5 ohm-cm [8, 9].

Conclusion

The present investigations on the resistivity of the Mn–Zn ferrite developed by sintering nanoparticle Mn–Zn ferrite, prepared by nitrilotriacetate precursor method in an inert atmosphere, show existence of phase transitions thus contributing to amazingly high electrical resistivity in comparison to the reported values. This is a very important parameter in minimizing the eddy current losses in power applications. It is evident that the material prepared by sintering nanomaterial Mn–Zn ferrite not only gives low loss material but also produces material with small grain size with large surface area as the grain growth is suppressed due to phase transitions. This feature can have remarkable effect on the other properties of the material. The semiconductor like behavior of the resistivity shown by this material makes it a favorable material for sensor applications.

References

1. Sugaya Y, Inoue O, Kugimiya K (1992) In: Yamaguchi T, Abe M (eds) Proceedings of the 6th Inter-national Conference on Ferrites. The Japan Society of Powder Metallurgy, Tokyo, pp 952–954

2. Drofenik M, Znidarsic A, Zajc I (1997) J Appl Phys 82(1):333
crossref ChemPort

3. Tangsali RB, Keluskar SH, Naik GK, Budkuley JS (2004) Int J Nanosci 3(4&5):589
crossref ChemPort

4. Mohan K, Venudhar YC (1999) J Mater Sci Lett 18:13
[SpringerLink] ChemPort

5. Makovec D, Drofenik M, Znidarsic A (2000) Aa I-8 Digest of 8th Int. Conf. on Ferrites. Kyoto, Japan

6. Keluskar SH, Tangsali RB, Naik GK, Budkuley JS (2006) J Magnetism Magn Mater 305:296
crossref ChemPort

7. Klinger MI, Samokhvalov AA (1977) Phys Status Solid B 79:9
ChemPort

8. Nakamura T, Okano Y (1996) J Appl Phys 79:7129
crossref ChemPort

9. Otsuki E, Yamada S, Oysuka T, Shoji K, Sato T (1996) J Appl Phys 69:5942
crossref

Papers Presented at National/International conferences:

1. "Fine Particle Magnetic Ferrite Material From Sulphite – Hydrazinate Based Precursors"

Proceedings of XXXI National Seminar On Crystallography (19 – 21 June 2001) organized by National Committee for Crystallography (INSA New Delhi) and National Facility for Macro-Molecular Crystallography (SSPD BARC Mumbai).

2.Preparation and Characterization of Nanoparticle Ferrite from Sulphite-Hydrazinate based Precursors

Proceedings of National Seminar on Solid State Spectroscopy (NSSSS 2001) (29-31 Aug. 2001) Organised by Dept of Sri Venkateswara University Tirupati under UGC-DRS program.

3."Effect of sintering temperature and environment on magnetic properties of nanoparticle Mn-Zn ferrite synthesized with Nitrilotriacetate precursor method" presented at National conference on recent advances in material science (NCMS2002) sponsored by CSIR &DRDO Organised by dept. of applied Physics Nehru memorial college Tiruchirapalli- India Dec. 2002.

4." Magnetic properties of nanoparticle Mn-Zn ferrite synthesized with Nitrilotriacetate precursor method" was presented in the workshop New Frontiers in Chemistry" organized by Dept. of Chemistry, Goa University, Feb 2003.

5"Temperature dependence of Magnetic properties of nanoparticle Mn-Zn ferrite prepared using Nitrilotriacetate precursor method" presented at National seminar on chemical physics (NSCP2003) organized by Dept. Of Physics Annamalai University, Tamilnadu India March2003.

6."Effect of sintering conditions on magnetic properties of nanoparticle Mn-Zn Ferrite synthesized with Nitrilotriacetate precursor method" presented in ICMAT 2003 International conference in Singapore, Asia, Dec. 2003.

7."Effect of sintering conditions on electric properties of nanoparticle Mn-Zn Ferrite synthesized with Nitrilotriacetate precursor method" was accepted for oral presentation in IUMRS-ICA-2004, International conference in Asia organized by Material Research society- Taiwan held in Nov.2004.

8." Sintering and microstructure development of Ultra fine particle Mn-Zn Ferrite prepared by Nitrilotriacetate Precursor method" was accepted for poster presentation 49th DAE Solid State Physics Symposium held in Amrutsar, India, Dec. **2004.**

9. **"Effect of Sintering conditions on resistivity of Nanoparticle Mn-Zn Ferrite prepared by Nitrilotriacetate precursor method"** presented in 3rd National conference on Thermophysical properties (NCTP-2005) organized by Thermophysical Society of India, Gauhati University, Assam & Dept. of Physics Goa University Goa.India, Jan. 2005.

10. **"High permeability of low loss Mn-Zn ferrite obtained by sintering nanoparticle Mn-Zn ferrite"** presented in ICMAT 2005 International conference in Singapore, Asia, July 2005.

11. **" Comparison of Physical and Magnetic Properties of Mn-Zn Ferrites prepared by Microwave Induced Decomposition and Ignition of Nitrilotriacetate based precursors"** presented in 4th National Symposium & conference on Solid State Chemistry and allied areas held jointly organized by Department of chemistry Goa University and Indian Association of Solid State Chemists and allied Scientists (ISCAS) in Dec.2005.

12. **"Effect of sintering temperature on Magnetic Properties of Nanoparticle Mn-Zn Ferrite prepared by Nitrilotriacetate Precursor method using Microwave Induced Decomposition"** presented in 4th National Symposium & conference on Solid State Chemistry and allied areas held jointly organized by Department of chemistry Goa University and Indian Association of Solid State Chemists and allied Scientists (ISCAS) in Dec.2005.

13. **"Effect of Microwave Induced Decomposition on Physical and Magnetic Properties of Nanoparticle Mn-Zn Ferrites prepared by Nitrilotriacetate precursor method"** presented in National Symposium on Current trends in Material Characterization organized by Indian Institute of Technology Kanpur held at IIT Kanpur in Dec.2005.

14. **"High performance Nanoparticle Mn-Zn Ferrite prepared by Nitrilotriacetate precursor method using Microwave Induced Decomposition"** presented in 50th DAE Solid State Physics Symposium held at BARC Mumbai in Dec.2005.

15. **"Preparation and Characterization of Nanoparticle Mn-Zn spinel ferrite using Microwave induced decomposition"** has been accepted for poster presentation in APCOT-2006, International conference in Asia organized by Asia-Pacific Conference of Transducers and Micro-nanotechnology at Singapore to be held in June2006.

16. "**High performance ultra loss nanoparticle Mn-Zn ferrite material prepared by nitrilotriacetate precursor with induced microwave combution"** presented in the Indo-Australian symposium on nanomaterials and nanotechnology, held in IISc, Bangalore from 31-1 April 2006.

17. " Preparation and Characterization of nanoparticle mn-zn spinel ferrite using Microwave induced decomposition" has been accepted for poster presentation in Nano-2006, Eighth International conference on nanostructured materials to be held in August 2006 in IISc. Bangalore.

18. "Dielectric properties of mn-zn ferrite prepared by microwave assisted autocombustion synthesis" presented in 51st DAE Solid State Physics Symposium held at Barkatullah university Bhopal in Dec.2006.

19. "Magnetic properties of nanoparticle $mn_{0.67}zn_{0.33}fe_2o_4$ spinel ferrite prepared by microwave induced combustion", presented at International conference on Advanced Nanomaterials 2007 organized by Indian Institute of Technology Powai, Mumbai, held in Jan 2007.

List of publications refereed Journals

1. "Effect of sintering conditions on magnetic properties of nanoparticle Mn-Zn Ferrite synthesized with Nitrilotriacetate precursor method" published in the International **Journal of Nanoscience Vol3 Nos 4&5 (2004) 1-9.**

2. "High permeability of low loss Mn-Zn ferrite obtained by sintering nanoparticle Mn-Zn ferrite" **Journal of Magnetism and Magnetic Materials, 305 (2006) 296-303**

3."Effect of Sintering conditions on resistivity of Nanoparticle Mn-Zn Ferrite prepared by Nitrilotriacetate precursor method" Journal of Material Sc. **Springer Link publications .**

4. " Preparation and Magnetic properties of cadmium substituted lithium ferrite using microwave-induced combustion " published in Journal of **Thin Solid Films, Elsevier publications,** 505 (2006) 168 – 172.

5. "Nanocrystalline Li-Cd ferrite using microwave assisted combustion reaction" published in **MSI Bulletin** Vol.29, 2005.

6. "Magnetic properties of nanoparticle $mn_{0.67}zn_{0.33}fe_2o_4$ spinel ferrite prepared by microwave induced combustion" **Journal of Nanoscience and Nanotechnology** (in review).